SVENSKA GEOFYSISKA FÖRENINGEN

VOLUME 12, NUMBER 3 **Tellus** AUGUST 1960

*A QUARTERLY JOURNAL OF GEOPHYSICS*

# Maximum Simplification of the Dynamic Equations

By EDWARD N. LORENZ, Massachusetts Institute of Technology[1]

(Manuscript received February 1, 1960)

## *Abstract*

When the dynamic equations are to be used to further our understanding of atmospheric phenomena, it is permissible to simplify them beyond the point where they can yield acceptable weather predictions. Through the use of double Fourier series, and with the omission of all but the largest scales of motion, the barotropic vorticity equation may be reduced to a system of three ordinary nonlinear differential equations. The analytic solutions of these equations are elliptic functions of time. The equations may also be solved rapidly by numerical integration.

Particular solutions of the equations picture the motion of finite disturbances on a zonal flow, with exchanges of kinetic energy between the zonal flow and the disturbances accompanying the meridional transport of zonal momentum by the disturbances. Other solutions picture the initial growth and eventual cessation of growth of small disturbances on an unstable zonal current. Still further solutions picture the destruction of a stable zonal flow by large disturbances, and lead to a plausible hypothesis concerning index cycles in the atmosphere.

Less extreme simplifications of the dynamic equations may be used when more complicated atmospheric phenomena are to be studied.

## 1. Simplification of the dynamic equations and the initial conditions

The various phenomena which are observed in our atmosphere, and the changes in the state of the atmosphere from one time to another, are supposedly governed by a set of physical laws. The dynamic meteorologist does not usually regard the discovery of these laws as one of his tasks, being willing to concede that the laws have already been established, at least in approximate form, by workers in other fields. Instead, he includes among his problems the prediction of future states of the atmosphere by means of these laws, and the explanation of typical observable phenomena in terms of these laws. He ordinarily finds it convenient to express the laws as a set of mathematical equations.

In order to make the best attainable forecast of the future weather, it would be desirable to express the physical laws as exactly as possible, and determine the initial conditions as precisely as possible. Yet the ultimate achievement of producing perfect forecasts, by applying equations already known to be exact to initial conditions already known to be precise, if such a feat were possible, would not by itself increase our understanding of the atmosphere, no matter how important it might be from other considerations. For example, if we should observe a hurricane, we might ask ourselves, "Why did this hurricane form?" If we could determine the exact conditions at an earlier time, and if we should feed these conditions, together with a program for integrating the exact equations, into an electronic computer, we should in due time receive a forecast from the computer, which would show the presence of a hurricane. We then might still be justified in asking why

[1] The research resulting in this work has been sponsored by the Geophysics Research Directorate of the Air Force Cambridge Research Center, under Contract No. No. AF 19 (604)-1000.

the hurricane formed. The answer that the physical laws required a hurricane to form from the given antecedent conditions might not satisfy us, since we were aware of that fact even before integrating the equations.

It is only when we use systematically imperfect equations or initial conditions that we can begin to gain further understanding of the phenomena which we observe. For if we omit the terms representing specified physical processes, such as friction, from the equations, or if we fail to include certain observable features, such as cloudiness, in the initial conditions, we may, by comparing the mathematical solutions with reality, gain some insight concerning the relative importance of the retained and omitted features. Of course, in so doing, we forgo the opportunity of simultaneously making the best attainable forecast.

Our present methods of weather observation, and also any foreseeable future methods, yield systematically incomplete initial conditions, and our present mathematical techniques do not allow us to solve the dynamic equations without previous systematic simplification, whether or not the equations may originally be expressed in exact form. Beyond these unavoidable inaccuracies, further simplifications have so far been necessary for the sake of economy. Thus it is that the recent studies in numerical weather prediction, besides yielding creditable although not optimum forecasts, have made vast contributions to our understanding of common weather phenomena. It should be added that these contributions are no accidental by-product; the investigators were concerned with explanation as well as prediction.

The customary simplifications of the dynamic equations are of two kinds. First, we omit or modify certain terms. By doing so, we neglect or alter certain physical processes believed to be of secondary importance. For example, the omission of terms representing the release of latent heat has become familiar, and the introduction of the filtering approximations, which prohibit the propagation of sound and gravity waves, has been one of the important recent advances in dynamic meteorology.

Further simplifications are then demanded by our present inability to solve the partial differential equations. Accordingly, by finite difference methods or otherwise, we convert each partial differential equation into a specified finite number of ordinary differential equations. These equations generally become algebraic when finite differences in time are also introduced. In this process, phenomena of such a small scale that they are lost in the differencing process are automatically excluded. There is no theoretical limit to the number of algebraic equations which may be handled, but for reasons of economy and convenience the number must be restricted. Several hundred equations is typical in short-range dynamic forecasting.

The simplifications of the initial conditions are analogous to those of the dynamic equations. First, we may omit or modify the description of certain observable quantities. For example, it may be logical to omit the field of humidity altogether, when the condensation process is not included in the dynamic equations.

Further simplifications are then demanded by our present system of observations, which yields values of observable quantities only at specified locations. Thus the true state of the atmosphere with its nearly infinite number of degrees of freedom is replaced by a state with a specified finite number of degrees of freedom. Again, phenomena small enough to be lost between observing stations will not be described. For reasons of economy and convenience, the number of degrees of freedom retained is often far less than the maximum number allowed by the observations.

When the problem is finally ready for solutions, it is logical that the finite set of quantities describing the initial conditions should be the finite set of dependent variables in the modified equations.

Although in meteorological practice the most common method of handling partial differential equations has been the use of finite differences, other methods are possible. An alternative method is the analysis of the field of a dependent variable into a series of orthogonal functions. Usually these orthogonal functions are eigenfunctions of a conveniently chosen equation (not the dynamic equation itself). A familiar example of such an analysis, in one dimension, is the Fourier series, in which the orthogonal functions are sines and cosines. The coefficients of these orthogonal functions

become the new dependent variables. The number of dependent variables and ordinary differential equations is then made finite by omitting reference to all but a finite number of variables. When the eigenfunctions can be arranged in the order of their eigenvalues, to represent features of successively smaller scale, this method also excludes the small-scale phenomena.

If our interest is confined to furthering our understanding of the atmosphere, we may simplify the equations and initial conditions to the point where good predictions can no longer be expected. In this study, we shall illustrate some of the advantages to be gained by simplifying the equations to the greatest extent possible, while still retaining the desired physical features. After simplifying the dynamic equations and initial conditions by omitting or modifying certain physical processes and features, we shall expand the equations and initial conditions into series of eigenfunctions. We shall then retain as dependent variables the coefficients of a minimum number of eigenfunctions, corresponding to features of the largest scale. As we shall see, in some cases the resulting set of ordinary differential equations is simple enough to be solved analytically. If this is not the case, we may convert the equations to algebraic equations by a finite difference approximation in time.

It should be evident that these remarks need not have been confined to the atmosphere. Similar remarks apply to a wide class of phenomena, which, in particular, includes controlled hydrodynamic experiments as well as such natural phenomena as oceanic flow.

## 2. The minimum hydrodynamic equations

As an illustration, we shall begin by letting the dynamic equations governing the atmosphere be simplified until they reduce to the familiar vorticity equation

$$\frac{\partial}{\partial t}\nabla^2\psi = -\mathbf{k}\cdot\nabla\psi\times\nabla(\nabla^2\psi), \qquad (1)$$

where $t$ is time, $\psi$ is a stream function for two-dimensional horizontal flow, $\nabla$ is a horizontal differential operator, $\nabla^2 = \nabla\cdot\nabla$ is the horizontal Laplacian operator, and $\mathbf{k}$ is a unit vertical vector. Equation (1) is equivalent to the barotropic vorticity equation, which approximately governs the vertically-averaged horizontal flow in the atmosphere. Equation (1) also governs the motion of a general two-dimensional homogeneous incompressible nonviscous fluid, and states that the vorticity of each material parcel of fluid is conserved.

We shall apply equation (1) to flow in a plane region, in which $\psi$ is doubly periodic at all times, i.e.,

$$\psi(x + 2\pi/k,\ y + 2\pi/l,\ t) = \psi(x,\ y,\ t), \qquad (2)$$

where the $x$ and $y$ axes point eastward and northward, respectively, and $k$ and $l$ are specified constants. In this way we have distorted the geometry of the spherical earth, but we have retained the important property that the effective area is finite but unbounded. We have also neglected the horizontal variations of the Coriolis parameter, although equation (1) is still consistent with a constant Coriolis parameter.

In such a plane region, the eigenfunctions of the equation

$$\nabla^2\psi = c\psi \qquad (3)$$

are trigonometric functions, or equivalently, complex exponential functions, of the variables $mkx + nly$, where $m$ and $n$ are integers, and the corresponding eigenvalues $c$ are the quantities $-(m^2k^2 + n^2l^2)$. Hence a series of eigenfunctions is in this case simply a double Fourier series. An expansion of $\nabla^2\psi$ in such a series is

$$\nabla^2\psi = \sum_{m=0}^{\infty}\sum_{n=n_0}^{\infty}[A_{mn}\cos(mkx + nly) + B_{mn}\sin(mkx + nly)] \qquad (4)$$

where $A_{mn}$ and $B_{mn}$ are real coefficients (and $A_{00} = 0$), and the lower limit $n_0$ in the second sum is $-\infty$ if $m > 0$ and 0 if $m = 0$, or in a more concise notation,

$$\nabla^2\psi = \sum_{\mathbf{M}} C_{\mathbf{M}} e^{i\mathbf{M}\cdot\mathbf{R}} \qquad (5)$$

where $\mathbf{M} = \mathbf{i}mk + \mathbf{j}nl$ and $\mathbf{R} = \mathbf{i}x + \mathbf{j}y$ are the vector wave number, or wave vector, and the radius vector, $\mathbf{i}$ and $\mathbf{j}$ are unit vectors parallel to the $x$ and $y$ axes, $m$ and $n$ assume all integral value from $-\infty$ to $\infty$, and

$$C_{\mathbf{M}} = \overline{C}_{-\mathbf{M}} = \frac{1}{2}(A_{mn} - iB_{mn}) \qquad (6)$$

Here the bar ($^-$) denotes a complex conjugate. The corresponding Fourier series for $\psi$ is

$$\psi = -\sum_{\mathbf{M}} (\mathbf{M}\cdot\mathbf{M})^{-1} C_{\mathbf{M}} e^{i\mathbf{M}\cdot\mathbf{R}} \qquad (7)$$

From (5), with the dummy index **M** replaced by **L**, and (7), with **M** replaced by **H**, it follows that

$$\mathbf{k}\cdot\nabla\psi\times\nabla(\nabla^2\psi) =$$
$$= \sum_{\mathbf{H},\mathbf{L}} (\mathbf{k}\cdot\mathbf{H}\times\mathbf{L})\,(\mathbf{H}\cdot\mathbf{H})^{-1} C_{\mathbf{H}} C_{\mathbf{L}} e^{i(\mathbf{H}+\mathbf{L})\cdot\mathbf{R}} \qquad (8)$$

Replacing $\mathbf{H}+\mathbf{L}$ in (8) by **M**, and substituting (5) and (8) into the left and right hand sides, respectively, of (1), we find that

$$\frac{dC_{\mathbf{M}}}{dt} = -\sum_{\mathbf{H}} \frac{\mathbf{K}\cdot\mathbf{H}\times\mathbf{M}}{\mathbf{H}\cdot\mathbf{H}} C_{\mathbf{H}} C_{\mathbf{M}-\mathbf{H}} \qquad (9)$$

Equation (9) is the Fourier transform of equation (1), and is actually the infinite set of ordinary differential equations which we sought to determine. The coefficients $C_{\mathbf{M}}$ are the dependent variables.

For the surface of a sphere, the eigenfunctions of equation (3) are spherical harmonics. An expansion of the vorticity equation into a series of spherical harmonics has been used by SILBERMAN (1954).

The final step in simplification is the omission of reference to all but a finite number of variables $C_{\mathbf{M}}$, corresponding to a specified set of values of $m$ and $n$. If these values are small, only large-scale features will be retained. The summation in (9) then becomes a finite sum, but the equations are otherwise unaltered.

Under equation (1), two integral quantities, namely, the mean kinetic energy and the mean square of the vorticity, remain unchanged with time. Since equations (1) and (9) are equivalent, equation (9) must also conserve these values. According to (5) and (7), the mean kinetic energy is given by

$$E = \frac{1}{2}\sum_{\mathbf{M}} \frac{C_{\mathbf{M}} C_{-\mathbf{M}}}{\mathbf{M}\cdot\mathbf{M}}, \qquad (10)$$

while the mean square of the vorticity is given by

$$V = \sum_{\mathbf{M}} C_{\mathbf{M}} C_{-\mathbf{M}}. \qquad (11)$$

According to (9), the time derivatives of $E$ and $V$ each involve sums of terms containing products $C_{\mathbf{H}} C_{\mathbf{M}-\mathbf{H}} C_{-\mathbf{M}}$. In these sums each product occurs six times, corresponding to the six permutations of $C_{\mathbf{H}}$, $C_{\mathbf{M}-\mathbf{H}}$, and $C_{\mathbf{M}}$, and the sum of the six coefficients may be readily verified to equal zero.

It follows that if all reference to specified variables is omitted, any specific product $C_{\mathbf{H}} C_{\mathbf{M}-\mathbf{H}} C_{-\mathbf{M}}$ will either be omitted altogether from the expressions for $dE/dt$ and $dV/dt$ or else it will occur six times, and the sum of the six coefficients will still vanish. Hence the simplified equations (9) still conserve the mean kinetic energy and the mean square of the vorticity, although the definition of these quantities has now been modified, in that the sums in (10) and (11) are now finite sums. Equations (9) are no longer able, however, to conserve the entire statistical distribution of vorticity. Equations (10) and (11) are two first integrals of (9).

Equation (9) may be regarded as describing a nonlinear interaction between the components whose coefficients are $C_{\mathbf{H}}$ and $C_{\mathbf{M}-\mathbf{H}}$, to alter a third coefficient $C_{-\mathbf{M}}$. Let us seek the maximum simplification of (9) which still describes this process. Clearly at least three terms with different eigenvalues must be retained.

A simple system may be formed by retaining only those eight significant terms for which $m$ and $n$ each assume a value of 1, 0, or $-1$ (the term $m = n = 0$ is superfluous). Then (4) reduces to

$$\nabla^2\psi = A_{10}\cos kx + A_{01}\cos ly +$$
$$+ A_{11}\cos(kx+ly) + A_{1,-1}\cos(kx-ly) +$$
$$+ B_{10}\sin kx + B_{01}\sin ly + B_{11}\sin(kx+ly) +$$
$$+ B_{1,-1}\sin(kx-ly). \qquad (12)$$

Further simplifications appear when it is noted that if $B_{10}$, $B_{01}$, $B_{11}$, and $B_{1,-1}$ all vanish initially, they will remain zero, and if, in addition, $A_{1,-1} = -A_{11}$ initially, $A_{1,-1}$ will remain equal to $-A_{11}$. Letting $A_{01} = A$, $A_{10} = F$, $A_{1,-1} = G$, we obtain, as the ultimate simplification of the vorticity and the stream function,

$$\nabla^2\psi = A\cos ly + F\cos kx +$$
$$+ 2G\sin ly\sin kx, \qquad (13)$$

$$\psi = -\frac{A}{l^2}\cos ly - \frac{F}{k^2}\cos kx - \\ -\frac{2G}{k^2+l^2}\sin ly \sin kx. \qquad (14)$$

The governing equations, obtained either from (9), or by substituting (13) and (14) directly into (1), are

$$\frac{dA}{dt} = -\left(\frac{1}{k^2} - \frac{1}{k^2+l^2}\right)klFG, \qquad (15)$$

$$\frac{dF}{dt} = \left(\frac{1}{l^2} - \frac{1}{k^2+l^2}\right)klAG, \qquad (16)$$

$$\frac{dG}{dt} = -\frac{1}{2}\left(\frac{1}{l^2} - \frac{1}{k^2}\right)klAF. \qquad (17)$$

The coefficients of $FG$, $AG$ and $AF$ are actually determined by the ratio $k/l$. The mean kinetic energy and the mean square of the vorticity,

$$E = \frac{1}{4}\left(\frac{A^2}{l^2} + \frac{F^2}{k^2} + \frac{2G^2}{k^2+l^2}\right), \qquad (18)$$

and

$$V = \frac{1}{2}(A^2 + F^2 + 2G^2), \qquad (19)$$

are readily seen to be conserved under equations (15—17).

In the remainder of this work we shall be primarily concerned with the simplifications appearing in equations (13—17). These equations presumably contain the minimum number of degrees of freedom required to picture nonlinear barotropic phenomena. We shall call this set of equations the *minimum hydrodynamic equations*, or sometimes simply the minimum equations.

In equation (14), the first term on the right is independent of $x$, and therefore represents the zonal flow. Because there are so few degrees of freedom, the latitudes ($y = \pi/2l$, $3\pi/2l$, — — —) of the zonal wind maxima are fixed, but the intensity $A/l$ may vary. Thus the variable $A$ agrees with the meteorologist's concept of the zonal index.

The remaining terms represent disturbances superposed on the zonal flow. Together they describe a wave of a single wave number, but a variable shape, and, except at certain latitudes, a variable phase. Again because there are so few degrees of freedom, the shape of the wave depends upon the phase, so that the model cannot picture the motion of disturbances without change of shape. It can, however, picture the nonlinear interaction between the zonal flow and the superposed disturbances.

In general, a set of nonlinear differential equations must be converted into a set of algebraic equations, by replacing time derivatives by finite differences, before a solution can be obtained. The minimum hydrodynamic equations (15—17), however, may be solved analytically. Either by eliminating two variables through the first integrals (18) and (19), and solving the remaining equation, or simply by observing that $A$, $F$, and $G$ are three quantities, each of whose derivatives is proportional to the product of the remaining two quantities, we find that the solutions of (15—17) are elliptic functions of time. The particular elliptic functions depend upon the ratio $\alpha = k/l$, and the ratio $V/E$ which is determined by the initial conditions.

If $\alpha > 1$, and if $V/E < 2k^2$, we find in view of (18) and (19) that $A$, $F$, and $G$ have maximum values $A^\star$, $F^\star$, and $G^\star$ given by

$$\left.\begin{aligned} A^{\star 2} &= A^2 + \alpha^{-4}F^2 \\ F^{\star 2} &= F^2 + 2(1-\alpha^{-4})^{-1}G^2 \\ G^{\star 2} &= G^2 + \frac{1}{2}(1-\alpha^{-4})F^2 \end{aligned}\right\} \qquad (20)$$

The solutions of (16—18) are then

$$\left.\begin{aligned} A &= A^\star\, dn\, h(t-t^\star) \\ F &= F^\star\, sn\, h(t-t^\star) \\ G &= G^\star\, cn\, h(t-t^\star) \end{aligned}\right\} \qquad (21)$$

where the modulus $k_0$ of the elliptic functions is given by

$$k_0^2 = \frac{2}{\alpha^4(\alpha^4-1)}\frac{F^\star G^\star}{A^{\star 2}} \qquad (22)$$

$h$ is given by

$$h^2 = \frac{1}{2}\frac{\alpha^2(\alpha^2-1)}{\alpha^2+1}A^{\star 2}, \qquad (23)$$

and $t^\star$ is the time when $A = A^\star$, $F = 0$, and $G = G^\star$, given by the elliptic integral

$$ht^\star = \int_{\tan^{-1}F_0/G_0}^{0} \frac{d\Theta}{\sqrt{1-k_0^2\sin^2\Theta}}. \qquad (24)$$

The solution is periodic of period $4K/h$, where $K$ is given by the complete elliptic integral

$$K = \int_0^{\pi/2} \frac{d\Theta}{\sqrt{1 - k_0^2 \sin^2 \Theta}}. \qquad (25)$$

With different initial conditions, or a different ratio $\alpha$, the elliptic functions $dn$, $sn$, and $cn$ may correspond to different permutations of $A$, $F$, and $G$.

When a numerical solution is desired, it is often simpler to solve equations (15—17) numerically than to use a table of elliptic functions. To convert the differential equations into algebraic equations which may be solved numerically, we choose a fixed time interval $\Delta t$, and let $A_n$, $F_n$, and $G_n$ be the values of $A$, $F$ and $G$ at time $t_0 + n\Delta t$. We may then use the centered difference formula

$$A_{n+1} = A_{n-1} + 2\left(\frac{dA}{dt}\right)_n \Delta t, \qquad (26)$$

with analogous equations for $F_{n+1}$ and $G_{n+1}$.

At the first time step, we cannot use a centered difference formula. Accordingly, we may obtain a first approximation $A_{(1)}$ to $A_1$ by the uncentered difference formula

$$A_{(1)} = A_0 + \left(\frac{dA}{dt}\right)_0 \Delta t, \qquad (27)$$

with analogous formulas for $F_{(1)}$ and $G_{(1)}$. We then obtain the final value $A_1$ by the formula

$$A_1 = A_0 + \frac{1}{2}\left[\left(\frac{dA}{dt}\right)_0 + \left(\frac{dA}{dt}\right)_{(1)}\right] \Delta t, \qquad (28)$$

with analogous formulas for $F_1$ and $G_1$.

When partial differential equations are integrated numerically through the use of finite differences in space and time, the phenomenon of computational instability may arise. In order to avoid such instability, the time interval $\Delta t$ must be chosen to be not too large compared to the space intervals $\Delta x$ and $\Delta y$. The corresponding condition for computational stability, when orthogonal functions are used, is that $\Delta t$ be not too large a fraction of the period of oscillation of the most rapidly oscillating variable. Thus, whichever method is used, the smaller the scale of the phenomena which are admitted, the smaller $\Delta t$ must be in order to avoid computational instability.

The phenomenon of computational instability is easily recognized when it arises, and may be eliminated by decreasing $\Delta t$. In the case of the minimum hydrodynamic equations, where only phenomena of very large scale are admitted, $\Delta t$ may be moderately large.

### 3. Particular solutions of the minimum hydrodynamic equations

We have seen that the minimum equations (15—17) preserve the average kinetic energy. At the same time, since they admit variations of $A$, they allow the kinetic energy of the zonal motion to vary, and hence allow exchanges of kinetic energy between the zonal flow and the disturbances. In actual barotropic flow, such exchanges can only accompany a net transport of momentum by the disturbances to or from the zones of maximum flow. In our first numerical example, we shall show that this phenomenon is adequately described by the minimum equations.

The quantity $2\pi/l$ is the distance between successive zonal wind maxima, while $2\pi/k$ is the wave length of the disturbances. Let us choose $2\pi/l$ = 10,000 kilometers and $2\pi/k$ = 5,000 kilometers, so that $\alpha = 2$. In so doing we shall be choosing systems of a size comparable to the large-scale flow systems in the earth's atmosphere. Equations (15—17) then become

$$\left.\begin{aligned} \dot{A} &= -\frac{1}{10} FG \\ \dot{F} &= \frac{8}{5} AG \\ \dot{G} &= -\frac{3}{4} AF \end{aligned}\right\} \qquad (29)$$

where a dot denotes a time derivative.

The unit of time may be conveniently chosen equal to 3 hours, so that the unit of vorticity is (3 hours)$^{-1}$, or approximately the value of the Coriolis parameter in middle latitudes.

For initial conditions, let us choose $A$ = 0.12 units, $F$ = 0.24 units, and $G$ = 0. The initial maximum zonal wind speed, occurring where $y = 3\pi/2l$, is then 64 kilometers per

hour, while the initial maximum vorticity, occurring where $x = 0$, and $y = 0$, is 0.36 time the Coriolis parameter. Since $F = 2A$, the zonal kinetic energy and disturbance kinetic energy are initially equal.

Applying equations (20—25), we find that the analytic solution of equation (29) is

$$\left.\begin{aligned} A &= 0.1342\, dn(0.147t + 11.03) \\ F &= 0.2400\, sn(0.147t + 11.03) \\ G &= 0.1643\, cn(0.147t + 11.03) \end{aligned}\right\} \quad (30)$$

where the modulus of the elliptic functions is $k_0 = 0.2$, while the period is 44.1 time units, or 132.3 hours.

Instead of consulting tables of elliptic functions, we may solve equations (29) numerically. If time interval $\Delta t$ is chosen to be 6 hours, or 2 time units, the algebraic approximations to (29) are

$$\left.\begin{aligned} A_{n+1} &= A_{n-1} - 0.4\, F_n G_n \\ F_{n+1} &= F_{n-1} + 6.4\, A_n G_n \\ G_{n+1} &= G_{n-1} - 3.0\, A_n F_n \end{aligned}\right\} \quad (31)$$

with appropriate modifications for the first time step.

The numerical integrations of (31) may be carried out with a desk computer, or even a slide rule, at a computation rate comparable to one minute per time step. The computations are presented in table 1.

The products $FG$, $AG$ and $AF$, which occur on the right hand side of (31), are included in the tabulation.

From the numerical point of view, we observe that $F$ becomes zero, and $A$ and $G$ reach maxima, after about 5 ½ time steps, or 33 hours, while $A$ and $G$ reach their original values after about 11 steps, after which the previous history must be repeated, except that $F$ and $G$ have opposite signs. The full period is therefore about 22 steps, or 132 hours, which agrees closely with the analytic solution, while the maxima of $A$ and $G$ also agree closely with $A^\star$ and $G^\star$ as determined by (20).

From the physical point of view, the initially symmetric disturbance is distorted by the zonal flow so as to transport momentum into the zones of maximum zonal winds, thereby increasing the zonal kinetic energy, at the expense of the disturbance kinetic energy. Eventually, the wave becomes distorted to a shape where it transfers momentum out of the zonal wind maxima, and the zonal kinetic energy decreases again to its original value.

From the synoptic point of view, the stream function field initially consists of alternate zones of high and low values of $\psi$, crossed by a series of troughs and ridges with axes oriented N—S, as shown in the first map in fig. 1. The troughs and ridges are carried eastward in the eastward flow, and westward in the westward flow, so that the axes acquire a NE—SW orientation across the latitudes of high $\psi$, and a NW—SE orientation across the latitudes of low $\psi$, as shown in the second map, which follows the first by 18 hours. As described by STARR (1948), eastward momentum is carried northward where the troughs and ridges tilt NE—SW, and southward where

**Table 1. Numerical integration of the minimum equations, with the indicated initial conditions, for the case $\alpha = 2$, with time steps equal to two time units.**

| $n$ | $A_n$ | $F_n$ | $G_n$ | $A_nF_n$ | $A_nG_n$ | $F_nG_n$ |
|---|---|---|---|---|---|---|
| 0 | 0.120 | 0.240 | 0.000 | 0.0288 | 0.0000 | 0.0000 |
| 1 | 0.121 | 0.232 | — 0.043 | 0.0281 | — 0.0052 | — 0.0100 |
| 2 | 0.124 | 0.207 | — 0.084 | 0.0257 | — 0.0104 | — 0.0174 |
| 3 | 0.128 | 0.165 | — 0.120 | 0.0211 | — 0.0154 | — 0.0198 |
| 4 | 0.132 | 0.108 | — 0.147 | 0.0143 | — 0.0194 | — 0.0159 |
| 5 | 0.134 | 0.041 | — 0.163 | 0.0055 | — 0.0218 | — 0.0067 |
| 6 | 0.135 | — 0.032 | — 0.163 | — 0.0043 | — 0.0220 | 0.0052 |
| 7 | 0.132 | — 0.100 | — 0.150 | — 0.0132 | — 0.0198 | 0.0150 |
| 8 | 0.129 | — 0.159 | — 0.123 | — 0.0205 | — 0.0159 | 0.0196 |
| 9 | 0.124 | — 0.202 | — 0.088 | — 0.0250 | — 0.0109 | 0.0178 |
| 10 | 0.122 | — 0.229 | — 0.048 | — 0.0279 | — 0.0059 | 0.0110 |
| 11 | 0.120 | — 0.240 | — 0.004 | — 0.0288 | — 0.0005 | — 0.0010 |
| 12 | 0.122 | — 0.232 | 0.038 | — 0.0283 | 0.0046 | — 0.0088 |

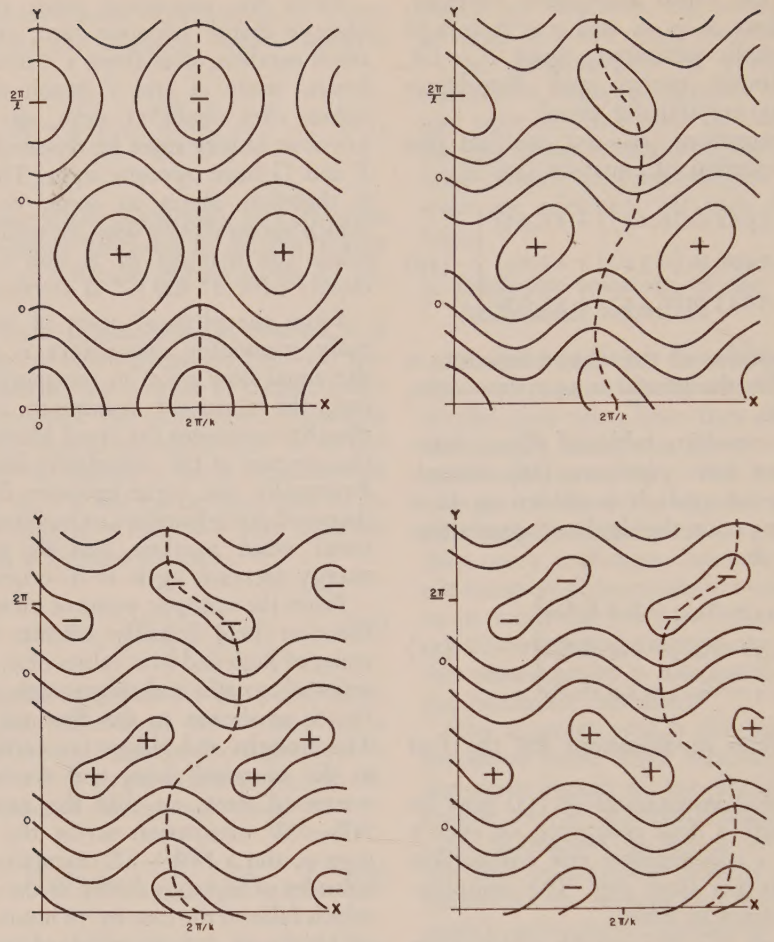


Fig. 1. Stream function patterns for the solutions of the minimum equations given in table 1. Upper left: 0 hours; upper right: 18 hours; lower left: 30 hours; lower right: 36 hours. Streamlines are drawn at intervals of 0.070 units. Dashed lines represent trough lines.

they tilt NW—SE, so that in this case eastward momentum is carried into the zones of eastward flow, in agreement with the increasing zonal index. After 30 hours, as seen in the third map, each center of high or low $\psi$ breaks into two centers. Still later, the NE lobe of each high center departs from the SW lobe altogether, and merges with the SW lobe of the next high center to the east, while the low centers perform a similar process, so that, shortly after 36 hours, as seen in the fourth map, the streamline patterns become the mirror image, in the line $x = 3\pi/2k$, of the map at 30 hours. Patterns after 36 hours become the mirror images of patterns before 30 hours, and, shortly after 66 hours, the pattern regains its initial appearance, except that it is displaced by one-half wave length. After 132 hours, the full cycle has taken place.

The solution presented in table 1 suggests that the zonal flow is stable, since the disturbances show no tendency for exponential growth. However, a stable flow strictly speaking is one which can exist by itself, and which does not tend to become further disturbed after being slightly disturbed. In a numerical study of stability we should therefore choose initial conditions where the

disturbance kinetic energy is small compared to the zonal kinetic energy.

According to the linear theory, in which the variable $A$ is replaced by a constant, equations (16) and (17) will govern a stable zonal flow if the coefficients of $AG$ and $AF$ have opposite signs, so that the solutions for $F$ and $G$ are trigonometric, and they will govern an unstable flow if the coefficients have the same sign, so that the solutions are exponential. Examining these coefficients in (16) and (17), we see that the zonal flow is stable if $\alpha > 1$, and unstable if $\alpha < 1$. In particular, the zonal flow in the previous example is stable. A similar condition for stability holds even when an infinite number of orthogonal functions are present in the series for $\psi$ and $\nabla^2\psi$, as shown by FJØRTOFT (1953).

Let us see what the nonlinear equations tell us about stability. Let us choose two cases, one where $\alpha = 1.05$, and one where $\alpha = 0.95$. The corresponding sets of differential equations are

$$\left.\begin{aligned} A^{\cdot} &= -0.453\,FG \\ F^{\cdot} &= \phantom{-}0.551\,AG \\ G^{\cdot} &= -0.049\,AF \end{aligned}\right\} \qquad (32)$$

and

$$\left.\begin{aligned} A^{\cdot} &= -0.553\,FG \\ F^{\cdot} &= \phantom{-}0.451\,AG \\ C^{\cdot} &= \phantom{-}0.051\,AF \end{aligned}\right\} \qquad (33)$$

We shall integrate these equations numerically by the same procedure as that used previously, again choosing 3 hours as our unit of time, and 6 hours as the length of a time step. In each case the initial eddy kinetic energy is about one per cent of the zonal kinetic energy. The integrations are presented in table 2.

In the first case, there is no tendency for the disturbance to grow. It simply progresses, with a period of about 18 time steps, or 108 hours, while the fluctuations of the zonal flow are very small. The solution differs only slightly from the trigonometric solution of the linearized equations.

In the second case, the disturbance begins to grow exponentially ($F$ resembles a hyperbolic cosine, while $G$ resembles a hyperbolic sine). Likewise, the rate of decrease of $A$ increases exponentially. The exponential increase of $F$ and $G$ does not proceed without limit, however, as in the linear case, but is inhibited as $A$ becomes smaller, and ceases altogether when $A$ reaches zero.

Thus, as might have been expected, the linearized equations describe the changes of the system very well while the disturbances remain small, but not after they become comparable in size to the zonal flow itself.

The unstable solution throws considerable light upon the whole phenomenon of instability, which is not apparent in considering the linear equations. Instability itself is pictured here as a nonlinear phenomenon. The growth of $F$ is due to the nonlinear interaction of $A$ and $G$, while the growth of $G$ is due to the nonlinear interaction of $A$ and $F$, or, taken as a whole, the disturbance grows because of

**Table 2. Numerical integration of the minimum equations, in the case of a disturbed stable zonal flow ($\alpha = 1.05$), and a disturbed unstable zonal flow ($\alpha = 0.95$).**

| $n$ | stable case, $\alpha = 1.05$ | | | unstable case, $\alpha = 0.95$ | | |
|---|---|---|---|---|---|---|
| | $A_n$ | $F_n$ | $G_n$ | $A_n$ | $F_n$ | $G_n$ |
| 0 | 1.000 | 0.100 | 0.000 | 1.000 | 0.100 | 0.000 |
| 1 | 1.000 | 0.094 | — 0.010 | 0.999 | 0.105 | 0.010 |
| 2 | 1.002 | 0.078 | — 0.018 | 0.998 | 0.118 | 0.021 |
| 3 | 1.003 | 0.054 | — 0.025 | 0.994 | 0.143 | 0.034 |
| 4 | 1.004 | 0.023 | — 0.029 | 0.987 | 0.179 | 0.050 |
| 5 | 1.004 | — 0.010 | — 0.030 | 0.974 | 0.232 | 0.070 |
| 6 | 1.004 | — 0.043 | — 0.027 | 0.951 | 0.302 | 0.096 |
| 7 | 1.002 | — 0.070 | — 0.021 | 0.910 | 0.397 | 0.129 |
| 8 | 1.001 | — 0.089 | — 0.013 | 0.838 | 0.514 | 0.170 |
| 9 | 1.000 | — 0.099 | — 0.003 | 0.717 | 0.654 | 0.217 |
| 10 | 1.000 | — 0.096 | 0.006 | 0.524 | 0.795 | 0.266 |
| 11 | 1.001 | — 0.086 | 0.016 | 0.249 | 0.908 | 0.303 |
| 12 | 1.003 | — 0.061 | 0.023 | — 0.085 | 0.931 | 0.312 |

its nonlinear interaction with the zonal flow. Eventually the disturbance ceases to grow, and begins to decay, also because of its nonlinear interaction with the zonal flow. The source or sink of disturbance kinetic energy during the entire process is the zonal kinetic energy.

We have seen that the minimum equations are capable of picturing the motion of disturbances in a zonal current, and the stability or instability of a zonal current. Another related atmospheric phenomenon is the index cycle, i.e., the tendency for the mean strength of the middle-latitude zonal westerly winds to undergo rather marked fluctuations in intensity, usually with periods of a few weeks. It is interesting to see what light may be thrown upon the index cycle by the minimum equations.

In the example appearing in table I, the zonal index $A$ undergoes fluctuations, but not the violent fluctuations of an index cycle. Moreover, the constraints of the model require some fluctuations of $A$ if the disturbances are to move at all. With different initial conditions, even though $\alpha > 1$, the fluctuations of $A$ need not be so weak. From (18) and (19), we observe that if $V/E < 2k^2$, and $\alpha > 1$, $A$ can never become zero, but if $V/E > 2k^2$, there is no apparent reason why $A$ cannot become zero. For $\alpha = 2$, the condition $V/E = 2k^2$ implies that $G^2 = \frac{15}{2} A^2$. Accordingly, we shall integrate equations (15—17) numerically for two cases of large disturbances, one case where $G^2 < \frac{15}{2} A^2$, and one where $G^2 > \frac{15}{2} A^2$. We shall choose all quantities except the initial conditions as in the first example. The solutions appear in table 3.

In the first case, where initially $G = 5/2\ A$, the solution is qualitatively like the example in table 1, although the fluctuations of the zonal index are more pronounced. In the second case, where $G = 10/3\ A$ initially, the situation is different. Here the zonal index changes sign, so that easterlies occupy the region where westerlies were originally present. Moreover, $G$ does not change sign, so that the disturbances do not continue to progress in one direction, but move back and forth, according to the sign of the zonal index. The index shows a period of about 26 time steps, or 6½ days.

Separating these cases there is a discontinuity in the amplitude of the fluctuations of $A$. Either the total range of $A$ is not greater than $A^\star$, if $V/E < 2k^2$, or it is twice $A^\star$, if $V/E > 2k^2$. We shall say that $A$ undergoes minor fluctuations in the former case, and major fluctuations in the latter. It seems reasonable to identify major fluctuations with an index cycle. It should be noted that, in contrast to the solution in table 2, the major fluctuations do not result from the instability of the zonal flow with respect to small disturbances. It is only because the disturbance is large that major fluctuations can occur.

**Table 3. Integration of the minimum equations for $\alpha = 2$, in the case of a subcritical disturbance ($G_0 = 5/2\,A_0$) and a supercritical disturbance ($G_0 = 10/3\,A_0$).**

| $n$ | subcritical case | | | supercritical case | | |
|---|---|---|---|---|---|---|
| | $A_n$ | $F_n$ | $G_n$ | $A_n$ | $F_n$ | $G_n$ |
| 0 | 0.120 | 0.000 | 0.300 | 0.120 | 0.000 | 0.400 |
| 1 | 0.117 | 0.115 | 0.290 | 0.114 | 0.154 | 0.386 |
| 2 | 0.107 | 0.217 | 0.260 | 0.096 | 0.282 | 0.347 |
| 3 | 0.094 | 0.293 | 0.221 | 0.075 | 0.367 | 0.305 |
| 4 | 0.081 | 0.350 | 0.179 | 0.051 | 0.429 | 0.265 |
| 5 | 0.069 | 0.386 | 0.136 | 0.030 | 0.451 | 0.239 |
| 6 | 0.060 | 0.410 | 0.099 | 0.008 | 0.475 | 0.225 |
| 7 | 0.053 | 0.424 | 0.062 | — 0.013 | 0.463 | 0.228 |
| 8 | 0.049 | 0.431 | 0.031 | — 0.034 | 0.454 | 0.243 |
| 9 | 0.048 | 0.434 | — 0.001 | — 0.057 | 0.410 | 0.274 |
| 10 | 0.049 | 0.431 | — 0.031 | — 0.079 | 0.354 | 0.313 |
| 11 | 0.053 | 0.424 | — 0.064 | — 0.101 | 0.252 | 0.358 |
| 12 | 0.060 | 0.409 | — 0.099 | — 0.115 | 0.122 | 0.389 |
| 13 | 0.069 | 0.386 | — 0.138 | — 0.120 | — 0.034 | 0.400 |
| 14 | 0.081 | 0.348 | — 0.179 | — 0.110 | — 0.185 | 0.377 |

This solution suggests a plausible hypothesis for the existence of index cycles in the atmosphere, which we shall now describe. According to this hypothesis, the ratio $V/E$ of the variance of vorticity to the kinetic energy is usually subcritical, so that only minor fluctuations of the zonal index take place. These fluctuations may occur within a high-index or low-index regime. Occasionally, as the result of a baroclinic process, the ratio $V/E$ will become supercritical, and the index will change from high to low, or low to high. The index change itself will be a barotropic effect, even though the cause of the supercritical value of $V/E$ will be baroclinic. Because of dissipative effects, the ratio $V/E$ will soon become subcritical again, after which the index will undergo minor fluctuations about its new value, until another baroclinic process makes the value $V/E$ supercritical again. If the time required for dissipative effects to make $V/E$ subcritical, after it becomes supercritical, is about one-half of the natural period of a major fluctuation of the index, the result will be a change from a high to low, or low to high, index regime.

Although this hypothesis may appear plausible, it cannot be claimed that the solution presented in table 2 is any more than a piece of evidence in its favor. To place the hypothesis on a firmer basis, it is necessary to integrate less drastically simplified systems of equations, to see whether major fluctuations still appear in the solutions. In addition, it is necessary to perform a careful observational study, to see whether changes in the zonal index actually do follow large increases in the ratio $V/E$, or in some equally significant parameter.

Nevertheless, this example demonstrates unmistakably how a plausible hypothesis, capable of being tested by further study, can be formulated on the basis of a dynamic equation which has been simplified far beyond the point where it will yield an acceptable short-range forecast.

## 4. Further applications of simplified equations

We have shown that it is possible to simplify the dynamic equations governing the atmosphere to the point where they may either be solved analytically, or else be integrated numerically with very little effort, while still retaining the nonlinear character of the equations. At the same time, these simplified equations are realistic enough to describe qualitatively some of the important physical phenomena in the atmosphere, and even to lead to plausible hypotheses concerning phenomena as yet not fully explained.

The degree of simplification which we are permitted to use depends upon the particular phenomena which we wish to investigate. For example, the belts of westerly winds pictured in fig. 1 do not resemble the atmospheric jet stream, since winds of nearly maximum strength occupy a large fraction of the belt. In order to study the behavior of a jet under barotropic flow, and in particular to observe such phenomena as the splitting of a jet into two streams, we must retain considerably more terms in the Fourier series, capable of picturing narrow bands of very strong flow.

Again, if we wish to study simple baroclinic flow, we may use one of the two-layer numerical prediction models in place of the barotropic vorticity equation. The maximum allowable simplification would then retain three degrees of freedom for the flow in each layer, or a total of six dependent variables. With such a system, the instability of zonal baroclinic flow, among other phenomena, could be studied.

As a final example, if we are interested in studying forced baroclinic flow, such as that which characterizes the general circulation of the atmosphere, we may again use the same six dependent variables, and modify the equations by appending terms representing nonadiabatic heating and friction. If, however, we wish to describe the increase in static stability which must accompany the conversion of potential and internal energy into kinetic energy through the sinking of cold air and rising of warm air, we must add at least one dependent variable, the space-averaged static stability. Such a system with seven degrees of freedom has been integrated by BRYAN (1959). Among other phenomena, the system is capable of duplicating the appearance or lack of appearance of waves superposed upon the symmetric flow occurring in the dishpan experiments (FULTZ, 1953), according to whether the external heating is weak or strong. Further refinements introduced by Bryan include the

spherical geometry of the earth, whereupon thirteen degrees of freedom are sufficient.

There is virtually no limit to the number of phenomena which one might study by means of equations simplified according to the manner we have described. In each case, the simplified equations may seem to be rather crude approximations, but they should clarify our understanding of the phenomena, and lead to plausible hypotheses, which may then be tested by means of careful observational studies and more refined systems of dynamic equations.

## REFERENCES


Bryan, K., 1959: A numerical investigation of certain features of the general circulation. *Tellus* **11**, pp. 163—174.

Fjørtoft, R., 1953: On the changes in the spectral distribution of kinetic energy for two dimensional nondivergent flow. *Tellus* **5**, pp. 225—230.

Fultz, D., 1953: A survey of certain thermally and mechanically driven systems of meteorological interest. *Proceedings of the first symposium on the use of models in geophysical fluid dynamics*. Johns Hopkins Univ., Baltimore.

Silberman, I., 1954: Planetary waves in the atmosphere. *J. Meteor.* **11**, pp. 27—34.

Starr, V. P., 1948: An essay on the general circulation of the earth's atmosphere. *J. Meteor.* **5**, pp. 39—43.

# On the motion of a cyclone embedded in a uniform flow[1]

By JULIÁN ADEM and PEDRO LEZAMA, Instituto de Geofísica, Universidad Nacional de México, México 20, D. F.

(Manuscript received November 10, 1959)

*Abstract*

Using the barotropic model, an analytical expression for the motion of a cyclone embedded in a uniform flow is obtained. The solution contains as parameters the radius of the vortex, the maximum velocity in the vortex, the velocity of the uniform flow and the variation of the Coriolis parameter.

It is shown that, if the variation of the Coriolis parameter is neglected, a cyclone initially embedded in a uniform flow moves with the velocity of the flow. However, superimposed with that motion there always exists a north-westward translation due to the variation of the Coriolis parameter that in some cases represents a non-negligible percentage of the total displacement of a hurricane.

Let us consider as initial flow the one given by the stream function

$$\psi(r, \Theta, 0) = DF(r/r_0) + Ar \sin \Theta + Br \cos \Theta \quad (1)$$

where $(r, \Theta)$ are polar coordinates and $A$, $B$, $D$ and $r_0$ are constants. This stream function represents a vortex embedded in a uniform flow. The term $Ar \sin \Theta$ is the zonal component of the flow that has a velocity $u = -\partial\psi/\partial y = -A$, the term $Br \cos \Theta$ is the meridional component that has a velocity $v = \partial\psi/\partial x = B$, and the term $DF(r/r_0)$ represents a vortex. We choose $F(r/r_0) = 0$ for $r \geqslant r_0$, so that the radius of the vortex is $r_0$.

Let

$$\left.\begin{aligned} DF(r/r_0) &= D[1 - (r/r_0)^2]^4 \quad \text{for } r \leqslant r_0 \\ DF(r/r_0) &= 0 \qquad\qquad\qquad\quad \text{for } r \geqslant 0 \end{aligned}\right\} \quad (2)$$

This stream function represents a vortex of radius $r_0$; it is a cyclone for $D$ negative and an anticyclone for $D$ positive. The maximum velocity in the vortex is at $(r/r_0) = \sqrt{1/7}$ and $D$ can be expressed as a function of the radius and of the maximum velocity by

$$D = -0.525\, r_0\, v_m \quad (3)$$

The vortex is therefore completely determined by the radius $r_0$ and the maximum velocity $v_m$.

From the barotropic vorticity equation and the equations obtained by differentiating the vorticity equation with respect to time, we can compute $\partial\psi/\partial t$, $\partial^2\psi/\partial t^2$, $\partial^3\psi/\partial t^3$, etc. by solving equations of the Poisson type in the same way as described in a previous paper (ADEM, 1956).

From the vorticity equation we obtain

$$\nabla^2 \frac{\partial \psi}{\partial t} = -\beta D \cos \Theta \frac{dF}{dr} + AD \cos \Theta \frac{d\nabla^2 F}{dr} - BD \sin \Theta \frac{d\nabla^2 F}{dr} - \beta B$$

For the range of values in which we are interested, the term $\beta B$ is small and will be neglected.

[1] This research was partially supported by Instituto Nacional de la Investigación Científica (México).

If we prescribe $\partial\psi/\partial t = 0$ at the boundary $r = R_0$ we obtain

$$\frac{\partial\psi}{\partial t} = \left[ AD\frac{dF}{dr} - \frac{\beta D}{r}\int_0^r rF dr + \right.$$

$$\left. + \frac{\beta D r}{R_0^2}\int_0^{r_0} rF dr \right] \cos\Theta - BD\frac{dF}{dr}\sin\Theta \quad (4)$$

We will assume that $R_0 \gg r_0$ so that the term that depends on the boundary can be neglected.

Similarly, by prescribing $(\partial^2\psi/\partial t^2)_{r=R_0} = 0$ and assuming that $R_0 \gg r_0$ we obtain $\partial^2\psi/\partial t^2$.

Using a series expansion with respect to $t$, the stream function after a sufficiently small interval of time is given by

$$\frac{\psi(r,\Theta,t)}{D} = -\frac{As\sin\Theta}{0.525\,v_m} - \frac{Bs\cos\Theta}{0.525\,v_m} + F(s) +$$

$$+ \left[\frac{A}{r_0}\frac{dF}{ds} - \frac{\beta r_0}{s}\int_0^s F(s)\,s\,ds\right] t\cos\Theta -$$

$$- \left[\frac{B}{r_0}\frac{dF}{ds}\, t + 0.525\,\beta v_m G(s)\, t^2\right]\sin\Theta + R \quad (5)$$

where we have made use of (3), $R$ is the residue in the series expansion and

$$G(s) = \frac{s}{4}\int_1^s F_1(s)\,ds - \frac{1}{4s}\int_0^s s^2 F_1(s)\,ds$$

is a function of the non-dimensional variable $s = r/r_0$, in which

$$F_1(s) = -\frac{1}{s}\left(\frac{dF}{ds}\right)^2 + \frac{1}{s^2}\frac{d\nabla^2 F}{ds}\int_0^s sF(s)\,ds$$

Solution (5) has been normalized dividing all the terms by $D$ and using the non-dimensional variable $s = r/r_0$. It contains as parameters the components of the velocity of the uniform flow $A$ and $B$, the variation of the Coriolis parameter $\beta$, and the two vortex parameters: The maximum velocity in the vortex $v_m$ and the radius of the vortex $r_0$. The solution is therefore useful in a study in which any of these five parameters needs to be varied.

Solution (5) has the following physical interpretation:

1) The first three terms represent the initial stream function, namely, a vortex of radius $r_0$ and maximum velocity $v_m$ immersed in a uniform flow, with velocity components $u = -A$ and $v = B$.

2) The terms

$$\left[\frac{A}{r_0}\frac{dF}{ds} - \frac{\beta r_0}{s}\int_0^s F(s)\,s\,ds\right] t\cos\Theta$$

when added to the initial stream function, displace the vortex in the direction parallel to the $x$-axis. They are, therefore, the terms responsible for the east-west component of the displacement of the vortex. The first term represents the steering effect of the zonal component of the uniform flow. The second is due to the effect of the variation of the Coriolis parameter on the vortex. For the purpose of comparing their relative value and determining their contribution in the displacement of the vortex, we multiply both terms by $r_0$. We see then that the first term is proportional to the velocity of the zonal flow ($A$), while the second one is proportional to the square of the radius of the vortex and to the variation of the Coriolis parameter ($\beta r_0^2$).

3) The terms

$$-\left[\frac{B}{r_0}\frac{dF}{ds}\, t + 0.525\,\beta v_m G(s)\, t^2\right]\sin\Theta$$

when added to the initial stream function, displace the vortex in the meridional direction. For the purpose of comparing their relative value we multiply them by $r_0$. The first one is the steering effect of the meridional component of the uniform flow proportional to $B$, while the second one, which is due entirely to the variation of the Coriolis parameter, is proportional to $\beta r_0 v_m$.

Before we carry out the numerical computations we shall prove the following result:

*Within the framework of the barotropic model, if we neglect the variation of the Coriolis parameter, a circular vortex embedded in a uniform flow moves with the velocity of the flow.*

*Proof.* — Neglecting the $\beta$-terms and using

the $x$, $y$ coordinates, solution (5) can be written as

$$\psi^{\star}(x, y, t) = Ay + Bx + F^{\star}(x,y) + \\ + \frac{\partial F^{\star}}{\partial x} At - \frac{\partial F^{\star}}{\partial y} Bt \qquad (6)$$

$$\text{where } \psi^{\star}(x, y, t) \equiv \psi(r, \Theta, t)$$

$$\text{and } F^{\star}(x, y) = DF(s)$$

For small $t$ the last three terms of the second member of (6) are the Taylor's expansion of $F^{\star}(x + At, y - Bt)$, and this function represents a vortex equal to the initial one, but with its center at the point $(-At, Bt)$. Therefore, the vortex moves with the velocity $(-A, B)$ of the uniform flow.

The next step is to establish the importance of the $\beta$-terms in the translation of the vortex. For that purpose we have numerically computed the different terms that enter in solution (5), using the function given in (2), for $\beta = 2.15 \times 10^{-13}$ sec$^{-1}$ cm$^{-1}$ (that corresponds to latitude 20°), for $t = 1$ hour and different values of $A$, $B$, $r_0$ and $v_m$ in the range of those that appear in the case of tropical cyclones. The results of the computations are shown in Table 1 where normalized quantities are shown. To obtain actual quantities we have to multiply all the values by $D$.

**Table 1**

Terms in solution (5) for $\beta = (2.15)\ 10^{-11}$ sec$^{-1}$ m$^{-1}$, $t = 1$ hour, $A = 10$ m/s, $B = 10$ m/s, $v_m = 50$ m/s and different values of $r_0$ in Km.

| 1 | 2 | 3 | 4 | 5 | 6 |
|---|---|---|---|---|---|
| | Cyclone | Uniform flow | $\left\{ \begin{matrix} At \\ Bt \end{matrix} \right\}$ terms | $\beta t$-term | $\beta t^2$-term |
| $s = \frac{r}{r_0}$ | $F(s)$ | $-\frac{s}{0.525\, v_m} \left\{ \begin{matrix} A \sin \Theta \\ B \cos \Theta \end{matrix} \right\}$ | $\frac{1}{r_0} \frac{dF}{ds} \left\{ \begin{matrix} A \cos \Theta \\ B \sin \Theta \end{matrix} \right\} t$ | $-\frac{\beta r_0}{s} \int_0^s F(s) ds \cos \Theta$ | $\beta v_m G(s)\, t^2 \sin \Theta$ |
| | | for $\left\{ \begin{matrix} \sin \Theta \\ \cos \Theta \end{matrix} \right\} = -1$ | for $\left\{ \begin{matrix} \cos \Theta \\ \sin \Theta \end{matrix} \right\} = -1$ | for $\cos \Theta = -1$ | for $\sin \Theta = 1$ |
| | | $v_m = 50$ | $r_0 = 1000$ | $r_0 = 1000$ | $v_m = 50$ |
| 0 | 1 | 0 | 0 | 0 | 0 |
| .2 | .8493 | .0762 | .0510 | .0076 | .0011 |
| .4 | .4974 | .1524 | .0680 | .0114 | .0015 |
| .6 | .1678 | .2290 | .0450 | .0121 | .0009 |
| .8 | .0178 | .3048 | .0100 | .0096 | .0003 |
| 1.0 | 0 | .3800 | 0 | .0082 | 0 |
| | | | $r_0 = 350$ | $r_0 = 350$ | |
| 0 | | | 0 | 0 | |
| .2 | | | .1460 | .0027 | |
| .4 | | | .1940 | .0038 | |
| .6 | | | .1290 | .0044 | |
| .8 | | | .0286 | .0034 | |
| 1.0 | | | 0 | .0029 | |
| | | | $r_0 = 200$ | $r_0 = 200$ | |
| 0 | | | 0 | 0 | |
| .2 | | | .2550 | .0015 | |
| .4 | | | .3400 | .0023 | |
| .6 | | | .2750 | .0024 | |
| .8 | | | .0500 | .0019 | |
| 1.0 | | | 0 | .0016 | |

Comparison of the values of columns 4 and 5 of Table 1 shows that a cyclone of radius $r_0 = 1000$ Km is translated to the west due to the variation of the Coriolis parameter, approximately at the rate of 1.5 m/sec; for $r_0 = 500$ Km at the rate of 0.4 m/sec; for $r_0 = 350$ Km at 0.2 m/sec; and for $r_0 = 200$ Km at 0.1 m/sec. If we consider that the effective radius of our vortex model is practically 0.7 $r_0$, we conclude that in a hurricane of effective radius of 700 Km embedded in an easterly flow of 5 m/sec, the $\beta$-term contributes 23 % of the easterly translation of the hurricane, while for effective radius of 350 Km and 140 Km, its contribution is of 7 % and 4 %, respectively.

The northward translation of the cyclone, due to the variation of the Coriolis parameter that is given in column 6 of Table 1, contains $t^2$ as factor and therefore cannot easily be compared with the translation due to the meridional flow which contains only $t$ as factor.

From the values of column 6 and its comparison with column 4 it is clear that the importance of this term increases when we deal with cyclones with a large radius and strong-wind velocities.

When the meridional component of the flow is zero ($B = 0$) the $\beta t^2$-term is the only one responsible for the northward displacement of tropical cyclones (in the Northern Hemisphere).

Regarding the importance of the $\beta$-terms, it can be stated that while the steering effect due to the uniform flow can reverse the sign or be zero, the northwestward translation due to the $\beta$-terms is always present and, therefore, in the long run contributes a non-negligible part to the displacement of a cyclone.

Besides the $\beta t^2$-term, the computation of $\partial^2\psi/\partial t^2$ yields additional terms in solution (5) of the form

$$\frac{A^2 + B^2}{4\, r_0^2}\, \nabla^2 F(s)\, t^2,$$

$$\frac{1}{4\, r_0^2}\left\{\frac{1}{2}\,(A^2 - B^2)\cos 2\Theta\right\}\left\{\frac{d^2F}{ds^2} - \frac{1}{s}\,\frac{dF}{ds}\right\} t^2,$$

$$\frac{1}{4\, r_0^2}\left\{-\,AB \sin 2\Theta\right\}\left\{\frac{d^2F}{ds^2} - \frac{1}{s}\,\frac{dF}{ds}\right\} t^2$$

and negligible $\beta A \cos 2\Theta$-term, $\beta B \sin 2\Theta$-term and $\beta^2$-terms.

As $A$ or $B$ increase, these terms become of the order of magnitude equal and even greater than the $\beta t^2$-term. This is due to the fact that for large $A$ or $B$ the motion of the vortex depends more on the steering effect of the uniform flow than on the variation of the Coriolis parameter. However, these terms do not contribute to the motion of the cyclone. In fact, the terms that have factors $\cos 2\Theta$ and $\sin 2\Theta$ have the effect of deforming the circular cyclone in an elliptical one, and the terms that depend only on the radius represent a change in the initial axially-symmetric pattern of the cyclone.

As $A$ or $B$ increase, the terms containing these parameters become the dominant ones; however, since the scale of motion decreases when $A$ or $B$ increase, we have to reduce the time step, reducing, hence, the contribution of the $t^2$-terms which become negligible compared with the $At$- and $Bt$-steering terms.

The $t^2$-terms containing $A$ or $B$ can in fact be considered as due to the neglection of the residue in the series expansion, and similar terms should appear in the higher derivatives that cancel out their contribution to the solution.

## REFERENCE

ADEM, J., 1956: A series solution of the barotropic vorticity equation and its application in the study of atmospheric vortices. *Tellus* **8**, pp. 364—372.

# Tropospheric Geopotential and Velocity Variances over the Arctic

By WARREN L. GODSON, Meteorological Service of Canada, Toronto,

and

M. AYLMER MacFARLANE, Arctic Meteorology Research Group, McGill University, Montreal

(Manuscript received January 11, revised version May 20, 1960)

## *Abstract*

As an elaboration of recent studies by BUELL (1954, 1957) and JENKINSON (1956), the relation between the standard deviation of contour height and the vector standard deviation of geostrophic wind velocity is formulated, both for point values (variations in time) and for chart values (variations in space). The relation between wind and contour variances for a simple schematic contour pattern is examined, from the point of view of both space and time statistics.

The relationship between the space variance of contour height ($S^2$) and the space variance of the geostrophic wind ($\sigma^2$) was evaluated over the Arctic (north of about 60° N) at the 500-mb level. A high degree of correlation was found to exist between these two quantities, although the form of the relationship ($\sigma^2$ proportional to $S$) did not agree with the results of previous studies (BUELL, JENKINSON, loc.cit.) of time variances. However, a reanalysis of such data for northern latitudes yielded results virtually identical with those of the present study.

In both cases, the standard error of estimate was too large to enable one to calculate accurately the wind variance from the height variance for synoptic purposes, but the relationships do allow climatological estimates (seasonal, etc.) to be made of the mean kinetic energy and of the size and amplitude of the dominant wave systems.

## 1. Introduction

KLEIN (1951) was one of the first to recognize that there must exist a high correlation between the variability of pressure and the variability of pressure gradient or wind. This correlation has recently been investigated, both theoretically and numerically, by JENKINSON (1956) and by BUELL (1954, 1957). Earlier studies have considered only standard deviations at a point; here we shall treat the problem of variability in space and time, separately and simultaneously, although the tests on actual data to be reported refer specifically to space variability.

## 2. Relations between space and time variances

The statistical measure of variation most commonly employed is the variance, or its square root, the standard deviation. We may discuss variation in time, at a point, variation in space, at a given time, variation in space for time-meaned quantities and variation in time for space-meaned quantities. There are thus four different standard deviations which may usefully be investigated, and we shall here carry out such an analysis, both for the vector standard deviation of geostrophic wind velocity (represented by $\sigma$ with a defining sub-

script) and for the standard deviation of contour height (represented by $S$ with a similar set of subscripts). It will be convenient to use a horizontal bar to denote a time average and square brackets to denote a space average; $u$ and $v$ will denote the $x$- and $y$-components of wind velocity (more strictly, of geostrophic velocity).

Consider first the vector standard deviation of wind velocity for variation in time (at a point), $\sigma_4$.

$$\sigma_4^2 = \sigma_{u_4}^2 + \sigma_{v_4}^2 = \overline{V^2} - V_r^2, \tag{1}$$

where $V_r$ denotes the resultant velocity, the absolute value of the time-mean vector velocity. EADY (1951) pointed out that $\sigma_4^2$ was a quantity of fundamental importance in dynamic climatology, being a measure of the turbulent (large-scale, chiefly) kinetic energy. We shall return to this concept a little later.

Consider now the vector standard deviation of wind velocity for variation in space (at a single time), $\sigma_1$.

$$\sigma_1^2 = \sigma_{u_1}^2 + \sigma_{v_1}^2 = [V^2] - V_s^2, \tag{2}$$

where $V_s$ denotes the space-mean vector wind velocity.

Consider now the vector standard deviation of space-mean wind velocities (in time), $\sigma_2$. For a large area, this will be a relatively small quantity.

$$\sigma_2^2 = \overline{V_s^2} - V_{rs}^2, \tag{3}$$

where $V_{rs}$ denotes a space and time vector-resultant mean wind velocity.

Consider finally the vector standard deviation of time-mean wind velocities (over an area), $\sigma_3$.

$$\sigma_3^2 = [V_r^2] - V_{rs}^2. \tag{4}$$

Taking the space average of (1), and the time average of (2), and introducing (3) and (4), one may express the total variance of vector velocity in the alternate forms

$$[\overline{V^2}] - V_{rs}^2 = \overline{\sigma_1^2} + \sigma_2^2 = \sigma_3^2 + [\sigma_4^2]. \tag{5}$$

$[\overline{V^2}]$ is simply equal to twice the space and time average of the kinetic energy per unit mass. For a temperate-latitude area, the term $V_{rs}^2$ in (5) will make an appreciable contribution, but this will not be so for an area centred at the pole. On individual occasions for such a polar area, $V_s$ would be small for quasi-zonal flow or for a quasi-symmetric cellular pattern; it would have an appreciable value, in fact, only with a pronounced trans-polar circulation.

Exactly analogous relations can be written down for the standard deviations of contour height, here denoted by $S_1$, $S_2$, $S_3$ and $S_4$.

$$\begin{aligned} S_1^2 &= [Z^2] - [Z]^2, \\ S_2^2 &= \overline{[Z]^2} - \overline{[Z]}^2, \\ S_3^2 &= \overline{[Z^2]} - \overline{[Z]}^2, \\ S_4^2 &= \overline{Z^2} - \overline{Z}^2. \end{aligned} \tag{6}$$

Once again the total variance, in both space and time, of contour height is

$$\overline{[Z^2]} - \overline{[Z]}^2 = \overline{S_1^2} + S_2^2 = S_3^2 + [S_4^2]. \tag{7}$$

### 3. Relations between velocity and height variances

Let us consider a cartesian grid, with grid spacings of $\delta x$ and $\delta y$. For the time being, at least, we shall neglect variations over this grid of map magnification and of Coriolis parameter ($f = 2\Omega \sin \Phi$, where $\Omega$ = earth's angular velocity and $\Phi$ = latitude). Let us denote two immediately adjacent grid points by the subscripts $p$ and $q$ (separated by either $\delta x$ or $\delta y$). Let us first analyze the problem treated by JENKINSON (1956) and BUELL (1954, 1957)—that of finding $\sigma_4^2$ in terms of ${S_4}^2$. Making the geostrophic assumption (denoting the ratio $f/g$ by $\lambda$), we obtain from (1) and (6) a relation derived by JENKINSON (1956),

$$\lambda^2 \delta y^2 \sigma_{u_4}^2 = (S_{p_4} S_{q_4})^2 + 2 S_{p_4} S_{q_4} \{1 - r_4(\delta y)\}, \tag{8}$$

where $r_4(\delta y)$ denotes the correlation coefficient between $Z_p$ and $Z_q$ (a time correlation).

In terms of derivatives, the approach adopted by Buell (loc. cit.), (8) is equivalent to

$$\lambda^2 \sigma_{u_4}^2 = \left(\frac{\partial S_4}{\partial y}\right)^2 - S_4^2 \left[\frac{\partial^2}{\partial y^2} r_4(y)\right]_{y=0}, \tag{9}$$

where we have invoked l'Hospital's Rule for the final term.

Differentiation of the final set of (6) with respect to $\gamma$ and substitution into (9) give the relation

$$\lambda^2 \sigma_{u_4}^2 = - S_4^2 \frac{\left[\frac{\partial^2}{\partial \gamma^2} r_4(\gamma)\right]_{\gamma=0}}{\{1 - R_4^2(Z, u)\}}, \qquad (10)$$

where $R_4$ $(Z, u)$ indicates the correlation coefficient (in time, at a point) between contour height and the $x$-component of the velocity.

An analogous relation can be derived for $\sigma_{v_4}^2$, which, in combination with (10), gives

$$\lambda^2 \sigma_4^2 = \\ = - S_4^2 \left( \frac{\left[\frac{\partial^2}{\partial x^2} r_4(x)\right]_{x=0}}{\{1 - R_4^2(Z, v)\}} + \frac{\left[\frac{\partial^2}{\partial \gamma^2} r_4(\gamma)\right]_{\gamma=0}}{\{1 - R_4^2(Z, u)\}} \right). \qquad (11)$$

According to JENKINSON (1956), the coefficient of $S_4^2$ in (11) is approximately a universal constant in space and time, throughout the troposphere. Without necessarily accepting this view (which we shall later show to be of dubious validity), we may write (11) in the form

$$\sigma_4^2 = \frac{k_4^2 S_4^2}{\sin^2 \phi}. \qquad (12)$$

Computations by BUELL (1954) of $k_4^2$ (see his figures 7, 8 and 9) indicate systematic geographical variations of this quantity, quite marked in polar areas, but rather less variation between troposphere and stratosphere than claimed by JENKINSON (1956).

The relation between $\sigma_1^2$ and $S_1^2$ (areal variances) can be found by carrying out the above analysis with space means rather than time means. Assuming that $\sin \phi$ has a small range or is only weakly correlated with $S_1$ or $\sigma_1$, one obtains

$$[\lambda^2] \sigma_1^2 = \\ = - S_1^2 \left( \frac{\left[\frac{\partial^2}{\partial x^2} r_1(x)\right]_{x=0}}{\{1 - R_1^2(Z, v)\}} + \frac{\left[\frac{\partial^2}{\partial \gamma^2} r_1(\gamma)\right]_{\gamma=0}}{\{1 - R_1^2(Z, u)\}} \right), \qquad (13)$$

where the subscript 1 indicates a correlation over space, rather than in time. Without implying a constancy for the ratio of variances, let us set

$$\sigma_1^2 = \frac{k_1^2 S_1^2}{[\sin^2 \phi]}. \qquad (14)$$

If $k_4$ were invariant in space and time, then one would expect $k_1$ to have similar properties (and a similar value). The explicit formulations of $k_4$ and $k_1$ (see (11) and (13)) do not in themselves lend much support to such beliefs, nor do they indicate what would be the implications of such a quasi-constancy if real. Accordingly, it was decided to investigate a very simple contour model, to provide a useful basis for the discussion of various sets of experimental data.

## 4. Variance relations for a simple contour pattern

Let us now evaluate $k_1^2$ for a simple cellular type of contour pattern, defined by

$$Z = A \sin \mu x + B \sin \nu y + C, \qquad (15)$$

where $\mu = 2\pi/L_x$ and $\nu = 2\pi/L_y$. $L_x$ and $L_y$ are wavelengths, and $A$ and $B$ amplitudes, in the $x$- and $y$-directions, respectively. For simplicity we shall imagine that a given map contains an integral number of waves (or cellular systems) in both coordinate directions so that it is adequate to average any parameters required over one wavelength in each direction.

For this contour pattern,

$$S_1^2 = (A^2 + B^2)/2, \qquad (16)$$

$$[\sin^2 \phi] \sigma_1^2 = \frac{g^2 \pi^2}{2\Omega^2} \left( \frac{A^2}{L_x^2} + \frac{B^2}{L_y^2} \right). \qquad (17)$$

From (14), (16) and (17),

$$k_1^2 = \frac{g^2 \pi^2}{\Omega^2 (A^2 + B^2)} \left( \frac{A^2}{L_x^2} + \frac{B^2}{L_y^2} \right). \qquad (18)$$

In the case that $L_x = L_y = L$,

$$k_1^2 = \frac{g^2 \pi^2}{\Omega^2 L^2}. \qquad (19)$$

If $L_x \neq L_y$, we may define $L$ as the effective or weighted wavelength by the above relation. This effective wavelength, $L$, is closely related to the "radius" of contour systems, $R_h$, intro-

duced by BUELL (1954, 1957) through the extrapolation of $\partial^2 r(x)/\partial x^2$ to a zero correlation at the rate observed at $x = 0$. It may be shown, in fact, that

$$L = \pi R_h = 2\pi/m, \tag{20}$$

where $m$ is the characteristic "wave number" utilized by THOMPSON (1957) in his interpretation of the meaning of the quasi-constant $k_4$ deduced by JENKINSON (1956). Incidently, with the particular contour system envisaged here, the correlation would actually drop to zero at a distance $L/4$. Thus, from (19) and (20),

$$k_1 = \frac{g\pi}{\Omega L} = \frac{g}{\Omega R_h} = \frac{gm}{2\Omega}. \tag{21}$$

In order to compute variances applicable to a point (time variances), one may assume a fixed speed and direction for contour system motion. It then follows directly that (16) applies equally well to $S_4^2$, (17) to $\sigma_4^2$ and (18) and (19) to $k_4^2$. Thus, for a reasonably homogeneous area for which space and time sampling are essentially equivalent, the two sets of statistical variance parameters should be numerically very similar. Contour-height variance, from (16), will be a direct measure of the root-mean-square "system amplitude", and the variance ratio, $k$, from (19), will be a direct measure of the effective "system wavelength".

It can be seen from (19) that $k$ would be approximately constant from one map to another ($k_1$) or from one point to another ($k_4$) only if the effective wavelength remained the same, regardless of amplitude (i. e., intensity) changes. Thus, one might expect rather similar ranges of $k$ from one season to the next in regions where the "size" of contour systems does not vary greatly from one season to another. Within any given season, it would be unreasonable to expect the effective wavelength to remain constant. In fact, one should expect a tendency for amplitude to increase as wavelength increases, leading to a more rapid increase of the intensity (and hence variability) of the contour-system than of the wind regime. In such a case, $k$ would decrease as $S$ increases.

One may adduce evidence for this latter belief from the quasiisotropic nature of wind-component variance, first demonstrated by Brooks et al. (1950) for variances in time, at a point. For the schematic contour model represented by (15), $\sigma_{u_1} = \sigma_{v_1}$ implies that $Bv = A\mu$, or that $B/L_y = A/L_x$. The empirical evidence for isotropic wind behaviour implies that the ratio of amplitude to wavelength in the two component directions tends to remain constant and thus one would expect that readjustment of wavelength to amplitude changes (or vice versa) should be such that the ratio itself would not change greatly. Undoubtedly, the actual variation of $\sigma_1$ with $S_1$, from day to day (or of $\sigma_4$ with $S_4$ from point to point), is rather complex so that it would not be fruitful to examine more realistic contour models. Instead, one should carry out analyses on the actual atmosphere, and results of such analyses will be presented in the next two sections.

## 5. Experimental testing of variance relations

From the considerations of the previous section it appeared likely that the height variance (in space) of a pressure surface and the geostrophic wind variance would be significantly correlated but that the regression coefficient for a simple linear regression would not prove to be a universal constant. Although the concept is quite general (i.e., holds wherever the geostrophic assumption is valid), it was tested in the Arctic at 500 mb because the basic data were already available from a previous study.

The experiment consisted simply of computing the height and geostrophic wind variances for a number of sample days, and of determining the nature of their correspondence and the accuracy with which the wind variance could be estimated from the variance of height. A detailed account of the testing procedures, with data tabulations, has appeared elsewhere (GODSON and MACFARLANE, 1958). It should be noted that a close relationship would imply that the space-mean kinetic energy could also be estimated from contour-height variance (which latter parameter could then function as a highly efficient and readily calculable circulation index), since, from (2) and (14),

$$[V^2] = V_s^2 + \frac{k_1^2 S_1^2}{[\sin^2 \phi]}. \tag{22}$$

The source of data for this experiment was the 500-mb (0300 GMT) synoptic charts for

1955 drawn by the Department of Transport Arctic Forecast Team at Edmonton. In connection with another project (HARE, GODSON et al. 1957), arrays of contour height had been abstracted from these maps on a $13 \times 13$ point grid extending from the pole to 60° N (on the average). The values of $S_1$ for these arrays had also been calculated and only $\sigma_1$ had to be computed. To satisfy the differential relations of (13), $[\sin \phi]\sigma_1$ was formed for grid sizes of $\delta$, $\sqrt{2}\delta$ and $2\delta$ ($\delta x = \delta y = \delta$), and then extrapolated analytically to a zero grid size.

The sample used in this study consisted of sixty days chosen to include all the seasons and the complete range of $S_1$. Because of the deliberate inclusion in the sample of the extreme values of $S_1$, a weighting factor had to be introduced so that the frequency distribution simulated the actual distribution of $S_1$ for 1955.

Scatter diagrams were made showing the relation between $[\sin \phi]\sigma_1$ and $S_1$, and between $k_1$ and $S_1$. Neither plot appeared to represent a linear correlation, but before attempting to fit a non-linear regression equation the data were converted to natural logarithms as it was thought most probable that the errors in computing $S_1$ and $[\sin \phi]\,\sigma_1$ were proportional to their magnitudes.

The new scatter diagram of the converted standard deviations (fig. 1) seemed to indicate a linear relationship between the two quantities and a straight line was fitted to the data, of the form

$$\ln [\sin \phi]\sigma_1 = a + b \ln S_1. \qquad (23)$$

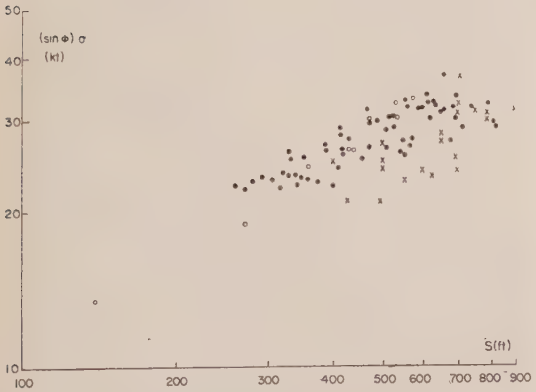


Fig. 1. Relation between contour-height standard deviation ($S$) and vector wind standard deviation ($\sigma$) at 500 mb at high latitudes (on logarithmic scales): closed circles—this study, open circles—JENKINSON (1956) and crosses—BUELL (1957).

Then, from (14),

$$k_1 = e^a S_1^{b-1}. \qquad (24)$$

The statistical parameters pertaining to the regression equation (23) are shown in Table 1.

**Table 1. The linear regression of ln $[\sin \phi]\sigma_1$ on ln $S_1$**

| Statistic | | Sample Value | 5% Confidence Limits | |
|---|---|---|---|---|
| | | | Lower | Upper |
| Regression Coefficient | $b$ | 0.403 | 0.306 | 0.500 |
| Regression Intercept | $a$ | 1.768 | 1.394 | 2.141 |
| Correlation Coefficient | $r$ | 0.736 | 0.590 | 0.836 |

Thus, from (24)

$$k_1 = 5.860\ S_1^{-0.597}. \qquad (25)$$

These results differ markedly from those of the previous studies (Buell and Jenkinson, loc. cit.) in which $b$ was assumed equal to unity (so that $k_4$ became a constant). Jenkinson computed $k_4$ directly from eq. (12), whereas Buell computed both his regression coefficient and intercept but found that the latter was approximately zero. Because of the apparent discrepancies between the results, it seemed desirable to combine and reanalyse the data that Buell and Jenkinson had presented in their papers.

## 6. Comparison of space and time variances

As it was felt that any valid comparison of these space and time statistics should be made with overlapping data, only the values of $\sigma_4$ and $S_4$ at 500 mb and from the northern stations ($\phi \geq 45°$) were used. The analysis described in section 5 was repeated and the results are given in Table 2 (see figure 1 for data points).

**Table 2. The linear regression of ln $(\sin \phi)\sigma_4$ on ln $S_4$**

| Statistic | | Sample Value | 5% Confidence Limits | |
|---|---|---|---|---|
| | | | Lower | Upper |
| Regression Coefficient | $b$ | 0.426 | 0.300 | 0.533 |
| Regression Intercept | $a$ | 1.580 | 1.078 | 2.081 |
| Correlation Coefficient | $r$ | 0.788 | 0.578 | 0.895 |

From (24)

$$k_4 = 4.853 \; S_4^{-0.574}. \qquad (26)$$

The confidence limits are somewhat wider than before (smaller sample) but otherwise these values are similar to those obtained from the space variances (see Table 1).

Although the high correlation between the space variance of contour height and the space variance of the geostrophic wind is the first conclusion of this study, it is not an unexpected one in the light of the underlying theory and the results obtained by Buell and Jenkinson; on the other hand, the most interesting result is the nature of the relationship between these two quantities.

The general form of the dependence of wind variance on contour height variance can be expressed as

$$\sigma \alpha S^b, \; 0.3 \leq b \leq 0.5, \qquad (27)$$

which is applicable to either the space or time values. At least a superficial explanation of this proportionality can be made on the basis of the contour model discussed in section 4. That is, those pressure patterns in which there is a pronounced coupling of the wave amplitude with the wavelength dominate over the patterns of variable amplitude but more or less constant wavelength. This coupling would most probably occur in long-wave patterns, such as those of the circumpolar westerlies, rather than in short-wave disturbances which are more likely to be of roughly uniform size though of widely varying intensity.

Moreover, it appears from the similarity of (25) and (26) that the space and time statistics are both sampling the same information, and the form of (27) suggests that this information is concerned with the largest features of the pressure patterns. Although this conclusion ($k_1 = k_4$) had appeared plausible, the empirical evidence seemed to be against it until the time statistics were reanalysed.

Naturally, even in a region of long-wave disturbances, the ratio of amplitude to wavelength would not be constant from day to day or from place to place; hence the considerable scatter of points in figure 1 is only to be expected. That the standard error of estimate of $\sigma_4$ is noticeably larger than that of $\sigma_1$ is probably due, in part at least, to the location of the samples. The space grid is embedded at the centre of the circumpolar vortex, which is made up of a core of small cellular disturbances surrounded by long-wave patterns; hence the values of $S_1$, $\sigma_1$ and $k_1$ probably represent some sort of weighted average of the values that would have been obtained by sampling the two regimes separately. This might tend to damp down the range of residuals about the regression line. As opposed to this, regional differences would be emphasized by point sampling in time. Buell (1954) has shown that in fact there are considerable variations in the size of pressure systems from one area to another. Thus the time sample used here is somewhat unsatisfactory because the stations not only tend to be near centres of action but they do not sample more than the fringe of the space grid (Godson and MacFarlane, 1958, fig. 10).

In the face of these possible sources of difference it is encouraging to find that there is no significant difference between the relationships in space and time of the standard deviations of height with the standard deviations of wind. This has a bearing on the remark by Buell (1957) that the statistical theory of turbulence (Batchelor, 1953) leads to the relation: $\sigma^2 \alpha S$. Since homogeneous turbulence, by definition, is such that space and time sampling give identical results, one might think it possible to consider the large scale features of the 500-mb circulation as being two-dimensionally isotropic homogeneous turbulence. However, it is pertinent to note that the isotropic turbulence prediction ($\sigma^2 \alpha S$) is formulated for a system in which Coriolis forces can be ignored. This is clearly not true in the present case, so that the apparent agreement between the $\sigma$—$S$ relations in the two cases should be regarded as largely accidental.

Equations (25) and (26) are of considerable climatological value. From these relations it is possible to obtain estimates, albeit crude, of the standard vector deviation of the wind, the mean kinetic energy and the r.m.s. amplitude and effective wavelength of dominant pressure systems, all from an easily obtained parameter—the variance of contour height. For not only can $S_1$ be readily computed from constant pressure charts, but it is a standard parameter developed in all types of numerical specification techniques.

In the year 1955 (using theWadsworth specification data described in section 5) the annual mean value of $S_1$ (i.e., the r.m.s. amplitude from (16)) was almost 500 ft., representing a mean radius of some 750 n. miles (12½° of latitude). This corresponds well with the mean size of Arctic pressure systems obtained by direct measurement from 500-mb charts.

**Acknowledgement**

The research reported in this document has been sponsored in part by the Geophysics Research Directorate of the Air Force Cambridge Research Center, Air Research and Development Command, under Contract No. AF 19 (604)-1141. Participation by Dr. W. L. Godson in this research is with the permission of the Director, Meteorological Branch, Department of Transport, Canada.

The authors wish to acknowledge the interest and encouragement provided by Prof. F. Kenneth Hare, Project Director, Arctic Meteorology Research Group, McGill University.

## REFERENCES

Batchelor, G. K., 1953: *The Theory of Homogeneous Turbulence.* Cambridge University Press, 197 pp.

Brooks, C. E. P., et al., 1950: Upper winds over the world. *Geophys. Mem.*, London, No. **85**, 105 pp.

Buell, C. E., 1954: Some relations among atmospheric statistics. *J. Meteor.*, **11**, pp. 238—244.

Buell, C. E., 1957: An approximate relation between the variability of wind and the variability of pressure or height in the atmosphere. *Bull. Am. Meteor. Soc.*, **38**, pp. 47—51.

Eady, E. T., 1951: Upper winds over the world (a review of). *Quart. J. Roy. Meteor. Soc.*, **77**, pp. 145—146.

Godson, W. L., MacFarlane, M. A., 1958: Pressure-contour variance and kinetic energy over the Arctic. *Sci. Report No. 5*, Contract AF 19 (604)-1141, Arctic Meteorology Research Group, McGill University, Montreal.

Hare, F. K., Godson, W. L., MacFarlane, M. A., Wilson, C. V., 1957: Specification of pressure fields and flow patterns in polar regions. *Sci. Report No. 3*, Contract AF-19 (604)-1141, Arctic Meteorology Research Group, McGill University, Montreal.

Jenkinson, A. F., 1956: The relation between standard deviation of contour height and standard vector deviation of wind. *Quart. J. Roy. Meteor. Soc.*, **82**, pp. 198—208.

Klein, W. H., 1951: A hemispheric study of daily pressure variability at sea level and aloft. *J. Meteor.*, **8**, pp. 332—346.

Thompson, P. D., 1957: The relation between standard deviation of contour height and standard vector deviation of wind. *Quart. J. Roy. Meteor. Soc.*, **83**, pp. 553—554.

# Midwinter Ozone Variations and Stratospheric Flow over Canada, 1958—1959

By K. ALLINGTON, B. W. BOVILLE and F. K. HARE
McGill University

(Manuscript received December 9, 1959)

*Abstract*

The total ozone variations at Edmonton and Moosonee during December, 1958 and January, 1959 are examined in relation to daily synoptic analysis up to the 25-mb level. The stratospheric perturbations of the polar-night westerlies appear to dominate the ozone record when that régime is over the station. Otherwise, the usual Normand tropospheric perturbation effect is indicated. Correspondence is analyzed using adiabatic vertical motions computed at the 200, 100 and 25-mb levels, in addition to the 200-mb geopotential height and the 100—25-mb thickness.

## 1. Introduction

The work of Sir CHARLES NORMAND (1953) and others has shown that daily ozone variations are related to the perturbed circulation of the upper troposphere. Negative correlations have been obtained between total ozone and 300-mb geopotentials, implying that ozone is more abundant over troughs than over ridges. Since these correlations were mostly established in northern Europe, one can safely assume that these troughs and ridges are parts of the travelling wave-trains of the circumpolar westerly vortex. It is known, furthermore, that the 300-mb waves extend without significant change of phase to 100 mb or above, i.e., into the lower stratosphere. Above the tropopause, the westerlies descend into troughs and climb on to ridges. Theoretical demonstrations by REED (1950), GODSON (1959), and others have shown that subsidence in the stratosphere must contribute to increases in total ozone, as long as ozone mixing ratio increases with height; similarly uplift decreases the total ozone. The Normand effect—high ozone in troughs, low in ridges—is hence qualitatively consistent with theory.

Quantitatively, however, the picture is less satisfactory, since the amplitude of the ozone variations considerably exceeds expectation. Moreover there are periods, especially in winter, when the Normand effect seems to vanish; even at their best, the computed correlations rarely explain more than 25 to 35 per cent of the ozone variance. No doubt advection complicates the effects of vertical motion, but it can hardly account for the width of the disparity. Hence it is obvious that other causes of ozone variation exist.

The present writers suggest that much of the remaining variance of total ozone is due to vertical motion in the newly-discovered baroclinic waves of the polar-night westerly vortex (HARE, 1960; GODSON and LEE, 1958). This vortex affects the layers from 150 mb to above 25 mb. It develops in high latitudes in the darkness of midwinter—hence the term

*polar-night vortex* introduced by KOCHANSKI (1955)—and sometimes extends below the U.S.-Canadian border for a few weeks before collapsing in the spectacular sudden-warmings well-known from the work of SCHERHAG (1952), CRAIG and HERING (1959), TEWELES (1958) and others. Since vertical motion of the order of 2 to 3 cm $sec^{-1}$ over long trajectories occurs within the wave-perturbations of this vortex, it seems reasonable to expect that ozone variations should occur in response to it.

To subject this idea to a preliminary test, the time-series of total ozone at Edmonton, Alberta, and Moosonee, Ontario, were examined alongside synoptic charts and cross-sections for the stratosphere over North America. Because of the large amount of work involved, the study was restricted to the months of December, 1958 and January, 1959. Both ozone stations were far enough north to be affected by the polar-night vortex, but had enough daylight even in midwinter for continuous ozone determination. The results are suggestive, but far from conclusive. They do, however, show that the middle stratospheric temperature field and total ozone are closely related.

## 2. The data employed

The daily ozone values used in this study were obtained by Dobson spectrophotometers maintained by the Canadian Meteorological Service during the I.G.Y. period at Edmonton and Moosonee. Values are in cm of $O_3$ at S.T.P. and it is estimated that the standard error of the measured 24-hour change in total ozone is about 0.010 cm. All temperature values were derived from radiosonde ascents for 0000 hrs G.C.T., with interpolated values from synoptic charts where necessary.

The synoptic charts and cross-section were drawn at the Central Analysis Office, Canadian Meteorological Service, by the Arctic Meteorology Research Group, McGill University, as part of a routine analytical project. The area of analysis at 200 mb was circumpolar, north of 35° N. The 100-mb maps were analyzed over North America, the Atlantic and Europe, also north of 35° N. At 25 mb daily analysis was carried out over North America, every fifth day's map being extended to a circumpolar area by suitable extrapolation techniques. The values of vertical motion (in cm $sec^{-1}$) were computed from charts at the 200, 100 and 25-mb levels by the adiabatic trajectory method. The values plotted are those for the 24-hour trajectory centered on 0000 hrs G.C.T. for the specified date. In view of the errors in the original contour analysis, and the length of trajectory involved, these values can be taken only as crude estimates of the order of magnitude and sign of the vertical motion.

## 3. Results

Fig. 1 presents time cross-sections for December, 1958, at Edmonton and Moosonee. Fig. 2 gives similar diagrams for January, 1959 at the same stations. The upper section in each diagram gives total ozone (cm at S.T.P.) and the thickness of the 25 to 100-mb layer in geopotential meters. The central section gives vertical motion in cm $sec^{-1}$, subsidence being considered negative; the negative periods

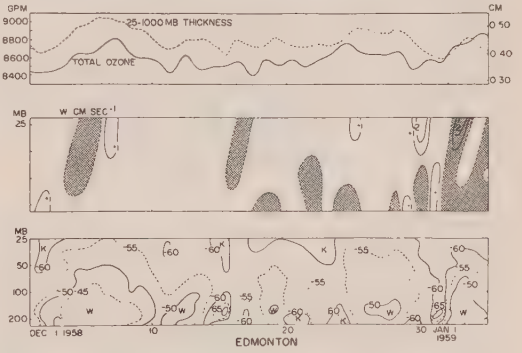


Fig. 1 a.

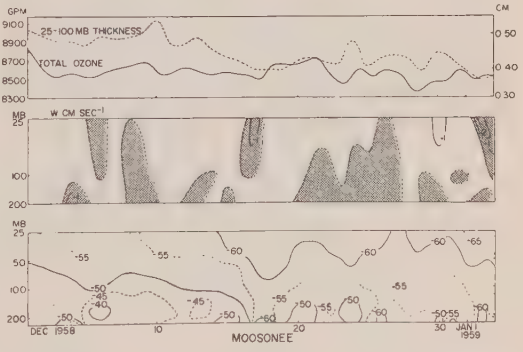


Fig. 1 b.

Fig. 1. Time sections of— observed 25—100 mb thickness and total ozone; 24-hour average adiabatic vertical motion (w), subsidence areas stippled; observed temperature (°C), warm areas (W), and cold areas (K).

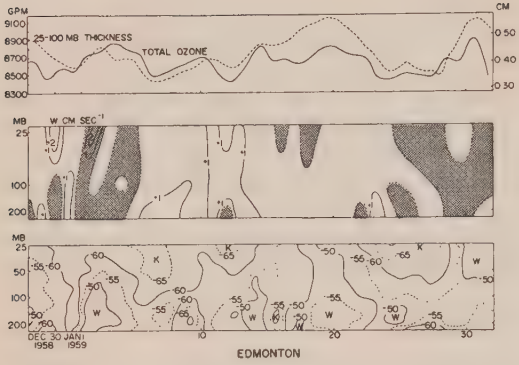


Fig. 2a.

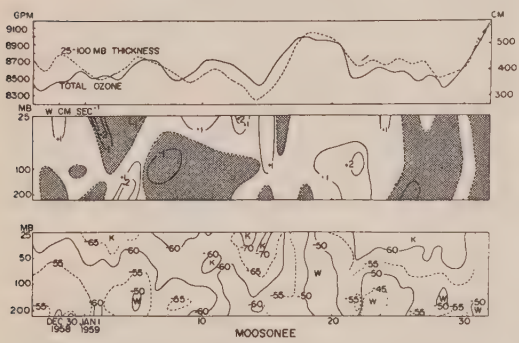


Fig. 2b.

Fig. 2. Similar to Fig. 1.

are stippled for convenient inspection. The bottom sections give temperatures in deg. Celsius.

The vertical motion values vary between 24-hour averages of above $+2$ cm sec$^{-1}$ and below $-2$ cm sec$^{-1}$. Over trajectories of this duration, an average of $\pm 2$ cm sec$^{-1}$ is equivalent to a vertical displacement of 1.7 km. Hence uplift and subsidence at rates of 1—2 km in 24 hours must be assumed typical of the stronger stratospheric disturbances over these stations. It is obvious from the diagrams that the vertical motion systems fall mainly into two suites—those centered at or above 25 mb (arising from perturbations in the polar-night vortex) and those centered at or below 200 mb. The latter are, of course, associated with the familiar travelling waves in the tropospheric westerlies. The 100-mb level has a minimum of vertical motion. Only during two short periods at Moosonee do systems appear centered at 100 mb. It is noteworthy that the time-average of vertical motion at Edmonton is clearly positive at all levels.

The temperature fields show a similar division. At 200 mb there is a very high variability due to the lower suite of vertical motion systems, as well as longer-period spells of warmth (e.g., December 1—13 at Edmonton). All these thermal systems diminish rapidly with height, few of them being visually identifiable above 50 mb. The upper part of each section shows the much longer-period fluctuations typical of middle stratospheric waves (Hare, 1960).

The 25 to 100-mb thickness curves naturally reflect the vertically integrated thermal field of the middle stratosphere, and hence show predominantly long-period variations. At both stations the largest fluctuations occur in early December and again in January. It is obvious at a glance that the total ozone curve is closely related to these thermal curves, more especially at Moosonee. The closeness of correlation is reduced by variable phase-lags in the major oscillations, but it is quite clear that each warm phase is ozone-rich, each colder period ozone-poor. Table I gives linear correlation coefficients between total ozone and (a) 25 to 100-mb thickness and (b) 200-mb geopotential height for both stations in both months. As an additional indicator of the processes at

**Table 1. Linear correlation coefficients between total ozone ($O_3$), 25 to 100-mb thickness ($\Delta Z$), and 200-mb geopotentials ($Z_{200}$), Edmonton & Moosonee**

| Line | Variates | Edmonton | | Moosonee | |
|---|---|---|---|---|---|
| | | Dec. | Jan. | Dec. | Jan. |
| (a) | $O_3$, $\Delta Z$ | +0.73 | +0.65 | +0.25[2] | +0.65 |
| (b) | $O_3$, $Z_{200}$ | −0.55 | −0.23[2] | −0.53 | −0.46 |
| (c) | $Z_{200}$, $\Delta Z$ | −0.55 | +0.28[1] | +0.16[2] | −0.64 |

[1] Significant at 5 % level. Remainder significant at 1 % level.
[2] Not significant at 5 % level.

work, line (c) give the correlation between 25 to 100-mb thickness and 200-mb geopotential height.

Table 1 shows that total ozone and the temperature of the 25 to 100-mb layer marched together except in December over Moosonee, when the correlation fell to an insignificant value, while retaining its positive sign. Reductions of variance for the other months ranged from 42 to 53 per cent. It has already been suggested that part of the unexplained variance arose from unsystematic phase lags, and that the resemblance between the two curves was closer than these reductions may suggest. The $O_3$ versus $Z_{200}$ correlations, which correspond closely to those of Normand, were all negative, and were smaller. It is of interest that the cross-correlation of $Z_{200}$ versus $\Delta Z$ gave very erratic results. At Edmonton in January, however, significant correlation between $O_3$ and $\Delta Z$ existed in the absence of both the Normand effect and a significant correlation between $Z_{200}$ and $\Delta Z$.

## 4. Interpretation

An attempt will now be made to interpret these results in the light of the stratospheric circulation during these months. A summary of that circulation has been given elsewhere by HARE (1960). It was there shown that the principal developments were as follows:—

(i) *From December 1—11, 1958*, a warm stratospheric ridge lay over Alaska and arctic Canada, with a closed anticyclone at 25 mb. This ridge drifted slowly southeastward. Fig. 1 shows the deep warm layer at Edmonton associated with this system. Moosonee lay throughout the period along the southern margin of the ridge, experiencing a slight warming on December 10.

(ii) *On December 11—15*, a drastic cooling of the middle stratosphere occurred over the arctic coast, as the polar-night vortex moved across the pole towards North America. The leading baroclinic trough reached western Alaska on December 11, reaching Edmonton on December 15 and Moosonee on December 18. *Thereafter for the remainder of the midwinter* the polar-night vortex dominated all Canada. The polar-night jet lay on the average across northern Alaska, dipping southward to about 65° N in the quasi-permanent east Canadian trough. Fig. 3 presents circumpolar 500-mb and 25-mb charts for December 29, 1958, showing the two circumpolar vortices, that of the troposphere having maximum winds

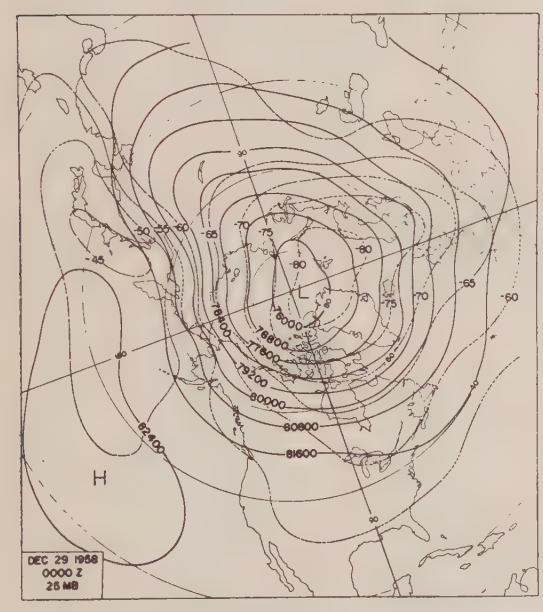


Fig. 3 a.

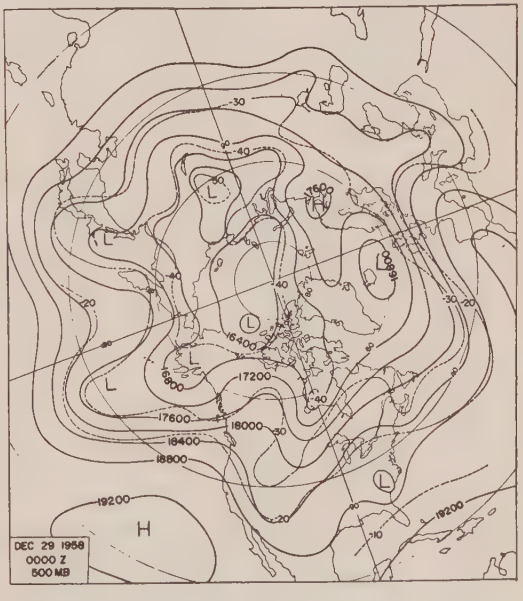


Fig. 3 b.

Fig. 3. Constant pressure charts. Solid lines—contours (gp ft) Dashed lines—isotherms (° C)

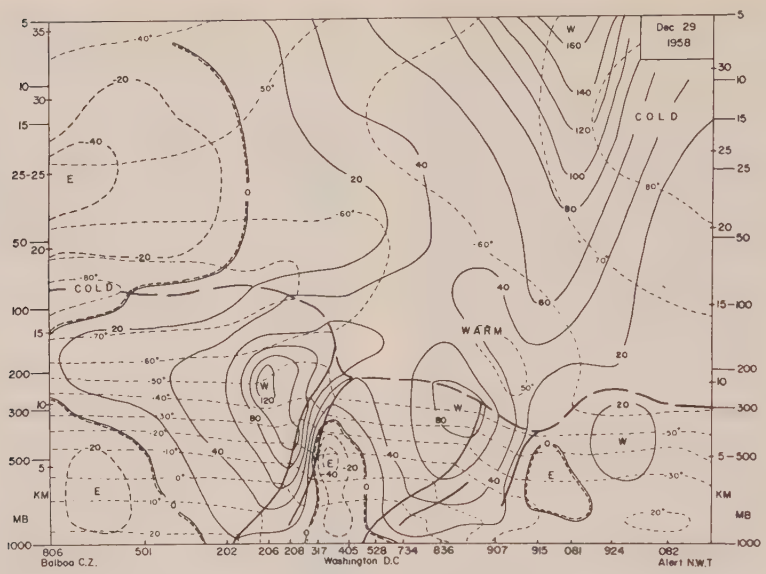


Fig. 4. 80° W cross-section for December 29th, 1958. Thick lines—fronts, tropopause. Thin dashed lines—isotherms (° C). Medium solid and dashed lines—zonal isotachs (kts)

in latitudes 35°—50° N. The essential separateness of the two vortices, stressed previously by HARE (1960), shows up in the cross-section along 80° W for December 29 (Fig. 4).

(iii) *From December 15 until January 30*, a series of baroclinic waves in the polar-night westerlies moved east across Canada, with a consistent phase velocity of about 11° longitude per day. For the sake of easy identification, these waves have been arbitrarily numbered. Table 2 gives their dates of passage at Edmonton and Moosonee. As Figs. 1—2 show, these waves were clearly marked in the thickness and temperature records, but no simple association with vertical motion was shown. The scale of these features is indicated by Fig. 5, which shows troughs IV and V.

The Edmonton ozone curve will now be examined in the light of this history. The warm, anticyclonic phase of December 1—10

**Table 2. Baroclinic waves in middle stratosphere December 15—January 30, 1958—59**

| Perturbation | Date past Edmonton | Date past Moosonee |
|---|---|---|
| Trough I | December 15 | December 18 |
| Ridge I (insignificant) | — | — |
| Trough II | December 22 | December 25 (weak) |
| Ridge II | December 27 | December 30 (weak) |
| Trough III | December 30 | January 2 |
| Ridge III | January 2 | January 5 |
| Trough IV | January 6 | January 9 (weak) |
| Ridge IV (insignificant) | — | January 11 (weak) |
| Trough V | January 12 | January 15 |
| Ridge V | January 18 | January 19[1] |
| Trough VI | January 24 | January 23[1] |
| Ridge VI (insignificant) | — | — |
| Trough VII | January 27 | January 30 |
| Ridge VII | January 30 | January 31[2] |

[1] Waves moving from NNW, with marked tilt.
[2] Sudden warming effect, with collapse of trough VII east of Hudson's Bay.

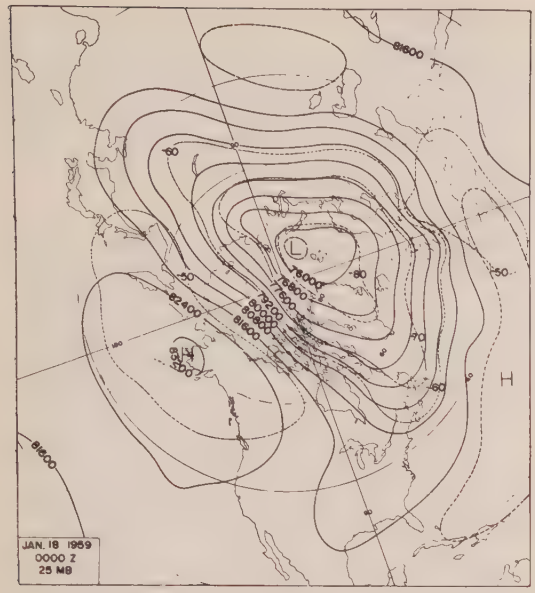


Fig. 5. Similar to Fig. 3.

had high ozone, with the $\Delta Z$ and $O_3$ curves behaving alike. Troughs I and II were of small amplitude, and had no discernible effect on ozone. Hence December 11—22 was a period when ozone variations were of small amplitude, and were probably governed by the motion of tropospheric waves; the effects of these waves on the 200-mb temperature field is well shown in Fig. 1. Ridge II, well-developed over western Canada, produced a warm stratosphere and high ozone, the ozone rise preceding the thickness rise by two days. No subsidence could be detected except at 200 mb on December 24, feeble uplift being typical of the period. Trough III amplified vigorously near Edmonton, with 24-hour ascent of 2 cm $sec^{-1}$ at 25 mb. The uplift was, however, offset by subsidence at 200 mb; ozone amounts rose slightly.

In January, Edmonton's record is unmistakably dominated by the middle stratospheric waves. At these levels troughs are cold, ridges warm; hence the ridges show up in Fig. 2 as maxima of $\Delta Z$, and troughs as minima. It is quite obvious that the $O_3$ curve behaves in a closely similar fashion, though, as the +0.65 correlation coefficient shows, there are phase-lags and marked differences in relative amplitude. The Normand effect is largely suppressed, even though the lower stratospheric temperature field shows that tropospheric waves were active for much of the month.

At Moosonee, it will be recalled (Table I) that December produced only a small correlation between $O_3$ and $\Delta Z$. As Fig. 1 shows, until December 17 (when the polar-night westerlies invaded the area) ozone hardly varied. Thereafter the $O_3$ and $\Delta Z$ curves are similar, but with marked phase-lags. A significant, though small, negative correlation between $O_3$ and $Z_{200}$ shows that the Normand effect was at work, in spite of the fact that the tropospheric westerlies lay well to the south for much of the month. In January, however, the middle stratospheric systems increased in amplitude, and as at Edmonton, dominated the ozone variation. The parallelism of the $O_3$ and $\Delta Z$ curves is very striking. Ridges III and IV produced small ozone peaks, but the much more profound ridging of January 23—24 produced a 50 per cent increase in ozone in 48 hours. Even more striking was the ozone increase—almost a doubling—between January 29 and February 1, associated with the sudden warming that followed the collapse over eastern Canada of trough VII. It is noteworthy that $\Delta Z$ and $Z_{200}$ were significantly correlated in January, with a negative sign. This may account for the persistence of a small negative correlation between $O_3$ and $Z_{200}$, in spite of the displacement of the tropospheric westerlies far south of Moosonee.

If one compares the Edmonton and Moosonee January records, it is apparent that the ozone "waves" stayed roughly in phase with the thermal waves, and that these in turn remained in phase with those of the motion field (as, of course, hydrostatic considerations require). Throughout the month the stream velocity of the polar-night circulation was much stronger than the phase-velocity of the waves. Hence the wind blew through the isotherms of the thermal field, which was advected by the phase velocity of the baroclinic waves. It follows that in the middle stratospheric waves, the wind also blew through the ozone maxima and minima, since these remained in phase with the thermal systems.

Little has been said about the computed values of vertical motion. Since they were computed by an approximate method from

very long trajectories, it is perhaps too much to expect that they will show any very close correlation with ozone variation; moreover, it is at present quite impossible to estimate the stream-advection of ozone, which obviously obscures the vertical motion effect. It is of some interest, however, to take the computed values and assess the order of magnitude of the ozone changes they might be expected to produce. Daily observations of the vertical ozone profile were unavailable, but a representative profile for winter at Edmonton was supplied by Dr. W. L. Godson, Meteorological Branch, Canadian Department of Transport. The original profile (derived from Umkehr determinations) was expressed in cm of $O_3$ at S.T.P. per 6 km layer. These values were converted into units of microns ($10^{-4}$ cm) of $O_3$ per millibar layer—i.e., mixing ratio. These values were then plotted as a linear function of pressure to give an equal-area transformation of ozone change for given vertical displacements of the curve. The slope of the ozone mixing ratio curve was found to be as follows:—

| Pressure Surface | Slope of $O_3$ Profile ($\mu$ mb$^{-2}$) |
|---|---|
| 25 mb | 0.7 |
| 50 mb | 0.25 |
| 100 mb | 0.1 |
| 200 mb | 0.04 |

For convenience, the Umkehr values were also integrated over pressure and time. This gave an increase of *0.008 cm* for each of two stratospheric layers, *20 mb to 100 mb* and *100 mb to 250 mb* for a unit vertical motion of *1 cm sec*$^{-1}$ over a *twelve-hour* period. The computed vertical motions at Edmonton gave an average daily change of 0.005 cm in the upper layer and 0.006 cm in the lower layer. The largest change computed for either layer was about 0.03 cm in 24 hours as compared to the largest total ozone change of 0.09 cm. The correspondence between the computed ozone changes for both layers and daily total ozone changes, over the two-month period, was not impressive, confirming the expected complexity of the vertical and horizontal advective processes.

## 5. Conclusions

The writers suggest that these results support (though they do not finally prove) the importance of baroclinic waves of the polar-night vortex in daily ozone variation in the midwinter months in high latitudes. In summary:—

(i) when the polar-night westerlies were present over Edmonton and Moosonee, and their baroclinic waves were of high amplitude (as in January), the variation in total ozone followed fairly closely the motion of these waves, ozone maxima and minima seeming to move with their phase-velocity, as did thermal maxima and minima;

(ii) the correlation between ozone and middle stratospheric temperature was high at such times; at Edmonton, moreover, it was also high in the anticyclonic phase of early December. In general, this correlation exceeded the well-known Normand correlation;

(iii) no obvious correlation with local vertical motion could be established.

If conclusion (i) is valid, it is clear that ozone and temperature variation along trajectories must be governed by similar conservation equations; if vertical motion and divergence are considered to be the appropriate mechanism, these must be so adjusted along the trajectories as to permit the isolines of ozone concentration to remain in phase with the ridges and troughs in the contour pattern.

These tentative findings cannot be extended to other latitudes or seasons. At all other times of year the middle stratosphere has undisturbed flow, with little vertical motion in middle and high latitudes. At such times the Normand effect must dominate the ozone record. Even in winter, moreover, the polar-night waves have a high amplitude only in sub-arctic latitudes, and there is some evidence that amplitudes over Eurasia are less, and the wave-structure more complex, than over Canada.

## Acknowledgement

The research reported in this paper was conducted with the support of the Geophysics Research Directorate, United States Air Force

Cambridge Research Center, under contract AF 19(604)-3865. Facilities for the analysis were made available by the Meteorological Branch, Department of Transport, Canada at the Central Analysis Office, under Mr. J. Leaver. The paper was read before the meeting of the International Ozone Commission, Oxford, England, July 22nd, 1959.

## REFERENCES

Craig, R. A., and Hering, W. S., 1959: The stratospheric warming of January—February 1957, *J. Meteor.*, **16**, pp. 91—107.

Godson, W. L., 1959: Unpublished paper presented to Seminar in Arctic and Stratospheric Meteorology, McGill University, July 27—August 7, 1959.

Godson, W. L. and Lee, R., 1958: High-level fields of wind and temperature over the Canadian arctic, *Beitr. zur Phys. der Atmos.*, **31**, pp. 40—68.

Hare, F. K., 1960: The disturbed circulation of the arctic stratosphere, *J. Meteor.*, **17**, p. 36—51.

Kochanski, A., 1955: Cross-sections of the mean zonal flow and temperature along 80° W, *J. Meteor.*, **12**, (2), pp. 95—106.

Normand, Sir Charles, 1953: Atmospheric ozone and the upper-air conditions, *Quart. J. Roy. Meteor Soc.*, **79**, pp. 39—50.

Reed, R. J., 1950: The rôle of vertical motions in ozone-weather relationships, *J. Meteor.*, **7**, pp. 263—267.

Scherhag, R., 1952: Die explosionsartigen Stratosphären-erwärmungen des Spätwinters 1951—52, *Ber. Deutsch. Wetterdienst.*, **6**, (38), pp. 51—63.

Teweles, S., 1958: Anomalous warming of the stratosphere over North America in early 1957, *Mon. Wea. Rev.*, **86**, (10), pp. 377—396.

# On the Exchange of Carbon Dioxide between the Atmosphere and the Sea

By BERT BOLIN, University of Stockholm

(Manuscript received March 3, 1960)

*Abstract*

The physical and chemical processes responsible for exchange of carbon dioxide between the atmosphere and the sea are analyzed. It is shown that the rate of transfer is considerably decreased due to the finite rate of hydration of $CO_2$ in water. This is the case both for a smooth water surface where molecular diffusion plays a rôle in the first few hundredths of a millimeter as well as for a rough sea where turbulence extends all the way to the surface. A general agreement is found between the transfer rate deduced in this way and the rate of exchange estimated on the basis of the $C^{14}/C^{12}$ ratio in the atmosphere and the sea.

## 1. Introduction

Recent studies of the exchange of carbon dioxide between the atmosphere and the sea (Revelle and Suess, 1957; Craig, 1957; Arnold and anderson, 1957; Bolin and Eriksson, 1959) using measurements of radiocarbon in the atmosphere and the sea have given a residence time for carbon dioxide in the atmosphere of 3—7 years. This result has been obtained considering the atmosphere and the sea as well mixed reservoirs (the latter one divided into an upper and a lower part) and assuming the exchange between them being directly proportional to the concentrations. The value of the residence time is roughly proportional to the difference of $C^{14}/C^{12}$ in the atmosphere and the surface layers of the ocean (after correction for fractionation). A large number of new measurements has recently become available (Broecker et al., 1959) and they agree in general with the previous measurement reported by Revelle and Suess (l.c.). Considerable variations occur, however, for example between the surface waters around the Antarctica and the Northern Atlantic. We shall here accept a value for this average residence time of about 5 years but keep in mind that this is an average value applicable to the ocean as a whole.

Obviously the model of the atmosphere and the sea adopted in these studies is a gross oversimplification of actual conditions and it therefore seems desirable to investigate a little more in detail the processes that bring about this exchange. It is of particular interest to analyze the proposal by Eriksson (1959), that the comparatively slow rate of hydration is of importance.

## 2. Chemical and physical processes governing the exchange

The carbon system of the sea consists of dissolved carbon dioxide, carbonic acid, bicarbonate and carbonate ions, which are all in approximate equilibrium. We may write (Buch et al., 1932)

$$\left.\begin{aligned} &\text{(a)}\ \ CO_2 + H_2O \rightleftharpoons H_2CO_3 \rightleftharpoons H^+ + \\ &\quad + HCO_3^- \rightleftharpoons 2H^+ + CO_3^= \\ &\text{(b)}\ \ CO_2 + OH^- \rightleftharpoons HCO_3^- \rightleftharpoons H^+ + CO_3^= \end{aligned}\right\} \quad (1)$$

The first reaction is the only one of importance for $pH \leq 8$ and the latter one is the

dominating process for pH ≥ 10 (cf. MILLS and UREY, 1940). When dealing with the ocean surface (pH = 8.0—8.2) we may disregard the second one.

The dissociation of carbonic acid into bicarbonate ions and further into carbonate ions is a fast process and may for all practical purposes be considered as instantaneous. The hydration (and dehydration) expressed by the first reaction in (1 a) proceeds with a finite speed, which is a function of pH and temperature. It has been determined experimentally (MILLS and UREY, 1940, ROUGHTON, 1941) for neutral solutions for temperatures ranging between 0° C and 35° C. Denoting the rate of hydration by $\alpha_1$ and dehydration by $\alpha_2$ we have

$$K = \frac{\alpha_2}{\alpha_1} \qquad (2)$$

where $K$ is the equilibrium constant. Table 1 gives values for these quantities as a function of temperature.

**Table 1**

| Temp. °C | $\alpha_1$ $sec^{-1}$ | $\alpha_2$ $sec^{-1}$ | $K$ |
|---|---|---|---|
| 0° | 0.002 | 2 | 1000 |
| 27° | 0.028 | 31 | 1100 |
| 37° | 0.10 | 80 | 800 |

It is probably not permissible to neglect reaction (1 b) completely at the ocean surface and the rates given in table 1 may therefore be somewhat too small. We shall use a value of $\alpha_1 = 0.03$ $sec^{-1}$ in the following. It will be seen, however, that the value does not enter critically into any of the results deduced.

The dissociation equilibrium between $H_2CO_3$ and the bicarbonate and carbonate ions is, on the other hand, very sensitive to the pH (cf. HARVEY, 1955, BOLIN and ERIKSSON, 1959). Since we here shall be considering steady state processes, we need not, however, be concerned with this in the following.

The transfer of carbon dioxide through the atmosphere and the sea takes place by turbulent processes except possibly in the intermediate vicinity of the sea surface where molecular diffusion may play a role at least in the case of a smooth surface. The transfer across the sea surface is dependent on the number of molecules colliding with the interphase and being retained in the water when coming from the air and *vice versa*.

Transfer in the *atmosphere* has been studied in connection with evaporation (cf. SVERDRUP, 1951). It has been shown that the observed rates can be explained if considering a boundary layer with molecular diffusion above which the turbulent transfer is dominating. The characteristics of this boundary layer are not very well known and it is doubtful whether it exists at all in case of a rough sea surface. Its thickness is of the order of 1—10 mm except in calm weather. Very little is also known about a corresponding boundary layer in the *sea*. The rate of molecular diffusion of a gas through water is, however, about $10^4$ times less than the corresponding rate of diffusion through a gas at standard pressure and temperature. Thus if the thickness of the boundary layer in the sea were considerably more than $10^{-4}$ of the thickness of the boundary layer in the air, i.e. more than about 1 μ and the solubility close to unity or less the diffusion through this water layer would be much more decisive in determining the rate of transfer between the atmosphere and the sea, than molecular diffusion through the lowest layer of the atmosphere. Now we know that the residence time for water in the atmosphere, obviously controlled by mixing processes in the atmosphere, is only about 10 days as compared with about five years for carbon dioxide. This fact in itself tells us that the comparatively long residence time for carbon dioxide in the atmosphere depends on slow transfer in the surface layers of the ocean rather than the lowest layers of the atmosphere. We shall indeed find that the transfer is essentially due to transfer of dissolved $CO_2$ in which case the solubility may be considered close to unity and furthermore studies of gas bubbles in sea water (WYMAN ET AL., 1952) indicate a thickness of the molecular boundary layer of about 35 μ. In the following we shall assume that the gas phase above the sea surface is well mixed and consider the processes in the sea as rate determining.

In case of strong winds and a rough sea surface most likely no molecular boundary layer exists. The turbulent eddies reach all the way to the surface which is clearly indicated by the fact that air bubbles may be found

at considerable depth under these conditions. Since the turbulence in this case is induced by the wind, one might even expect the eddy diffusivity to have a maximum at the surface as was found for the eddy viscosity in a case studied by ROSSBY and MONTGOMERY (1935). Values for the eddy diffusivity range between 0.2 and 100 $cm^2$ $sec^{-1}$ (SVERDRUP, 1942).

According to kinetic theory of gases the number of molecules ($S$) penetrating into the water surface is given by

$$S = 1/4\, c \cdot \nu \cdot \bar{v} \qquad (3)$$

where $\nu$ is the number of molecules per unit volume, $\bar{v}$ is the mean molecular speed and $c$ the fraction of all colliding molecules that is retained in the water. In our case $\bar{v} \approx 10^4$ cm $sec^{-1}$. The residence time of carbon dioxide in the atmosphere of about 5 years corresponds to a transfer velocity of $7 \cdot 10^{-3}$ cm $sec^{-1}$ (in terms of $CO_2$ at the pressure prevailing in the atmosphere).[1] Thus the molecular transfer velocity across the sea surface is larger than this observed transfer velocity as long as $c > 4 \cdot 10^{-6}$. Recent studies by MÜNNICH and VOGEL (1959), indicate that the molecular transfer across the surface of a NaOH solution may be considerably greater than 0.1 cm $sec^{-1}$ indicating that the transfer across the surface is not a limiting factor for the observed rate of transfer. It would, however, be of great interest to determine the constant $c$ in (3) experimentally and not merely know that $c \geq 10^{-5}$ as implied by MÜNNICH and VOGEL's experiment.

The previous discussion is valid for a smooth water surface. In case of a rough sea with breaking waves droplets in the air and bubbles in the water probably take same part in the exchange of $CO_2$. This is, however, not of principle importance since in such a case the turbulence in the atmosphere and the sea is so violent and still plays the most important rôle. This can be seen from the fact that the amount of $CO_2$-gas in a bubble is about the same as the amount of dissolved $CO_2$-gas in the same water volume. In the case of bubbles penetrating into the sea turbulent motion extends to the surface and due to the great solubility of $CO_2$ in water much more $CO_2$ is transferred by this turbulent motion of the *water* than the comparatively very small quantities of gas present in form of bubbles. With regard to droplets in the air we recall that the residence time for carbon dioxide in the air of about five years means a transfer across the sea surface equal to the total amount of $CO_2$ present in a 20 m deep layer of the ocean every year. Due to the slow hydration process it takes of the order of minutes to establish an equilibrium between the drops and the surrounding air. Only very small drops that stay an appreciable time in the air therefore are of importance. Assuming for the moment that all transfer were due to exchange between the drops and the surrounding air. This would imply a transfer of sea salt into the atmosphere at such a rate that even if assuming the highest observed air concentration of salt (see Station Vinga, EGNÉR, ERIKSSON, 1955) the amount of salt present in a layer of about 25 m were transferred into the atmosphere in a second. This is obviously unrealistic.

In the previous discussion we have already used the word residence time several times. In the case of exchange between *well-mixed* reservoirs this concept is uniquely defined as the inverse of the exchange coefficient (cf. e.g. CRAIG, 1957). Obviously the residence time for molecules in incompletely mixed reservoirs is a function of the initial position of the molecule considered. Thus molecules immediately above the sea surface on an average stay a much shorter time in the atmosphere than those in the middle of the troposphere. An *average* residence time is of course a function of the internal mixing in the atmosphere and the rapidity of the molecular transfer across the sea surface. According to our previous discussion the latter implies a transfer velocity larger than 0.1 cm $sec^{-1}$ or a residence time less than three months and the internal mixing of the troposphere has a characteristic time scale of one to two months (LAL, PETERS, 1959). The five years' residence time for carbon dioxide in the

[1] We shall use the term transfer velocity in the following as the depth of a column of the gas at prevailing pressure in the gas phase that is transferred across a horizontal surface (usually the sea surface) per unit time. Clearly a transfer velocity in the water in the case of a steady state is the velocity defined above divided by the solubility of the gas in water (cf. equ. 7). Solubility of $CO_2$ gas will be assumed to be unity in the following.

atmosphere must then mean that only a small fraction of molecules entering the sea surface ever have a chance to be transferred into the main part of the sea, i.e. beyond a very thin boundary layer. The residence time as deduced from $C^{14}/C^{12}$ measurements therefore is the average time for bringing a molecule from the *interior* of one reservoir to the *interior* of the other. The residence time for carbon dioxide *in the atmosphere* defined in this way is essentially dependent on incomplete or slow mixing *in the sea*.

### 3. Molecular and turbulent transfer of carbon dioxide in the sea

The transfer of carbon dioxide in the ocean has been studied by DINGLE (1954). He treated, however, the hydration process as a one-way reaction and furthermore a thorough discussion of the molecular and eddy diffusivity is lacking. The residence time of about one day arrived at is not compatible with our previous discussion. We shall here reconsider the problem. In accordance with our previous discussion we shall assume complete mixing in the atmosphere and an immediate adjustment of conditions at the sea surface.

Consider an infinite surface, horizontal homogeneity of the water and no net vertical velocity. We denote by $n'$ the amount of dissolved carbon dioxide and by $n''$ the sum of the remaining inorganic carbon compounds in the water. We shall assume that the dissociation in (1 a) is very fast. The rate constant ($\alpha_2^*$) expressing the rate of transfer of $H_2CO_2$, $HCO_3$ and $CO_3$ into dissolved $CO_2$ then is given by

$$\alpha_2^* = \alpha_2 \frac{1}{K} \frac{N'}{N - N'} \tag{4}$$

where $N'$ and $N$ denote equilibrium values for dissolved $CO_2$ and total amount of carbon in the system. Considering now the vertical distribution of $n'$ and $n''$ being dependent both on the chemical reaction (1 a) and molecular or turbulent diffusion we obtain

$$\left.\begin{aligned} \frac{\partial n'}{\partial t} &= -\alpha_1 n' + \alpha_2^* n'' + \frac{\partial}{\partial z}\left(A \frac{\partial n'}{\partial z}\right) \\ \frac{\partial n''}{\partial t} &= \alpha_1 n' - \alpha_2^* n'' + \frac{\partial}{\partial z}\left(A \frac{\partial n''}{\partial z}\right) \end{aligned}\right\} \tag{5}$$

where $A$ is the molecular or eddy diffusivity. The boundary conditions at the sea surface express the fact that only the dissolved carbon dioxide is in exchange with the atmosphere. Thus

$$\left.\begin{aligned} &\text{(a)} \quad -A \frac{\partial n'}{\partial z} = \beta_1 n' - \beta_2 n_a \\ &\qquad\qquad\qquad\qquad\qquad\qquad z = 0 \\ &\text{(b)} \quad -A \frac{\partial n''}{\partial z} = 0 \end{aligned}\right\} \tag{6}$$

Here the coefficients $\beta_1$ and $\beta_2$ express the number of molecules leaving the water or penetrating into it respectively and $n_a$ is the concentration in the gas phase. In case of an equilibrium we have $\partial n'/\partial z = 0$ and thus

$$n' = \frac{\beta_2}{\beta_1} n_a = n_0' \tag{7}$$

$\beta_2/\beta_1$ is an expression for the solubility of carbon dioxide. If the coefficient $c$ in equ. (3) is large (cf. sec. 2) the left side of equ. (6 a) is small compared with the two terms on the right side and we may use the boundary condition (7) also in case of a net transfer taking place. In addition we shall assume complete mixing below a certain depth, $d$ and thus have

$$\left.\begin{aligned} &n' = n_d' \qquad n'' = n_d'' \qquad z = -d \\ &\alpha_1 n_d' = \alpha_2 n_d'' \end{aligned}\right\} \tag{8}$$

The complete time-dependent problem as outlined above leads to a nonhomogeneous partial differential equation of fourth order with variable coefficients. We shall here only treat a few special cases which still are of considerable interest.

#### a. Molecular diffusion through a boundary layer

Let us assume that the turbulence in the interior of the water mass is intense enough to maintain any necessary transport and that all gradients of $n'$ and $n''$ are confined to a boundary layer through which molecular diffusion is predominant. Consider furthermore a steady state, where the transfer still is too small to affect conditions in the air ($n_0'$) or in the turbulent part of the fluid ($n_d'$ and $n_d''$) over

the time interval considered. The equations (5) are transferred into

$$\left.\begin{aligned} -\alpha_1 n' + \alpha_2^\star n'' + \varkappa \frac{\partial^2 n'}{\partial z^2} = 0 \\ \alpha_1 n' - \alpha_2^\star n'' + \varkappa \frac{\partial^2 n''}{\partial z^2} = 0 \end{aligned}\right\} \qquad (9)$$

with the boundary conditions (6 b) (7) and (8). $\varkappa$ is the molecular diffusivity and $d$ now denotes the thickness of the boundary layer. We here deduce the following expression for the flux of total amount of carbon dioxide towards the interior of the fluid

$$F = \frac{n_0' - n_d'}{d} \cdot \frac{\alpha_1 + \alpha_2^\star}{\alpha_1} \cdot \gamma d \cdot \frac{e^{\gamma d} + e^{-\gamma d}}{e^{\gamma d}\left(1 + \frac{\alpha_2^\star}{\alpha_1}\gamma d\right) - e^{-\gamma d}\left(1 - \frac{\alpha_2^\star}{\alpha_1}\gamma d\right)} \qquad (10)$$

where

$$\gamma^2 = \frac{\alpha_1 + \alpha_2^\star}{\varkappa} \qquad (11)$$

Obviously the flux depends upon the total gradient imposed $(n_0' - n_d') \cdot d^{-1}$ and $\gamma d$ which expresses the ratio of the rate of hydration and dehydration to the rate of molecular diffusion through a layer of thickness $d$. We have the two limiting cases $\gamma d \to \infty$ (diffusion is slow compared to hydration) and $\gamma d \to 0$ (diffusion through the layer considered is fast compared to the rate of hydration). We get

$$\lim_{\gamma d \to \infty} F = F_\infty = \varkappa \frac{n_0' - n_d'}{d} \cdot \frac{\alpha_1 + \alpha_2^\star}{\alpha_2^\star} \qquad (12)$$

$$\lim_{\gamma d \to 0} F = F_0 = \varkappa \frac{n_0' - n_d'}{d} \qquad (13)$$

In the former case the hydration equilibrium is established everywhere $\alpha_1 n' = \alpha_2^\star n''$ and the downward transfer is due to diffusion of both dissolved gas and bicarbonate and carbonate ions. In the latter case, on the other hand, no gradients of $n''$ are ever established and the transfer is only due to transfer of dissolved gas. Figure 1 illustrates the principle difference between these two cases with regard to the distribution of $n'$ and $n''$ in the boundary layer. Figure 2 shows the flux

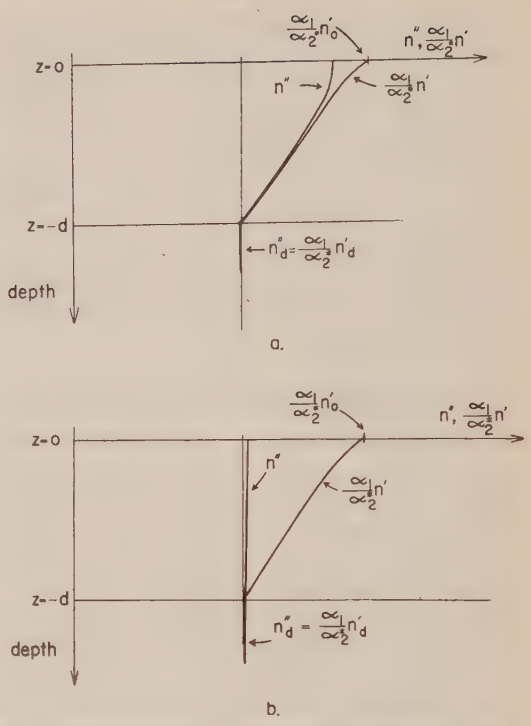


Fig. 1. Distribution of $n'$ and $n''$ as a function of depth in a thin boundary layer with a steady flux of carbon dioxide. (a) shows conditions when $\gamma d$ is large ($\to \infty$), (b) shows conditions when $\gamma\ d$ is small ($\to$ 0).

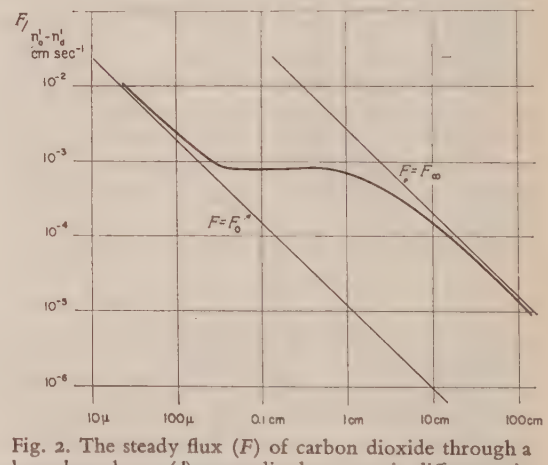


Fig. 2. The steady flux ($F$) of carbon dioxide through a boundary layer ($d$) normalized to a unit difference in concentration between the boundaries of the layer. The straight lines show the asymptotic values given by equations (12) and (13).

as a function of $d$. We have here assumed $\varkappa = 2 \cdot 10^{-5}$ cm$^2$ sec$^{-1}$, $\alpha_1 = 0.03$ sec$^{-1}$ and $\alpha_2 = 150 \cdot \alpha_2^\star$ (according to equ. (4) and the

values for $N$ and $N'$ as given by BOLIN and ERIKSSON, 1959). We find $F = F_0$ within 10 % for $d < 130\ \mu$ while $F = F_\infty$ within again 10 % for $d > 20$ cm. We furthermore note that the thickness of the boundary layer should be about 35 $\mu$ to yield a transfer rate corresponding to the residence time of $CO_2$ as obtained from $C^{14}/C^{12}$ data. It is interesting to note that this is equal to the value of 35 $\mu$ derived by WYMAN ET AL. (1952) using a similar model of diffusion of $O_2$ and $N_2$ when studying bubbles in sea water. The exact agreement may be a coincidence since we have not yet considered the relative importance of carbon dioxide transfer in areas with a rough sea surface. The general agreement is, however, no doubt significant.

In his treatment of the $CO_2$-transfer into the ocean DINGLE (1954) assumed that we may put $\alpha_2^\star \equiv 0$ in equation (5). The first of the two equations may then be solved independently of the second yielding

$$F = n_0' \cdot \sqrt{\alpha_1 \cdot \varkappa} \tag{14}$$

This gives a transfer velocity of $8 \cdot 10^{-4}$ cm sec$^{-1}$, i.e. much less than the velocities actually observed. The interpretation is obviously that the turbulence in the interior can maintain a steeper gradient of $n'$ than the hydration and thus the thickness of the boundary layer, dependent on the intensity of mixing in the interior of the fluid, is the rate-determining factor. It is interesting to note that for an increasing thickness of the boundary layer the transfer remains constant at $\sqrt{\varkappa \alpha_1} \approx 8 \cdot 10^{-4}$ cm sec$^{-1}$ over a wide range of values for $d$. The decreasing effectiveness of diffusion is compensated by the increasing importance of hydration. Since a stagnant layer within which only molecular transfer takes place can hardly be more than a millimeter thick in the ocean we find that the rate given by (14) is the minimum transfer rate for $CO_2$.

## b. Turbulent diffusion of carbon dioxide into a water body

Let us next consider a case in which the diffusivity is equal to the molecular diffusivity $\varkappa$ at the sea surface and then increases linearly towards the interior of the fluid. The results are, however, not sensitive to the profile. As long as $A = \varkappa$ at the surface (a *smooth* surface) the results apply and we shall in this way be able to make use of our knowledge about turbulence in the sea as deduced from eddy exchange of heat and salt (eddy diffusivity of the order of 10—50 cm$^2$ sec$^{-1}$, cf. SVERDRUP et al., 1942).

We may thus replace $A$ in equation (5) by

$$A = -kz + \varkappa \qquad (z \leq 0) \tag{15}$$

In steady state our differential equations (5) applied to a layer, $d$, now become

$$\left.\begin{aligned} -\alpha_1 n' + \alpha_2^\star n'' + \frac{\partial}{\partial z}\left[(-kz+\varkappa)\frac{\partial n'}{\partial z}\right] &= 0 \\ \alpha_1 n' - \alpha_2^\star n'' + \frac{\partial}{\partial z}\left[(-kz+\varkappa)\frac{\partial n''}{\partial z}\right] &= 0 \end{aligned}\right\} \tag{16}$$

again with the same boundary conditions as before (6 b), (7) and (8). The solution of this system of equations yields

$$\left.\begin{aligned} n' &= \frac{\alpha_2^\star}{\alpha_1 + \alpha_2^\star}[B_0 \ln x + B_1] + \\ &\quad + C_1 J_0(2i\sqrt{bx}) + C_2 Y_0(2i\sqrt{bx}) \\ n'' &= \frac{\alpha_1}{\alpha_1 + \alpha_2^\star}[B_0 \ln x + B_1] - \\ &\quad - C_1 J_0(2i\sqrt{bx}) - C_2 Y_0(2i\sqrt{bx}) \end{aligned}\right\} \tag{17}$$

Here $J_0$ and $Y_0$ are Bessel functions of zero order and of the first and second kind with imaginary argument, $x = -kz + \varkappa$, $b = k^{-2}(\alpha_1 + \alpha_2^\star)$ and $B_0, B_1, C_1$ and $C_2$ are integration constants. For $k = 10^{-3}$—1 cm sec$^{-1}$ and $d = 1$—$10^3$ cm, we have $C_1 \approx 0$ and we obtain the following expression for the flux

$$F = (n_0' - n_d')\frac{\alpha_1 + \alpha_2^\star}{\alpha_1} \cdot k \frac{1}{\frac{\alpha_2^\star}{\alpha_1}\ln\frac{kd+\varkappa}{\varkappa} - \frac{1}{\sqrt{b\varkappa}}\frac{Y_0(2i\sqrt{b\varkappa})}{Y_1(2i\sqrt{b\varkappa})}} \tag{18}$$

$Y_1$ being the Bessel function of first order and second kind. As two limiting cases we have

$$F_\infty = (n_0' - n_d') \frac{\alpha_1 + \alpha_2^*}{\alpha_1} k \frac{1}{\ln\left(1 + \frac{kd}{\varkappa}\right)} \quad (19)$$

$$F_0 = (n_0' - n_d') k \frac{1}{\ln\left(1 + \frac{kd}{\varkappa}\right)} \quad (20)$$

for relatively rapid respectively slow hydration rate as compared with the rate of diffusion. In order to have a transfer velocity of $7 \cdot 10^{-3}$ cm sec$^{-1}$, we must have $k \geq 0.1$ cm sec$^{-1}$ regardless of the value chosen for $d$ between 1 and $10^3$ cm, which in turn means that the mixing at these depths is that intense that no appreciable gradients are necessary to bring about the transfer determined by processes in the vicinity of the sea surface. The value of $k$ thus obtained implies an eddy diffusivity of $A = 10$ cm$^2$ sec$^{-1}$ at the depth of about 1 m. If we permit a thin layer of molecular diffusion at the surface an even more rapid increase of the eddy diffusivity with depth must exist in order to have a transfer velocity of $7 \cdot 10^{-3}$ cm sec$^{-1}$. In any case we are close to the case given by equ. (20), i.e. hydration is of little importance in determining the transfer away from the surface.

In case of a rough sea surface the turbulence elements presumably reach to the surface and no boundary layer with molecular diffusion exists. The turbulence is now intense enough that once a $CO_2$-molecule has been hydrated it will with all likeliness be mixed throughout the mixed layer before being returned to the atmosphere. The rate of transfer of $CO_2$ molecules into the water is then approximately given by equation (14), where, however, we insert the turbulent diffusivity $A$ instead of the molecular one $\varkappa$. For $A = 1$ cm$^2$ sec$^{-1}$ the transfer velocity becomes 0.17 cm sec$^{-1}$ and for $A = 10$ and 100 cm$^2$ sec$^{-1}$ we obtain respectively 0.6 and 1.7 cm sec$^{-1}$. These values correspond to an atmospheric residence time of 60, 20 and 6 days respectively. These rates are now comparable to the rate of overturning of the mixed layer as a whole, which we know has a characteristic time scale of a month or two indicated by the almost in phase variations of $O_2$ in the ocean and temperature disregarding effects caused by biological activities (cf. REDFIELD, 1948). A value of $A = 10$ or 100 cm$^2$ sec$^{-1}$ also implies a characteristic mixing time of a layer 100 m deep of 100 and 10 days respectively.

## 4. Conclusions

It has been shown above that droplets in the air and bubbles in the sea play an insignificant role for the exchange of $CO_2$ between the atmosphere and the sea. Similarly the turbulent and molecular transfer in the atmosphere is rapid as compared to the corresponding processes in the sea. In case of a smooth water surface a transfer velocity of $7 \cdot 10^{-3}$ cm sec$^{-1}$ (corresponding to a residence time for $CO_2$ in the atmosphere of about five years) implies a boundary layer not thicker than about 35 $\mu$ in fair agreement with the thickness of the boundary layer around a bubble as deduced from observation of the rate of solution of bubbles in water. For a rough sea surface the transfer velocity may be 10 to 100 times larger.

By far the greatest part of the ocean surface is smooth but it seems impossible to say what the importance is of the increased transfer in stormy regions. Off hand one would for example expect a smaller difference in the $C^{14}/C^{12}$ ratio between the atmosphere and the sea in a stormy area (after correction for fractionation). The turbulent transfer within the sea also becomes larger in such a case, whereby such an effect may be masked. It would be of great interest to study this ratio in the surface layers of the sea and the atmosphere above. A comparison between the stormy areas around latitude 50° and the relatively calm regions in the subtropics would be of particular interest. An especially interesting phase prevails at present in that the excess radiocarbon introduced by hydrogen bombs is being transferred into the oceans.

## Acknowledgement

The present study was carried out at Woods Hole Oceanographic Institution and Scripps Oceanographic Institution with the support from the Carnegie Institution of Washington, D.C. The generous support from all these institutions is gratefully acknowledged. I also wish to thank for stimulating discussions with Drs. J. Kanwisher and D. Keeling.

## REFERENCES


ARNOLD, J. R., and ANDERSON, E. C., 1957: The distribution of carbon-14 in nature. *Tellus* **9**, pp. 28—32.

BOLIN, B., and ERIKSSON, E., 1959: Changes in the carbon dioxide content of the atmosphere and the sea due to fossil fuel combustion. *Rossby Memorial Volume* (Rockefeller Institute Press, New York), pp. 130—142.

BROECKER, W. S. et al., 1959: Geochemistry and physics of ocean circulation. *Proceedings of the Oceanographic Congress, New York, Sept. 1959.*

BUCH, D., HARVEY, H. W., WATTENBERG, H., and GRIPENBERG, S., 1932: Ueber das Kohlensäuresystem in Meerwasser. *Conseil Perm. Int. pour Expl. de la Mer. Rapports et procès verbaux des Réunions* **LXXIC**.

CRAIG, H., 1957: The natural distribution of radiocarbon and the exchange time of carbon dioxide between atmosphere and sea. *Tellus* **9**, pp. 1—17.

DINGLE, A. N., 1954: The carbon dioxide exchange between the North-Atlantic Ocean and the atmosphere. *Tellus* **6**, pp. 343—350.

EGNÉR, H and ERIKSSON, E., 1955: Current data on the chemical composition of air and precipitation. *Tellus* **7**, pp. 134—139 and following issues.

ERIKSSON, E., 1959: The exchange of matter between atmosphere and sea. *Proceedings of the Oceanographic Congress, New York, Sept. 1959.*

LAL, D., and PETERS, B., 1959: Cosmic ray produced isotopes for studying large scale atmospheric circulation. *Proceedings of the second international conference on peaceful uses of atomic energy, Geneva, 1958.* **18**, pp. 533—544.

MILLS, A., and UREY, H. C., 1940: The kinetics of isotopic exchange between carbon dioxide, bicarbonate ions, carbonate ions and water. *J. American Chem. Soc.* **62**, pp. 1019—1026.

MÜNNICH, K. O., and VOGEL, J. C., 1959: Variations in $C^{14}$-content during the last years. *Presented at the International $C^{14}$-symposium in Groningen, Sept. 1959.*

REDFIELD, A. C., 1948: The exchange of oxygen across the sea surface. *J. Marine Research* **7**, pp. 347—361.

REVELLE, R., and SUESS, H., 1957: Carbon dioxide exchange between atmosphere and ocean and the question of an increase of atmospheric $CO_2$ during the past decades. *Tellus* **9**, pp. 18—27.

ROSSBY, C.-G., and MONTGOMERY, R., 1935: The layer of frictional influence in wind and ocean currents. *Papers in Physical Oceanography and Meteorology* **III**, No. 3.

ROUGHTON, F. J. W., 1941: The kinetics and rapid thermochemistry of carbon acid. *J. American Chem. Soc.* **62**, pp. 1019—1026.

SVERDRUP, H. et al., 1942: *The ocean.* Prentice Hall, Inc., New York.

SVERDRUP, H., 1951: Evaporation from the oceans. *Compendium of Meteorology*, Am. Met. Soc., pp. 1071—1080.

WYMAN, J. et al., 1952: On the stability of gas bubbles in sea water. *J. Marine Research* **XI**, pp. 47—62.

# On the Appearance of Ninhydrinpositive Substances in the Atmosphere

By F. MUNCZAK, First Institute of Physics, Vienna

(Manuscript received November 17, 1959)

*Abstract*

This report is part of a larger work (entered at the Austrian Academy of Sciences on 20th June, 1959) which appears here without significant alteration and translated into English; it deals with the investigation of atmospheric organic nitrogen compounds. On some days in the course of these investigations the appearance of ninhydrinpositive substances could be established and at least some of them could be identified with great probability as amino acids. Observations are made about the appearance of these substances in relation to meteorological factors, and about the sizes in which particles of these substances may appear. Some remarks are added about their possible origin and the influence their appearance may have on life.

**Introduction**

Since the middle of the last century there have been a great many investigations into the presence of nitrogen compounds in the atmosphere and in precipitations. By far the largest number of these investigations have involved both ammonia and its salts and nitrates and nitrites, whilst only relatively few investigations about organic nitrogen compounds have been made. The different views on the formation and cycles of these substances (and the significance which individual authors attribute to the various sources of atmospheric nitrogen compounds) prove the complexity of this problem. Although a number of questions connected with the atmospheric inorganic nitrogen compounds remain unsolved, the uncertainty increases as soon as the appearance of organic nitrogen compounds is considered, especially since there are very few works which deal with the nature of these compounds. Indeed one dare say that this field of research is hardly explored, as until now almost the only goal of investigation has been the determination of the amount of albuminoid nitrogen, i.e. the ammonia released from organic matter in precipitation when treating it with oxidizing agents, or by Kjeldahl digestion. (These are both summary methods.) Thus it is not possible to decide whether this albuminoid nitrogen is produced by fragments of organic matter, bacteria, pollens etcetera, or from more simple nitrogen compounds, e.g. amino acids or amines. As far as is known, FONSELIUS (1954) was the first to find in precipitations the most simple nitrogen compounds of organic matter (i.e. amino acids) using the methods of chromatography, which are especially fitted for this kind of research.

Different explanations of the appearance of amino acids in the atmosphere are conceivable. They may be set free by the decomposition of organic matter or even perhaps arise in connection with the combustion of solid or liquid fossil fuels. Finally it is possible that higher organic nitrogen compounds arise from a synthesis from more simple compounds, similar perhaps to that of MILLER (1953, 1955, 1957) or from other synthesis hitherto unknown. All these possibilities may be taken into con-

sideration. As early as 1934 TREIBS (1934, 1935) produced evidence of relatively unchanged chlorophyll- and hæmin-derivatives in crude oils, coal and bituminous rocks. (In crude oils he found porphyrinderivatives in an amount of 2γ—10 mg per 50 g crude oil.) It is quite possible that during combustion small amounts of these derivatives or fragments of them, escape into the air. Since these compounds contain nitrogen in the form of the pyrrol ring, according to the preservation of this ring or its splitting, the formation of more or less simple nitrogen compounds is possible. Just as these hæmin- and chlorophyll-derivatives survived almost unchanged for millions of years, so did amino acids in fossils. Thus alanine, glutamic acid, glycine, leucine or isoleucine and proline have been identified beyond doubt and valine less certainly by ERDMAN, MARLETT and HANSON (1954). These are almost the same amino acids which ABELSON (1957) lists as the most stable; so alanine may survive in solution for billions of years at room temperature, 100 years at 120 degrees and a few hours at 250 degrees. To the more stable amino acids may be added also aminobutyric acid, glycine, isoleucine, leucine, proline and valine, whilst all others are less stable. Even if the existence of free amino acids in fossil fuels is not very probable, because in organic fuel of lesser age only such higher compounds as sugars, waxes, fats and resins have been found (cited after ABELSON, 1957), it is possible that aliphatic nitrogen compounds may be present from which under special conditions amino acids or similar compounds could be synthesized. In view of the preferred absorption of nitrogen compounds in water which is favoured by certain weather conditions, this synthesis could take place in little water droplets whereby the smallest particles of dust, aerosol or seasalt could act as catalysts for chemical or photochemical processes. Thus in the smallest space, i.e. in the droplets themselves, it is possible to conceive conditions which sometimes differ from those predominant in the atmosphere as a whole. So, for example, in contradiction to the surrounding oxidizing atmosphere, reducing conditions, at least for short periods, would be possible in these small spheres, producing reactions which could otherwise occur only with considerable activation energy and in very small yield in an oxidizing atmosphere. The oxidation of $SO_2$ to $SO_3$ could be cited as an example for the establishment of such conditions, since, owing to industry, home heating and traffic aerosol, a relatively large amount of these compounds is brought into the air. This or similar processes would, like a Miller synthesis, in which u.v. radiation provides the necessary energy, lead to the formation of amino acids. However, the great reactivity of many rather simple organic nitrogen compounds and their great affinity for water and carbon dioxide makes a large number of reactions possible.

The substances found, or the compounds from which they originate, could have been formed near the place where the sample is taken or carried from further afield by air or winds. Thus, e.g. ÅNGSTRÖM and HÖGBERG (1952), gave evidence that the content on $NH_4N$ resp. $NO_3N$ in precipitations depend on the air masses out of which they are formed (see table 1).

**Table 1.**

| Number of invest. precipitations | air-mass | $NH_4N$ | tropic air = 1 | $NO_3N$ | tropic air = 1 |
|---|---|---|---|---|---|
| 20 | tropic | 0,0354 | 1,00 | 0,0142 | 1,00 |
| 92 | polar | 0,0262 | 0,74 | 0,0131 | 0,92 |
| 5 | arctic | 0,0172 | 0,49 | 0,0094 | 0,66 |

## Description of Apparatus and experimental Conditions

The air investigations were carried out in a laboratory at Strudlhofgasse 4, Vienna IX, within the centre of the city, close to streets with heavy traffic. Just below and immediately opposite the laboratory is situated a small petrol station. The air-samples were taken out of the atmosphere at an approximate height of 10 metres above the ground by a glass tube with a diameter of 10 mm. The outer end of the glass tube was bent downwards. To keep out dust and those nitrogen compounds which together with the dust enter into the atmosphere, the air was filtered with filters of different pore-size. The air was then passed into a bubble-tube, as already described in similar form by other authors (see fig. 1). A water-jet vacuum-pump sucked the air in; the rate of flow of the air was regulated

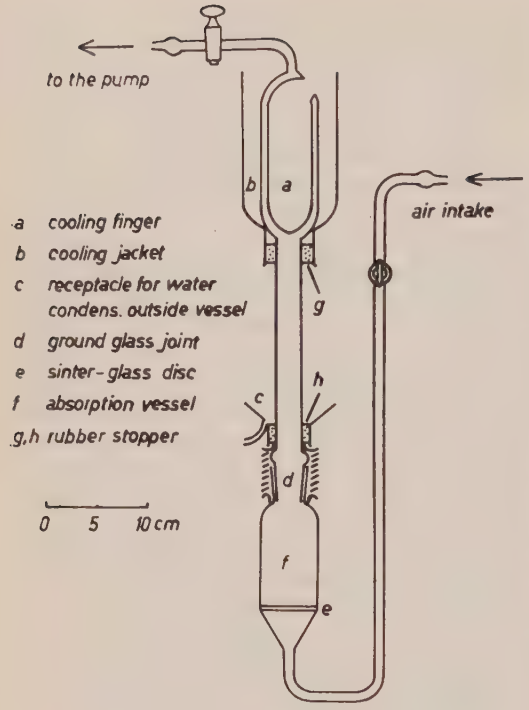


Fig. 1. Absorption-vessel.

by a set of capillaries and pressure variations were eliminated by a glass reservoir positioned in front of the water-jet pump. The air volume was determined by a rotameter used in connection with a manometer. The passing of the air between a cooling finger and a cooling jacket (both ice-cooled) ensured a sufficient cooling of the water-saturated air to make losses of absorption-fluid insignificant (even in experiments lasting some days and in outside temperatures of 25 degrees C and higher).

The flow-rate was about 120 litres an hour under normal pressure, which meant approximately 1 $m^3$ if the test lasted for 9 hours (as was usual). 150 $cm^3$ of twice-distilled water was used as absorption-fluid (for the second distillation a quartz distillation set was used) and to it was added 0.2 $cm^3$ glacial acetic acid per analysis. Acidification of the absorption-fluid with acetic acid instead of with hydrochloric acid proved more useful, as the fine bubbles formed while using the former remained longer without much coalescence on their way through the liquid; a good mixture of the air with the liquid was thereby assured.

Under reduced pressure (water pump) the absorption-fluid was evaporated to dryness at a temperature of 35° C. The residue was taken up with a drop of doubly-distilled water and investigated by circular paper chromatography. To filter the air, either Weissband filters of Schleicher and Schüll or membrane filters No. 5 of Sartorius, Göttingen, were used. The exact pore-size of the "Weissband" filter is unknown to the author, but according to RÖMPP (1958) it may be about 5 μ. The manufacturer of the membrane filter used gives its pore-size as 0.25—0.40 μ. The air was filtered prior to its examination to prevent greater contamination of the sample. Later, when two devices both with these filters were running simultaneously, the different pore-size of the filters made possible a separation of the investigated particles according to size and so gave evidence about the approximate particle-size of the different fractions.

Owing to its good discriminating power and long running-time which permitted an easier control of the running chromatogram, filter paper 2045 b made by Schleicher and Schüll was used. The substances were arranged in a circle with a radius of 2.0 cm around the centre of the chromatogram in 6—8 equal distances. This arrangement and the applying of test substances besides the substances under investigation made it possible to compare $R_f$-values and colours, and corresponds to the method described by GIRI and RAO (1952). A butanol/acetic acid/water-mixture was generally used as solvent for the chromatography, also several times water-saturated phenol. For the few two-dimensional chromatograms which were carried out, the above-mentioned combinations of solution mediums were used. In general the chromatograms were developed by a 0.2 % ninhydrin solution in butanol and acetic acid and then heated. The development aiming at finding ninhydrinpositive substances in the atmosphere was used because, in the adopted arrangement of tests, the test for reducing substances (with ammoniacal silver nitrate solution, benzidine and with triphenyltetrazolium chloride) as well as for phenols (with $FeCl_3$) remained negative. Repeated blank tests as well as investigations of the air with a negative ninhydrin reaction on the chromatogram, which can be counted as negative blank tests, showed the freedom of the

chemicals used from ninhydrinpositive substances.

From the local meteorological conditions, temperature, air pressure, relative humidity, wind and cloudiness were recorded, though summarily. At the end of the experiments, the filter contamination was estimated visually. To these data were added those of the Central Institution of Meteorology and Geodynamics in Vienna, concerning air masses and duration of sunshine at the time of experiment.

## Results of Investigations

### *Duration and Classification of Experiments*

On average, tests were run for 9 hours, mostly between 9.00 a.m. and 6.00 p.m. Longer investigations were carried out from January 28th to March 1st, 1958, covering a period of 33 days, another from March 24th to March 29th, followed by one from March 31st to April 4th, 1958, and finally one running from April 17th to April 26th, 1958. A day-and-night series was run uninterrupted from 3rd to 13th July, 1958 and carried through with 3 devices so that 46 air samples were collected and tested. All in all the atmospheric air was tested for ninhydrinpositive substances on more than 100 days, and the results of these investigations were correlated with general meteorological conditions, prevailing air masses and local weather conditions.

The experiments can be divided into two groups. Firstly when two similar devices were available, an attempt was made to find out the approximate order of magnitude of the investigated substances by inserting filters of different pore-size in front of the absorption vessel. Later on, when the interest was directed more to the identification of the substances, one apparatus was used to provide the material for the daily air examinations, whilst in the second apparatus material was collected (during a longer period) for chromatographic investigations of substances absorbed out of the air. These longer tests were always run for several days and during this period the same acetic acid solution remained in the absorption vessel. In the first investigations the same filter as used in the other apparatus was kept in the filter holder for the whole test. Later on it was replaced daily by a new filter to eliminate changes which might have been caused by filter contamination. Thus analogous working conditions were obtained on both devices. On the whole, the long running test did not show any other quantitative and qualitative result as would correspond to the sum of the individual test-results obtained within the same period.

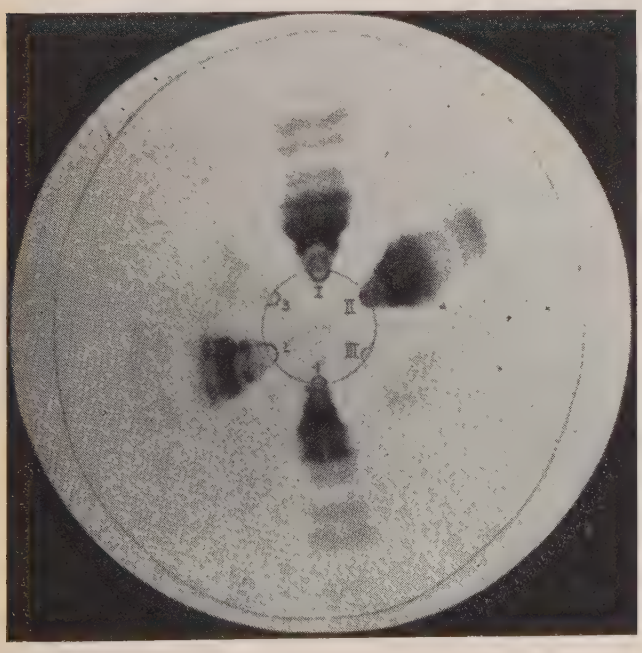


Fig. 2. Chromatogram of substances obtained beyond Weissband- and membrane filter.

I, II, III — Samples taken beyond the Weissband filter on October 14th, 15th and 18th, 1957.

1, 2, 3 — Samples taken beyond the membrane filter No. 5, taken on the same days.

III and 3 — almost negative results (obtained beyond both filters) of samples taken on 18th October, 1957.

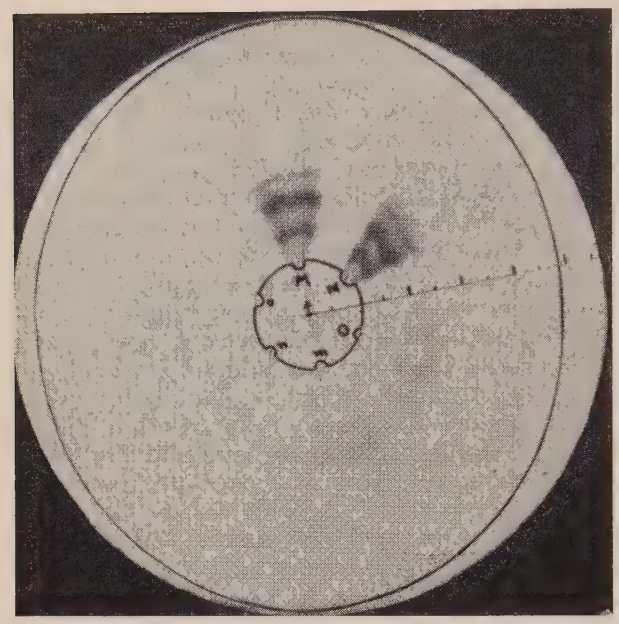

Fig. 3.

*Result of using Filters with different Pore-Size*

Unfortunately there exist only a few results giving information about the size of particles which cause ninhydrinpositive reactions or which occlude ninhydrinpositive substances. So, for instance, the chromatogram of the 14th and 15th October, 1957 (fig. 2 black and white photograph from a colour slide) shows that on both days the chromatographically discovered substances were present in the air in such size that they passed through the Weissband filter (pore-size approximately 5.0 μ) as well as the membrane filter (pore-size 0.25—0.40 μ) in almost the same amount and compo-

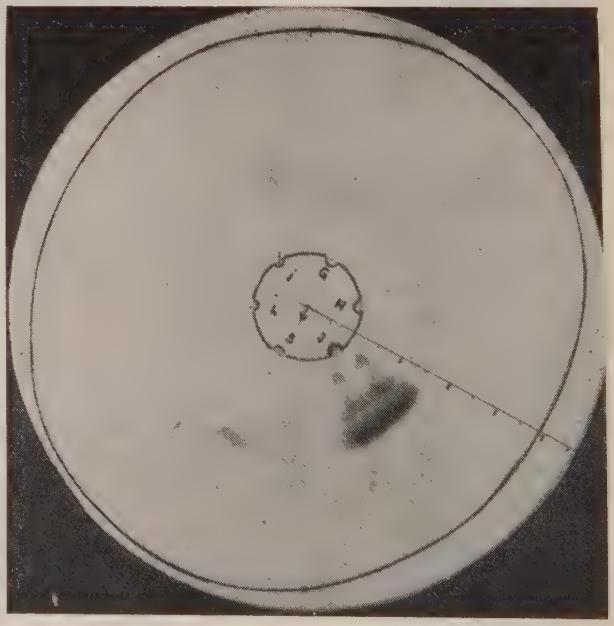

Fig. 3. Fig. 4. Chromatograms of substances obtained beyond Weissband- and membrane filter.

Capital letters — Samples taken beyond Weissband filter.

Small letters — Samples taken beyond membrane filter No. 5.

J (j) — indicates tests from 29th October, 1957.

M (m) and N (n) — those from 6th and 7th November, 1957, respectively.

The other letters denote days on which beyond the Weissband filter as well as beyond the membrane filter negative or almost negative results were obtained.

sition. Chromatographically there can be found only little difference of substance composition between samples collected beyond the Weissband filter and these found beyond the membrane filter.

Different results were obtained from similar investigations carried out on 29th October and 6th and 7th November, 1957. Beyond the Weissband filter a decrease in the number and intensity of the spots was observed and there was a more or less complete absence of positive results beyond the membrane filter (fig. 3 and fig. 4).

Using the same experimental arrangement for several tests, results similar to the last were obtained.

As a result of these investigations it seems to be evident that with the decrease in the number and intensity of the spots, either the particles increase in size or else they are occluded to larger particles.

It was unfortunate that on days with many ninhydrinpositive substances in the air, investigations with only one kind of filter were carried out, so that it was not possible to confirm the results of the 14th and 15th October, 1957.

From air pollutions according to KATZ (1956) only the smoke of oil, tobacco and carbon and $NH_4Cl$ fumes could pass both filters. In addition to this, the Weissband filter allows $SO_3$ mist and some of the smaller bacteria, to pass through.

*Results of chemical Investigations*

During extensive preliminary trials positive results were obtained only by the before-mentioned method when using ninhydrin as developer. This result by no means proves the absence of other substances in the atmosphere but is due to the limitations inherent in the method used. Among the ninhydrinpositive substances chiefly amino acids, amines and perhaps aminoaldehydes have to be considered. By evaporation to dryness at 35° C, no compounds volatile at this temperature, i.e. the greater part of the gaseous or liquid simple aliphatic amines, are included in this investigation. Substances insoluble in water were likewise excluded. However, salts of these compounds often show a different reaction with regard to solubility in water and volatility. A partial salt formation could take place either in the air or later during the absorption in the bubble tube. Assuming

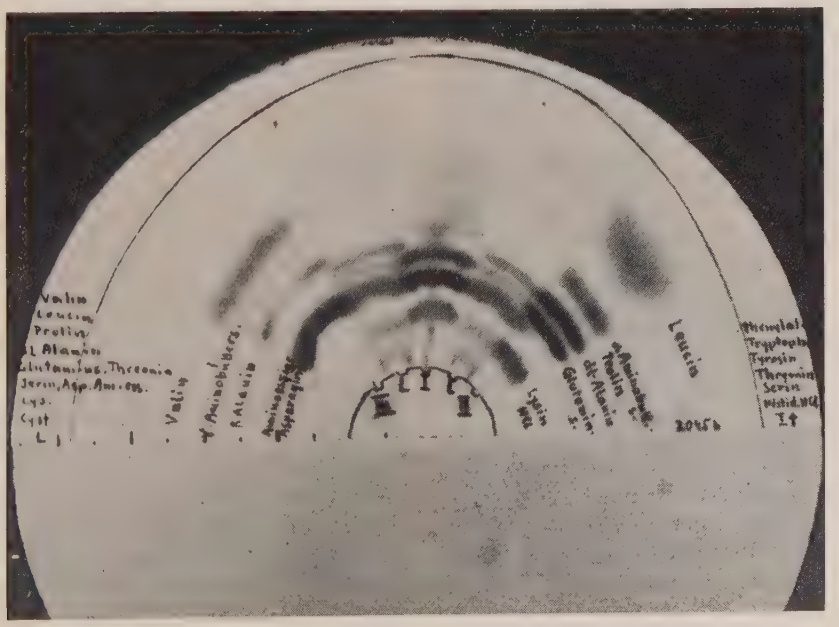


Fig. 5. Test substances and substances obtained from the air, chromatographically compared.
L — means the mixture of substances from the air.
I, II, III—the test substances used on the chromatogram.

that the last-mentioned reaction is of no great importance, at least a certain number of the substances found can be considered as amino acids, for the following reasons:

1. The substances obtained from the air behaved similarly to the amino acids used as test substances, both in chromatograms with a butanol/acetic acid/water-mixture as solvent (see fig. 5), and in those where the sample was divided and one part chromatographed with the above solvent, the other with water-saturated phenol.

2. The ninhydrinpositive substances did not show up if the chromatogram was treated with copper carbonate before its treatment with ninhydrin. According to CRUMPLER and DENT (1949), this is charateristic of $\alpha$-amino acids, as other ninhydrinpositive substances remain ninhydrinpositive after such treatment.

3. A spot which appeared yellowish after ninhydrin treatment, and which behaved similarly to proline used as a test substance, appeared after isatine-spraying as a faint blue. (A similar blue was shown by some of the other substances in question, and the same reaction is known for some amino acids.)

4. The only investigation of precipitation (snow) which was made showed ninhydrinpositive substances in such quantity that they remained unseparated on the chromatogram. As this sample was not subjected to any other treatment besides filtering and boiling down, formation of these substances, while being collected in the absorption-vessel, does not seem to take place. FONSELIUS' (1954) findings on amino acids in precipitation would support this view.

In cases where distinct positive results were obtained on the chromatogram, the concentrated absorption-fluid showed a yellowish tinge, a fact which agrees with the information the author received from Fonselius, who also got a yellowish residue from the distilled sample when investigating precipitations. Yellow-coloured substances had been observed as early as 1853 by BARRAL (1853) in rainwater and BOUSSINGAULT (1858) in fog. Both authors considered them as organic substances and found that they released ammonia on treatment with alkali. At MILLER'S (1953, 1955, 1957) successful experiments to produce amino acids under possible primitive earth conditions yellow polymers were formed too showing a very intense ultraviolet absorption.

From the chromatographic results, those substances isolated from the atmosphere seem almost certainly to be glycine, alanine, valine and leucine and (less certainly) glutamic acid, aspartic acid and proline.

The absence of ammonium acetate, which as a hygroscopic substance should have appeared, was remarkable. Only during longer experiments were hygroscopic substances found, particularly when only one filter was used for the whole experiment. It is possible that such small quantities of ammonia can be absorbed on the filter, or that it combines with sulphuric acid on the filter or in the absorption-fluid, thereby forming ammonium sulphate which is hardly hygroscopic.

**Relation to meteorological Factors**

On approximately 25 days out of more than 100 investigated days positive results were obtained. Among them were one third faintly positive. Though the strongly positive results were to some extent dependent on the prevailing air masses, the number of these results is too small (16) to establish a real relation. Considering all different tropical air masses together, positive results for tropical air masses were obtained 9 times, for mixed air masses 2 times, and for arctic 5 times. As tropical air masses prevailed during the testing period the results loose some of their significance. On the other hand, lightly foggy or hazy weather with high air-humidity and little altered or falling air pressure was, almost without exception, a precondition for positive results. On days with heavy fog the presence of these substances could not be proved, either because this kind of weather does not assist their formation or because they are absorbed by droplets too large to pass the filter. In this connection the only investigation of precipitation (snow), carried out on February 27th, 1958, may be mentioned. In that instance so great was the amount of ninhydrinpositive substances present that they remained chromatographically unseparated, whilst the air investigation of the same day showed a wholly negative result. Air investigations on the two preceding days, i.e. February 25th and 26th, 1958, days without precipitation, showed the presence of a large number of ninhydrinpositive substances. Of

course it is not possible to decide from this single test whether these substances are absorbed to a high degree by snow flakes (or rain drops). The much higher frequency of positive results obtained during the cold seasons with rather stagnant air masses and little turbulence may indicate a possible connection between the appearance of these substances and the combustion of solid and liquid fossil fuels. Nevertheless, more or less positive results were also found during the warm season, though only in small number. There existed no distinct correlation between the visible filter contamination and the occurrence of positive results. The substances found could also be derivatives of compounds diffused from the sewers and the nearby Danube Canal into the atmosphere, where they accumulate. In such places decomposition of organic matter may take place on a large scale, and under favourable atmospheric conditions these decomposition products may escape in relatively large quantities into the air. Suitable meteorological conditions would be falling or at least constant air pressure and a larger temperature gradient from the warmer sewers to the colder open air. Inversion layers and little air motion would favour an accumulation of these substances in the atmosphere, where they can be subjected to different chemical alterations. In this context it may be mentioned that according to CAUER (1956) a higher decomposition rate of organic substances and greater biological activity, whereby the so-called "ammoniacal substances" are formed, produce a rise in the pH-values of the atmospheric condensation water.

That the turbulence is of some importance could be concluded from the investigations run day and night in July, 1958, where the results obtained during the least turbulence (viz. in the early morning and evening) though poor, turned out to be better than those produced in investigations carried out at midday, the time of the highest turbulence, when there were almost no results at all. The vapour layer, which varies in thickness, according to the season, must also be considered. Since, according to LÖHLE cited after Band, 1957, the upper limit of the vapour layer lies during the cold season at approximate heights of 400—500 m, the thickness of this layer can increase by convection during summer to 3,000 metres and more. The differences of results between summer and winter may thus be at least partially explained, for during summer the substances looked for might be diluted to such an extent that they escape detection.

It could also be that some of the substances in question were assimilated by green plants during the vegetation period.

In general, negative or only faintly positive results proved to be independent of meteorological factors.

**Error analysis**

Among the various possible errors there are only a few relevant enough to alter the results significantly. Summarizing them, two main sources have to be distinguished:

1. errors which occur in taking and treating the sample,

2. those which may be due to chromatography.

With reference to 1.

a. Fluctuation of the air-intake volume is of no importance as qualitative results were the principal aim. The filter contamination after sucking 1 $m^3$ of air does not lower the flow-rate significantly. Only the air humidity seems to influence the flow-rate by altering the pore-size of the filters. This rather unimportant effect was compensated by adjusting the appropriate capillary in the capillary set. From the readings of the rotameter and manometer a flow-rate accuracy of $\pm$ 10% was established.

b. Two faults caused by the filtering could falsify the results qualitatively and quantitatively in a way difficult to correct and to estimate. The first, described by JUNGE (1956), is the considerable absorption of some gaseous air constituents by millipore filters. THOULET (1903), noted an extraordinary ammonia absorption on paper filters. Secondly, there is the possibility that substances absorbed on the filter react and that the reaction products diffusing after saturation through the filter show compounds which do not exist in the open air.

c. Owing to the cooling at the end of the apparatus and the low air flow-rate, losses of absorption-fluid by spraying and evaporation are, as measurements showed, insignificant.

d. Substances remaining in the frit after removal of the absorption-liquid have no influence on the investigations which follow; this is proved by the absence of any reaction after high positive results. Whether a loss of material in the process of the thorough cleaning of the absorption-vessel takes place would have to be investigated separately.

e. Losses during the evaporation depend on the vapour pressure of the substances under examination. As the evaporation of volatile substances was the purpose of the method used, this effect need not be considered as an error.

f. For the insolubility in water, par. e. applies, as only substances soluble in water were the aim of the investigation.

g. Any losses resulting from the application of the substances on the filter paper for chromatography need not be considered.

h. Finally, the argument that the acetic acid used may serve as culture medium for spores and bacteria passing the filter, must be taken into consideration. Owing to the low temperature, which is unfavourable to the growth of microorganisms, and the relatively short time between absorption and evaporation, the formation of these compounds seems very improbable, although not quite impossible. Such effects should certainly occur more frequently during the warm seasons, but in fact positive results from the air investigations were much more often obtained during the cold period. Finally, the finding of amino acids in precipitation by FONSELIUS (1954) and of ninhydrinpositive substances by the author in snow do not support the view of a genesis of these substances through bacterial activity in the absorption-fluid.

re. 2.

a. Not only the $R_f$-values themselves but also their relation to each other can be altered as well by the contamination of the substances examined with other compounds in the atmosphere, as by inconstant temperature during the chromatography. Also the colours of the developed chromatograms may to some extent be influenced by contamination. The variation of these possible hindrances to the chromatography is responsible for the impossibility of reproducing the chromatograms exactly. Hindering substances could be removed, for example, by ion exchange.

b. Especially in these chromatograms where heating is necessary for the removal of solvent, e.g. such as run with phenol, losses occur according to BRUSH, BONTWELL, BARTON and HEIDELBERGER (1951). Thus substances which are only present in low concentration may disappear in some chromatograms and so make it difficult to compare them with those where heating is not necessary.

**Summary and Discussions of Results**

On some days in the course of investigating the atmospheric air over a period of more than a year, ninhydrinpositive substances were found, which can fairly safely be considered as amino acids. Glycine, alanine, valine and leucine have been identifired almost to acertainty, glutamic acid, aspartic acid and proline less surely. Some of the substances may be amines. These substances appeared much more often and in greater quantity during the cold season. The amount of the individual compounds reached a maximum of a few $\gamma$ per $m^3$. A more abundant appearance of the substances was paralleled by a yellowish tinge of the concentrated absorption-fluid.

A direct connection with the atmospheric conditions and air masses could not be confirmed beyond doubt, but local meteorological factors like high humidity with haze, reduced visibility and falling or almost stable air pressure, indeed seem to be suitable conditions for the formation or preservation of these substances. The greater frequency of their appearance during the cold season can hardly be related to the combustion of liquid and solid fossil fuels alone. Meteorological factors prevailing at this season may be involved in the formation, preservation or decay of these compounds. Such meteorological factors could also stipulate conditions which enable nitrogen compounds, formed in connection with decomposition of organic matter in sewers and rivers to escape in greater amounts into the air and to accumulate there. To find a possible connection between the appearance of the above-mentioned substances and the different air masses, further investigations would have to be carried out simultaneously in several places. Independent of any hypothesis about the genesis and source of the substances found,

the changes they have to undergo by chemical or photochemical influences, must also be considered. Thus the genesis and preservation of the substances could be due to the simultaneous influence of certain local factors and of those which are effective over extended areas.

It is possible that in some methods of $NH_3$ determination a part of these substances is included.

Many nitrogen compounds have a direct effect on human organism and it seems possible, therefore that the amount of these compounds found on certain days in the atmosphere, may be sufficient to alter the pH-values of skin or mucous membranes (CAUER, 1956) or to cause troubles of an allergic nature in persons so disposed. But also these nitrogen compounds could become effective indirectly, through microorganisms whose growth, metabolism and augmentation they can further or hinder, characteristics which allow the determination of such substances by biological methods, i.e. with the aid of microorganisms. Thus the old miasma theory, however restricted or altered might possibly have some justification after all.

There may be a connection between these compounds and vegetation. The decrease of the substances could, during the vegetation period, be related to their assimilation by plants, the uptake of nitrogen compounds in small amounts by plant elements above ground being well known. Alternatively, WARBURG (1957) referred to the importance of two systems, alanine-aspartic acid and glutamic acid in connection with the carbon dioxide transfer at the photosynthesis of green plants. It would be of interest to know definitely whether a direct supply of those or other amino acids in the air would influence the assimilation by plants.

In view of limited means and the difficulties inherent in all kinds of investigations depending on meteorological factors, the results obtained cannot be considered as final. Therefore it may be of some interest to continue the investigations and to advance the position so far reached. By these and other investigations it seems already that known amino acids or substances closely related to them are, though in extremely small amounts, widely spread in nature outside of organic matter.

**Acknowledgement**

The author would like to thank Prof. G. Stetter, in whose institute he was allowed to carry out this work, for his advice, for reading and commenting on his manuscript and for means put at his disposal. Furthermore, he would convey his thanks to Mr. M. J. K. Biggs for supervising the English manuscript.

## REFERENCES

ABELSON, P. H., 1957: Some Aspects of Paleobiochemistry, *Annals of the New-York Ac. of Sciences* **69**, Art 2, p. 277.

ÅNGSTRÖM, A., HÖGBERG, L., 1952: On the Content of Nitrogen ($NH_4N$ and $NO_3N$) in Atmospheric Precipitation, *Tellus* **4**, p. 31.

BARRAL, M., 1853: Note sur l'analyse d'eaux de pluie recueillies et distillées dans la platine, *Comptes rendus* **36**, p. 184.

BOUSSINGAULT, M., 1858: Recherches sur la quantité d'acide nitrique contenue dans la pluie, le brouillard, la rosée (Suite), *Comptes rendus* **46**, p. 1175.

BRUSH, M. K., BONTWELL, R. K., BARTON, A. D., HEIDELBERGER, CH., 1951: Destruction of Amino Acids during Filter Paper Chromatography, *Science* **113**, p. 4.

CAUER, H., 1956: Die pH-Werte von Aerosolen in Niederschlägen und ihre lufthygienische und bioklimatische Indikatorbedeutung. *Zeitschrift für Aerosolforschung und Therapie*, Jahrgang V/6, p. 459.

CRUMPLER, H. R., DENT, C. E., 1949: Distinctive Tes for α-Amino-acids in Paper Chromatography, *Nature* **164**, p. 441.

ERDMAN, J. G., MARLETT, E. M., HANSON, W. E., 1954: Survival of Amino Acids in Marine Sediments, *Science* **124**, p. 1026.

FONSELIUS, S., 1954: Amino Acids in Rainwater, *Tellus* **4**, p. 90.

GIRI, K. V., RAO, N. A. N., 1952: A Technique for the Identification of Amino Acids separated by Circular Paper Chromatography, *Nature* **169**, p. 923.

JUNGE, CHR. E., 1956: Recent Investigation in Air Chemistry *Tellus* **8**, p. 127.

KATZ, M., 1956: City Planning, Industrial-Plant Location and Air Pollution, *Air Pollution Handbook* (Editors: P. L. Magill, F. R. Holden, Ch. Ackley) New-York—Toronto—London, McGraw-Hill Book Comp. Inc. 2—41.

LÖHLE, F., 1941: Sichtbeobachtungen vom meteorologischen Standpunkt, Berlin, cited by G. Band 1957

in: Ein Beitrag zur Globalstrahlung, *Geofisica pura e applicata* **37**, p. 230.

Miller, St. L., 1953: A Production of Amino Acids under Possible Primitive Earth Conditions, *Science* **117**, p. 528.

— 1955: Production of Some Organic Compounds under Possible Earth Conditions, *Journ. of the Am. Chem. Soc.* **77**, p. 2351.

— 1957: The Formation of Organic Compounds on the Primitive Earth, *Ann. of New-York Ac. of Sciences* **69**/2, p. 260.

Römpp, H., 1958: Filter und Filtrieren, *Chemielexikon* 4. Aufl., Franck'scher Verlag, Stuttgart, p. 1467.

Thoulet, G., 1903: Absorption de l'ammoniaque par l'eau de mer, *Comptes rendus* **136**, p. 477.

Treibs, A., 1934: Über das Vorkommen von Chlorophyll-Derivaten in einem Ölschiefer aus dem oberen Trias, *J. Liebigs Ann. d. Chemie* **509**, p. 103.

— 1934: Chlorophyll- und Hämin-Derivate in bituminösen Gesteinen, Erdölen, Erdwachsen und Asphalten, *J. Liebigs Ann. d. Chemie* **510**, p. 42.

— 1935: Chlorophyll- und Hämin-Derivate in bituminösen Gesteinen, Erdölen, Kohlen, Phosphoriten, *J. Liebigs Ann. d. Chemie* **517**, p. 172.

Warburg, O., 1957; O. Warburg zur Photosynthese (Report about a lecture of O. Warburg, Berlin, October 5th, 1957), *Naturwisenschaftliche Rundschau* **10**. Jahrg. 11, p. 427.

# Meteorological Fractionation of Nuclear Bomb Debris

By PER B. STOREBÖ, Norwegian Defence Research Establishment, Kjeller, Norway

(Manuscript received December 7, 1959)

*Abstract*

Radioactive particles are produced by nuclear bomb explosions which are widely different in size and nature. Systematic differences in properties are expected for particles formed under different conditions. Differences in particle properties may cause sorting during deposition because of systematic differences in weather trends at different geographical locations and thus bring to light information about the particles.

Deposits at a mountain station in Norway appear to have contained more short-lived fission products than those at lowland stations, especially during periods when considerable fresh fission products have been present in the atmosphere. This could be due to a substantial chemical fractionation on particle sizes taking place during formation, or to the general formation of particles somewhat larger than 0.5 micron diameter during high-yield explosions.

## 1. Introduction

Nuclear bomb explosions produce radioactive particles which are measured all over the world. The explosions are widely different in nature and size, and for each explosion, particle formation occurs over an interval of time during which physical conditions are drastically changed. Differences in particle size and composition are, therefore, to be expected.

If the world-wide distributions of radioactive deposition and air concentration are properly analyzed, influences of these differences might turn up. This question will be further examined.

## 2. Formation of particles

Part of the energy liberated in an explosion is used in evaporation of the bomb material and material from the ground. The resulting warm mass rises rapidly through the atmosphere, is cooled, and particles are formed.

STEWART ET AL. (1956) have microscopically examined bomb debris particles present in samples from the atmosphere and they found that most of the particles bore resemblance to condensation particles.

The conditions under which the particles are formed vary widely. Early substances in some decay chains are gaseous or very volatile, and particles starting to grow very early or very late in the condensation phase may be enriched or diminished in content of certain isotopes. Systematic differences may also arise between particles from larger and smaller bombs due to the slower cooling and later condensation for the former.

After formation, the particles may agglomerate. Some debris clouds may be held tightly together for a long time while others may be torn to pieces at once. The behaviour might be quite different for particles inserted into the dry and stable stratosphere than for those in the much more moist and turbulent troposphere.

Ground deposition of the particles is influenced by the weather, and because weather varies systematically from place to place, the particles may, to a certain degree, be sorted during deposition in such a way that different locations may get particles with different

physical and chemical properties. Such effects may appear between different climates or due to variations within climatic regions, between low and high level ground or between the leeward and windward side of mountain ridges where a predominant wind direction exists.

### 3. Representativity and analysis of samples

It seems to be plausible that in a climate with a reasonable amount of precipitation, pot samples of bomb debris are fairly representative for the content in precipitation. Such samples are taken regularly in Norway and Figure 1 shows a map over the southern part of the country with 4 sampling stations indicated.

The western part of Norway between the west coast and the top of a south-north mountain ridge forms an area where orographic precipitation very often occurs due to the mean westerly wind bringing moist air over the country. The air current crosses the mountain ridge and is forced to rise as it moves towards the top. This will strengthen precipitation systems and sometimes form precipitation in air masses where it otherwise would not occur. When streaming from the coast towards the mountain ridge, more and more precipitation is exhausted from the same air elements. New dry air entrained into the system tends to decrease the precipitation formed in that part of the clouds, and most precipitation might be expected to be formed in air which existed in the clouds when they crossed the coast. This effect will be most obvious when the air masses are stably stratified, which is often the case for the large precipitation systems giving the bulk of the precipitation in the area.

Fig. 1. Map of Southern Norway showing measurement stations. Mountain areas are shaded.

Most particles brought down with rain must for some time have resided in the lower air layers, where precipitation is more or less evenly or arbitrarily distributed. Air concentration of different particles in the cloudbearing layers will then be adjusted to conform with the quasi-constant removal fraction of particles and the rate of incorporation of new particles. When precipitation is suddenly strengthened orographically, a more rapid removal of particles sets in, and a new and lower air concentration of particles tends to be formed in accordance with the removal rate and the incorporation rate now existing. The adjustment will take some time, and one might expect an excess of particles most easily brought down at the start of the orographic area, at Bergen and Sola, and an excess of the more slowly captured particles towards the end of the area, at Finse.

The sampling periods for radioactive deposition are too long to make it possible to select convenient weather situations. The next best thing might be to add observations for such a long time that one may have a fair confidence that the mean conditions prevail. One month is regarded as a lower limit for Norwegian samples.

In this way some masking of an orographic fractionation effect must be expected because of the different origins of precipitation systems. Heavy precipitation may occur partly or all over the area with wind direction inside a large angle, nearly 180 degrees. Showers may occur, and although they may be orographically strengthened, the incorporation of new air is probably much greater than in the more stable precipitation systems. In the upper part of western Norway, precipitation also occurs when the wind comes from the east. The

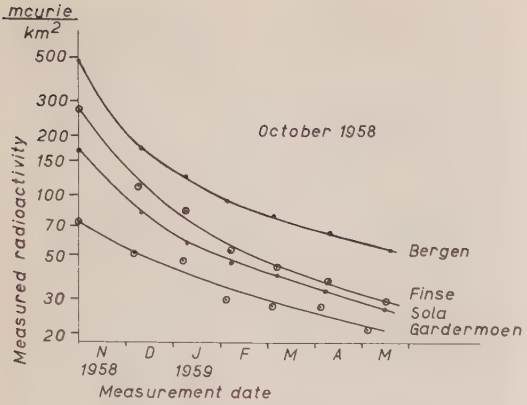


Fig. 2. Decay of October 1958 samples.

mountain station, Finse, lies however at the end of the orographical precipitation area also in this case, while Gardermoen has a position somewhat similar to that usually held by Bergen and Sola.

In one sampling period, the bulk of radioactivity in a sample from one station need not be deposited simultaneously with the bulk of the material at another station.

For meteorological fractionation processes time elapsed since explosion might be decisive, and equal weighting of all deposition with regard to time of deposition is desirable. This meets difficulties.

If $t$ is time since explosion, fission product activity varies roughly as $t^{-1.2}$. If, for instance, products four days old are deposited at the beginning of the month, they will be weighted only $^1/_{10}$ compared with similar products deposited at the end of the period, provided the samples are measured just after the end of the period. Measured one month after the end of the sampling period the former will be weighted about $^1/_2$ of the latter. For older products the weighting factor will be more nearly one, but a discrimination will always exist.

If particles of different ages exist in the samples, the older particles gain more weight the longer time elapses before measurements. A compromise must be sought if comparatively fresh fission products are to be measured. The author feels that if monthly samples are measured one month after the end of the sampling period, fair weight is given to both old and new particles.

From the actual decay curves of Figure 2 it appears that the Finse sample has a more rapid decay than the other samples. Due to the unique position of the Finse site, this is very interesting. For a closer inspection, a decay index has been used. This index is the ratio between the radioactivity of a sample measured six months after end of the sampling period and the radioactivity of the same sample measured one month after end of the period. A relatively high decay index indicates a relatively high content of isotopes with half-life longer than about 2 months.

The decay indices have been computed from smoothed decay curves covering 8—10

Fig. 3. Decay indices for monthly samples from July 1957 to April 1959.

months of measurements, and are assumed to be correct within 5 per cent. The variation with time has been plotted on Figure 3 for the four stations in question. The general impression is that the same pattern is roughly reproduced in all curves. The Finse decay index has however a tendency to be lower than the others, especially during periods when much fresh debris is present in the air, this appears as a dip on the curves. This feature might point to some sort of selection of particles in the deposits, the reason for which might be found in the mechanism of orographical precipitation.

**4. Discussion of measurements**

It was earlier mentioned that in an orographic precipitation region the particles most easily brought down by precipitation should be found in excess at the geographical beginning of the precipitation area, and other particles should be found in relatively greater amounts near the end of the precipitation area. It seems logical to associate the less rapid decay of radioactivity at Sola, Bergen and Gardermoen with the particles most easily brought down. The washout by precipitation may be due to the physical or chemical properties of the particles, but it is at present difficult to pursue the last possibility.

Particle capture by water droplets has been examined by GREENFIELD (1957). For larger particles capture by coalescence is predominant, for smaller particles capture by Brownian motion. The border between these two effects is found when the particle diameter is about 0.5 micron, and this corresponds to minimum capture efficiency.

Capture by coalescence will favour large droplets, and from LANGMUIR's (1948) or MASON's (1957) tables for the coalescence collection efficiency of droplets, it can be deduced that larger droplets have a higher probability for reaching the raindrop stage. Confronted with Greenfield's results, this means that larger particles should be more easily transported downward by rain than smaller particles. Deposition in precipitation may therefore cause more of the larger particles to be deposited at the lowland stations than at the mountain station. In the periods when the decay index at Finse is lower than at the other stations, it may be that the air pollution either consists of many large particles containing more medium and long-lived fission products, or many small particles containing more short-lived fission products, or both.

The enrichment of large particles with medium and long-lived fission products may be due to chemical fractionation during particle formation. Such an effect is generally dealt with by RAND (1953) and is used for explaining specific problems by STOREBÖ (1959) and EDVARSON ET AL. (1959). It may be mentioned that the authors of the last paper by use of gamma spectrometry on stratospheric samples have found enrichment of a certain mass number in large particles.

If the effect on the decay index on Figure 3 shall be most pronounced when the debris is young, the bulk of the large particles must be cleaned out of the atmosphere within some months after an explosion. For debris from small explosions this agrees with present opinion about residence time in the atmosphere before deposition. However if the large particles are identical with those found in stratospheric air samples (EDVARSON ET AL., 1959), they must have significant velocity of fall if they shall selectively disappear within some months. Calculations show (RAND, 1953, page 86) that a particle diameter about 5—7 micron should be in the right size range.

The other possible explanation of the meteorological fractionation effect is the presence of many small particles when the debris is young. During a test series of mixed small and high yield explosions, most radioactivity in the lower air layers is expected to originate from small bombs, because the bomb clouds do not rise through the tropopause. Most debris from high yield explosions is inserted in the stratosphere, and will generally remain there some time before being deposited. During this period much of the short-lived fission products will decay to a low level, and the particles, will appear as being composed of more long-lived fission products when they reach the ground. The described effect might appear if these particles are generally larger than particles from low yield explosions.

Particles from high yield explosions are generally spoken of as "very small" or "in submicron range". However, if the particles in worldwide fallout are condensation particles, the particle size in high yield explosions

might be larger than for low yield explosions. The rate of cooling of the debris vapour is much slower for the former, leading to a longer period of condensation phase. It is generally known in physics that condensation occurring under such circumstances tend to give larger condensation elements. This is counteracted by the lower atmospheric pressure at the heights at which condensation takes place, and by the greater dilution of the materials which may have taken place. On the other hand, more rapid agglomeration of the particles formed may occur in a particle cloud in the stratosphere due to less turbulent spreading and dilution afterwards.

It thus seems possible that the orographic effect examined here could be due to generally larger particles being formed in high yield explosions than in low yield explosions. The fact that differences in decay index are most pronounced when new debris is present in the troposphere, must then be explained by a lack of younger smaller particles at other times. This must also in this case be due to the rapid disappearance of debris from smaller bombs inserted only into the troposphere.

## 5. Conclusion

The meteorological fractionation of bomb debris in Norway indicates that a substantial part of the radioactivity might be associated with particles somewhat larger than 0.5 micron diameter, at least during periods when considerable fresh fission products are present. These particles contain, in the mean, less fission products with half-lives shorter than 1—2 months than is the case for the gross activity in the air.

Particles of this size have an appreciable rate of fall if times of years are considered, and they may have an heavy influence on the residence time of the bulk of the debris in the atmosphere. For estimates of bomb debris behaviour in the atmosphere, it might be necessary to take this into consideration. The exchange of air between stratosphere and troposphere may not play such an important part as thought earlier.

## Acknowledgments

The author would like to thank Mr. Stuart H. Small and Mr. H. Stuart Muench for reading and commenting upon the manuscript.

## REFERENCES

Edvarson, K., Löw, K., and Sisefsky, J., 1959: Fractionation Phenomena in Nuclear Weapons Debris. *Nature*, **184**, pp. 1771—1774.

Greenfield, S. M., 1957: Rain Scavenging of Radioactive Particulate Matter from the Atmosphere. *J. Meteor.*, **14**, pp. 115—125.

Langmuir, I., 1948: The Production of Rain by a Chain Reaction in Cumulus Clouds at Temperatures above Freezing. *J. Meteor.*, **5**, pp. 175—192.

Mason, B. J., 1957: *The Physics of Clouds*. Oxford, Clarendon Press, p. 424.

Rand Corporation, 1953: *World-Wide Effects of Atomic Debris. Project Sunshine*. R-251-AEC (Amended) AECU-3488.

Stewart, N. G., Crooks, R. N., and Fisher, E. M., 1956: *The Radiological Dose to Persons in the U.K. due to Debris from Nuclear Test Explosions prior to January 1956*. AERE HP/R 2017, Harwell.

Storebö, P. B., 1959: Orographical and Climatological Influences on Deposition of Nuclear Bomb Debris. *J. Meteor.*, **16**, pp. 600—608.

# Measurements of the Air Concentration of Gross Fission Product Radioactivity during the IGY July 1957—December 1958

By L. B. LOCKHART, Jr. and R. L. PATTERSON, Jr.

(Manuscript received January 29, 1960)

*Abstract*

Measurements of the gross fission product radioactivity in the air at 21 sites along the 80th meridian and 4 sites in the North Pacific area are reported for the period July 1957—December 1958. The activity levels at the various sites are related both to the stratospheric deposition of nuclear debris and to the direct introduction of radioactive material into the troposphere upwind of the collecting sites.

Radioactive debris injected into the troposphere at any particular site spreads rather rapidly throughout the same hemisphere but rarely crosses the equator in any quantity. An exception to this occurred during the Hardtack series in the Pacific when massive quantities of activity were transported to the Southern Hemisphere by winds in the upper troposphere.

It is again shown that periods of heavy rainfall, such as occur during the rainy season in Panama, cause a general decrease in the concentration of fission products in the air.

## 1. Introduction

In 1956 the U.S. Naval Research Laboratory, with the assistance of the U.S. Atomic Energy Commission, the U.S. Weather Bureau, and interested groups in Canada and South America, initiated a program of measurement of the fission product radioactivity in the air at a carefully selected group of sites along the 80th meridian. During 1957 this program was expanded to include collections at several other locations which were of interest to the U.S. Air Force Cambridge Research Center. This work has been carried out as part of the International Geophysical Year Program on Atmospheric Nuclear Radiation and was financed, in part, by the Division of Biology and Medicine, U.S. Atomic Energy Commission.

As the result of a study of several collecting devices (LOCKHART, JR., BAUS and BLIFFORD, JR., 1959), air filtration was found to be the method which gave the most readily interpretable information and which, in addition, furnished samples suitable for radiochemical analysis. It was further decided that data on the air concentration of fission products would be required ultimately for any understanding of the information obtained from methods which measure deposited radioactivity. The entire effort was therefore directed toward obtaining reliable measurements of the concentration of fission products in the ground-level air at the 25 collecting sites associated with this program (Table 1).

## 2. Experimental procedure

Each collecting station employed an identical positive-displacement blower having a free-air capacity of about 40 cubic feet per minute. The stations making daily air-filter

**Table 1. Collecting Sites Associated with the NRL/IGY Program of Atmospheric Nuclear Radiation**

| Station | Latitude | Longitude | Elevation (m) | Operator |
|---|---|---|---|---|
| **Daily Filter Collections** | | | | |
| Thule, Greenland | 76° 35′ N | 68° 35′ W | 259 | IGY Thule Coordinator, U.S. Air Force |
| Coral Harbour, N.W.T., Canada | 64° 12′ N | 83° 22′ W | 59 | Meteorological Branch, Department of Transport (Canada) |
| Moosonee, Ontario, Canada | 51° 16′ N | 80° 39′ W | 10 | Meteorological Branch, Department of Transport (Canada) |
| Bedford, Mass., USA | 42° 27′ N | 71° 22′ W | 80 | USAF Cambridge Research Center |
| Silver Hill, Maryland, USA (Washington, D.C.) | 38° 50′ N | 76° 57′ W | 88 | U.S. Weather Bureau |
| Columbia, S.C., USA | 33° 57′ N | 81° 07′ W | 69 | U.S. Weather Bureau |
| Miami, Florida | 25° 49′ N | 80° 17′ W | 4 | U.S. Weather Bureau |
| San Juan, Puerto Rico | 18° 26′ N | 66° 00′ W | 10 | U.S. Weather Bureau |
| Miraflores, Panama Canal Zone | 9° 00′ N | 79° 35′ W | 10 | Canal Zone Corrosion Laboratory U.S. Naval Research Laboratory |
| Bogotá, Colombia | 4° 37′ N | 74° 04′ W | 2640 | Instituto Geofisico de los Andes Colombianos |
| Quito, Ecuador | 0° 08′ S | 78° 26′ W | 2818 | Astronomic Observatory |
| Guayaquil, Ecuador | 2° 10′ S | 79° 52′ W | 7 | Meteorological Office |
| Iquitos, Peru | 3° 45′ S | 73° 11′ W | 117 | Corporación Peruana de Aeropuertos y Aviación Comercial (CORPAC) |
| Lima, Peru | 12° 06′ S | 77° 01′ W | 134 | Corporación Peruana de Aeropuertos y Aviación Comercial (CORPAC) |
| Huancayo, Peru | 12° 07′ S | 75° 20′ W | 3353 | Instituto Geofisico de Huancayo |
| Chacaltaya, Bolivia | 17° 10′ S | 68° 15′ W | 5220 | Universidad Mayor de San Andres, Laboratorio de Fisica Cosmica de Chacaltaya |
| Antofagasta, Chile | 23° 37′ S | 70° 16′ W | 519 | NASA Satellite Tracking Station |
| Porto Alegre, Brazil | 30° 02′ S | 51° 13′ W | 24 | Servico de Meteorologia |
| Santiago, Chile | 33° 27′ S | 70° 42′ W | 520 | Oficina Meteorologica de Chile |
| Puerto Montt, Chile | 41° 27′ S | 72° 57′ W | 5 | U.S. Weather Bureau |
| Punta Arenas, Chile | 53° 08′ S | 70° 53′ W | 3 | Oficina Meteorologica de Chile |
| **Weekly Filter Collections** | | | | |
| Drifting Station Alpha* | 83°-86° N | 110°-180° W | 3 | U.S. Weather Bureau/IGY |
| Mauna Loa, Hawaii, T.H. | 19° 28′ N | 155° 36′ W | 3394 | U.S. Weather Bureau/IGY |
| Pearl Harbor, Oahu, T.H. | 21° 22′ N | 157° 58′ W | 5 | U.S. Naval Air Station, Ford Island |
| Subic Bay, Philippines | 14° 49′ N | 120° 17′ E | 18 | U.S. Naval Station, Subic Bay |

*Station evacuated November 1, 1958.

collections used a circular piece of filter paper 8 inches in diameter which decreased the flow rate to about 30 cfm. Those stations making week-long collections employed a larger filter (17 × 13 inches) with a somewhat higher flow rate. The filter was an asbestos-based paper (U.S. Army Chemical Corps type 6) having essentially 100 % retention for particles as small as 0.3μ at the flow rate employed. The pumps were intercalibrated under standard conditions before being sent into the field and adjustments were made to take into account the effect of local conditions at each site on the flow rate. The equipment was housed in a louvered shelter to protect it from rain.

The exposed samples were returned to Washington, D.C., via air where they were ashed at 650° C and compressed to thin disks about 3 cm in diameter by an hydraulic press. Two weeks after collection, these were counted in an automatic sample changer which held each sample in turn under a shielded, end-window GM tube and recorded the time required to obtain a preset total of 2,000 counts.

Each day the count of a standard sample and the background were measured. The counter was calibrated against standards of filter paper ash of the same size and shape and containing known amounts of RaD (RaE) activity. The radioactivity has been reported in disintegrations per minute per cubic meter of air under the pressure existing at the collecting site.

### 3. Radioactivity profiles along the 80th Meridian

Profiles of the gross fission product concentration in the ground-level air along the 80th

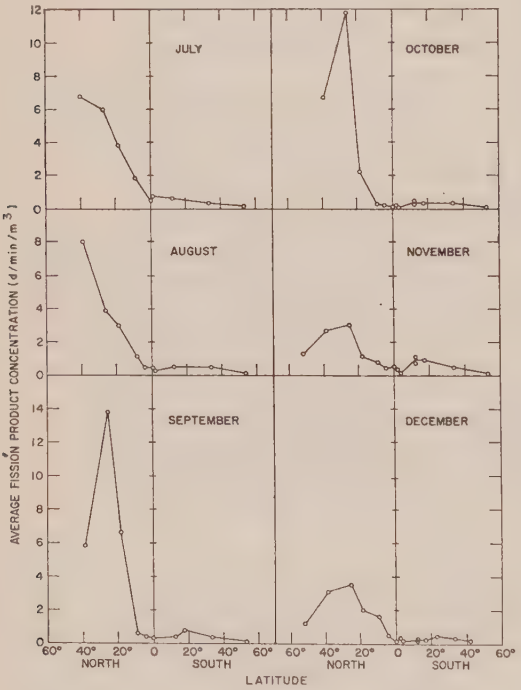


Fig. 1. Radioactivity Profiles, July—December 1957.

Meridian are shown in Figs. 1—3. The effect of nuclear tests can be readily noted by the increases in radioactivity of the air in the Northern Hemisphere during the Plumbbob tests in Nevada (May—October 1957), the Soviet tests of February and March 1958, when the effect lasted well into June, and the Soviet tests of 30 September—3 November 1958, when the effect was strong throughout the remainder of 1958 (and well into 1959). Neither of the U.S. test series of 1958 had any great effect in this hemisphere, though

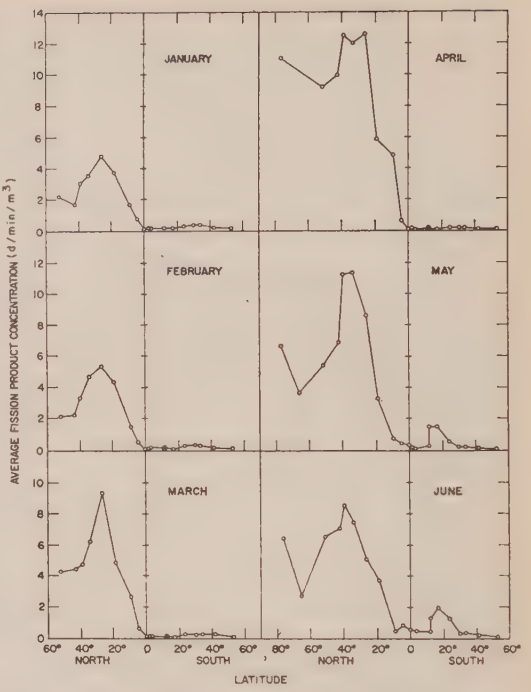


Fig. 2. Radioactivity Profiles, January—June 1958.

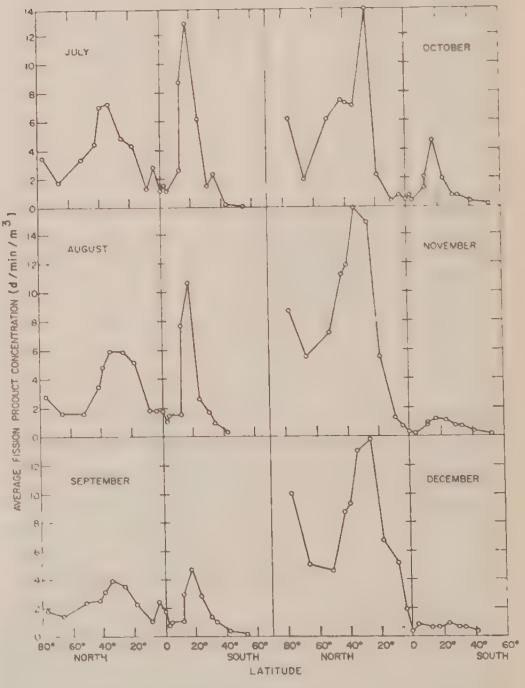


Fig. 3. Radioactivity Profiles, July—December 1958.

the presence of the debris from the Pacific tests of April—July was detected through the $W^{185}$ isotope produced in this series of tests as a tracer (LOCKHART, JR., BAUS, PATTERSON, JR. and SAUNDERS, JR., 1959). The Nevada tests of September and October 1958 were generally of small yield or were carried out underground.

In the Southern Hemisphere, where the background of radioactive debris was considerably lower, fresh injections of fission products were more readily noted. This is reminiscent of the conditions in the Northern Hemisphere some five years earlier. The residual activity present in South America during July and August 1957 was due principally to the British tests held at Christmas Island in June. A small effect may be noted during September from a test held at the Maralinga Proving Ground in South Australia, and a stronger but short-lived effect from the Christmas Island test of November 8, 1957. During January—April 1958, a period when no testing occurred south of the Equator, very low activities were encountered there in spite of the high activities prevalent in the Northern Hemisphere. The sharp gradient occurring near the Equator during April and again during December 1958 (and several times in early 1959) indicated that, in general, little transfer of particulate matter in the tropospheric air took place across this "barrier".

That sometimes the equatorial barrier breaks down became evident during the U.S. Hardtack tests in the Eniwetok-Bikini area during April—August 1958. The activity appearing primarily at Huancayo and Chacaltaya during May may have been due in part to the British test held at Christmas Island on April 28, 1958. The large amounts of $W^{185}$ tracer activity, however, identified the source of a large portion of this activity to have been the U.S. Pacific tests (LOCKHART, JR., BAUS, PATTERSON, JR., and SAUNDERS, JR. 1959). The enormous increases in activity during July and August, when the activity at some sites in South America for the first time exceeded that at all North American sites along the 80th Meridian, indicated a massive transfer of activity had taken place across the Equator. Radiochemical data has indicated that at least two bulk exchanges of air between the hemispheres occurred during May—July (LOCKHART,

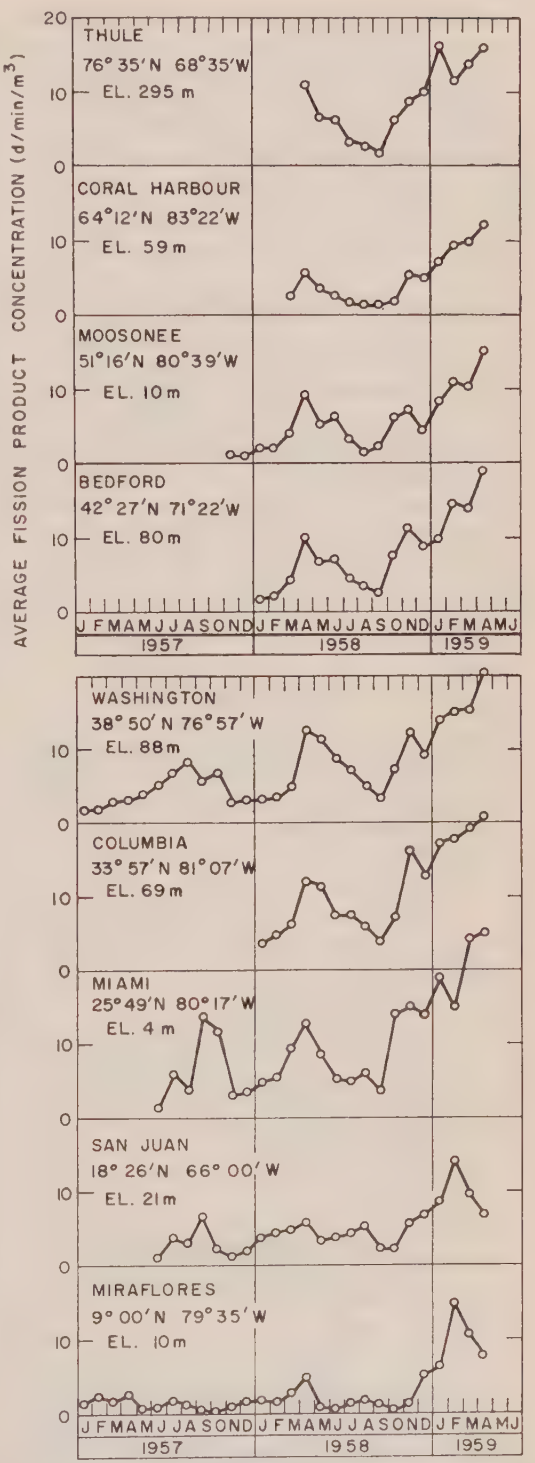


Fig. 4. Fission product radioactivity in the air of the Northern Hemisphere.

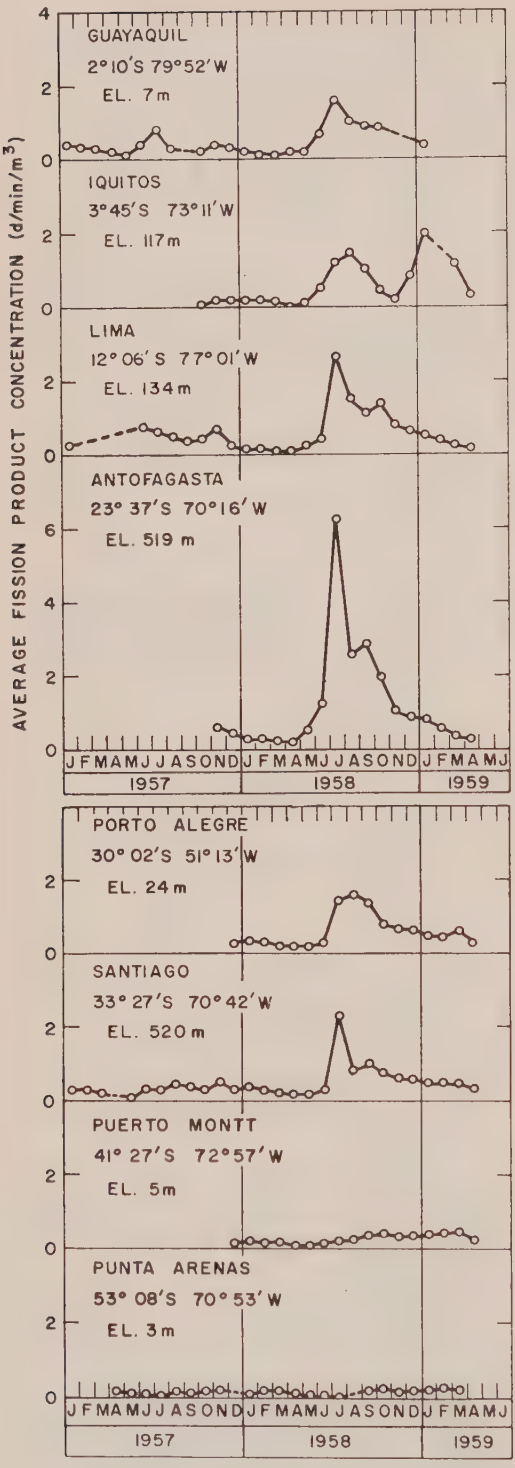


Fig. 5. Fission product radioactivity in the air of the Southern Hemisphere.

Jr., Baus, Patterson, Jr. and Saunders, Jr. 1959).

It is important at this point to consider the mechanism by which this activity crossed the Equator. In the Northern Hemisphere high fission product concentrations were found in the Philippines during May and July (Fig. 7) and in Japan during early July (Lockhart, Jr. 1959), which were obviously due to the transport of activity from the test site to collecting station by winds of the lower troposphere. (Prevailing winds at lower altitudes in the test area are easterlies.) The debris appearing in South America, initially at the high altitude stations, must have been carried primarily by winds in the upper troposphere, which could account for their rapid transport and rapid detection at ground level. A large fraction of the activity, however, must have gone into the stratosphere as this normally occurs with explosions of high yield. (In fact, $W^{185}$ from the Hardtack series of tests has been found at all collecting sites more than a year after the tests, demonstrating that debris from this series did contribute to the stratospheric inventory of radioactivity.)

## 4. Variations of activity concentrations with time

The data presented in the radioactivity profiles has been replotted in Figs. 4—6 to show the changes in activity levels with time, and to show the relative arrival times of debris at the different sites. The principal point of interest in the curves made at sites along the 80th Meridian in the Northern Hemisphere (Fig. 4) is the apparent lack of response to the U.S. Pacific Tests of 1958 and the long-continuing, high levels of activity caused by the Soviet tests of October and November 1958. Radiochemical data, however, does indicate the presence of some Hardtack debris at these sites. The highest monthly averages of activity ever encountered at any of these sites were recorded in early 1959, months after any nuclear explosion had taken place. Because of the age of the fission product mixtures, they must have been relatively rich in such longer-lived isotopes as $Sr^{90}$, $Cs^{137}$ and $Ce^{144}$.

In Fig. 5, similar curves for the Southern Hemisphere show the great effect of the U.S. Pacific tests of 1958 on the radioactivity of

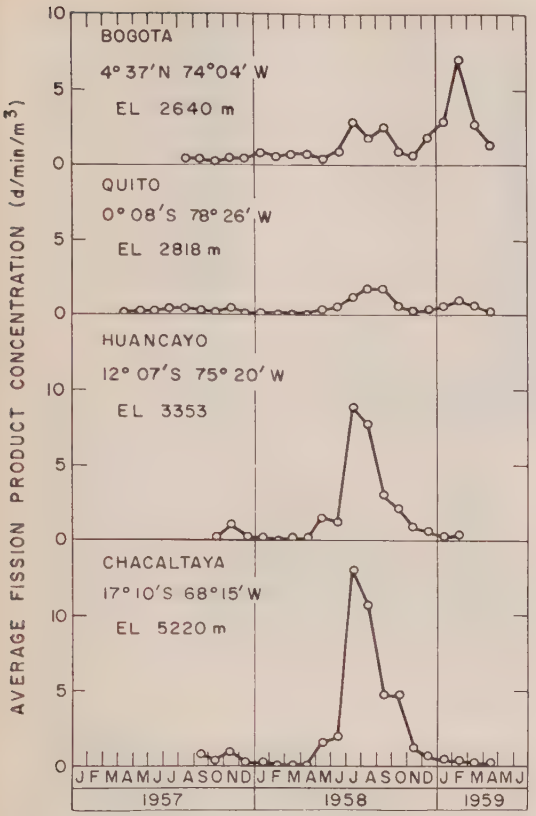
BOGOTA
4° 37′N 74°04′ W
EL 2640 m
QUITO
0° 08′S 78° 26′ W
EL 2818 m
HUANCAYO
12° 07′S 75° 20′ W
EL 3353
CHACALTAYA
17° 10′S 68° 15′W
EL 5220 m
AVERAGE FISSION PRODUCT CONCENTRATION (d/min/m³)
J F M A M J J A S O N D J F M A M J J A S O N D J F M A M J
1957
1958
1959

Fig. 6. Fission product radioactivity in the air at high altitude sites in South America.

the air at latitudes as far as 33° S (Santiago). The low response at Puerto Montt and Punta Arenas is noteworthy. The high altitude stations in South America are shown separately in Fig. 6 on a scale intermediate to those of Figs. 4 and 5. The maximum response to the U.S. Pacific tests occurred at the high altitude sites some 750 to 1,000 miles south of the Equator rather than at those sites due east of the test area. During the last months of 1958 and in early 1959, Bogotá (4° 37′ N) showed the typical behavior of stations north of the Equator, while Quito (0°) and the more southerly stations showed a return to the low background of fission products in the air which has been typical to the Southern Hemisphere.

In Fig. 7, the monthly average concentrations of fission products in the air are shown for the stations in the North Pacific area where week-long collections were made. The activity pattern at Drifting Station Alpha in the Arctic was not unlike that at Thule and Coral Harbour; the lack of sharpness of the maxima at Drifting Station Alpha and at Coral Harbour was due to the longer elapsed time between collection and counting at these sites occasioned by transportation difficulties, with the result that fresh fission product collections underwent considerable radioactive decay before being assayed.

Results from the triad of stations at Pearl Harbor, Mauna Loa, and Subic Bay are most interesting in that the activity patterns are so different. Pearl Harbor responded more strongly to the Soviet tests of early 1958 than did Mauna Loa, which is less than 200 miles away but situated at an altitude of 3,394 meters. (Actually, the gross activity per unit mass of air was higher at Mauna Loa, but radiochemical analyses indicated the debris there consisted of an older fission product conglomerate than that at Pearl Harbor.) This would indicate that the

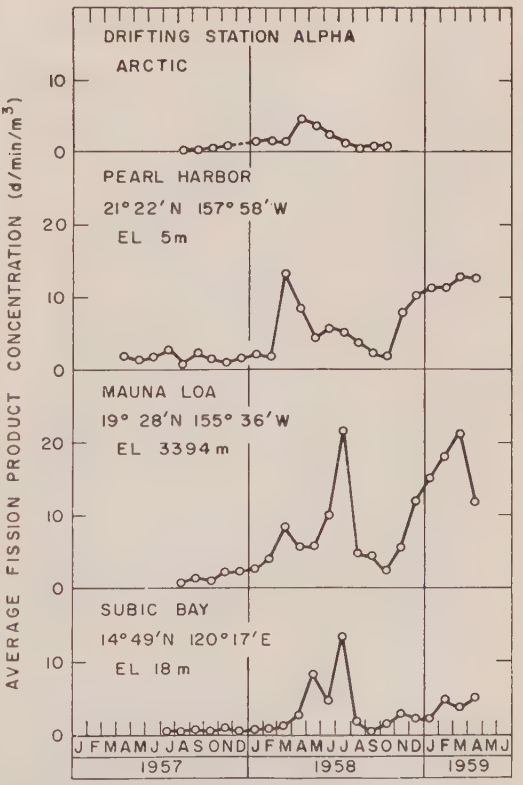
DRIFTING STATION ALPHA
ARCTIC
PEARL HARBOR
21° 22′N 157° 58′W
EL 5m
MAUNA LOA
19° 28′N 155° 36′W
EL 3394 m
SUBIC BAY
14° 49′N 120° 17′E
EL 18 m
AVERAGE FISSION PRODUCT CONCENTRATION (d/min/m³)
J F M A M J J A S O N D J F M A M J J A S O N D J F M A M J
1957
1958
1959

Fig. 7. Fission product radioactivity in the air at sites in the North Pacific area.

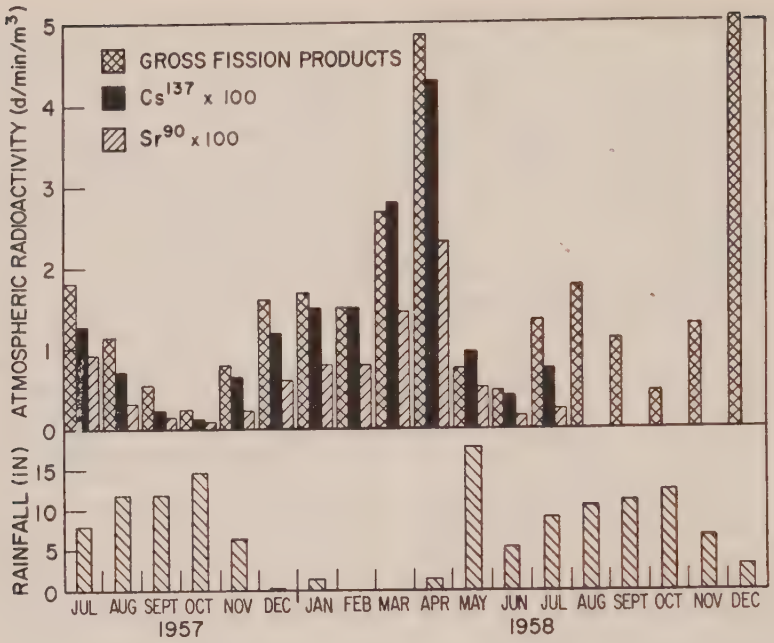
GROSS FISSION PRODUCTS
Cs137 x 100
Sr90 x 100
ATMOSPHERIC RADIOACTIVITY (d/min/m3)
RAINFALL (IN)
JUL AUG SEPT OCT NOV DEC JAN FEB MAR APR MAY JUN JUL AUG SEPT OCT NOV DEC
1957
1958

Fig. 8. Relationship between rainfall and the radioactivity of the air at Miraflores, Panama Canal Zone.

contamination was brought into this area by winds of the lower troposphere. Subic Bay received little activity from the USSR tests of either the spring or fall of 1958, but did intercept large quantities of debris from the U.S. Pacific series of 1958 (Hardtack) in both May and July. The transport of the activity was again by the prevailing easterlies of the lower atmosphere. Mauna Loa experienced its highest activity in July, also from Hardtack debris. Tungsten-185 data showed no Hardtack debris were collected at either Pearl Harbor or Mauna Loa during May. During the months of June and July, the contamination due to Hardtack debris was over ten times greater at Mauna Loa than at Pearl Harbor. This is consistent with the observations made at the South American sites where debris from these tests in the Eniwetok-Bikini area appeared in highest concentration at the high altitude sites.

### 5. Effect of rainfall on the radioactivity of the air

The relationship between rainfall and fallout is of great interest since rain is considered to be the principal mechanism by which radioactivity is removed from the air. Some work on this problem was done at NRL a number of years ago (Blifford, Jr., Lockhart, Jr. and Rosenstock, 1952; King, Lockhart, Jr., Baus, Patterson, Jr., Friedman and Blifford, Jr., 1956). More recently, a correlation of the gross radioactivity in the air with the rainfall at Miraflores, Panama, has been reported (Lockhart, Jr., Baus and Blifford, Jr., 1959). As would be expected, the lowest air concentrations of fission products were obtained during the rainy season. New data on the relation between rainfall and fission products in the air at Panama are shown in Fig. 8. Here the monthly average $Sr^{90}$, $Cs^{137}$, and gross fission product activities are plotted against the total rainfall during the month. The increase in the air activity during the period December 1957—April 1958 correlates well with the dry season. The large increase in April must have been due at least in part, however, to the Soviet tests of February 23 to March 22. This is confirmed by the decrease in the amounts of $Sr^{90}$ and $Cs^{137}$ relative to the gross fission products during April as compared to the earlier months. Nevertheless, there is evidence of a spring maximum in

stratospheric deposition since the ratio of $Sr^{90}$ activity to the gross fission product activity was too high to be representative of fresh debris. It seems that both increased stratospheric fallout and fresh debris were involved. In May the advent of the rainy season resulted in a great decrease in the total activity in the air and an apparent increase in the age of the radioactive material. The migration of tropospheric debris to this area was so inhibited by

**Table 2. Monthly Maxima of Fission Product Concentrations at Sites along the 80th Meridian during July 1957—December 1958**

**Activity in micromicrocuries per cubic meter of air[1]**

| Location | 1957 | | | | | |
|---|---|---|---|---|---|---|
| | July | Aug. | Sept. | Oct. | Nov. | Dec. |
| Thule | — | — | — | — | — | — |
| Coral Harbour | — | — | — | — | — | — |
| Moosonee | — | — | — | — | 2.5 (4) | 1.27 (26) |
| Bedford | — | — | — | — | — | — |
| Washington | 16.6 (22) | 23.7 (12) | 8.9 (24) | 7.0 (10) | 3.3 (1) | 3.0 (28) |
| Columbia | — | — | — | — | — | — |
| Miami | 7.9 (22) | 6.2 (27) | 32.3 (25) | 22.9 (6) | 5.9 (4) | 2.7 (25) |
| San Juan | 4.1 (26) | 6.0 (3, 25) | 19.2 (30) | 2.6 (15) | 1.32 (11) | 2.9 (11) |
| Miraflores | 3.2 (10) | 1.41 (15) | 1.62 (7) | 0.75 (2) | 1.47 (1) | 1.16 (4, 5) |
| Bogotá | — | 0.72 (1) | 0.28 (8, 12) | 0.19 (4) | 0.72 (29) | 0.59 (13) |
| Quito | 0.75 (7) | 0.52 (4) | 0.27 (12) | 0.09 (5) | 1.10 (19) | 0.14 (1, 19) |
| Guayaquil | 0.71 (10) | 0.32 (2) | — | 0.21 (16) | 0.52 (25) | 0.37 (4) |
| Iquitos | — | — | — | 0.09 (6, 8) | 0.29 (21) | 0.32 (8) |
| Lima | 0.71 (25) | 0.53 (15) | 0.39 (30) | 0.82 (31) | 0.89 (4) | 0.17 (13) |
| Huancayo | — | — | — | 0.31 (29) | 1.78 (19) | 0.22 (4) |
| Chacaltaya | — | — | 0.56 (23) | 0.38 (28) | 1.32 (21, 22) | 0.51 (1) |
| Antofagasta | — | — | — | — | — | 0.62 (4) |
| Porto Alegre | — | — | — | — | — | — |
| Santiago | 0.44 (17) | 0.46 (31) | 0.46 (26) | 0.38 (21) | 0.80 (23) | 0.22 (20) |
| Puerto Montt | — | — | — | — | — | 0.17 (28) |
| Punta Arenas | 0.09 (22,28) | 0.34 (17) | 0.14 (26) | 0.21 (21) | 0.16 (1) | — |

| Location | 1958 | | | | | |
|---|---|---|---|---|---|---|
| | Jan. | Feb. | Mar. | Apr. | May | June |
| Thule | — | — | — | 14.1 (2) | 6.4 (5) | 7.8 (8) |
| Coral Harbour | — | — | — | — | 3.9 (14) | 3.3 (25) |
| Moosonee | 1.92 (10) | 1.81 (20) | 4.0 (28) | 7.6 (4) | 5.5 (5) | 6.6 (4) |
| Bedford | 2.2 (14) | 2.5 (7) | 9.8 (29-31) | 9.9 (4) | 11.8 (1) | 5.7 (7, 30) |
| Washington | 3.1 (17) | 3.4 (22) | 10.0 (31) | 11.8 (6) | 13.6 (1) | 8.4 (15) |
| Columbia | 3.9 (21) | 3.5 (6) | 9.1 (11) | 13.1 (7) | 10.7 (9) | 7.7 (1) |
| Miami | 5.1 (13) | 4.4 (20) | 17.0 (24) | 13.1 (20) | 12.4 (16) | 5.1 (7) |
| San Juan | 4.6 (14) | 4.4 (6) | 5.0 (3) | 7.8 (27) | 5.2 (1) | 3.3 (13) |
| Miraflores | 2.4 (19) | 1.22 (7) | 1.82 (12) | 6.9 (19) | 1.24 (1) | 0.54 (15) |
| Bogotá | 0.92 (14) | 0.64 (26) | 0.73 (23) | 0.96 (7) | 0.76 (26) | 1.15 (2) |
| Quito | 0.23 (21) | 0.15 (5) | 0.09 (25) | 0.17 (24) | 0.71 (27) | 1.36 (3) |
| Guayaquil | 0.13 (6) | 0.16 (5, 16) | 0.20 (19) | 0.22(24, 26) | 0.32 (23) | — |
| Iquitos | 0.28 (17) | 0.28 (9) | 0.25 (22) | 0.14 (3) | 0.12 (7) | 0.50 (3) |
| Lima | 0.11 (5, 15) | 0.14 (11) | 0.09 (6, 31) | 0.12 (12) | 0.50 (17) | 0.79 (11) |
| Huancayo | 0.14 (17) | 0.09 (1) | 0.10 (25) | 0.07 (29) | 2.7 (26) | 2.5 (30) |
| Chacaltaya | 0.14 (30) | 0.14 (1) | 0.07 (16) | 0.09 (25) | 3.4 (28) | 5.7 (29) |
| Antofagasta | 0.27 (31) | 0.42 (5) | 0.22 (3) | 0.18(21, 22) | 0.99 (31) | 1.22 (5) |
| Porto Alegre | 0.39 (29) | 0.26 (10) | 0.25 (9) | 0.17 (1, 14) | 0.14 (4) | 0.52 (9) |
| Santiago | 0.26 (10) | 0.24 (8) | 0.20 (16) | 0.17 (8, 9) | 0.12 (20, 30 | 0.53 (30) |
| Puerto Montt | 0.18 (25) | 0.14 (6) | 0.24 (3) | 0.09 (18) | 0.11 (13) | 0.44 (21) |
| Punta Arenas | 0.12 (6) | 0.14 (21) | 0.16 (7) | 0.12 (30) | 0.07 (14) | 0.07 (30) |

| Location | 1958 | | | | | |
|---|---|---|---|---|---|---|
| | July | Aug. | Sept. | Oct. | Nov. | Dec. |
| Thule | 4.0 (8) | 3.7 (15) | 1.88 (27) | 13.0 (26) | 7.2 (8, 27) | 9.2 (27) |
| Coral Harbour | 2.8 (3) | 1.59 (30) | 1.42 (4) | 2.4 (20, 30) | 6.0 (4) | 4.4 (26) |
| Moosonee | 4.0 (15) | 1.57 (6) | 3.3 (25) | 8.9 (24) | 8.8 (3) | 4.9 (31) |
| Bedford | 5.3 (3) | 3.2 (8) | 2.2 (16) | 18.1 (18) | 10.9 (4) | 7.7 (13) |
| Washington | 8.0 (3) | 5.1 (7) | 4.9 (11) | 11.1 (22) | 10.9 (15) | 7.0 (2) |
| Columbia | 8.4 (18) | 4.3 (11) | 3.0 (11) | 10.6 (13) | 12.8 (15) | 12.8 (1) |
| Miami | 3.5 (31) | 4.8 (1) | 5.3 (5) | 18.9 (31) | 29.9 (3) | 19.3 (1) |
| San Juan | 3.6 (30) | 4.0 (2) | 2.4 (3) | 2.8 (31) | 7.0 (6) | 5.7 (14) |
| Miraflores | 1.58 (21) | 1.32 (9, 22) | 1.30 (8) | 0.54 (27) | 1.89 (13) | 4.5 (16, 19) |
| Bogotá | 4.5 (21) | 2.3 (1) | 2.4 (10) | 1.09 (5) | 1.29 (1) | 2.0 (12) |
| Quito | 1.86 (21) | 2.3 (15, 24) | 1.96 (24) | 1.13 (14) | 0.31 (20) | 0.45 (14) |
| Guayaquil | 2.0 (14) | 0.95 (14) | 0.87 (2) | — | — | — |
| Iquitos | 1.15 (15) | 1.43 (7) | 1.21 (14) | 0.39 (5) | 0.17 (5, 30) | 1.03 (30) |
| Lima | 3.3 (13) | 1.54 (11) | 1.39 (6) | 1.52(24,26) | 0.86 (16) | 0.87 (13) |
| Huancayo | 7.3 (19) | 7.7 (6) | 3.2 (25) | 3.3 (9) | 1.56 (3) | 0.55 (8, 10) |
| Chacaltaya | 15.6 (6) | 10.4 (7) | 4.3 (2) | 7.8 (9) | 1.79 (1) | 0.58 (8) |
| Antofagasta | 6.6 (18) | 3.2 (17) | 5.2 (4) | 3.9 (4) | 0.88 (7) | 0.69 (3) |
| Porto Alegre | 1.78 (27) | 3.5 (16, 17) | 2.1 (21) | 0.65 (28) | 1.03 (15) | 0.43 (2, 22) |
| Santiago | 2.9 (11, 12) | 1.65 (14) | 1.35 (28) | 0.84 (8) | 0.96 (1) | 0.54 (6) |
| Puerto Montt | 0.54 (9) | 0.35 (1) | 0.50 (10, 11) | 0.67 (22) | 0.51 (23) | 0.36 (29) |
| Punta Arenas | 0.07 (12) | — | 0.21 (7, 8) | 0.98 (1) | 0.16 (4) | — |

Note: Figures in parentheses refer to the day (or days) on which the maximum occurred (date of end of collection).

[1] 1 $\mu\mu$ curie/m$^3$ = 10$^{-18}$ curie/cc.

rain that the radioactivity collected was more nearly representative of stratospheric material. During June, but especially during July, some fresh material from the Hardtack tests did penetrate to this Panama site in spite of the rainy weather. This is shown by the low $Sr^{90}$ and $Cs^{137}$ values relative to the gross activity and also was demonstrated by the presence of $W^{185}$ activity in the air filter collections. (No radiochemical analyses of Panama collections were made after July 1958.)

### 6. Maxima of fission product concentrations

In Table 2 the maxima readings of the concentration of fission products in the air for each month of the IGY are compared in terms of micromicrocuries per cubic meter of air. The two highest concentrations were recorded at Miami, Florida: 32.3 $\mu\mu$ c/m$^3$ on September 25, 1957 and 29.9 $\mu\mu$c/m$^3$ on November 3, 1958. These maxima occurred during periods when tests were being carried out both by the United States (Nevada) and the Soviet Union. The maximum concentration in South America was recorded at Chacaltaya, Bolivia, for the 24-hour collection ending July 6, during the U.S. Hardtack tests in the Pacific. This value of 15.6 $\mu\mu$ c/m$^3$ is some seven times that recorded in June 1957 at Lima, Peru, following U.K. tests at Christmas Island (LOCKHART, JR., BAUS and BLIFFORD, JR., 1959).

### 7. Conclusions

The fission product radioactivity of the air increased markedly in the Northern Hemisphere during 1958 as the result of the intensive test programs carried out there during this period. This activity has continued to increase during early 1959 because of the delayed deposition of debris injected into the stratosphere by the recent high-yield nuclear explosions. (In spite of this great increase in the quantity of nuclear debris in the air, this material still contributes only a small fraction of the total radioactivity in the ground-level air.)

Radioactive debris injected into the troposphere at any particular site spread rapidly throughout the entire hemisphere but rarely cross the Equator in quantity. An exception to this

rule occurred during the U.S. Hardtack series in the Pacific (1958) when massive quantities of activity were transported to the Southern Hemisphere by winds in the upper troposphere. Radiotungsten ($W^{185}$) produced during the Pacific Hardtack tests has enabled debris from this one series to be traced as they spread throughout the ground-level air of both the Northern and Southern Hemispheres.

Periods of heavy rainfall, such as occur during the rainy season at Panama, cause a general decrease in the concentration of fission products in the air.

**Acknowledgement**

The authors wish to express their appreciation to the personnel at the various collecting sites whose cooperation has made this program possible.

## REFERENCES

Blifford, Jr., I. H., Lockhart, Jr., L. B. and Rosenstock, H. B., 1952: "On the Natural Radioactivity in the Air", *J. Geophys. Res.* **57**, p. 499.

King, P., Lockhart, Jr., L. B., Baus, R. A., Patterson, Jr., R. L., Friedman, H. and Blifford, Jr., I. H., 1956: "RaD, RaE and Po in the Atmosphere", *Nucleonics* **14**, p. 78.

Lockhart, Jr., L. B., Baus, R. A. and Blifford, Jr., I. H., 1959: "Fission Product Radioactivity in the Air Along the 80th Meridian — January—June 1957", *Tellus* **11**, p. 83.

Lockhart, Jr., L. B., Baus, R. A., Patterson, Jr., R. L. and Saunders, Jr., A. W., 1959: "Contamination of the Air by Radioactivity from the 1958 Nuclear Tests in the Pacific", *Science* **130**, p. 161.

Lockhart, Jr., L. B., Baus, R. A., Patterson, Jr., R. L. and Saunders, Jr., A. W., 1959: "*Radiochemical Analyses of Air-Filter Samples Collected During 1958*", NRL Report 5390.

Lockhart, Jr., L. B., 1959: "Atmospheric Radioactivity Levels at Yokosuka, Japan, 1954—1958", *J. Geophys. Res.* **64**, p. 1445.

# Wet and Dry Deposition of Fallout Materials at Kjeller

By S. H. SMALL, Norwegian Defence Research Establishment, Kjeller, Norway

(Manuscript received December 7, 1959)

*Abstract*

Daily measurements of fallout air activity and deposited activity at Kjeller, Norway, from 1 Sept. 1956 to 30 Sept. 1959 are given as monthly means for days with and without obvious precipitation. It seems that significant concentrations of fallout particles reach the earth about 3 months after high-yield test explosions. Dry deposition may reduce the amounts of fallout materials available for capture by precipitation.

## 1. Introduction

It has been thought for some time that particle sizes vary with yield (PROJECT SUNSHINE, 1953, p. 19), and this could have an important effect upon the general pattern of world-wide deposition. It is not an easy matter to measure particle sizes directly, and it is therefore interesting to see what might be deduced from routine measurements of air activity and deposited activity.

An apparent relationship between surface-air activity and deposition with precipitation has already been pointed out (STOREBÖ, 1957), and it might be important to see if dry deposition and surface-air activity are connected in any way. This could help in forecasting the extent of dry deposition in very dry periods.

It is shown here that wet and dry deposition and surface-air activity may all be interrelated, and that the amounts of fallout materials available for capture by precipitation may depend upon the amounts of materials removed from near-surface air layers by processes of dry deposition.

## 2. Measuring procedures

Daily samples of suspended particles are collected by drawing about 400 $m^3$ of air through asbestos fibre filters at a height of about 2 m. The exposed filters are ashed and measured with an end-window beta counting tube after a delay of 48 hours. The counting arrangement is calibrated with potassium 40.

Samples of deposited materials are collected in open vessels which are emptied daily. When necessary the vessels are washed-out with distilled water. Samples are dried by infra-red lamps and measured in the same way as air dust samples. Precipitation amounts are determined from wet sample volumes.

## 3. Basic data

Daily measurements made at Kjeller during the period 1 Sept. 1956—30 Sept. 1959 have been divided into two groups, covering days with and without obvious precipitation. Monthly means of air activity and deposited activity have been calculated for each of these groups. Monthly means of deposition velocity $\left(\frac{\text{rate of deposition of activity per unit area}}{\text{conc. of activity per unit volume of air}}\right)$ and air to precipitation activity ratios for equal volumes, have also been calculated. Average precipitation activity and average daily air activity have been determined for different total amounts of daily precipitation.

Measurement data for Kjeller have been published in several earlier reports (HVINDEN,

**Table 1. Mean daily values of air activity and deposition on apparently dry days for each month between 1 Sept. 1956 and 30 Sept. 1959.**

| | 1956 | | 1957 | | 1958 | | 1959 | |
|---|---|---|---|---|---|---|---|---|
| | average air activity (dry days) $\mu\mu c/m^3$ | average daily deposition on dry days $\mu\mu c/cm^2$ | | | | | | |
| Jan. | | | 0.61 | 173 | 0.35 | 204 | 1.23 | 1161 |
| Feb. | | | 0.43 | 89 | 0.59 | 119 | 2.71 | 1147 |
| Mar. | | | 0.73 | 230 | 1.59 | 478 | 3.08 | 1324 |
| Apr. | | | 1.11 | 469 | 2.32 | 1132 | 3.04 | 1195 |
| May | | | 1.95 | 868 | 1.60 | 1354 | 4.50 | 1629 |
| June | | | 1.13 | 516 | 2.50 | 764 | 2.12 | 538 |
| July | | | 0.45 | 564 | 2.54 | 843 | 1.55 | 436 |
| Aug. | | | 0.70 | 166 | 0.57 | 432 | 0.53 | 256 |
| Sept. | 0.76 | 2254 | 0.84 | 290 | 1.11 | 1012 | 0.28 | 119 |
| Oct. | 0.97 | 803 | 1.30 | 325 | 1.86 | 2408 | | |
| Nov. | 0.61 | 761 | 0.45 | 218 | 2.18 | 2532 | | |
| Dec. | 0.67 | 728 | 0.34 | 210 | 1.43 | 793 | | |

1959), but are treated in a new way in this report. Daily routine measurements were started in the Spring of 1956, but results for the first 6 months have not been used in the investigation because of uncertainties in distinguishing between wet and dry days. A new system of recording data was started in Sept. 1956.

A number of measurements from March 1959 have been rejected because of minor accidental releases of I—131 from a nearby isotope laboratory.

## 4. Dry deposition

Monthly means of air activity and deposited activity on apparently dry days are given in table 1, the values being plotted in fig. 1.

Most of the points in figure 1 lie quite close to a line drawn through the point determined by the average values of air activity and deposited activity for the whole period. There are however a few points which obviously do not follow the general trend, and it might be important to find out why this is so.

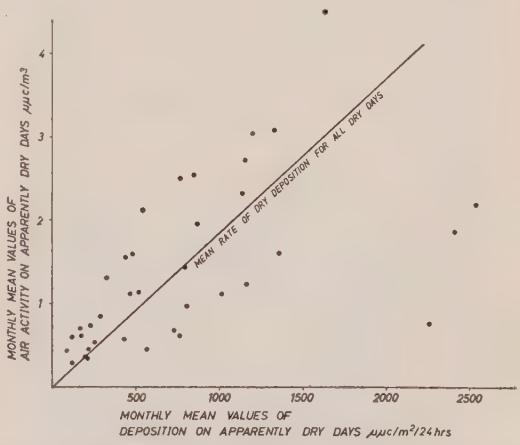


Fig. 1. Regression of deposition on air activity from values given in table 1.

**Table 2. Mean values of deposition velocity for each month between 1 Sept. 1956 and 30 Sept. 1959. The number of apparently dry days in each month and the total deposition on apparently dry days are given in columns 2 and 3.**

| | 1956 | | | 1957 | | | 1958 | | | 1959 | | |
|---|---|---|---|---|---|---|---|---|---|---|---|---|
| | deposition velocity cm/sec | number of dry days | deposition of dry days mc/km² | | | | | | | | | |
| Jan. | | | | 0.33 | 20 | 3.5 | 0.67 | 17 | 3.5 | 1.09 | 17 | 19.7 |
| Feb. | | | | 0.23 | 11 | 1.0 | 0.23 | 14 | 1.7 | 0.49 | 23 | 26.4 |
| Mar. | | | | 0.36 | 22 | 5.1 | 0.36 | 25 | 12.0 | 0.50 | 16 | 21.2 |
| Apr. | | | | 0.49 | 23 | 10.8 | 0.56 | 17 | 19.2 | 0.45 | 16 | 19.1 |
| May | | | | 0.51 | 18 | 15.6 | 0.98 | 18 | 24.4 | 0.42 | 25 | 40.7 |
| June | | | | 0.53 | 11 | 5.7 | 0.35 | 20 | 15.3 | 0.29 | 22 | 11.8 |
| July | | | | 1.45 | 14 | 7.9 | 0.38 | 18 | 15.2 | 0.33 | 17 | 7.4 |
| Aug. | | | | 0.27 | 17 | 2.8 | 0.88 | 16 | 7.0 | 0.56 | 24 | 6.1 |
| Sept. | 3.43 | 21 | 47.3 | 0.40 | 10 | 2.9 | 1.05 | 18 | 18.2 | 0.49 | 26 | 3.1 |
| Oct. | 0.96 | 22 | 19.7 | 0.29 | 10 | 3.2 | 1.50 | 15 | 36.1 | | | |
| Nov. | 1.44 | 19 | 14.5 | 0.56 | 12 | 2.6 | 1.34 | 14 | 35.4 | | | |
| Dec. | 1.25 | 9 | 6.6 | 0.71 | 23 | 4.8 | 0.64 | 15 | 11.9 | | | |

As shown in table 2 and figure 2,monthly mean values of deposition velocity seem to increase almost invariably about 3 months after reported high-yield test explosion series (STRONTIUM PROGRAM 1959), possibly due to the arrival near the surface of rather large particles. (The high value of deposition velocity in Sept. 1956 could be due to the American high yield tests carried out in the Summer of 1956.)

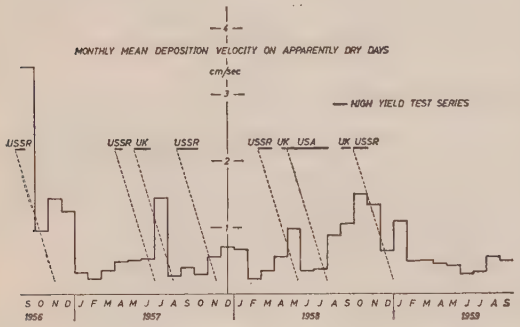
MONTHLY MEAN DEPOSITION VELOCITY ON APPARENTLY DRY DAYS
cm/sec
HIGH YIELD TEST SERIES
USSR
USSR UK
USSR
USSR UK USA
UK USSR
S O N D J F M A M J J A S O N D J F M A M J J A S O N D J F M A M J J A S
1956
1957
1958
1959

Fig. 2. Variations of deposition velocity from values given in table 2.

It can be deduced from table 1 that an average depth of about 500 m of surface air must have been emptied each day to account for the sampled amounts of deposited materials. It is interesting that particles of about 6—7 micron diameter which would fall from 20 km in about 3 months (PROJECT SUNSHINE, 1953, p. 86), would fall several hundred meters in still surface air in the course of a day or so. In fact the diurnal variation of fallout air activity reported from measurements at Kjeller (SMALL 1959), may be due to settling of rather large particles intosurface-air layers.

Fallout air activity which is reduced during the daytime by turbulent removal of fallout particles, tends to increase during the nighttime because of continued settling of particles into calmer air.

It might be important to investigate a possible diurnal variation of dry deposition rate. Such an investigation would probably provide some information about the way in which particle sizes near the ground change as a result of weather conditions etc. The possibility of important health effects in this connection has been pointed out from observations of 1—131 accidentally released to the atmosphere (SMALL and STOREBÖ, 1959).

The values of deposition velocity given in table 2 (approx. 0.2—3.4 cm/sec) are substantially larger than the value of 0.07 cm/sec obtained by STEWART ET AL. (1957). The British measurements were made using gummed surfaces and sampling funnels, and there is no apparent reason for the discrepancy. It might be suggested that fallout materials at Kjeller have contained a greater proportion of large particles.

## 5. Deposition with precipitation

Monthly means of average precipitation activity per litre and air activity for days with precipitation are given in table 3, and plotted in fig. 3.

Most of the points in figure 3 lie quite close to a line drawn through the point determined by the average values of air activity and average precipitation activity per litre for the

**Table 3. Mean daily values of air activity and precipitation activity on obviously wet days for each month between 1 Sept. 1956 and 30 Sept. 1959**

| | 1956 | | 1957 | | 1958 | | 1959 | |
|---|---|---|---|---|---|---|---|---|
| | average air activity (wet days) $\mu\mu c/m^3$ | average precipitation activity $\mu\mu c/l$ | | | | | | |
| Jan. | | | 0.61 | 785 | 0.40 | 400 | 1.17 | 670 |
| Feb. | | | 0.31 | 356 | 0.34 | 216 | | |
| Mar. | | | 0.85 | 1120 | 1.22 | 914 | 2.67 | 3154 |
| Apr. | | | 1.88 | 4990 | 2.02 | 1746 | 2.27 | 2347 |
| May | | | 1.55 | 1915 | 1.88 | 1638 | 4.61 | 3625 |
| June | | | 0.69 | 576 | 1.77 | 1289 | 2.54 | 2736 |
| July | | | 0.64 | 896 | 1.03 | 878 | 1.19 | 698 |
| Aug. | | | 0.51 | 342 | 0.48 | 652 | 0.67 | 403 |
| Sept. | 0.91 | 2894 | 0.90 | 1026 | 0.87 | 1397 | 0.17 | 83 |
| Oct. | 1.00 | 4168 | 1.35 | 1339 | 1.68 | 2052 | | |
| Nov. | 0.51 | 1364 | 0.51 | 680 | 2.53 | 4396 | | |
| Dec. | 0.58 | 1393 | 0.28 | 583 | 0.97 | 2124 | | |

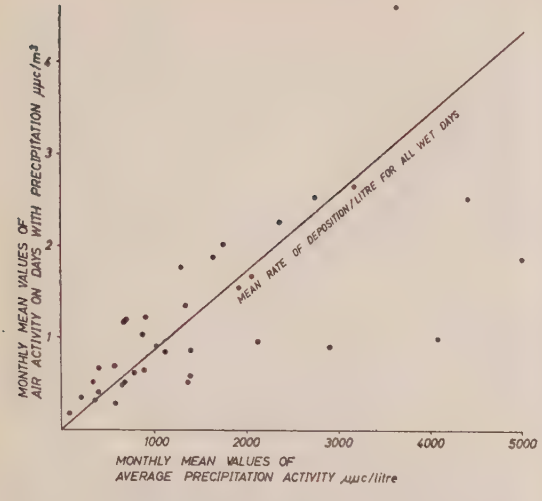
MONTHLY MEAN VALUES OF AIR ACTIVITY ON DAYS WITH PRECIPITATION μμc/m³
MEAN RATE OF DEPOSITION/LITRE FOR ALL WET DAYS
MONTHLY MEAN VALUES OF AVERAGE PRECIPITATION ACTIVITY μμc/litre
1000
2000
3000
4000
5000

Fig. 3. Regression of precipitation activity on air activity from values given in table 3.

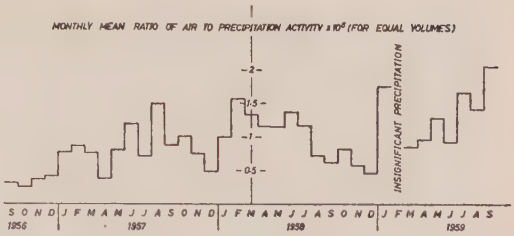
MONTHLY MEAN RATIO OF AIR TO PRECIPITATION ACTIVITY x 10⁶ (FOR EQUAL VOLUMES)
INSIGNIFICANT PRECIPITATION
S O N D J F M A M J J A S O N D J F M A M J J A S O N D J F M A M J J A S
1956
1957
1958
1959

Fig. 4. Variations of air to precipitation activity ratio from values given in table 4.

whole period. Consequently in view of what has been pointed out in section 4, it is interesting to see if the obvious exceptions to the general trend in fig. 3 can be explained by changes in particle sizes.

Comparing the air to precipitation activity ratios given in table 4 and figure 4 with the deposition velocities given in table 2 and figure 2, it seems that when deposition velocity increases, the air to precipitation activity ratio falls and vice-versa. This might indicate that some fraction of fresh fallout particles is removed by processes of dry deposition rather than by precipitation. One way of explaining this is that precipitation processes involve an upward movement of air from near the surface, and that larger particles in particular tend to be removed near the surface. This leads to the simplified model shown in fig. 5.

Consequently the amount of fallout materials available for capture and removal by precipitation, may depend to some extent upon the amount of dry deposition from surface air layers.

The mean values of air to precipitation activity ratio in themselves provide material for speculation about precipitation processes, since droplet growth by condensation might be expected to produce higher values of air to precipitation activity ratio than growth by coalescence. It appears from fig. 4 that relatively fresh fallout materials tend to reduce the air to precipitation activity ratio, and it might be argued that coalescence effects are more important than usual when fresh fallout materials are available. Consequently the simple model shown in fig. 5, which is based upon dry removal effects, may have to be elaborated to include effects of fallout particles in the formation of precipitation elements.

The mean value of air to precipitation ac-

**Table 4. Mean values of air to precipitation activity for equal volumes for each month between 1 Sept. 1956 and 30 Sept. 1959. Precipitation amount and total wet deposition for each month given in columns 2 and 3**

| | 1956 | | | 1957 | | | 1958 | | | 1959 | | |
|---|---|---|---|---|---|---|---|---|---|---|---|---|
| | $\frac{\text{air activity}}{\text{precip. activ.}} \times 10^{-6}$ | mm precipitation | deposition on wet days mc/km² | | | | | | | | | |
| Jan | | | | 0.78 | 49 | 38.1 | 1.00 | 49 | 19.4 | 1.76 | 108 | 71.7 |
| Feb | | | | 0.87 | 120 | 42.1 | 1.57 | 60 | 12.8 | | | 11.6 |
| Mar | | | | 0.76 | 37 | 41.8 | 1.34 | 9 | 8.2 | 0.85 | 45 | 140.0 |
| Apr | | | | 0.38 | 23 | 115.0 | 1.16 | 45 | 79.7 | 0.97 | 103 | 246.6 |
| May | | | | 0.80 | 48 | 92.5 | 1.15 | 91 | 149.4 | 1.28 | 23 | 82.5 |
| June | | | | 1.20 | 131 | 75.6 | 1.38 | 74 | 95.6 | 0.93 | 13 | 34.2 |
| July | | | | 0.71 | 112 | 100.4 | 1.17 | 102 | 92.4 | 1.67 | 80 | 55.7 |
| Aug | | | | 1.50 | 137 | 46.9 | 0.72 | 71 | 46.7 | 1.42 | 34 | 13.6 |
| Sept | 0.31 | 81 | 233.7 | 0.88 | 162 | 165.9 | 0.62 | 41 | 57.0 | 2.06 | 14 | 1.2 |
| Oct | 0.25 | 27 | 110.6 | 1.01 | 71 | 95.5 | 0.82 | 110 | 224.9 | | | |
| Nov | 0.37 | 42 | 57.3 | 0.75 | 61 | 41.7 | 0.58 | 55 | 241.1 | | | |
| Dec | 0.42 | 46 | 64.4 | 0.48 | 4.5 | 2.6 | 0.46 | 78 | 166.5 | | | |

tivity ratio for the whole period, $0.9 \cdot 10^{-6}$ (implying that 0.9 gms of precipitation have on the average contained as much activity as 1 $m^3$ of surface air) might be used to form a rough picture of the average precipitation process at Kjeller. Since average precipitation clouds probably contain about 0.3—0.4 gms/$m^3$ of water droplets, it seems that a moderate degree of extra condensation is necessary before precipitation occurs. This is of course not surprising, since cloud water must be replenished in order to provide appreciable precipitation. It seems that there may in fact be a very high degree of correspondence

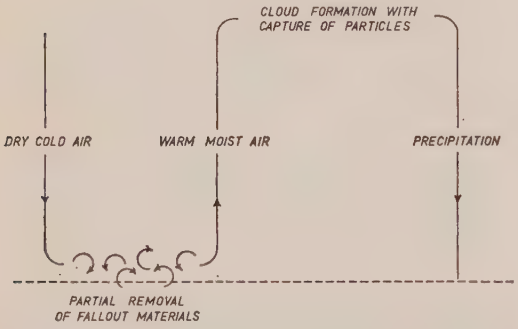


Fig. 5. Model showing connection between wet and dry deposition and surface air activity.

between the original activity of surface air/$m^3$ and the activity of condensed water/$m^3$ of clouds. It has for example been observed near Finse in the southern part of Norway at about 1,700 m above sea level, that the activity of hard rime during deposition was about the same as the activity of snow falling in clouds at the same height. This suggests that precipitation occurred as a result of droplet growth by condensation or sublimation followed by coalescence.

Although the amount of fallout materials in air which has come from near the surface may be overridingly important, extra amounts of materials could be mixed into the clouds from environmental air. This type of mixing is probably less important in the case of layer clouds than in the case of cumulus and cumulonimbus clouds.

For this reason fig. 6 showing the average volume activity of precipitation for different amounts of precipitation per day, might be explained in the following way. Observations

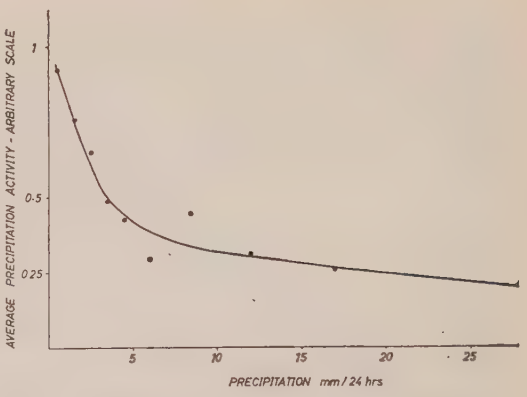


Fig. 6. Average precipitation activities for different daily amounts of precipitation.

covering days with small total amounts of precipitation are likely to be very much influenced by convectional precipitation, which although typically intense, tends to produce relatively small total amounts. However, the greater mixing with environmental air, and possibly greater coalescence in convection clouds, seem likely to produce precipitation which is more radioactive than orographic and cyclonic precipitation. On the other hand orographic and cyclonic precipitation tend to produce relatively large total amounts. Between these two extremes of small total amounts of convectional precipitation with relatively high volume activity and large total amounts of orographic and cyclonic precipitation with relatively low volume activity, occur different combinations of rain-

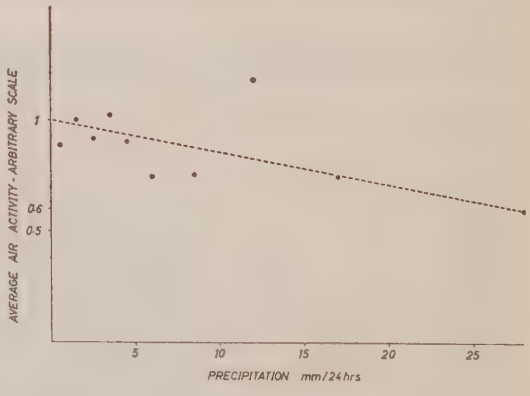


Fig. 7. Average air activities for different daily amounts of precipitation.

fall types and different degrees of mixing with environmental air.

Fig. 7 shows that air activity tends to be lowest on days with large total amounts of precipitation. This might be due to a large extent to differences in downward mixing rates near the surface, mixing being greatest when convectional clouds are formed. The rather haphazard grouping of points in the figure may point to significant variations in mixing rates between different days.

Figure 6 agrees very well with a corresponding figure given by STEWART ET AL. (1957), but does not show the steady increase reported by HINZPETER (1958), for precipitation amounts greater than 10 mm per day.

The values of air to precipitation activity ratio ($0{,}2 \cdot 10^{-6}$—$2.0 \cdot 10^{-6}$ between Sept. 1956 and Sept. 1959) agree well with those reported by BLOK in Holland (1957), $0.4 \cdot 10^{-6}$—$2.5 \cdot 10^{-6}$ between Sept. 1955 and April 1957, but are lower than the value of $3 \cdot 10^{-6}$ given by HINZPETER (1958) from measurements made in Germany in the period July—December 1957.

It might be suggested that Hinzpeter's measurements have been more influenced by convectional precipitation than corresponding measurements in England, Holland and Norway. This does not seem unlikely in view of the geographical and meteorological factors involved in precipitation processes.

## 6. General discussion of fallout deposition rates

Some of the deposition on days with obvious precipitation will have fallen without precipitation, but on the other hand some precipitation will have fallen and evaporated on apparently dry days. Consequently the measured dry to wet deposition ratio of about 1:6 deduced from table 6.1 may not be greatly in error for the open sampling vessels during this period.

To account for the total wet + dry deposition during the whole period an average depth of about 2,500 m of "surface" air must have been emptied each day. This probably corresponds to a depth of about 500 m of "average" tropospheric air, since air activity increases with height. This means that it would have been necessary to empty and refill the troposphere over Kjeller about once every 20 days in order to account for the measured deposition. Since deposition at Kjeller is not average on a worldwide scale, it might be reasonable to use figures for Sr-90 in soils to see how Kjeller compares with the rest of the Northern hemisphere. A rough average figure for most of the Northern hemisphere up to 1958 is about 10 mC/km², the value for Oslo being 28.6 (ALEXANDER, 1959). The 20 days tropospheric emptying time might then be multiplied by 3 to obtain a rough estimate of 60 days for the Northern hemisphere. This value can again be multiplied by 10 to obtain a rough estimate of 600 days for the average stratospheric emptying time over the Northern hemisphere, 10 being an approximate figure for the number of times "average" stratospheric air is more active than "average" tropospheric air (ENVIRONMENTAL CONTAMINATION FROM WEAPONS TESTS, 1958).

Assuming insertion heights of about 20 km, the average rate of downward transport in the stratosphere seems to have been about 15 m per day. It is very interesting that this is the same figure obtained by Storebö for the probable average rate of air subsidence in the Northern polar stratosphere (STOREBÖ, 1959).

## 7. Conclusions

Some fallout materials from test explosions have been deposited more quickly than expected, probably because of gravitational settling of relatively large particles.

Measurements show that there might be a rather acute deposition period beginning about

**Table 5. Summary of wet and dry deposition data**

| | | | | | | | | |
|---|---|---|---|---|---|---|---|---|
| 1117 daily observations — 655 dry days + 462 wet days | | | | | | | | |
| Total deposition on dry days | 0.51 | curie per km² | | | | | | |
| » » » wet | » | 3.17 | » | » | » | | | |
| Average air activity on dry days | 1.43 | micromicrocurie per m³ | | | | | | |
| » » » » wet | » | 1.15 | » | » | » | | | |
| » » » for all | » | 1.31 | » | » | » | | | |

2—3 months after a large-number of high-yield air bursts, and lasting probably a few months.

It looks as though it might be possible to forecast both wet and dry deposition rates, given sufficient measurements of surface air activity over land and ocean regions.

Dry deposition might be greatly influenced by a diurnal variation of removal rates.

**Acknowledgements**

The fallout measurements have been made by Mr. K. Sand, Mr. T. Lekvold and other members of the fallout laboratory staff of the Physic Department of the Norwegian Defence Research Establishment.

The writer wishes to thank Mr. T. Hvinden, Mr. P. Storebö and Mr. A. Lillegraven for valuable discussions and advice.

## REFERENCES

Alexander, L. T., 1959: *Strontium 90 Distribution as Determined by the Analysis of Soils*—Statement for Joint Committee on Atomic Energy Congressional Hearings, May 5—8, 1959. (Table 7 and p. 11).

Blok, J., 1957: Radioaktieve Besmetting van die Biodfeer in Nederland. *Academisch Proefschrift, Vrije Universiteit te Amsterdam.*

Environmental Contamination from Weapons Tests, 1958: HASL-42 p. 38.

Hinzpeter, M., 1958: *The Influence of Meteorological Parameters on the Propagation of Radioactive Fission Products in the Biosphere.* United Nations—Peaceful Uses of Atomic Energy—Proceedings of the Second International Conference, Geneva, Sept. 1958, Vol. 18, pp. 285—290.

Hvinden, T., 1959: Radioactive Fallout in Norway 1958. *NDRE Intern Rapport* **F-374** (latest report of a series).

Project Sunshine, 1953: *Worldwide Effects of Atomic Weapons.* AECU-3488 p. 19.

—, 1953: *Worldwide Effects of Atomic Weapons.* AECU-3488 p. 86.

Small. S. H., 1959: Some Observations on Changes in Air Activity Near Ground Level. *NDRE Intern Rapport* **F-379.**

Small, S. H. and Storebö, P. B., 1959: *On the Waste Disposal Potentiality of the Atmosphere.* (Paper accepted for the Scientific Conference on the Disposal of Radioactive Wastes, held from 16—21 Nov. 1959 in Monaco.)

Stewart, N. G., Osmond, R. G. D., Crooks, R. N. and Fisher, E. M., 1957: *The World-Wide Deposition of Long-Lived Fission Products from Nuclear Test Explosions.* AERE HP/R 2354.

Storebö, P. B., 1957: On the Deposition of Nuclear Bomb Debris in Relation to Air Concentration. *NDRE Intern Rapport* **F-344.**

Storebö, P. B., 1959: The Exchange of Air between Stratosphere and Troposphere. *NDRE Intern Rapport* **F-376.**

Strontium Program 1959: *Quarterly Summary Report,* HASL-65 p. 190—195.

# The Origin of Trade-Wind Orographic Shower Rains

By A. H. WOODCOCK, Woods Hole Oceanographic Institution[1]

(Manuscript received February 6, 1960)

*Abstract*

The purpose of the work reported here was to learn more about rain formation through a study of the extensive Project Shower and other data on the physics and the chemistry of rains. Most of the observations used have been published. It is demonstrated that the water and chloride content of orographic shower rains in Hawaii can be roughly computed from the observed amounts of sea-salt aerosols and water vapor in the sub-cloud layer over the sea, assuming wet adiabatic ascent of the air. From this and several other relationships among the properties of the air and rains, it is tentatively concluded that the showers originate within especially moist parcels of air which are carried into the orographic cloud by the trade winds, and which were previously formed in the sub-cloud layer over the windward sea. Specific suggestions are made for testing the degree to which potential shower-forming air may be identified over the sea or the windward shore prior to rain formation.

## 1. Introduction

Since the beginning of the century numerous workers have, for various reasons, been interested in the chemistry of precipitation (see review papers by ERIKSSON 1952 and JUNGE 1958). Among the many results of this world-wide interest has been the discovery that the chloride concentration in rains tends to decrease with increases in rain amount. In the present paper, the numerous data concerning the chlorinity and other properties of the rain and the atmosphere are examined in order to see what deductions can be made, if any, about rain-forming processes. Recently derived information about the individual sea-salt particles in the atmosphere is also utilized.

The presence of chlorides in precipitation waters has long been used as an example of the capacity of rain to "wash" particulate and other matter from the air as the drops fall from cloud base to ground. Recent tests in 1951 and 1952 (WOODCOCK and BLANCHARD 1955) revcaled, however, that similar chloride concentrations were also present in rains sampled within the rain-producing clouds, making it necessary to revise the "washout" idea of earlier workers to include washout from the cloudy air as well as sub-cloud air. In the present paper it is demonstrated that, through alterations in the time, duration and position of rainwater sampling, one can reveal useful relationships between the chloride concentrations and other characteristics of the rains and of the atmosphere from which they fall.

The Project Shower data resulting from a cooperative field study of Hawaiian trade-wind orographic showers (SQUIRES 1955), is the primary source of the information used in the present work. These data have been given in a series of reports in Tellus vol. 9, No. 4, 1957.[1]

## 2. Comparison of observed and computed chloride concentrations in rains

In a previous study of the rains of Hawaii (WOODCOCK and BLANCHARD 1955) is was computed from observational data and with certain assumptions, that about 20 to 40 per cent of the airborne salt could be found in solution in the rains which fall near cloud-base altitude

[1] Contribution No. 1094 of the Woods Hole Oceanographic Institution. Work supported by the Office of Naval Research, under Contract Nonr-798(00) (NR-082-124).

[1] Hereafter referred to by the abbreviation PST.

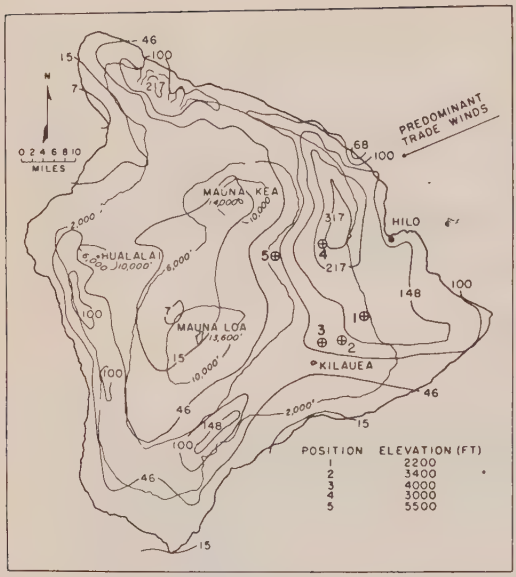


Fig. 1. Isohyetal map of the island of Hawaii, showing the locations of the earlier rainsampling stations. The later more elaborate study required the expanded network shown in Fig. 2.

(stations 1 and 4, Figure 1). These rain showers drift in the wind stream up the mountain slope, the rain being "winnowed" in the general direction of stations 3 and 5 as indicated by BLANCHARD (1957). Rain samples taken at position 5 were found to contain only about five per cent of the salt. It was suggested at the time that the remainder of the salt and water of the rains might be found among the drops which fall over the intervening distance of about 20 km.

During the Project Shower field program, daily rain amounts were sampled at closely spaced stations roughly along the average line of drift of the trade-wind air, with the purpose of examining this idea of winnowed drops. From these samples numerous data are available showing the daily rainfall and saltfall as a function of distance downwind and up the mountain slope from stations 32 and 5 on the Kulani and Saddle Roads (see Figure 2). In this section the properties of the rains from these locations will be shown to be related to the amounts of airborne salt particles and the amounts of water condensed in the clouds.

The purpose here is to present an analysis of a part of the published Project Shower data which indicates that the Hawaii orographic shower rains are produced in certain parcels of air. In simple terms, the actual operation performed here is a comparison of the ratios

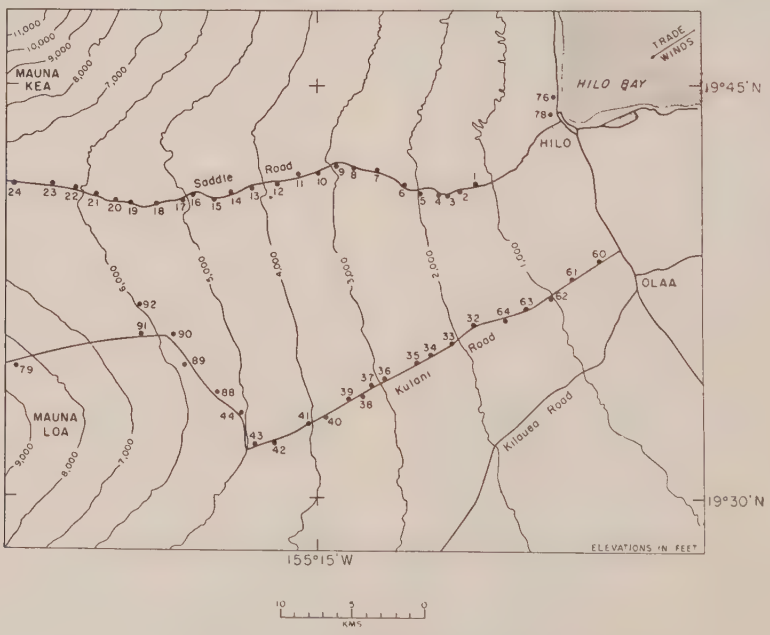


Fig. 2. Map of a section of the windward side of the island of Hawaii. The numbered dots on the Saddle and Kulani roads mark the positions of the Project Shower rain gages used in the present study.

**Table 1. Data used in comparing the average chlorinity of the orographic shower rains of Hawaii to the chlorinities derived by the use of the "shower parcel" model**

| | | | a | b* | c* | d | e | f | g | h |
|---|---|---|---|---|---|---|---|---|---|---|
| Date | Rain Sampling | | Airborne Chloride particles | Rainfall | Saltfall (in rain) | Cloud base altitude over sea | Cloud top altitude | Water content of rain | Chloride conc. of rain observed (c/b) | Chloride conc. of rain comp. (a/f) |
| | position | duration hours | μgms $kg^{-1}$ | $10^6$ liter | $10^6$ mg Cl | m | m | gms $kg^{-1}$ | mg $l^{-1}$ | mg $l^{-1}$ |
| Oct. 1954 | | | | | | | | | | |
| 19—20 | S | 24 | 3.1 | 0.34 | 0.36 | 336 | 2,410 | 3.8 | 1.0 | 0.7 |
| 20—21 | S | » | 9.2 | 1.08 | 3.96 | 610 | 2,740 | 4.0 | 3.7 | 2.3 |
| 25—26 | S | » | 6.4 | 0.80 | 0.05 | » | 2,920 | 4.2 | 0.1 | 1.5 |
| » | K | » | » | 0.49 | 0.20 | » | » | » | 0.4 | » |
| 26—27 | S | » | » | 0.51 | 0.23 | » | 2,470 | 3.5 | 0.5 | 1.5 |
| » | K | » | » | 0.67 | 1.02 | » | » | » | 1.5 | » |
| Nov. 1954 | | | | | | | | | | |
| 2—3 | S | 24 | 6.5 | 0.08 | 0.22 | 458 | 1,830 | 2.5 | 2.7 | 2.6 |
| » | K | » | » | 0.08 | 0.39 | » | » | » | 4.8 | » |
| 6—7 | S | » | 3.9 | 0.80 | 0.14 | 404 | 3,020 | 5.0 | 0.2 | 0.8 |
| » | K | » | » | 0.69 | 0.45 | » | » | » | 0.7 | » |
| 7 | S | 3 | 4.9 | 0.11 | 0.07 | 503 | 2,710 | 4.2 | 0.6 | 1.2 |
| » | K | » | » | 0.12 | 0.12 | » | » | » | 1.0 | » |
| 9—10 | S | 24 | 2.8 | 0.14 | 0.19 | 305 | 2,010 | 3.1 | 1.3 | 0.9 |
| » | K | » | » | 0.16 | 0.23 | » | » | » | 1.5 | » |
| 25—26 | S | » | 6.8 | 0.27 | 0.37 | 915 | 3,110 | 3.6 | 1.4 | 1.9 |
| 29—30 | S | » | 8.5 | 0.27 | 0.71 | 670 | 2,860 | 4.0 | 2.6 | 2.1 |
| » | K | » | » | 0.28 | 0.95 | » | » | » | 3.4 | » |
| Dec. 1954 | | | | | | | | | | |
| N30—1 | S | 22 | 11.9 | 0.40 | 1.34 | 610 | 2,840 | 4.1 | 3.3 | 2.9 |
| » | K | » | » | 0.49 | 2.23 | » | » | » | 4.6 | » |
| 1—2 | S | 24 | 10.7 | 1.24 | 2.38 | 630 | 3,260 | 4.8 | 1.9 | 2.2 |
| » | K | » | » | 0.88 | 3.14 | » | » | » | 3.5 | » |
| 2 | S | 2 | 11.1 | 0.17 | 0.34 | 640 | 3,020 | 4.4 | 2.0 | 2.5 |
| » | K | » | » | 0.09 | 0.35 | » | » | » | 3.9 | » |
| 2—3 | S | 21 | 9.3 | 1.10 | 0.93 | 610 | 3,140 | 4.5 | 0.8 | 2.1 |
| » | K | » | » | 1.34 | 0.82 | » | » | » | 0.6 | » |
| 3—4 | S | 24 | 5.2 | 0.11 | 0.19 | 900 | 2,220 | 2.1 | 1.8 | 2.5 |
| » | K | » | » | 0.15 | 0.37 | » | » | » | 2.4 | » |
| 3 | S | 2.5 | — | 0.06 | 0.09 | 670 | 3,050 | 4.5 | 1.5 | — |
| » | K | 2.5 | — | 0.05 | 0.03 | » | » | » | 0.7 | — |

* Rain and salt falling on a strip one meter wide, which extends from gages 5 and 32 to the upper limits of the rain areas.

of the total saltfall and rainfall on the mountain to the ratio of salt load of the sub-cloud air and the total water condensed as this air ascends in the clouds.

The information used to derive these ratios is listed in Table 1, along with other pertinent facts which will enable the reader to find the original data in PST. The primary observations are contained in columns a through h, Table 1, and are discussed in that order below.

a. The quantities of chloride in the sub-cloud air over the sea are taken from pages 522 and 523 (PST), and are the sums of the products of the median number particle weight in each weight range category and the number of particles in each range.

b. Integrated total amounts of rainfall in rain gages 5 through 25 on the Saddle Road and numbers 32 through 44 on the Kulani Road are given. Uniform steps of about 1,570 meters were used in this integration, in order to smooth out small differences in the spacing of the sampling station. The rainfall amounts given represent the total falling on a strip one meter wide.

Effectively samples are thus obtained at

various successive times in the life histories of the showers, which begin on the lower slopes and rain out as they drift up the slope about parallel with the lines of sampling stations (see Figure 2). Only stations within the orographic clouds are included in this analysis, thus avoiding any question of salt collected by the rain in falling from cloud base to ground. (Excluded from this analysis are the Kulani Road data of November 26—27, which included rains of the 25th to 26th, and the Kona Storm rains of the 27th to 29th of November, when flights were cancelled.)

c. Integrated total fall of chloride dissolved in the rains is derived in the same manner as the integrated rainfall discussed above under (b).

d. Cloud base altitudes over the sea as measured by aircraft are given. These were found on occasion to differ by one hundred meters or more in places only a few miles apart. The altitudes given are the minimum values observed during the flights.

e. The average altitude at which the radiosonde record showed drying of the air $\leq 50$ % relative humidity. Four ascents were made daily (PST pp. 569 to 580). This drying of the air was often associated with the trade-wind temperature inversion, but is thought to be a better indicator of average cloud top than is the temperature.

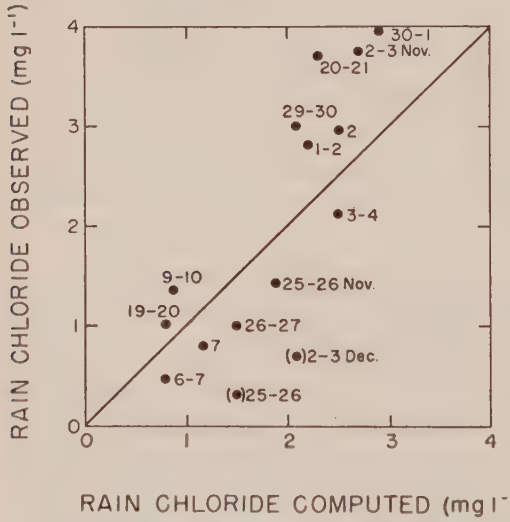


Fig. 3. A comparison of the average observed chlorinity of the integrated total rainfall on the Saddle and Kulani roads and the rainfall chlorinity computed from the "shower parcel" model. The numbers near the points refer to the days of the month, as given in Table 1.

f. The average water content of the rain is derived by assuming that an air parcel, equal in vertical extent to the distance from sea surface to cloud base (i.e., equal to d), flows into the orographic cloud and is lifted wet-adiabatically from cloud base to within one-half of the distance d below the cloud top. Cloud-base mixing ratio is approximated from the Hilo radiosonde records (PST pp. 569—580), a tephigram being used to derive the total condensed water.

g. Column g lists the ratios of the total saltfall to the rainfall (c/b). This chloride concentration is thought to be equal to that which would be found in rains if one could catch all of the water falling from the showers as they move up the mountain slopes.

h. These computed chloride concentrations (a/f) are compared to the average of those observed (g). The reason for making this comparison is the idea that the rains are generated in certain ascending parcels of air. It is thought that the salt content of these parcels is equal to the average in the sub-cloud layer over the sea and that their water content equals that released in the wet adiabatic ascent of the parcel.

Figure 3 shows the relationship between the average of the chloride concentrations observed on the Saddle and Kulani Roads (Table 1, column g) and those estimated through the use of the rain-generating parcel model mentioned in h, above. (On October 19th through 21st, the Kulani Road gages were not yet in operation.)

### 3. Discussion of Figure 3

At first glance the relationship of the observed and computed chlorinities in this graph may seem poor. The values seem remarkably similar however, when one reviews the variability of many important factors involved.

For instance, if many rains begin upwind of gages 5 and 32 (Figure 2) and near the coast during a 24-hour period, the higher salinity drops which are the first to come from the showers (Turner 1955, Woodcock 1953) will fall before the showers pass over the sampling stations, thus causing these drops to be inadequately represented in the two lines of gages. The low-chloride rains of October 25 to 26 and December 2 to 3 may be due to

this factor (see Figure 3 and the isoheytal maps pp. 587 and 589 PST).

Showers moving in directions not parallel to the lines of gages can also alter the assumed average pattern of the first larger drops falling in the lower-level gages and the smaller drops falling in gages successively further up the slope in the direction of shower drift. Such showers might serve to increase or to decrease the observed twenty-four hour average chlorinities such as those given in Figure 3.

On many occasions only one measurement of airborne salt was available for a 24-hour period. The data however show differences of two to three times in airborne salt in a day, thus adding a further potential error in the computed concentrations of Figure 3.

Errors can arise in the estimation of condensed water from uncertainties as to the time of occurrence of the most of the rain[1] and consequently as to which of the four daily radiosonde records to use in estimating cloud thickness and the amounts of condensed water. The average inversion altitude, as reflected in the drying of the air $\leq 50$ %, has been used here in estimating condensed water amounts, though if one knew the time of occurrence of most of the rain, it might be much more realistic to use only one of the radiosonde records as specifying the state of the lower atmosphere.

Leopold's suggestion of the possible existence of local convergence over the region of maximum rainfall (LEOPOLD 1949) may also be important here, though occasional observation from aircraft revealed no marked increase in cloud top altitudes in this region of the orographic cloud.

The presently most satisfactory explanation of the results on Figure 3 is one requiring the assumption that the major growth of the raindrops takes place in parcels of ascending air, and that in the drop growth process all of the salt particles in these parcels become dissolved in the rain waters. Alternative assumptions of fallout of all salt and condensed water in the whole cloud, or of washout of total cloud salt by rain formed in the parcels alone, produce computed salinity values which in all cases fall to the right of the forty-five degree line on Figure 3.

[1] The rain recorders should have been in continuous operation.

We might also suppose that the salt and water does not come from the sub-cloud parcels exclusively, but is fractionally extracted from most of the cloud in some accretion process such as that suggested by BOWEN (1950). If this occurs, then the relationship suggested by Figure 3 requires that this accretion process in each shower extract an amount of water and salt from the cloud which is approximately proportional to the cloud-base-to-inversion distance and to the weight of salt in the sub-cloud layer respectively.

Proportionalities such as these seem reasonable, but the sequence of events pictured in Bowen's model seems clearly inapplicable to the Hawaii orographic shower rains. For instance, WEXLER (1954) has shown that application of Bowen's model to the growth of marine aerosols in cumuli should result in an early fall out of the giant ($10^{-9}$ gm) sea-salt particles as small raindrops, whereas the more numerous smaller ($10^{-10}$ gm) particles should fall later in the shower as larger drops. However, WOODCOCK and BLANCHARD (1955) found that the initial drops falling at the beginning of a shower at cloud base were large and few in number and later Turner showed that the salt content of the large drops ranged from about $2 \times 10^{-9}$ to $10^{-8}$ grams (see TURNER 1955, Figure 4, curves b). WOODCOCK and BLANCHARD (1955) also showed that the numbers of these drops per cubic meter of air approximated the numbers of the giant salt particles of the masses given, suggesting a growth mechanism which tended to conserve the number per unit volume of air as the giant nuclei grow to raindrop size. Thus if one assumes that the coalescense of many droplets containing smaller amounts of salt have chanced to become one drop whose salt content is equivalent to the mass of the larger sea-salt particles, he is faced with the problem of explaining the number correspondence mentioned above.

The purpose of emphasizing here the large amounts of salt in the large raindrops, however, is to suggest that the evidence is against the Bowen mechanism as one which is consistent with the results given in Figure 3, since the mechanism fails to account for some of the details of the character of the rains represented. On the other hand, the salt nuclei hypothesis of raindrop formation outlined by the author

(WOODCOCK 1952) and tested in collaboration with BLANCHARD (1955), does not conflict with Turner's observations (WOODCOCK and BLANCHARD 1955). It is pertinent to repeat here that this hypothesis led to the suggestion that the fraction of the rain and chloride which was not found near cloud base, should be found among the drops distributed up the mountain slopes by the winnowing action of the wind. The integrated total fall of salt and water on these slopes (columns b and c, Table 1), does indeed appear to be a rough summation of the total amount of these substances in the rain-generating parcel of air.

Entrainment of air from the orographic cloud into the shower-producing parcels has not been considered. An implication of Figure 3 is that entrainment into the parcels, if it occurs, does not greatly alter their relative salt and water contents.

Impactor samples of salt aerosols taken by JUNGE (PST pp. 535) near ground levels well within the orographic clouds, and during "drizzle", showed an almost complete absence of chloride among the "giant particles" (0.8 to 8 $\mu$ radius). This might be mistakenly interpreted as indicating that the rains had washed out all of the particles with which we are concerned here. However, within the cloud most of the giant sea-salt particles would have grown into cloud droplets larger than Junge's upper limiting size of 8 $\mu$ (KEITH and ARONS 1957), and thus would have fallen out in the 50 cm long "precipitation tube", before reaching the sampling surfaces of his impactor (JUNGE 1958).

The foregoing discussion of Figure 3 is not regarded as proof that the major growth of the raindrops occurs exclusively in parcels of sub-cloud air ascending in the orographic cloud. At this time, however, the author is unable to think of a more plausible notion. Later in this paper a further method for testing this idea in the future is outlined.

The mechanics of rain formation which can lead to the observational results given in Figure 3 and to those upon which the salt-nuclei raindrop hypothesis (WOODCOCK and BLANCHARD 1955) is based remain unknown to the author, though KOMABAYASI (1958) has made an interesting approach to the latter problem. Recent work by C. G. H. Rooth (unpublished) on an additional theoretical model, involving drop growth in air parcels having the form of spherical vortices, is producing some useful results. In the meantime, some of the implications of the present air-parcel idea of shower rain origin seem worth additional investigation here in an effort to mark out promising paths for further exploratory field work.

The author has long entertained the idea that parcels of air in which showers are to form may be identifiable in the tradewind stream over the sea, prior to their passage over the windward shore and into the orographic clouds. The following study supports

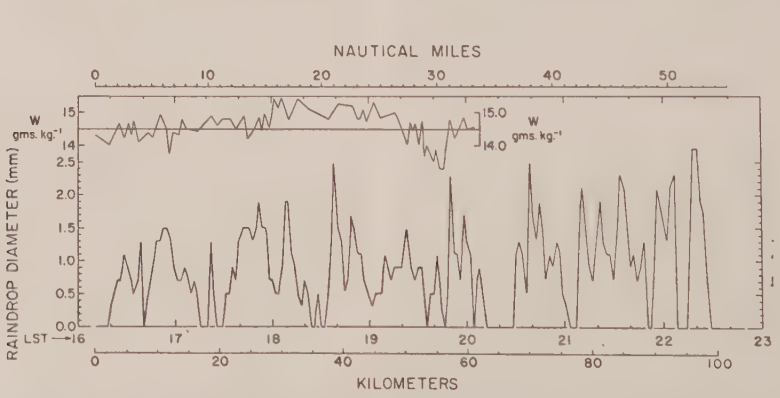


Fig. 4. The lower part of this graph gives the maximum drop diameter ($\pm$ 0.1 mm) found on the drop-recorder tape, exposed at station 4 on Oct. 21, 1954, as a function of time. The distance scales represent the motion of the lower air (at 8.5 knots) during the time the rain recorder was operating. The upper part of the graph shows horizontal differences in mixing ratio which were taken from Figure 5. (A correspondence of upper and lower traces on Figure 4 is not to be expected.) See text for more explanation.

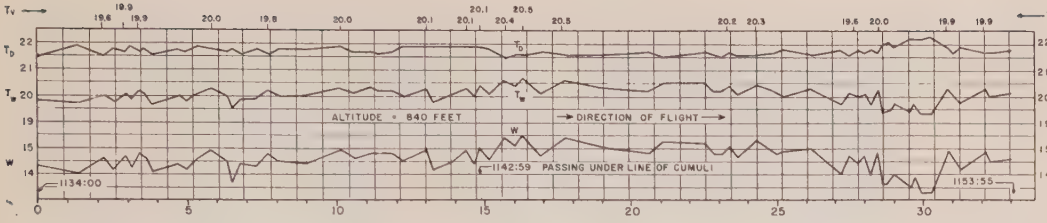


Fig. 5. Reproduction of some of Johnson's data (PST p. 498, Fig. 5) showing differences in the distribution of temperature and water vapor on Oct. 21, 1954, in a horizontal flight made about parallel to the surface wind and windward of Hawaii. The purpose here is to illustrate the effects of the differences in the amounts of vapor upon the virtual temperature when the sub-cloud layer is lifted above the saturation altitude. The numbers at the top of the figure were added to show the range of virtual temperatures which will exist in the moist parcels if the layer is lifted adiabatically to the 911 mb level. Note that the virtual temperature of these parcels exceeds that of the environmental air at the time (see Table 2).

this idea in a way which enables one to form some specific questions upon which to base suggestions for further work.

### 4. Identifying potential rain-forming air parcels

Concerning the idea of the existence of specific shower-producing parcels in the sub-cloud layer over the sea, it is interesting to ask how many showers fall each twenty-four hours, and what property differences in the layer might show a frequency of recurrence similar to that of the showers.

Unfortunately, there was only one day during the project when a rain recorder was in operation at a time when measurements were also made in the sub-cloud air over the sea and when the flight was made parallel with the surface wind.

On October 21, 1954, between 1610 and 2250 HST, a rain-recorder indicated about thirty-four showers passing station 4 (see map, Figure 1). Each increase in raindrop size, or each peak in recorded maximum size (see lower part of Figure 4) is counted as a separate shower, since there seems to be no clear physical basis for discrimination among them at this time.

Between 1054 and 1217 on the same day, wet- and dry-bulb temperature measurements were made in the lower air over the sea along a flight path parallel with the surface wind and windward of the sampling area on Hawaii (see PST p. 498). A part of the flight data is reproduced here in Figure 5 and at the top of Figure 4. The timing of these aircraft measurements was such that some of the air in which the flight was made would flow over the island sampling area during the rain-sampling period. The Hilo wind for the 300 m to 2,100 m layer, averaged 8.5 knots during the rain-sampling period (PST p. 570). Thus, about 57 nautical miles of air flowed over the Saddle Road during the rain-sampling interval (see distance scale on Figure 4).

Examination of Figures 4 and 5 shows that the factor which might significantly alter the stability of this lower air as it is forced up into the orographic cloud and one which varies spatially at frequent intervals in flight parallel with the wind, is the amount of water vapor.[1] It will be noted that there are 18 marked peaks in the mixing ratio (W) in the 33 nautical mile flight path. The vapor content and temperature of these moist air parcels was such that their virtual temperature, upon adiabatic lifting to 911 mb and higher, would exceed that of the environment at the time by at least 0.5 °C (see Table 2). Figure 6 shows graphically these excess temperatures, using the environmental conditions specified by the Hilo radiosonde and by Johnson's airplane sounding. These more unstable parcels of air from the sub-cloud layer should ascend

[1] The results of cross-wind flights by Johnson are not useful here because the rain recorders indicate the showers that occur along the line of flow of the trades, and not those that occur normal to them. It is noteworthy that the frequency of occurrence of horizontal differences in W in the sub-cloud air was not the same during the parallel-with-the wind flight on October 21, and cross-wind flights on other days (see PST, pp. 498, 501, 502 and 503). Measurements should have been made on both headings at about the same time and altitude on each of the days studied.

**Table 2. Results of airplane sounding made by Johnson (PST p. 499) at 1218 to 1241 HST, on Oct. 21, 1954, over the sea a few miles southeast of Hilo. The pressures were derived from the altimeter readings, and the virtual temperatures were derived through the use of Table 72 of the 1958 Smithsonian Meteorological Tables. The columns marked "moist parcels" give the virtual temperatures of the dryest and the wettest of the 18 moist parcels indicated on Figure 4, assuming adiabatic ascent above the condensation lifting level. Note that temperature ($T_V$) excess over that of the environment (columns 6, 9, 10 and 11) becomes large only above about 1,020 m.**

| Altimeter reading | Johnson's Sounding | | | | | "Moist Parcels" | | Hilo Radiosonde | | |
|---|---|---|---|---|---|---|---|---|---|---|
| | | | | | | dryest | wettest | interpolated values | | |
| | $P$ | $T_D$ | $T_W$ | $W$ | $T_V$ | $T_V$ | $T_V$ | 1100 $T_V$ | 1700 $T_V$ | 2300 $T_V$ |
| m | mb | C | C | gm kg$^{-1}$ | | | | | | |
| 256 | 983 | 22.1 | 20.2 | 14.6 | 24.7 | | | | | |
| 348 | 972 | 21.0 | 19.8 | 14.7 | 23.6 | | | | | |
| 430 | 963 | 20.1 | 18.8 | 13.9 | 22.6 | | | | | |
| 470 | 958 | 20.2 | 17.9 | 12.8 | 22.5 | | | | | |
| 510 | 953 | 19.8 | 17.9 | 13.0 | 22.1 | | | | | |
| 560 | 948 | 19.5 | 17.0 | 12.0 | 21.6 | | | | | |
| 607 | 942 | 19.3 | 16.6 | 11.7 | 21.4 | | | | | |
| 665 | 936 | 18.6 | 17.0 | 12.5 | 20.8 | | | | | |
| 760 | 926 | 18.4 | 15.8 | 11.2 | 20.4 | 20.4 | 21.1 | 21.0 | 19.2 | 20.2 |
| 850 | 915 | 17.8 | 15.5 | 11.3 | 19.8 | 19.9 | 20.6 | 20.4 | 18.9 | 19.6 |
| 890 | 911 | 17.1 | 15.9 | 12.0 | 19.1 | 19.6 | 20.4 | 20.2 | 17.9 | 19.3 |
| 940 | 905 | 16.8 | 14.8 | 11.0 | 18.7 | 19.4 | 20.1 | 19.8 | 17.3 | 18.8 |
| 1,020 | 897 | 16.6 | 14.8 | 11.1 | 18.5 | 19.0 | 19.8 | 19.3 | 16.6 | 18.2 |
| 1,050 | 894 | 16.1 | 14.7 | 11.3 | 18.1 | 18.9 | 19.6 | 19.2 | 16.4 | 18.0 |
| 1,280 | 868 | 14.9 | 12.6 | 9.7 | 16.6 | 17.7 | 18.4 | 17.5 | 15.5 | 16.0 |
| 1,320 | 864 | 14.7 | 12.5 | 9.7 | 16.4 | 17.4 | 18.3 | 17.2 | 15.4 | 15.7 |
| 1,380 | 858 | 14.5 | 12.1 | 9.5 | 16.2 | 17.2 | 18.0 | 16.8 | 15.3 | 15.2 |
| 1,460 | 849 | 13.8 | 11.0 | 8.6 | 15.3 | 16.8 | 17.5 | 16.2 | 15.0 | 14.5 |
| 1,495 | 846 | 13.8 | 11.2 | 9.0 | 15.4 | 16.7 | 17.3 | 16.0 | 15.0 | 14.3 |
| 1,640 | 831 | 12.7 | 10.8 | 9.1 | 14.3 | 15.9 | 16.7 | 15.0 | 14.5 | 13.2 |
| 1,680 | 827 | 12.2 | 10.9 | 9.5 | 13.8 | 15.7 | 16.4 | 14.7 | 14.2 | 12.8 |
| 1,700 | 825 | 11.9 | 10.5 | 9.2 | 13.5 | 15.6 | 16.4 | 14.6 | 14.0 | 12.7 |
| 1,780 | 817 | 11.5 | 10.2 | 9.1 | 13.1 | 15.1 | 15.9 | 14.1 | 13.6 | 12.1 |
| 1,830 | 812 | 11.0 | 10.0 | 9.2 | 12.6 | 15.1 | 15.7 | 13.8 | 13.2 | 11.7 |
| 1,975 | 797 | 10.6 | 8.2 | 7.7 | 11.9 | 14.0 | 15.0 | 12.8 | 12.1 | 10.5 |
| 2,130 | 782 | 9.4 | 8.9 | 9.0 | 10.9 | 13.2 | 14.1 | 11.8 | 11.0 | — |
| 2,300 | 765 | 8.8 | 6.2 | 6.8 | 10.0 | 12.4 | 13.2 | 10.7 | 9.8 | — |
| 2,440 | 753 | 8.3 | 5.8 | 6.7 | 9.4 | 11.8 | 12.6 | 9.8 | 8.9 | — |
| 2,560 | 744 | 10.6 | 0.7 | 1.5 | 10.9 | 11.0 | 11.9 | 10.4 | 8.0 | — |
| 2,750 | 723 | 10.7 | 0.5 | 1.5 | 11.0 | 10.0 | 10.9 | 11.8 | 6.6 | — |
| 3,040 | 697 | 8.5 | —0.9 | 1.4 | 8.7 | 8.3 | 9.3 | — | 9.0 | |

more rapidly in the orographic cloud than other parts of this layer. MALKUS (1954) has shown that virtual temperature excesses of 0.5 to 2 °C are commonly associated with the most rapidly ascending air in trade-wind cumulus clouds. It is assumed that it is within these moist parcels that the showers develop after the sub-cloud air passes up the windward slopes of the island and into the orographic cloud.

Thus, in the 57 nautical miles of air flow over station 4 on the Saddle Road, about 31 of these moist parcels should pass. Thirty-four showers were estimated from the rain-recorder tapes. The purpose here is that of simply emphasizing the rough similarity of the spatial distribution of showers and moist parcels (see Figure 4), and to point out that the parcels would have the highest virtual temperature in the clouds. We do not know the structure of the air which actually passed over the rain-recorder station. However, we do know that more than 75% of the 120 nautical miles of air measured by Johnson on the 21st showed structure similar to that represented at the top of Figure 4.

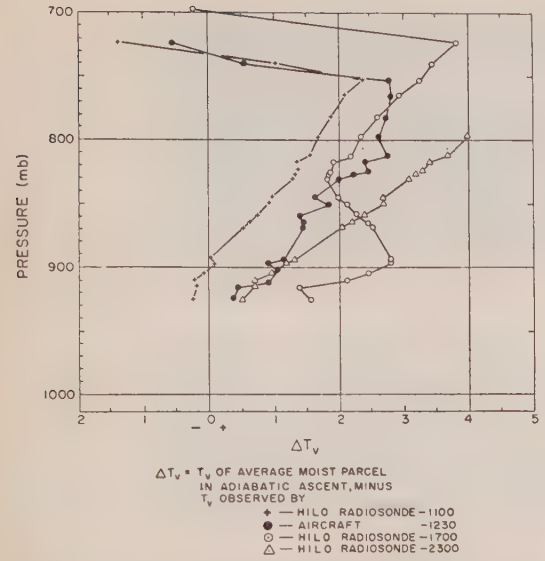
700
800
900
1000
PRESSURE (mb)
2 1 0 1 2 3 4 5
ΔTv
ΔTv = Tv OF AVERAGE MOIST PARCEL IN ADIABATIC ASCENT, MINUS Tv OBSERVED BY
+ — HILO RADIOSONDE – 1100
● — AIRCRAFT – 1230
○ — HILO RADIOSONDE – 1700
△ — HILO RADIOSONDE – 2300

Fig. 6. Virtual temperature differences between the average moist parcel (Fig. 5) in adiabatic ascent and that within the lower atmosphere at various times during the observation period. Aircraft sounding made over sea about ten nautical miles southeast of Hilo.

## 5. Discussion of Figures 4 and 5, and Table 2

It may be argued that the difference between the virtual temperature of the "moist parcels" and that of the adjacent "dryer parcels" (a few tenths to one degree) seems small. It should be remembered, however, that as the lower air orographically ascends, the moist parcels will be the first to reach the condensation lifting level, and hence will be the first to experience the additional buoyancy as latent heat is released. The recurring showers, and the similarity of their number to that of the moist parcels present a picture of chain-like rain-forming air masses linearly imbedded within the wind stream passing over the island. This perhaps explains the cellular nature of the orographic cloud, particularly towards its seaward edge, as noted by Squires and Warner among the records from their numerous flights made within this cloud to determine the droplet size distribution and liquid water content (see PST, p. 487). Many more measurements of moist parcel number and shower number are needed however. One naturally wonders what the moisture structure of the sub-cloud layer might be in the absence of shower activity on the island and when known influencing factors such as the temperature inversion and wind characteristics seem favorable for showers.

It will be noted that Johnson has indicated a mixing ratio accuracy of ± 0.2 gm $kg^{-1}$ as derived from his psychrometric measurements. This error is due primarily "to the inaccuracy in determining the correction for dynamic heating" (PST p. 496). We are largely concerned here with differences rather than absolute values in mixing ratio. Since air speed was constant, dynamic heating errors would also be constant. The wet- and dry-bulb temperature (and hence mixing ratio) differences encountered in flight are concluded theref re to be real.

Similar spatial differences in water vapor had been previously observed from ships and aircraft in trade-wind regions of the Atlantic and on the windward shore of one of the Hawaiian islands (see Figures. 7 and 8). It is thought that these features are common in the sub-cloud air of these and perhaps other latitudes. In fact the data on Figure 9 show that moist parcels are present in the lower wind stream a short time after continental air passes over the sea, though in this case it is thought that the moist regions are of very limited vertical extent.

Sensitive shielded mercury thermometers were used to make the measurements reported on Figure 9. Response time was 60 % full scale in seven seconds and thermometer error correction was applied to the nearest five-hundredths of a degree. Readings were made each thirty seconds at a fixed location on the

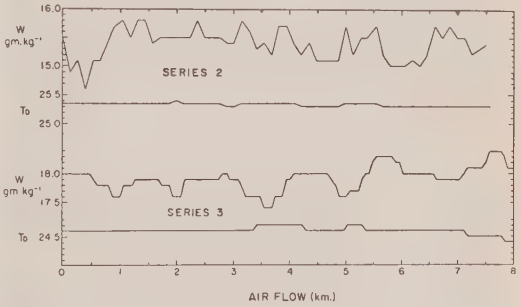


Fig. 7. Horizontal differences in the temperature and mixing ratio in the lower atmosphere of an Atlantic trade-wind area. It can be seen that these differences are very similar in frequency and amplitude to those presented in Fig. 4, 8 and 9. Table 3 and text give more information about these data.

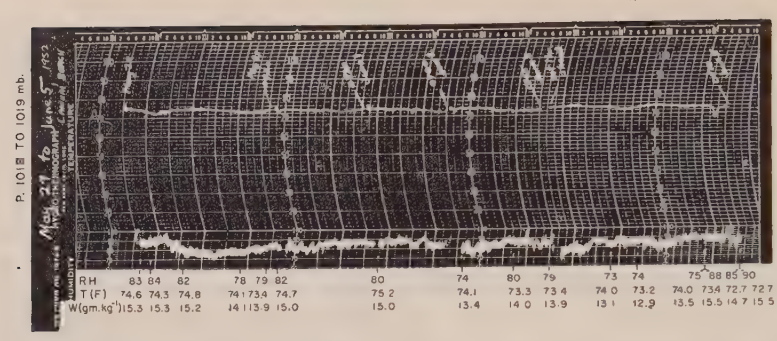


Fig. 8. One of five similar hygro-thermograph records from instrument exposed to trade winds at Lanikai Beach, Oahu, Hawaii. Location about 30 meters from windward shore, at site shielded from direct solar radiation and rain. For comparison, data from sling psychrometer measurements given in table below. Thermometer error corrected to nearest 0.1°, and times adjusted to error of the thermograph clock. Hygrothermograph shows short period RH changes of 4% to 10% with little dry temperature change. Mercury thermometers confirm these differences, when consecutive readings are made a few minutes apart (see results of last four measurements on table).

outer end of a pier near the Woods Hole laboratories, the passing air being metered with a recording anemometer.

The series two temperature measurements (Table 3 and Figure 7) were made at the bow of the research vessel Atlantis while it was in the Atlantic trade-wind area and moving windward. A sling psychrometer was used, and the thermometers were read each fifteen seconds. Radiation shielding was supplied by metal foil, and thermometer error corrected to the nearest one-tenth degree. The series three data were kindly supplied by Mr. A. F. Bunker of the Woods Hole Oceanographic Institution, from his aircraft measurements.

The effects of short-period variations in the thermal structure of the lower 3,000 m of the trade-wind atmosphere in altering the stability of the moist parcels (inadiabatic ascent), is clearly illustrated on Figure 6. A progressive increase in the $T_V$ difference within a short time and distance is apparent, showing the potential importance of almost continuous scanning of this part of the atmosphere in trying to understand events in the clouds which are imbedded therein.

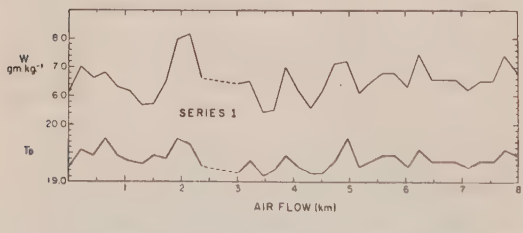


Fig. 9. Temperature and mixing ratio found within the wind stream shortly after air passed from land to water surface. See Table 3 and text for further information.

## 6. Estimate of shower diameters using parcel method

If most of the water condensing within the ascending shower-producing parcels eventually falls out along the lines of gages on the mountain slopes, one should be able to estimate the average sizes of the showers from the data on Table 1 and from the number of showers indicated by the rain recorders. The apparent average shower diameter ($S$) is estimated as follows:

$$S = \frac{R\,10^3}{Whn} \qquad (1)$$

where $R$ = average total rain; see Figure 2 and Table 1, column b (liters $m^{-1}$)

$W$ = total water condensed; Table 1, column f (gms $kg^{-1}$)

$h$ = vertical distance from sea surface to cloud base; Table 1, column d. ($m$)

$n$ = shower number (counted as on Figure 4).

**Table 3. Additional data concerning observations given on Figures 7, 8 and 9**

| Series | Date | Time zonal | Lat. N | Long. W | Alt. m | Surface Wind | | Atmos. Pressure mb | Sea Surface Temp. °C | Place | Fetch km |
|---|---|---|---|---|---|---|---|---|---|---|---|
| | | | | | | Speed m sec$^{-1}$ | Direction | | | | |
| 1 | July 11, 1945 | 1400 | 41°31′56″ | 70°40′15″ | 3 | 7 | 320 | 1015 | 22.6 | dock | 19 |
| 2 | Apr. 24, 1947 | 0630 | 20°38′ | 69°00′ | 4 | 3 | 90 | 1017 | 26.2 | ship's bow | > 1,000 |
| 3 | Nov. 14, 1958 | 1100 | 18°40′ | 65°50″ | 305 | 7 | 70 | 977 | — | aircraft | > 4,000 |

Unfortunately none of the Project Shower data properly fulfill the requirements of equation (1). This is not surprising, since the program of observations was not designed to answer the questions posed. During the best single twenty-four hour observation period (Dec. 1—2, Table 1 and PST pp. 548 and 549), the rain-recorders missed more than eight hours. The two- and three-hour intervals of Nov. 7 and Dec. 2 and 3, are also uncertain because the time required to read the numerous rain gages was about one-half of the total sampling time. Thus, on Dec. 2, the rainfall in the Saddle Road gage number 5 (see Figure 2 and PST p. 514) represents the period 1414 to 1612, while the last gage, number 25, caught rains falling between 1509 and 1715 (see data file Pineapple Research Institute, Honolulu, Hawaii).

Using interpolations and extrapolations of the rain gage and rain-recorder data to cover the unknown time intervals, shower diameters of from 1,700 to 4,100 meters were computed for the above dates, using equation (1).[1] This diameter range is consistent with the few individual showers distinguishable in the liquid water records obtained in the orographic cloud by SQUIRES and WARNER (PST, see especially Figure 12 and pp. 487—489). Also, the Hilo rawinsonde data indicate in general a sufficient air flow inland to transport air parcels of the number and size required. Examination of the rain-recorder records shows however that variability in shower activity with time makes the validity of extrapolations or interpolations very uncertain.

Thus the major usefulness of equation (1) at this time is to point out that it constitutes a further means of testing the shower-parcel idea, when applied to data obtained during a properly designed observation program.

## 7. Conclusions

The idea that the showers originate in specific moist parcels of air enables one to advance tentative explanations for the following characteristics of Hawaiian orographic rains which have been revealed by the Project Shower data.

1. Chloride concentration
2. Shower frequency
3. Total water content
4. Horizontal dimensions

This result suggests that these rains form in units of air within the trade wind stream which may be identifiable prior to their arrival over the land. Despite the limited extent of some of the data supporting this idea, a reasonably consistent shower model has evolved. The importance in meteorological studies of locating shower-forming air before the shower occurs, makes further work seem clearly worthwhile. Prior location would of course be a forecasting aid and would simplify and make more economic studies of the effects upon shower production of artificially altering the nuclei population and other characteristics of potential shower-producing air parcels.

Since the chloride and water contents of Hawaiian rains seem to be explicable through

[1] It will be noted that the drop maxima, shown by the peaks on rain records such as Figure 4, are represented by $n$ in equation (1) as if individual showers contributed equal amounts of rain to the lines of gages. It is clear however that these showers are widely different in intensity at any one location (e.g. PST p. 545). The high-rate rains have larger drops and presumably briefer duration, while the low-rate rains have smaller drops and presumably longer duration. Thus an equal value for $R$, in equation (1), can result from a 30 mm hr$^{-1}$ rain lasting three minutes or a 3 mm hr$^{-1}$ rain of thirty minutes duration.

the use of the moist-parcel idea, the application of this idea to rains in other areas, becomes a question worth consideration.

The parcel idea suggests that orographic shower frequency is related to the frequency of occurrence of certain moist parcels having virtual temperature excesses over those of the environment comparable to or exceeding those shown on Figure 6.

The occurrence of orographic showers in regions such as Hawaii should be predictable from measurements made within the cloud and sub-cloud layers of the lower atmosphere which are soon to pass over the area concerned. Horizontal runs and vertical soundings by aircraft, similar to those made by Johnson, are best; their number and extent depending upon the variability with time, distance and altitude of virtual temperature, mixing ratio, and perhaps other factors such as wind shear.

Figure 8 indicates that the moist air parcels of higher levels probably extend to within a few meters of the sea surface. If so, a simple means of testing them as a source of showers would be to set up a line of observing stations along the coast normal to the dominant winds and windward of a network of recording rain gages. Thus one could continuously scan the surface air two-dimensionally (or perhaps three-dimensionally using towers) for moist parcels and for showers. Frequent local radiosonde and rawinsonde ascents would also be needed as indicated in the present study.

Relatively long term field programs should be initiated at favorable locations, with the purpose of understanding and perhaps exploiting the relationships indicated here between certain properties of the air stream and the precipitation resulting when this air is subsequently lifted.

**Acknowledgements**

This paper is one of the results of Project Shower, a international cooperative field study to which many persons and organizations contributed (SQUIRES 1955). Without their simultaneous efforts, focused upon the complex of interrelated events often too simply termed "orographic showers", the present work could not have been performed. The author's co-workers, Mr. D. C. Blanchard and Mr. Claes Rooth contributed to this work through generous critical readings and discussions.

## REFERENCES

BLANCHARD, D. C., 1957: Discussion of raindrop distributions found during Project Shower, Hawaii, 1954. Artificial Stimulation of Rain, pp. 213—223, Pergamon Press, New York.

BOWEN, E. G., 1950: The formation of rain by coalescence. *Aust. Jour. Sci. Res.*, A, 3, pp. 193—213.

ERIKSSON, E., 1952: Composition of atmospheric precipitation. *Tellus* **4**, pp. 280—303.

— 1955: Airborne salts and the chemical composition of river waters. *Tellus* **7**, pp. 243—250.

JUNGE, C. E., 1954: The chemical composition of atmospheric aerosols, I: Measurements at Round Hill field station, June—July 1953. *J. Meteor.* **11**, pp. 323—333.

— 1958: Atmospheric chemistry; Advances in Geophysics, IV, pp. 1—108, Academic Press, Inc., New York, N.Y.

KEITH, C. H., and ARONS, A. B., 1954: The growth of sea-salt particles by condensation of atmospheric water vapor. *J. Meteor.* **11**, pp. 173—184.

KOMABAYASI, M., 1958: Some aspects of rain formation in warm cloud (I) Salinity of individual raindrops and other quantities concerning rainfall. *Coll. Met. Papers No.* **108**, pp. 205—220, Geophysical Institute, Tokyo Univ., Tokyo, Japan.

LEOPOLD, L. B., 1949: The interaction of trade wind and sea breeze, Hawaii, *J. Meteor.* **6**, pp. 312—320.

MALKUS, J. S., 1954: Some results of a trade-cumulus cloud investigation. *J. Meteor.* **11**, pp. 220—237.

PROJECT SHOWER DATA, 1957: An investigation on warm rainfall in Hawaii. *Tellus* **9**, pp. 471—590.

SQUIRES, P., 1955: Project Shower; An investigation on warm rain in the Hawaiian islands, *Nature* **175**, pp. 748—750.

TURNER, J. S., 1955: The salinity of rainfall as a function of drop size. *Quart. J. Roy. Met. Soc.* **81**, pp. 418—429.

WEXLER, R., 1954: Growth of rain in warm clouds. Unpublished manuscript. Woods Hole Oceanographic Inst.

WOOD, W. E., and WILSMORE, N. T. M., 1929: Salinity of rain in Western Australia. *J. Roy. Soc. W. Austr.* **15**, pp. 22—30.

WOODCOCK, A. H., 1952: Atmospheric salt particles and raindrops, *J. Meteor.* **9**, pp. 200—212.

— 1953: Salt nuclei in marine air as a function of altitude and wind force. *J. Meteor.* **10**, pp. 362—371.

WOODCOCK, A. H., and BLANCHARD, D. C., 1955: Tests of the salt-nuclei hypothesis of rain formation. *Tellus* **4**, pp. 437—448.

# The Effect of Monochromatic Light on the Concentration of Large Ions

By A. F. ELNADI[1] and N. FARAG[2]

(Manuscript received February 13, 1960)

*Abstract*

The divided electrode condenser is used to study the effect of monochromatic light of wave lengths between 4,030 and 6,610 Å (using 10 interference filters of Jena glass), on the concentration of large ions having mobilities below $10 \times 10^{-4}$ cm/sec: volt/cm.

The number of ions per c.c. is measured with the aid of the characteristics obtained for each wave length, at different group mobilities, both in the presence of light ($N_1$) and in complete darkness ($N_2$). The ratio ($N_1/N_2$) is obtained for each filter and for the four mobility groups, i.e. $6.90 \times 10^{-4}$, $2.22 \times 10^{-4}$, $1.02 \times 10^{-4}$ and $0.60 \times 10^{-4}$ cm/sec. : volt/cm.

The results are discussed on the basis of statistical analysis by applying the correlation and significance tests.

## Introduction

The influence of visible light on the mobility spectrum of large atmospheric ions was studied here at Giza by G. ORTNER and A. F. ELNADI (1955). They found that there is an increase in the ion concentration for ions with mobilities greater than about $2.0 \times 10^{-4}$ both in daylight and in case of light from a tungsten filament lamp. On the other hand, ions with mobilities smaller than $2.0 \times 10^{-4}$ show a decrease in the ion concentration.

H. ISRAËL, G. FRIES and H. DOLEZALEK (1956) in a report on "Parallelism occurring in the registration of potential gradient and general local brightness", came to the following conclusion:

"When continuously registering the atmospheric potential gradient and the air earth current on one hand and the general local brightness on the other hand, occasional parallelisms and antiparallelisms between the elements were observed.

F. VERZÁR and YVETTE KUNZ (1957) showed that in a closed air mass which has a very low nucleus count, direct sunlight produces, in a few minutes, large numbers of atmospheric condensation nuclei.

S. Williams and W. A. Morgan (Ireland) observed an increase in concentration of condensation nuclei, which are of the same size as large ions, with sunshine near the Atlantic at Valentia. A similar behaviour was found in Basel by M. Bider (POLLAK 1955). Later A. F. ELNADI (1958) at Giza, Cairo, showed that ordinary light decreases the concentration of small ions of mobilities $\geq 1.3$ while it causes an increase for lower mobilities ($\leq 0.045$).

In this paper the influence of monochromatic light on the large ion concentration is studied.

## Apparatus

The apparatus used in this investigation consisted of a cylindrical condenser composed of two concentric brass tubings. The inner electrode of 4.76 cm external diameter was divided

[1] Assiout University, Faculty of Sience, Assiout, Egypt. U.A.R.

[2] Cairo University, Faculty of Science, Giza, Egypt. U.A.R.

into three sections insulated from each other and fixed firmly together by perspex cylinders. The lengths of the sections were 140, 20 and 20 cm respectively in the direction of air flow. The first and third sections were grounded and the second section was connected to an electrometer of the Compton type having a sensitivity of about 1,800 mm/volt. The outer electrode was 160 cm in length and 7.30 cm internal diameter, connected to a variable voltage supply of dry batteries placed inside a shielded box. The cylindrical condenser was well shielded by a third tube of 10.5 cm in diameter.

The air was drawn from a rectangular box of 240 litres volume, through a short tube of galvanised iron of 5.0 cm internal diameter, into the cylindrical condenser. The box has one of its sides (100 × 60 cm) of thin glass covered by a thick black paper.

The upper part of the box was illuminated by a tungsten filament lamp of 500 watts in a projector with glass lenses at a distance of 100 cm from the box. Monochromatic light was obtained by using interference filters of Jena glass which can be attached to the projector lenses allowing light of a certain wave length to fall on the upper part of the box.

The experiments have been carried out in a dark room (9 metres from the ground level) in the Physics Department, Faculty of Science, Cairo University at Giza.

The effective wave lengths and the corresponding frequencies are given in table 1.

Table 1

| Filter number | Wave length $\lambda_{(max)}$ Å | Frequency $(\nu) \times 10^{12}$ cycles/sec. |
|---|---|---|
| 1 | 4,030 | 744 |
| 2 | 4,340 | 690 |
| 3 | 4,640 | 648 |
| 4 | 5,120 | 585 |
| 5 | 5,280 | 567 |
| 6 | 5,670 | 528 |
| 7 | 5,840 | 513 |
| 8 | 6,010 | 498 |
| 9 | 6,350 | 474 |
| 10 | 6,610 | 453 |

**Method and mode of calculation**

The divided-electrode method due to ZELENY (1900) was used as it is one of the most satisfactory methods of the blast type for the the mobility groups.

To check the apparatus, some characteristics of large ions with mobilities below $10 \times 10^{-4}$ were obtained, see fig. 1. In these characteristics the groups $6.90 \times 10^{-4}$, $2.22 \times 10^{-4}$, $1.02 \times 10^{-4}$ and $0.60 \times 10^{-4}$ appeared clearly, in good agreement with results previously obtained by one of the authors (ELNADI 1955).

The study was made on these groups as follows:

The current in the electrometer was measured for each group while the box was completely dark, then it was subjected to monochromatic light from the projector and after a few minutes the current was again measured for each group. Finally the box was again dark and the current was measured. The interval of time between every set of observations was to assure that the effect was complete.

This was done with the ten filters and repeated six times for positive ions and four times for negative ions.

It is clear that the ratio $(C_1+C_2)/C_1 = 1.15$ is less than the ratio $k/k'$, corresponding to two subsequent ion groups, as it must be, in order to assure a high resolving power.

As the ion concentration ($N$) does not remain constant throughout the series of observations, the current was measured with a standard potential at short intervals, then every reading was corrected relative to the mean of these readings if they were within reasonable limits; otherwise the whole series was repeated.

The mobility of ions was obtained from the formula:

$$K = \varphi / 4\pi V (C_1 + C_2)$$

where $\varphi$ is the volume of air passing per second, $V$ is the applied potential, $C_1$ is the capacity of the first section and $C_2$ is that of the second section.

The concentration of the ions was obtained from the formula:

$$N = E_m (C_2 + C_3/C_2)(C_1 + C_2)/\varphi e t$$

where $E_m$ is the increase of potential of the electrometer system in time $t$ for the applied voltage $V$, $C_3$ is the capacity of the electrometer and its connections and $e$ is the electronic charge. It is assumed that all ions carry a single charge.

Both expressions were derived by Hogg (1939).

**Results**

In the characteristics of large ions obtained with the apparatus, four peaks corresponding to four groups appeared clearly, namely: $k_1$ ranging from 6.2 to $6.9 \times 10^{-4}$, $k_2$ from 2.2 to $2.4 \times 10^{-4}$, $k_3$ from 0.95 to $1.03 \times 10^{-4}$ and $k_4$ from 0.60 to $0.63 \times 10^{-4}$. Two of these characteristics are shown in fig. 1 for both positive and negative ions.

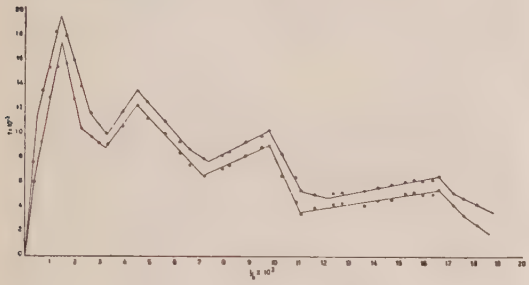

Fig. 1. Large ion characteristics for both positive and negative ions.

△ (—) ve ion
⊙ (+) ve ion

Characteristics were then obtained using monochromatic light. The four groups appeared in the same position as in the case when the box was completely dark. Fig. 2 is an example for positive ions when using monochromatic light of wave length $\lambda_{max} = 4{,}030$ Å.

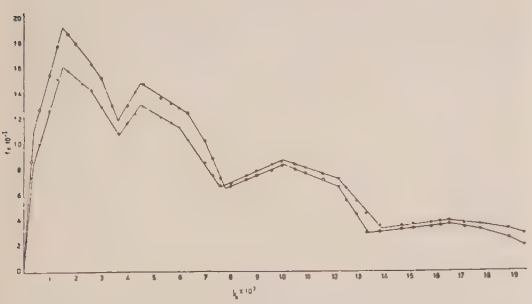

Fig. 2. Large ion characteristics for positive ions:

a) Dark box: The air sample was drawn from the covered box.

b) Box enlighted: The air sample was drawn from the box while it was exposed to monochromatic ligtht of wavelength 4030 A°.

(+) ve ion
× Dark box
⊙ Box irradiated with monochromatic light (4030 Å)

The number of ions $N_1$ and $N_2$ and also the ratio $(N_1/N_2)$ for each group are given in table 2.

**Table 2**

| Mobility | Ion concentration (+ *ve*) | | Ratio $N_1/N_2$ |
|---|---|---|---|
| | Box subjected to light of 4,030 Å $N_1$ ions/c.c. | Dark box $N_2$ ions/c.c. | |
| $6.67 \times 10^{-4}$ | 1249 | 1034 | 1.21 |
| 2.22 | 965 | 792 | 1.22 |
| 1.00 | 543 | 548 | 0.99 |
| 0.61 | 323 | 340 | 0.95 |

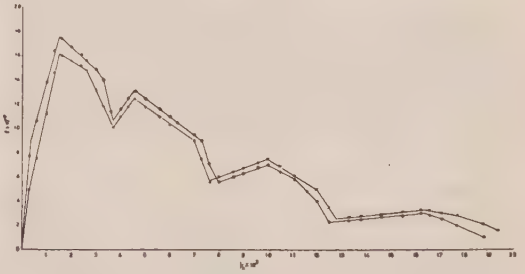

Fig. 3. Large ion characteristics for negative ions:

a) Dark box: The air sample was drawn from the covered box.

b) Box enlighted: The air sample was drawn from the box while it was exposed to monochromatic light of wavelength 6610 A°.

(—) ve ion
× Dark box
⊙ Box irratiated with monochromatic light (6610 Å)

Fig. 3 is an example for negative ions when using monochromatic light of wave length $\lambda_{max}$. $= 6{,}610$ Å. The number of ions $N_1$ and $N_2$ and also the ratio $(N_1/N_2)$ for each group are given in table 3.

**Table 3**

| Mobility | Ion concentration (— *ve*) | | Ratio $N_1/N_2$ |
|---|---|---|---|
| | Box subjected to light of 6,610 Å $N_1$ ions/c.c. | Dark box $N_2$ ions/c.c. | |
| $6.67 \times 10^{-4}$ | 1,146 | 1,051 | 1.09 |
| 2.17 | 861 | 784 | 1.10 |
| 1.00 | 448 | 471 | 0.95 |
| 0.61 | 265 | 283 | 0.94 |

**Table 4**

| Wave length $\lambda_{max}$ Å | The ratio $(N_1/N_2)$ | | | | | | | |
|---|---|---|---|---|---|---|---|---|
| | $k_1$ | | $k_2$ | | $k_3$ | | $k_4$ | |
| | + ve | — ve | + ve | — ve | + ve | — ve | + ve | — ve |
| 4,030 | 1.220 | 1.215 | 1.194 | 1.188 | 0.970 | 0.968 | 0.955 | 0.955 |
| 4,340 | 1.215 | 1.210 | 1.185 | 1.185 | .966 | .965 | .950 | .950 |
| 4,640 | 1.210 | 1.208 | 1.185 | 1.180 | .965 | .960 | .946 | .945 |
| 5,120 | 1.210 | 1.205 | 1.180 | 1.180 | .960 | .960 | .940 | .945 |
| 5,280 | 1.200 | 1.200 | 1.180 | 1.175 | .960 | .956 | .940 | .940 |
| 5,670 | 1.200 | 1.195 | 1.160 | 1.160 | .970 | .965 | .950 | .955 |
| 5,840 | 1.170 | 1.168 | 1.140 | 1.136 | .970 | .960 | .955 | .955 |
| 6,010 | 1.130 | 1.127 | 1.130 | 1.130 | .980 | .985 | .960 | .960 |
| 6,350 | 1.110 | 1.108 | 1.110 | 1.110 | .985 | .985 | .975 | .965 |
| 6,610 | 1.100 | 1.085 | 1.100 | 1.100 | .990 | .990 | .980 | .980 |

It appears from the above results that there is a slight increase in the ion concentration in case of the group mobilities $k_1$ and $k_2$, whereas a slight decrease in the ion concentration in case of the other two mobilities $k_3$ and $k_4$ can be observed.

When this effect was tested several times for both positive and negative ions using the ten filters, the same conclusion was reached but in different ratios. In table 4 a summary is given for the observations obtained during the period from October 1957 to July 1958.

By analyzing these results statistically, the following deductions were obtained.

a) The correlation test showed a very strong connection between the wave length $\lambda$, or the frequency $\nu$, and the ratio $(N_1/N_2)$ for the first two groups $k_1$ and $k_2$. This can be shown clearly from the graph relating the frequency $\nu$ and the ratio $(N_1/N_2)$ (fig. 4).

b) When applying the significance test on the ratios $(N_1/N_2)$ obtained with 4,030 Å and those obtained with 6,610 Å, for the groups $k_1$ and $k_2$, it appeared to be highly significant. Also the ratios $(N_1/N_2)$ obtained with 5,670 Å and those obtained with 6,610 Å were highly significant. On the other hand the ratios $(N_1/N_2)$ obtained with 4,030 Å and those obtained with 5,670 Å were not significant.

c) In case of the other two groups $k_3$ and $k_4$, the correlation test showed a significant connection between the wave length $\lambda$, or the frequency $\nu$, and the ratio $(N_1/N_2)$. This is shown graphically in fig. 5 relating the frequency $\nu$ and the ratio $(N_1/N_2)$.

d) The significance test showed, in case of the groups $k_3$ and $k_4$, that the ratios $(N_1/N_2)$ obtained with 4,030 Å and those obtained with 5,280 Å, and also the ratios obtained with

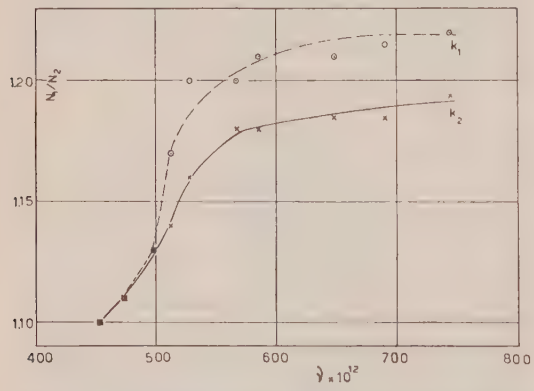


Fig. 4. The relation between $N_1/N_2$ and the frequency $\nu$ of the incident light for the two mobilities $k_1$ and $k_2$.

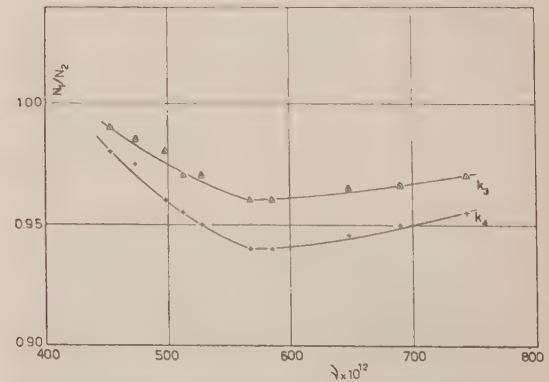


Fig. 5. The relation between $N_1/N_2$ and the frequency $\nu$ of the incident light for the two mobilites $k_3$ and $k_4$.

4,030 Å and those obtained with 6,610 Å, were not significant, while the ratios obtained with 5,280 Å and those obtained with 6,610 Å were almost insignificant.

**The above discussions can be summarized in the following:**

1. There is a slight increase in the ion concentration in the presence of monochromatic light in case of the group mobilities $k_1$ and $k_2$. This increase is more clear within the range 4,030—5,670 Å (i.e. from violet to green), and it decreases gradually from 5,670 to 6,610 Å (i.e. from green to red).

This increase in the ion concentration may be explained as due to an increase in the number of nuclei formed from the constituents of air (mainly oxygen and nitrogen) as a result of photo effect.

2. There is a slight decrease in the ion concentration in the presence of monochromatic light in case of the group mobilities $k_3$ and $k_4$. This decrease is clear in the range 4,030—5,840 Å and is less clear in the range 6,010—6,610 Å.

This decrease in the ion concentration may be due to coagulation of particles as a result of chance collisions between the nuclei, which leads to an increase in their size and hence a decrease in their concentration.

3. In general the increase in the ion concentration in case of the groups $k_1$ and $k_2$ is small, and also the decrease in the ion concentration in case of the groups $k_3$ and $k_4$ is very small, as the transmitted light from the interference filters was $\leq 57$ %.

4. The ratios $(N_1/N_2)$ obtained in case of positive ions were approximately the same as those obtained in case of negative ions but sometimes they are slightly higher.

## REFERENCES


ElNadi, A. F., 1958: On the effect of ordinary light on small ion concentration. *Math. and Phys. Soc. of Egypt No.* **22**, p. 59.

Hogg, A. R., 1939: The intermediate ions in the atmosphere. *Proc. Phys. Soc.* **51**, p. 1014.

Israel, H., Fries, G. and Dolezalek, H., 1956: Technical Note No. 7. Contract No. AF 61 (514) 640. *Air Research and Development Command U.S. Air Force.*

Ortner, G. and ElNadi, A. F., 1955: Intermediate and large atmospheric ions at Cairo—Giza. *J. Atmosph. Terr. Phys.* **7**, p. 31.

Pollak, L. W., 1955: Condensation nuclei. Symposium in Dublin. *Nature*, **175**, p. 1072.

Verzár, F. and Kunz, Y., 1957: Production of atmospheric condensation nuclei by solar radiation. *Geofisica pura e applicata*, **38**, p. 215—221.

# The Daily Variation of the Cosmic Ray Nucleonic Component at Murchison Bay and Uppsala

By ARNE ELD SANDSTRÖM, ERIC DYRING and STIG LINDGREN

Institute of Physics, University of Uppsala, Sweden

(Manuscript received February 13, revised version March 7, 1960)

*Abstract*

In both places the monitors were of the standard pattern with 12 proportional counters filled with 97 per cent enriched $B^{10}F_3$. The first and second harmonics of the mean daily variation have been determined both for yearly periods and for each sun rotation period. Vector sum diagrams for the first harmonics in the latter case are given covering the intervals 31 Aug. 1956 to 15 Aug. 1959 for Uppsala and 13 Sept. 1957 to 29 April 1959 for Murchison Bay. In some instances a considerable phase shift has taken place from one sequence of sun rotation periods to another. These phase shifts were not contemporary at the two stations. The first harmonic of the 12-month means displays a high degree of constancy with only a small secular phase shift. The amplitudes of the second harmonics are very small. Conditions are especially favourable concerning the deviation in the earth's magnetic field of the particles registered by the Murchison Bay monitor. Accordingly it has been possible to determine the direction of the anisotropy with a fairly good accuracy. The Murchison Bay records do not show any prominent phase shift with the $K_p$ index. Concerning Uppsala, days with $[K_p]_{\max} \leqq 1^+$ have a later time of maximum than other days. The influence of single days with an abnormal daily variation is discussed.

## Introduction

When plans were made for a Swedish arctic station during the IGY it was deemed essential to include a neutron pile monitor among the equipment for cosmic ray studies. The plans were realized through the Swedish-Finnish-Swiss IGY-expedition 1957—58 to Murchison Bay (LILJEQUIST 1959). The site of the arctic station is on the island Nordaustlandet of the Svalbard (Spitzbergen) archipelago. Its geographic coordinates are 80° 03′ N and 18° 18′ E. It is nearly on the same meridian as the cosmic ray station at Uppsala (59° 55′ N and 17° 55′ E).

The continuous records from the Murchison Bay monitor start with Aug. 27, 1957. After the end of the Swedish-Finnish-Swiss IGY expedition the base was maintained for another year. However, owing to very adverse ice-conditions at the end of the 1958 summer it became impossible to refurnish the base with an adequate supply of diesel oil for the generators. As a consequence the continuous running of the latter had to end with April 1959. The first year's results from the Uppsala monitor have already been published (SANDSTRÖM and LINDGREN 1959).

## Experimental details

Both monitors are of the type (SIMPSON, FONGER and TREIMAN 1953) recommended as the international standard instrument for the geophysical year. The few details in which the monitors differ from those of Simpson et al. were described in a previous paper (SANDSTRÖM and LINDGREN 1959). The monitor for the arctic station was designed in such a way

as to make it possible to assemble the monitor for tests in the laboratory at Uppsala and then remove it in pieces to be reerected at Murchison Bay with the least possible trouble.

Although the site of the arctic station was in a region believed to be comparatively free from heavy snow falls, an iron scaffold was constructed to carry the monitor at a level well above the height of any snow drifts which might possibly collect along the walls of the C.R. building. The top of the scaffold consisted of a frame of beams supporting a thick wooden floor. The monitor itself stood on this floor. The roof of the building was given a shape expected to favour the snow being blown away by the prevailing winds. The scheme turned out very well. During the first year of recording the amount of snow staying on the roof never exceeded some few grams per cm². The mass of the heat insulated roof itself is less than 10 g/cm². Twice during the second year snow had to be removed from the roof.

The electronics of the Murchison Bay monitor is a true replica of that at Uppsala (SANDSTRÖM and LINDGREN 1959). The power was supplied by two diesel-engined generators, one of them always being kept ready to take over the load in an emergency.

As the research station at Murchison Bay included a very complete meteorological service and the pressure was registered in an adjacent building it was deemed quite unnecessary to equip the monitor with an instrument for independent barometric measurements. The general cosmic ray equipment includes an auxiliary recording instrument (SANDSTRÖM and LINDGREN 1959). From these auxiliary records the counting rates can be derived for periods of any length from half a minute to one hour.

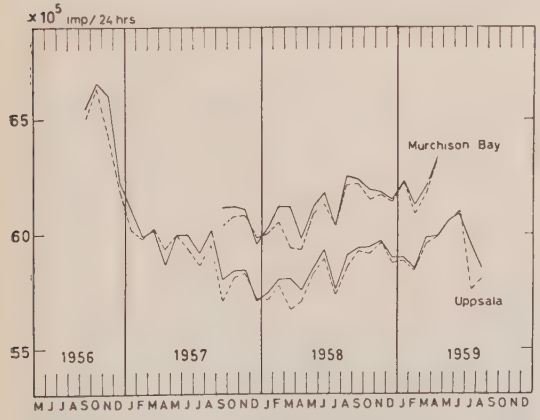


Fig. 1. Monthly means of the 24-hr values of the nucleon component in Uppsala and Murchison Bay. Full lines: days with $[K_p]_{max} \leq 3^+$. Dotted lines: all available days.

The monitors were calibrated by means of RaBe neutron sources of 1 mc. Calibrations were made whenever a readjustment of amplifiers or discriminators took place as well as after repairs or at any suspicion of a change of counting rate. No regular time schedule was followed as it was our aim to disturb the continuous performance of the monitors as little as possible. The two monitor sections were always calibrated separately. By limiting each calibration run to 25 minutes the whole calibration could be completed within one hour. This was necessary with regard for the continuity of the records as one section could not be calibrated without affecting the counting rate of the other. Likewise the neutron source affected the counting rate of the counter telescopes in the vicinity of the monitors.

With cadmium covers on the proportional counters the counting rate of the Uppsala monitor was 4 per cent of the normal counting rate with the cadmium tubes removed, while that of the Murchison Bay monitor was only 2.5 per cent. In both cases it was constant all along the plateau of the counters.

During Sept. 1957 the average counting rate of the Murchison Bay monitor was 420 c/min., while that of the Uppsala monitor was as low as 400 c/min. The Murchison Bay records cover the period of minimum intensity of the nucleonic component (Fig. 1) as well as what appears to be the start of a slow increase. The monthly averages appear to follow one another comparatively closely regardless of whether all days are included or only those with $K_p$ indices less than $3^+$.

In the records from Murchison Bay 17 days are affected by breaks of such an extent as tc make them unsuitable for harmonic analysis. For the same reasons 29 days have to be excluded from the Uppsala records between 1 Sept. 1957 and 31 Aug. 1959. For both monitors there are instances in which days could be saved for the harmonic analysis by interpolating values for single hours or, in a few cases, two consecutive hours. In no case single events or abrupt intensity changes are

known to have taken place during the interval for which such an interpolation was performed.

All data have been referred to intervals of 2 hours. They have been reduced to an atmospheric pressure of 1,010 mb (the yearly average for Uppsala is 1,008 mb and that for Murchison Bay 1,012 mb). The pressure coefficient = 0.737 per cent/mb has been adopted for both the monitors (SANDSTRÖM 1958, SANDSTRÖM and LINDGREN 1959).

**The daily variation**

The yearly mean daily variations of the nucleonic component as recorded in Murchison Bay and Uppsala during the period 1 Sept. 1957 to 31 Aug. 1958 are shown in Fig. 2. The statistical variations are also plotted for each 2-hour interval. The figure displays how the points of measurement are distributed relative to the first and second harmonics. A corresponding diagram for the records from the Uppsala monitor from 1 Sept. 1956 to 31 Aug. 1957 has been published in a previous paper. A comparison does not display any differences in either phase or amplitude between the two yearly means as recorded by the Uppsala monitor. The points of measurement constitute a time series. Therefore, it is difficult to calculate the standard error for the amplitude as well as for the phase. In previous papers (SANDSTRÖM 1955, SANDSTRÖM and LINDGREN 1959), this difficulty was surmounted by exchanging the standard error for another limit of error. The latter was based on the assumption that the error in the differences between the daily mean and the number of pulses during each 2-hr period was twice the standard deviation of each point of measurement (SANDSTRÖM 1955). The error determined in this way will give a confidence of 90—99 per cent. It meets the purpose well when high confidence is desirable. However, comparisons become difficult with other papers, where, usually, limits of error are based only on the Poisson distribution of pulses. In the present paper we have therefore returned to this method of defining the accuracy.

At the same time it appears to us essential to determine the limits of error so as to correspond to real facts. This can be done by calculating the standard error from the residuals of the points of measurement after fitting the first harmonic, resp. the sum of the first and second harmonics. The deduction of the formulas for this error will be given elsewhere (DYRING and ROSÉN 1960). In some of the clock diagrams we have indicated this limit of error by dotted circles. It is our opinion that this kind of error should be employed for the calculation of significances rather than that deduced solely from an assumed Poisson distribution of pulses. The standard deviation of the points of measurement from the resulting curve will evidently include all statistical fluctuations. There is no constant relation between the two kinds of errors. That including all statistical fluctuations is usually bigger than that covering only the Poisson

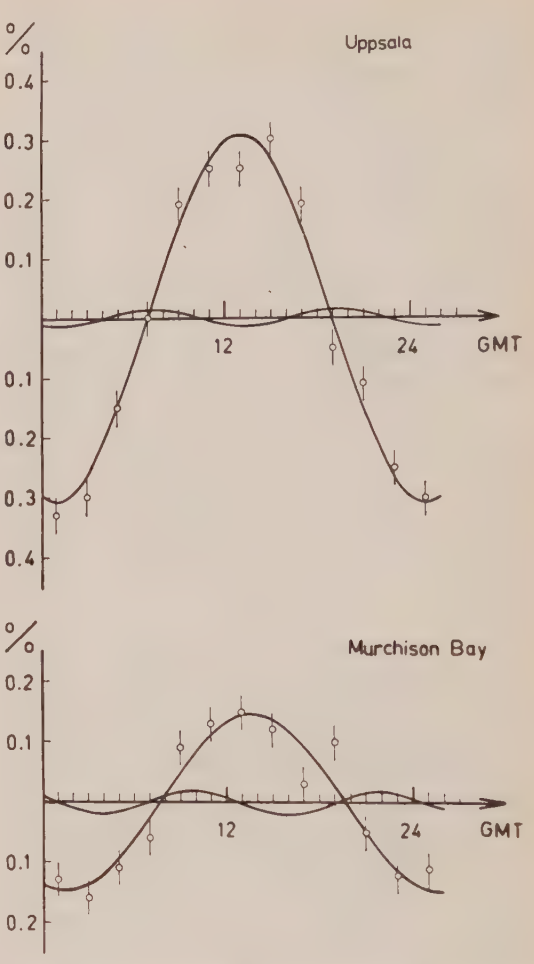


Fig. 2. First and second harmonics of the mean daily variation for 1 Sep. 1957 to 31 Aug. 1958 at Murchison Bay and Uppsala. The statistical fluctuations are indicated.

distribution. Concerning the additional variations we wish to remark that one of us (Dyring 1960) has found that the statistical fluctuations calculated according to Poisson's law have to be multiplied by a factor of 1.2 to cover the actual hour by hour fluctuations.

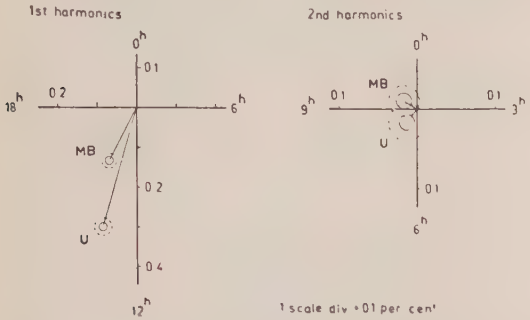


Fig. 3. First and second harmonics of the nucleon component 1 Sep. 1957 to 31 Aug. 1958. MB: Murchison Bay, U: Uppsala. Full circles: standard error from Poisson distribution. Dotted circles: standard error calculated from residuals after fitting first and second harmonics.

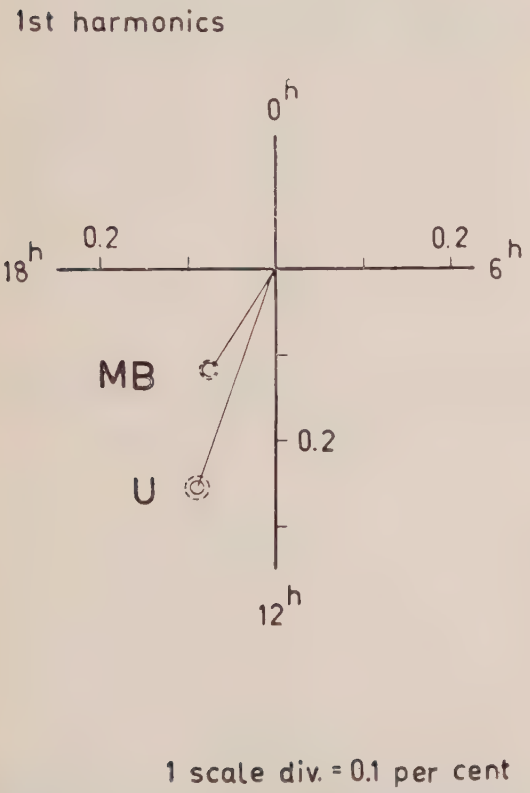


Fig. 4. First harmonics for the mean daily variation of the nucleonic component 26 Aug. 1957 to 30 Apr. 1959, MB: Murchison Bay, U: Uppsala. Full circles: standard error from Poisson distribution. Dotted circles: standard error calculated from residuals after fitting first and second harmonics.

The amplitude of the first harmonic is evidently smaller at the latitude of Murchison Bay than at the latitude of Uppsala. This is displayed also by the clock diagrams in Figs. 3 and 4. The phase difference is 45 minutes in both cases. A small phase shift is indicated by the records from the Uppsala monitor during three consecutive years (Fig. 5). The small amplitude at Murchison Bay causes an error in the time of maximum approximately twice as big as that affecting the time of maximum at Uppsala. Concerning the phase difference between Uppsala and Murchison Bay it undoubtedly exists even with due regard for the wider limits of error deduced from the standard deviations of the points of measurement from the first harmonic (Fig. 3 and 4).

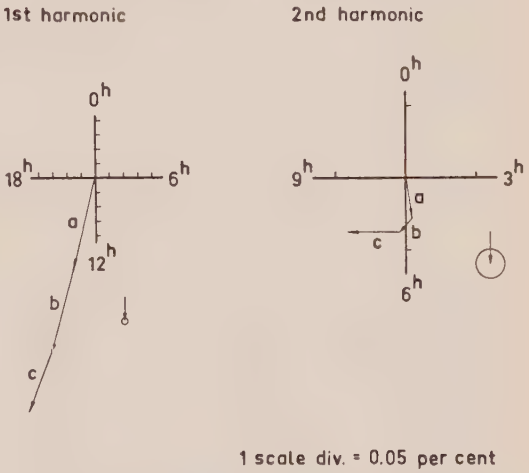


Fig. 5. Vector sum diagrams for the first and second harmonics of the nucleon component at Uppsala. a: 1 Sep. 1956—31 Aug. 1957; b: 1 Sep. 1957—31 Aug. 1958; c: 1 Sep. 1958—31 Aug. 1959.

Turning to the vector sum diagram of the yearly means from Uppsala (Fig. 5) we note that a small but persistent phase shift is indicated during three consecutive 12-monthly periods. It ought to be remarked, however, that there appears to be a phase difference of 45 minutes between the two calendar years 1957 and 1958 (Table 1). This difference is far outside any limits of error. The reason for such a shift depending on the starting point for the twelve-monthly periods is more easily

Fig. 6. Vector sum diagrams for the 27-day periods. The Murchison Bay vectors are twice the scale of those for Uppsala. The numbers denote sun rotation periods covering the following dates: 1690: 17 Dec. 1956—12 Jan. 1957; 1695: 1 May 1957—27 May 1957; 1700: 13 Sep. 1957—9 Oct. 1957; 1705: 26 Jan. 1958—21 Feb. 1958; 1710: 10 Jun. 1958—6 Jul. 1958; 1715: 23 Oct. 1958—18 Nov. 1958; 1720: 7 March 1959—2 Apr. 1959; 1725: 20 Jul. 1959—15 Aug. 1959.

understood after studying the vector sum diagrams in Fig. 6. These diagrams represent the phase and amplitude of the first harmonic of the mean daily variation for separate sun rotation periods. Naturally, the influence from the statistical fluctuations will be considerable although very few days had to be excluded. Although such an exclusion of a couple of days from a 27-day period usually does not affect the mean values of either the phase or the amplitude there are instances, especially during periods with a small amplitude, when a considerable change is caused by excluding only one single day (SANDSTRÖM and LINDGREN 1959). Therefore, the means for the sun rotation periods have been calculated using exactly the same days for both stations. In general the Murchison Bay records display a small amplitude. Consequently the random fluctuations will tend to mask most of the phase variations. For both stations it can be said that in most instances where there is a considerable variation in phase the amplitude is small and consequently the whole phase change can be regarded as due to a random distribution around a mean. In other instances the more or less persistent trend of the phase indicates variations which apparently are real.

The vector sum diagram for Murchison Bay displays a couple of very marked phase shifts. Starting with August and through October 1958 the phase differed definitely from that before as well as after this period. It appears

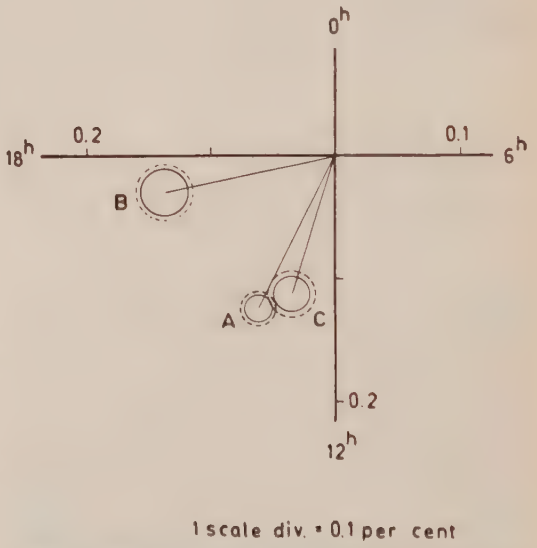


Fig. 7. Phase shifts of the first harmonic of the nucleon component registered at Murchison Bay. Full circles: standard error from Poisson distribution. Dotted circles: standard error calculated from residuals after fitting first and second harmonics.
A: 10 Oct. 1957—2 Aug. 1958; B: 3 Aug. 1958—18 Nov. 1958; C: 19 Nov. 1958—29 Apr. 1959.

**Table 1. First and second harmonics of the mean daily variation.**
**The standard error of the amplitude calculated from the Poisson distribution of primary values ranges from 0.006 to 0.010. Calculated from residuals after fitting first harmonic it ranges from 0.008 to 0.020. Calculated from residuals after fitting first + second harmonics it ranges from 0.006 to 0.017 (Detailed tables complete with limits of error are distributed on application).**

| Station Int.number | Period | First harmonic | | Second harmonic | |
|---|---|---|---|---|---|
| | | Amplitude Per cent of daily mean | Phase GMT | Amplitude Per cent of daily mean | Phase GMT |
| Uppsala B 003 | 1 Sept. 1956—31 Aug. 1957 | 0.322 | 12 55 | 0 028 | 05 43 |
| | Calendar year 1957 | 0.333 | 12 44 | 0.040 | 05 53 |
| | 1 Sept. 1957—31 Aug. 1958 | 0.306 | 12 57 | 0.014 | 07 24 |
| | Calendar year 1958 | 0.219 | 13 29 | 0.009 | 09 54 |
| | 1 May 1958—30 Apr. 1959 | 0.217 | 13 29 | 0.030 | 08 42 |
| | 1 Sept. 1958—31 Aug. 1959 | 0.222 | 13 24 | 0.036 | 09 02 |
| | 26 Aug. 1957—30 Apr. 1959 | 0.263 | 13 15 | 0.020 | 07 34 |
| | 1 Sept. 1956—31 Aug. 1959 | 0.283 | 13 03 | 0.018 | 07 33 |
| Murchison Bay A 010 | 1 Sept. 1957—31 Aug. 1958 | 0.147 | 13 40 | 0.020 | 09 56 |
| | Calendar year 1958 | 0.131 | 14 31 | 0.019 | 01 25 |
| | 1 May 1958—30 Apr. 1959 | 0.131 | 14 14 | 0.027 | 03 46 |
| | 26 Aug. 1959—20 Apr. 1959 | 0.139 | 14 06 | 0.008 | 04 22 |

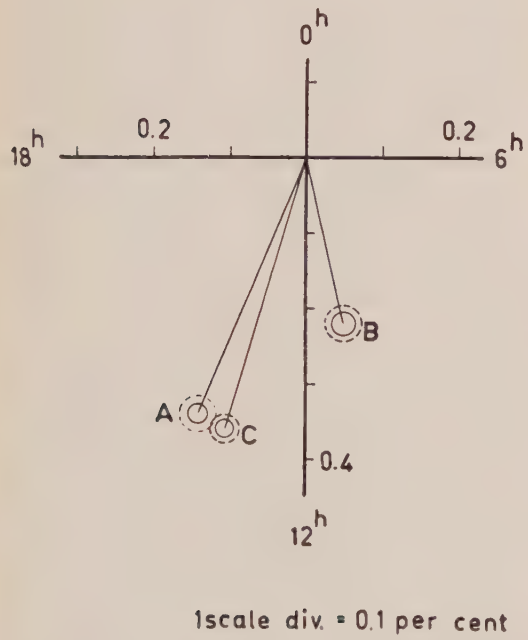


Fig. 8. Phase shifts of the first harmonic of the nucleon component registered at Uppsala. Full circles: standard error from Poisson distribution. Dotted circles: standard error calculated from residuals after fitting first and second harmonics.

A: 31 Aug. 1956—7 March 1957; B: 8 March 1957—20 Jul. 1957; C: 21 Jul. 1957—3 March 1958.

also as if a phase shift had taken place shortly after the start of recording. However, the discussion will be confined to the other two instances when a phase shift appears to have taken place. Accordingly we calculate the means for the periods 10 Oct. 1957—2 Aug. 1958; 3 Aug.—18 Nov. 1958, and 19 Nov. 1958—29 April 1959. The result is illustrated by the clock diagram in Fig. 7. With due regard for standard errors it is evident from this diagram that the phase is the same during the first and third periods. Combining these two periods we find a time of maximum intensity of 1328 GMT ± 17 min. For the period 3 Aug.—18 Nov. 1958 the time of maximum was 1723 GMT ± 31 min. From Fig. 7 it is apparent that the phase shift is real. The phase shift is 56° ± 22°. It is clearly indicated still if we demand a confidence of 95 per cent.

It is possible that the phase shift of the mean daily variation in Uppsala for the two calendar years as compared to the three twelve-monthly periods is due, also, to short periods of a differing phase (Table 1). A study of the details of the vector sum diagram for this station (Fig. 6) reveals the existence of such periods although they are less conspicuous than in the Murchison Bay records. The clock diagram in Fig. 8 illustrates the mean daily

variation during the three periods 31 Aug. 1956—7 March 1957; 8 March—20 July 1957, and 21 July 1957—3 March 1958. This case exhibits a striking resemblance to that illustrated in Fig. 7. It is evident that during the middle period the phase differed from that during the two adjacent periods. A phase difference between the two latter is also indicated, the time of maximum being 1327 GMT ± 8 min. for the first one and 1305 GMT ± 8 min. for the third period. During the intervening time, 8 March—20 July 1957, the time of maximum was 1117 GMT ± 16 min. This period with an early maximum falls inside the calendar year 1957. In the following year there does not exist any prolonged period with such a comparatively early maximum (during the sun rotation period no. 1711 the mean time of maximum was 1030 GMT). If the period 8 March—20 July is excluded from the 1957 records the mean time of maximum will be practically the same as that during 1958.

The two vector sum diagrams (Fig. 6) reveal also that the variations of the amplitudes in the two places are not well correlated. This is especially true for the last quarter of 1957 and the first quarter of 1958.

The amplitude of the second harmonic is very small. It is of the same order of magnitude in Uppsala and Murchison Bay (Fig. 3). Both phase and amplitude are severely affected by the exclusion of only a few days. Further, as was shown by the first year's records from the Uppsala monitor, periods exist which have a prominent second harmonic while the amplitude of the first harmonic is of the same order of magnitude or even less (SANDSTRÖM and LINDGREN 1959).

The three consecutive 12-monthly periods combined with the calendar years 1957 and 1958 from the Uppsala monitor provide running means for a study of the second harmonic (Table 2). The vector sum diagram for the three 12-monthly periods is to be found in Fig. 5. This diagram as well as the figures in Table 1 strengthen the picture of a considerable variation both in phase and amplitude. If we consider only the Poisson distribution of the number of pulses during the 2-hr intervals the existence of the second harmonic does not seem to be in doubt. If the standard errors are calculated from residuals of the points of measurement after fitting first plus second harmonics the second harmonic appears doubtful (Fig. 3).

**Table 2.**

| | Uppsala | Murchison Bay |
|---|---|---|
| Geomagn. lat..... | 58° 36′ | 75° 30′ |
| Geomagn. long. .... | 107° | 137° 30′ |
| Dip..... | 72° 30′ | 82° 30′ |
| Declination..... | 0°30′E | 1° 0′ E |

### The longitude correction

Terrella experiments (MALMFORS 1945, BRUNBERG 1953, BRUNBERG and DATTNER 1953) made it possible to calculate the asymptotic directions of primaries for various rigidities and directions of registration (BRUNBERG 1956). The knowledge thus gathered can be utilized to determine the true direction of the anisotropy responsible for the daily variation (BRUNBERG and DATTNER 1959). However, several obstacles have to be overcome before it becomes possible to determine the correction for the deviation of the primaries in the geomagnetic field with a precision corresponding to that of present day C.R. registrations (DORMAN 1957). Three factors are involved: the rigidity spectrum of the primaries, the solid angle of acceptance of the detector, and the shape of the geomagnetic field. The multiplicity of the nucleon production is a function of the rigidity. It is thus a part of the first one of the three factors listed. The effective rigidity to be ascribed to the primaries of the nucleonic component at the geomagnetic latitude of Uppsala has been discussed elsewhere (SANDSTRÖM and LINDGREN 1959). Concerning Murchison Bay especially favourable conditions govern the angular correction in the east-west plane for particles observed by the monitor in the zenith direction. At this latitude secondaries accepted by the monitor at zenith angles up to 48° originate from primaries having asymptotic directions inside a comparatively narrow cone (ÅSTRÖM 1956; compare also Fig. 32 in BRUNBERG 1956). Under these conditions we have found it permissible to regard the Murchison Bay monitor as observing predominantly in the zenith direction.

The longitude correction $\psi$ and the latitude correction $\phi$ for the zenith direction and

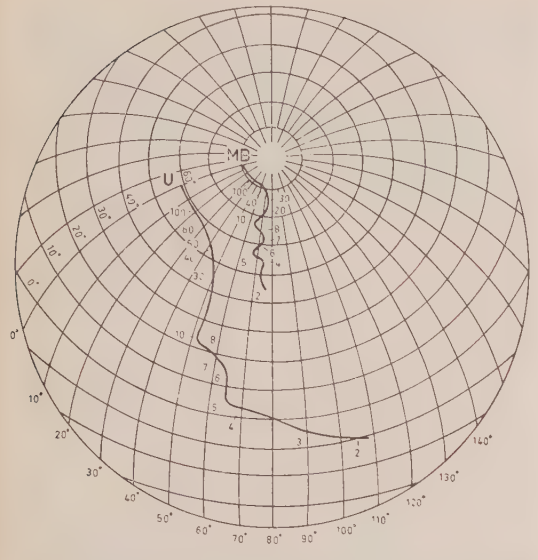


Fig. 9. Longitude and latitude corrections for the zenith directions in Uppsala (U) and Murchison Bay (MB). The rigidities are indicated in the figure. The unit is $10^9$ eV/c.

varying rigidities have been plotted in a diagram (Fig. 9) according to BRUNBERG (1956). The values have been recalculated to the geographic lat. 80° (Murchison Bay), Brunberg's original Svalbard values being calculated for geographic lat. 78° (Longyearbyen). In high latitudes a couple of degrees make quite a marked difference. For rigidities below 10 GeV/c the values have been calculated from the measurements by MALMFORS (1945).

The corresponding curve for the zenith direction in Uppsala has been entered into the same figure. The conditions are not as favourable in this case as in the former one. Nevertheless, as has been pointed out by ÅSTRÖM (1956) the spherical representations by BRUNBERG (1956) of $\psi$ and $\phi$ reveal a certain focussing effect even for latitudes down to 50°. However, the cones limiting the asymptotic directions will not have as small a solid angle as in the case of the Murchison Bay monitor.

What concerns us most is the longitude correction $\psi_{MB}$. Fig. 9 reveals that for rigidities below 40 GeV/c this correction does not vary very much with the rigidity. Most of the primaries responsible for the nucleonic component will have rigidities below 10 GeV/c. Accordingly it appears to be realistic to put

$$\psi_{MB} = 72° \pm 5° \qquad (1)$$

The most remarkable fact is that even a considerable change in spectral distribution will leave this value unaffected. On the contrary, for Uppsala, the longitude correction will vary strongly with the spectral distribution of the primaries.

The longitude correction was discussed concerning the first year's records from the Uppsala monitor (SANDSTRÖM and LINDGREN 1959). This discussion led to

$$\psi_U = 71° \pm 15° \qquad (2)$$

It is very tempting to try to find a value with smaller limits of error by comparing the curves in Fig. 9. Such a comparison would have to be based on the assumption that above the knee of the latitude effect the rigidity spectrum does not vary with the latitude. Naturally, it has also to be assumed that the direction of the anisotropy is the same regardless of the fact that the Uppsala monitor mainly registers primaries entering the earth's magnetic field parallel or nearly parallel to the equatorial plane while the Murchison Bay monitor registers primaries entering the field in directions 45° to 70° from this plane.

The values in Table 1 show that the phase difference between the two stations varies with the starting point of the 12-monthly periods. On the average it is $12° \pm 5°$. The limits of error are difficult to determine in this case. The variations between the three 12-monthly periods are covered by $\pm 3°$. The standard errors calculated from the residuals after fitting the first plus second harmonics yield $\pm 5°$. The values all refer to 12-monthly means. Such abnormal phase shifts as those illustrated by Figs. 8 and 9 are not considered. The correction for Uppsala calculated from $\psi_{MB}$ and the phase difference between the two stations would then be

$$\psi_U = 84° \pm 10° \qquad (3)$$

Accordingly the curves in Fig. 9 indicate that the "effective" rigidity has to fall between 3 and 5 GeV/c to correspond to the same original direction of the anisotropy in both cases. This is reasonable, considering what is known of the rigidity spectrum of the primaries generating the nucleonic component.

Recent studies of the latitude effect have shown that the actual magnetic field configuration near the surface of the earth has a certain influence on the geomagnetic cut off of C.R. (ROTHWELL 1958, SANDSTRÖM 1958, POMERANTZ, SANDSTRÖM, POTNIS, and ROSE 1959). It has not been proved that there exists a corresponding effect on the trajectories of the primaries. Most of the length of each trajectory will certainly fall in a region where the geomagnetic field is regular and free from anomalies. In Murchison Bay as well as in Uppsala the magnetic meridian plane nearly coincides with the geographic meridian. Dip and geomagnetic coordinates are listed in Table 2.

**The direction of the anisotropy**

The direction of the observed anisotropy is most conveniently defined through the angle $\alpha$ it makes with the radius vector from the sun. For this angle we have

$$\alpha = \lambda + \tau + \psi \qquad (3)$$

Here $\lambda$ represents the geographic longitude (Table 3). $\tau$ is the difference, in angular measure, between the time of maximum and noon i.e. $\tau = 15^\circ (t_{max} - 12)$. The values of $\tau$ for the periods under discussion are listed in Table 3. The value of the longitude correction $\psi$ for Murchison Bay is that given by eq. (1). For Uppsala $\alpha$ has been calculated both with a longitude correction according to eq. (2), viz. deduced independently of any comparisons with Murchison Bay, as well as with that according to eq. (3). The results covering the period of recording at Murchison Bay are listed in the last three columns of Table 3, where $\alpha_U$ refers to Uppsala and $\alpha_{MB}$ to Murchison Bay. Naturally, the way of deducing the longitude correction represented by eq. (3) results in nearly coinciding pairs of values in the two last columns of the table. Nevertheless, the direction of the anisotropy as recorded by the Uppsala monitor will still be inside the limits of error asigned to the longitude correction according to eq. (2).

In the discussion concerning the vector sum diagrams in Fig. 6 and the clock diagrams in Figs. 7 and 8 it was remarked that the yearly mean of the daily variation might vary slightly with the starting points of the twelve-monthly periods. This is apparent from the values in Table 3 also. As long as we do not know the reason for the non-periodical phase shifts causing these variations we are not able to eliminate them. Influences from short period variations are probably eliminated to a large extent in every yearly mean (compare final section). Therefore, it should be emphasized that the present discussion on the direction of the anisotropy is concerned only with 12-monthly averages.

A simple way of studying the directions of C.R. anisotropies is to resolve the corresponding vector into components along two axes, one along the radius vector from the sun and one along a tangent to the orbit of the earth (SANDSTRÖM 1956). Concerning the records from Murchison Bay there is no doubt about the existence of the component along the radius vector. It is directed towards the sun. Exactly the same can be said of the Uppsala records if the longitude correction according to eq. (3) is used. A radial component towards the sun is still present when the longitude correction is that given by eq. (2).

**The daily variation as a function of the $K_p$ index**

Concerning the meson component there exists comparatively strong evidence that the

Table 3.

| Period | $\tau_U$ | $\tau_{MB}$ | $\alpha_U$ | | $\alpha_{MB}$ |
|---|---|---|---|---|---|
| | | | $\psi = 71^\circ$ | $\psi = 84^\circ$ | |
| 1 Sept. 1957—31 Aug. 1958 ... | $14.5^\circ \pm 5^\circ$ | $25.0^\circ \pm 5^\circ$ | $103^\circ \pm 20^\circ$ | $116^\circ \pm 15^\circ$ | $115^\circ \pm 10^\circ$ |
| Calendar year 1958 ..... | $22.3^\circ \pm 5^\circ$ | $37.7^\circ \pm 5^\circ$ | $111^\circ \pm 20^\circ$ | $124^\circ \pm 15^\circ$ | $128^\circ \pm 10^\circ$ |
| 1 May 1958—30 Apr. 1959.. | $22.3^\circ \pm 5^\circ$ | $33.5^\circ \pm 5^\circ$ | $111^\circ \pm 20^\circ$ | $124^\circ \pm 15^\circ$ | $124^\circ \pm 10^\circ$ |

phase of the daily variation depends on the prevailing geomagnetic conditions (SEKIDO and KODAMA 1952, SANDSTRÖM 1955). For a similar treatment of the present data on the nucleonic component the days were divided into five classes determined by the maximum $K_p$ index of each day (SANDSTRÖM 1955). These classes are

$$\text{I: } [K_p]_{\max} \leqq 1^+$$

$$\text{II: } 1^+ < [K_p]_{\max} \leqq 3^+$$

$$\text{III: } 3^+ < [K_p]_{\max} \leqq 5^+$$

$$\text{IV: } 5^+ < [K_p]_{\max} \leqq 7^+$$

$$\text{V: } 7^+ < [K_p]_{\max} \leqq 9^-$$

For the sake of comparison between Uppsala and Murchison Bay one of the periods was selected so as to include the whole set of neutron monitor records from the latter place. As the records from Uppsala show good agreement in phase as well as in amplitude for the three 12-month periods illustrated by the vector sum diagram in Fig. 5 it was considered appropriate to combine these three periods into one.

A study of this kind has already been published concerning the first year of the Uppsala records (SANDSTRÖM and LINDGREN 1959). As regards the days employed in the comparison between Uppsala and Murchison Bay those belonging to class I are exactly the same in both cases. In classes II and III the number of days is so big as to make the few cases of odd days completely insignificant. Concerning class IV the available number of days is anyhow so low as to necessitate the employment of as many days as possible for the sake of the statistical fluctuations. Moreover, variations correlated with the geomagnetic conditions might be responsible for some of the day to day phase shifts which undoubtedly exist. From this point of view it appears desirable to accumulate as many days as possible for each $K_p$ index class. If the number of days in one group is as large as 60 the removal of a few days does not affect either amplitude or phase in a serious way (SANDSTRÖM and LINDGREN 1959).

Concerning the most disturbed days (class V) we encounter another problem. These days are usually those on which a prominent Forbush decrease occurred. An ordinary linear trend correction is then often inadequate for the separation of the true daily variation from the singular event (SANDSTRÖM and LINDGREN 1959). Therefore, no vector corresponding to class V has been included in the clock diagrams of Figs. 10 and 11. However, in the Uppsala records there is a sufficient number of days available during which C.R. conditions were undisturbed despite the very high $K_p$ indices. These days have been employed for a special study illustrated in Fig. 12.

Concerning Murchison Bay (Fig. 10) the vectors for all four classes of days fall together inside the limits of error. Also the contemporary Uppsala records display small variations, the class I days excepted. Despite the

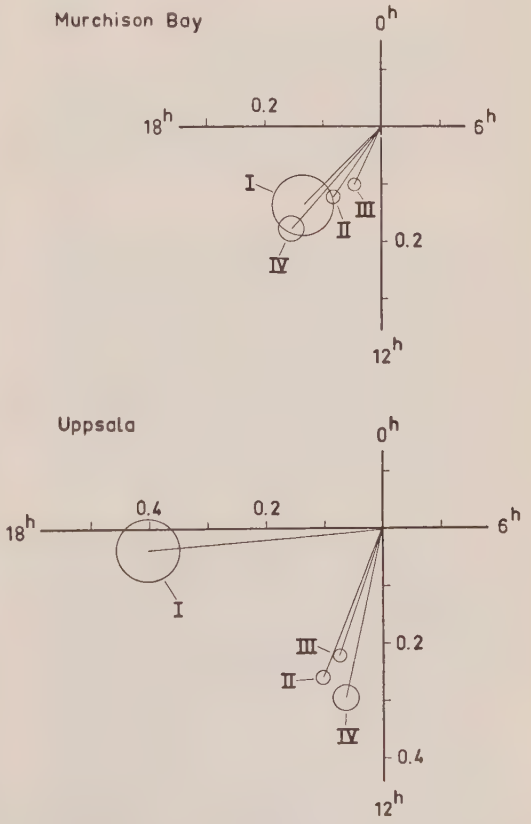


Fig. 10. The mean first harmonics for days divided into classes according to their maximum $K_p$ index. Period: 26 Aug. 1957 to 30 Apr. 1959. The Roman numbers mark the grouping of days according to the classification on p. 341.

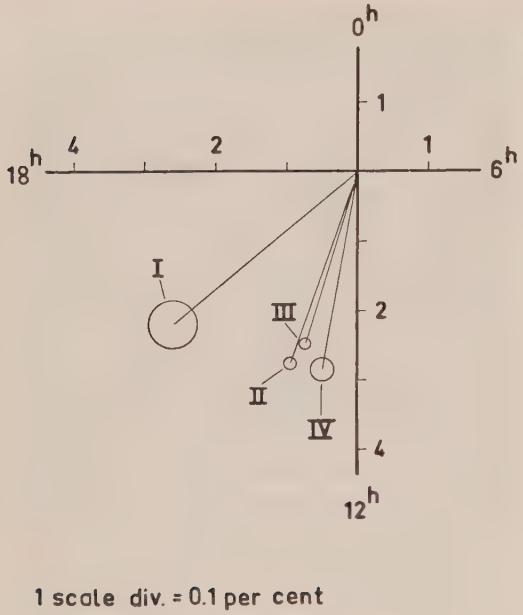


Fig. 11. The mean first harmonics at Uppsala for days divided into classes according to their maximum $K_p$ index. Period of 36 months: 1 Sep. 1956 to 31 Aug. 1959. The Roman numbers mark the grouping of days according to the classification on p. 341.

small number of days the limits of error are sufficiently narrow to prove the reality of the phase shift for quiet days (class I). Likewise there is little doubt that on class IV days the maximum tends to appear earlier than on the days of classes II and III. Space forbids the introduction into Figs. 10 and 11 of the standard errors based on the residuals of the experimental points after fitting the first plus second harmonics.

During the period 31 Aug. 1956—31 Aug. 1957 the phase of the class I days in Uppsala was the same as that of classes II and III. The introduction of accurately calculated limits of error does not change this aspect. The phase shift for the class I days from this period to the following 12-month period is more than twice the standard errors calculated from the Poisson distribution. From this point of view it is perhaps not suitable to found an analysis on as long a period as 36 months. But, this special shift excepted, the changes from one year to another are small. A period over several years will present, through better statistics, a more accurate determination of the phase shifts between the other classes of days. From Fig. 11 can be seen that the class IV days certainly have an earlier mean time of maximum than days with $[K_p]_{max} \leqq 5^+$. In all the three clock diagrams (Figs. 10 and 11) the phase appears to be nearly the same for classes II and III.

The long period of 36 months has also yielded a sufficient number of days with $7^+ < [K_p]_{max} \leqq 9^-$ for the study illustrated in Fig. 12. In this case we have found it important to calculate also the limits of error from the residuals after fitting the first and second harmonics. They are illustrated by dotted circles in Fig. 12. During the whole period 11 days of class V were found which did not have any single event disturbing the normal variation. The 2-hr values for each single day can be read from the curves in columns 1, 2, and 4 in the upper part of Fig. 12. To these 11 days can be added six days with small Forbush decreases or parts of such decreases (curves in column 3, Fig. 12). The corresponding vectors are to be found in the clock diagram in the lower part of the same figure. In the first case the phase is nearly the same as for the class IV days in Fig. 11. In the second case it lags 22° behind (1.5 hrs). The amplitude has also increased. If all available days of class V are employed the phase lag increases to 27° and the mean amplitude becomes twice that of the group of 11 days first considered. As the added days are such with prominent Forbush decreases it is evidently the decreases and not a change in the normal daily variation which produce the big amplitude.

The change in phase is not as easily brought back to the same source. Nevertheless, days with $[K_p]_{max} > 7^+$ but undisturbed by actual decreases (11 d vector in Fig. 12) have nearly the same phase and amplitude as those belonging to class IV.

The variation of the amplitude with $[K_p]_{max}$ differs from that observed for the meson component (SANDSTRÖM 1955). At present the nucleon component has its biggest amplitude on days with $[K_p]_{max} \leqq 1^+$. It decreases with increasing $[K_p]_{max}$ until $[K_p]_{max} = 5^+$. After that it appears to increase slightly (class IV). The same picture is offered by all the three clock diagrams (Figs. 10 and 11).

From the small spread of the vectors for the nucleonic component at Murchison Bay it

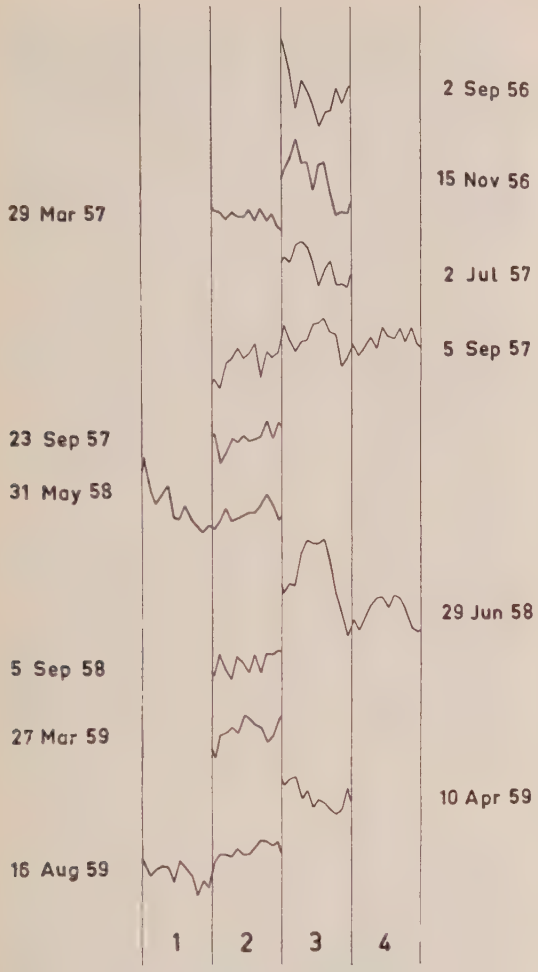


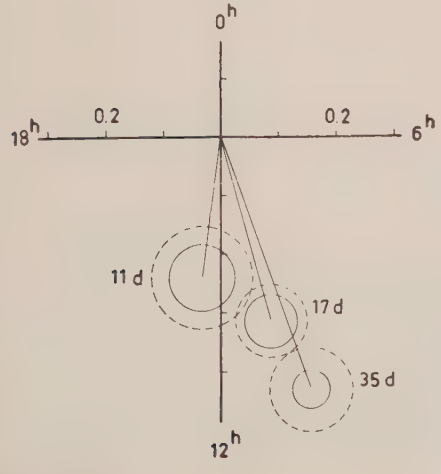


follows that the direction of the anisotropy outside the earth's magnetic field depends only slightly on the disturbances causing the variations of the $K_p$ index. The same can be said about the Uppsala values, days with $[K_p]_{max} \leqq \leqq 1^+$ excepted. Concerning the latter the Uppsala records (Fig. 11) indicate a late time of maximum. Correcting for the deviation of the primaries by the earth's magnetic field we find the direction of the anisotropy to be $174° \pm 20°$ to the evening side for $\psi_U = 71°$ (eq. 2) and $187° \pm 15°$ for $\psi_U = 84°$ (eq. 3). A comparison with the contemporary measurements from Murchison Bay makes both these values look meaningless. Resolving the anisotropy into radial and tangential components we find that at the latitude of Uppsala the latter would be either non-existent or smaller than that at Murchison Bay. If the correction according to eq. 3 is accepted it would even be possible that it had the opposite direction. At the same time the radial component would have a very much bigger amplitude at Uppsala than at Murchison Bay. Even considering the very wide limits of error of the longitude correction this seems contradictory.

If instead, the first year of the Uppsala records (SANDSTRÖM and LINDGREN 1959) is studied, the picture will be different. The same is to some extent true also of the whole 36-month period. In the first case the vector for the class I days has almost the same direction as that for the period unresolved according to the $K_p$ index. In the second case the angles of direction will be $139° \pm 20°$ for $\psi_U = 71°$ and $152° \pm 15°$ for $\psi_U = 84°$. This appears at least more reasonable. But the erratic phase shifts still call for a special study.

During the period 26 Aug. 1957 to 30 Apr. 1959 the records contain only 12 days belonging to class I. The very big amplitude of the first harmonic at Uppsala indicates that it might be possible to study the daily variation on single days. The vector sum diagrams in Fig. 13

Fig. 12. Mean daily variation for days with $[K_p]_{max} > 7^+$. The vector marked 11 days represents the days illustrated by the curves in columns 1, 2, and 4. The vector marked 17 days shows phase and amplitude when those days are added which are illustrated by the curves in column 3. The third vector (35 days) represents the mean of all available days with $[K_p]_{max} > 7^+$. The curves in the upper part show the variation in relative intensity for each day.

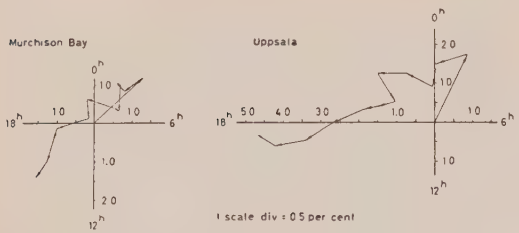


Fig. 13. Vector sum diagrams for the first harmonics of single days with $[K_p]_{max} \leqq 1^+$. From the origin the vectors represent 23 and 28 Dec. 1957, 24 May, 13 Sep., 12 Oct., 5, 6, and 30 Nov., 1 Dec. 1958, 1 and 21 Jan., and 22 Apr. 1959.

are the result of such a study. It is interesting to note that on the first one of the 12 days under discussion the phase of the first harmonic differs considerably from the mean of the whole class of days. Because of the unavoidably big standard errors the phases are not significantly different at Murchison Bay and Uppsala. However, the removal of this particular day has a remarkable effect on the means for the remaining 11 days (Fig. 14). At Murchison Bay the phase remains the same while the amplitude increases by a factor of approximately two. At Uppsala the phase decreases. In this case, too, the amplitude increases. In Fig. 14 the dotted vectors represent the means of the original 12 days, while the full drawn vectors represent the means of the remaining 11 days.

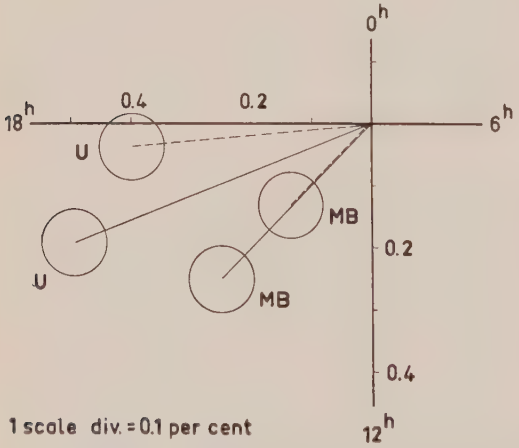


Fig. 14. Diagram showing amplitude and phase of the first harmonic for the class I days at Uppsala (U) and Murchison Bay (MB). Dotted vectors: all days with $[K_p]_{max} \leqq 1^+$ included. Full drawn vectors: the same days exclusive 23 Dec. 1957.

A comparison between Figs. 10 and 14 reveals that the exclusion of 23 Dec. 1957 does not bring the Uppsala and Murchison Bay vectors of the class I days into phase inside the standard errors as calculated from the Poisson distribution. However, the results indicate that 12 days is too short a period for the elimination of disturbances in the daily variation not correlated with the phenomena characterized by the $K_p$ indices.

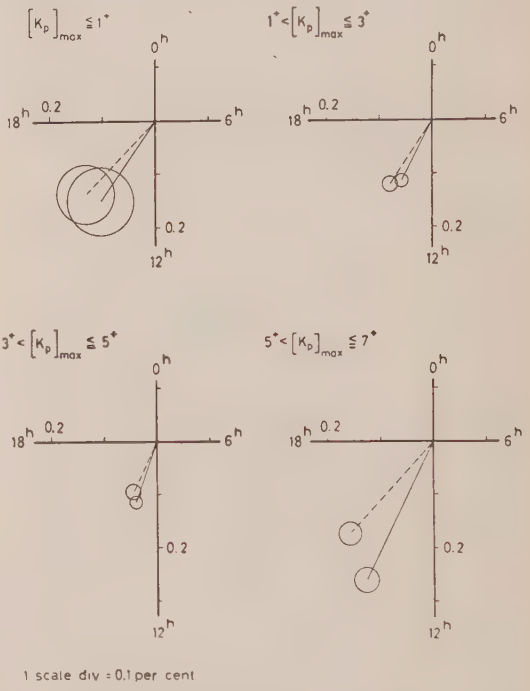


Fig. 15. Clock diagrams for the mean daily variation at Murchison Bay showing the phase shifts for the first four classes of days when the period 3 Aug. to 18 Nov. 1958 is being removed (full drawn vectors).

It ought to be observed that 23 Dec. 1957 is at the end of the recovery period after a Forbush decrease (compare SANDSTRÖM and LINDGREN 1959).

It is of some interest to study how the removal of the period 3 Aug. to 18 Nov. 1958 affects the phases and amplitudes of classes I—IV. This period had a phase which differed markedly from the phase during the rest of the Murchison Bay records (Figs. 6 and 7). In the case of Uppsala the phase change as well as the change of amplitude is negligible. For Murchison Bay the shifts are significant through

their consistency although they are relatively small in comparison with the limits of error. As can be seen from Fig. 15 the shifts are in the same direction in all four cases. The direction is that expected from the removal of the period with abnormal phase. The results indicate also that the late time of maximum is unconnected with the geomagnetic conditions during the period in question.

Although the amplitude of the second harmonic is very small in comparison with the limits of error there is no doubt of its existence especially for days with $[K_p]_{max} > 3^+$. However, for the geomagnetically most disturbed days ($7^+ < [K_p]_{max} \leq 9^-$) the mean amplitude does exceed the limits of error.

The first year's records from the Uppsala monitor reveal a significant amplitude of the second harmonic for days belonging to class IV (SANDSTRÖM and LINDGREN 1959). However, for the whole period of 36 months the mean amplitude for this class is insignificant. Disregarding those cases where the amplitude is less than the limits of error no variation in phase can be observed. This might be due, partly, to the inaccuracy caused by the small amplitudes.

**Concluding remarks and summary**

Undoubtedly there is a considerable day to day variation both in phase and amplitude. They have been commented upon by FIROR ET AL. (1954), and by MC CRACKEN (unpublished thesis 1959). It is possible that some of these variations are due to local effects. In other cases, for instance 28 June 1958 (Fig. 12) it is doubtful whether the big amplitude is to be ascribed to the normal daily variation or to some superimposed single event. Under these circumstances the mean value over a long period becomes important not only as a means of reducing the influence of statistical fluctuations. If, as most of the evidence indicates, the main component of the daily variation can be regarded as being due to a particle wind blowing along the earth's orbit, the tilting of the axis of rotation of the earth will possibly give rise to a small seasonal variation in the amplitude. This seasonal variation will disappear in the yearly mean. A sideral component with constant amplitude will also disappear in the yearly mean. Should the amplitude not be constant it would still be diminished to a minimum through the process of averaging.

DATTNER and VENKATESAN (1959) have listed seven possible components of the diurnal variation. The existence of these components has been derived from the theory by ALFVÉN (1954) concerning the origin of cosmic rays. One of these components is identical with the solar time variation which is the main subject of the present investigation. According to Dattner and Venkatesan most of the other components should more or less cancel one another in an annual average. This also indicates the yearly mean as a less complicated object of study than short period means. Nevertheless, as is shown by the Murchison Bay and Uppsala records, the yearly means can be affected by non-recurrent periods with a differing phase (Figs. 7 and 8). If only they were contemporary the existence of such periods could be explained by the appearance or disappearance of one or two of the components listed by Dattner and Venkatesan. As in this case non-contemporary phase shifts occur at two stations on the same meridian it appears as if an explanation through such components is invalidated. A recent investigation has led PARSONS (1960) to suggest that at least part of these phase shifts are due to a universal time component of limited durability.

When means for periods as short as one month or 27 days are being studied it is necessary to bear in mind that the day to day variability will play a prominent part. This fact might be responsible also for the phase shifts revealed by the vector sum diagrams in Fig. 6.

A period of 20 months has been employed for the correlation of the phase and amplitude variations with $[K_p]_{max}$. It could be argued that in this case, too, 12-month periods would offer a better elimination of the influence from certain variable components. However, such an elimination becomes possible only when nearly all the days of the 12 month periods can be employed. It might also be partly successful if an evenly distributed number of days is employed. Neither is possible for days sorted into classes according to their $[K_p]_{max}$ values. Therefore it is necessary to allow for certain disturbing influences. These will not be serious for classes II and III, which contain the majority of days. As has already been

shown such influences might be considerable where days of class I are concerned. The results presented here can be summarized as follows:

The harmonic analysis of the Uppsala and Murchison Bay records shows the amplitude of the yearly mean daily variation of the nucleonic component to be bigger at the former place than at the latter. The quotient between the two amplitudes is in full accordance with the assumption that the direction of the anisotropy is parallel to or nearly parallel to the orbital plane of the earth.

The Murchison Bay records reveal that the anisotropy makes an angle of more than 90° with the radius vector from the sun. Therefore, if resolved in one tangential and one radial component the mean yearly anisotropy will have a radial component directed towards the sun.

Making it a condition that the direction of the anisotropy should be the same when calculated from the Uppsala records as when calculated from the Murchison Bay records, a longitude correction can be found for Uppsala.

During three consecutive years the Uppsala records reveal only minor changes in the phase and amplitude of the yearly mean first harmonic.

When short periods are analyzed phase shifts are found which do not appear simultaneously in the records from the two stations.

At Murchison Bay the first harmonic exhibits a small negative phase shift with increasing values of $[K_p]_{max}$. At Uppsala the first harmonic displays clearly the same small phase shift, days with $[K_p]_{max} \leqq 1^+$ excepted. In this latter case the phase is sometimes strongly shifted towards late hours, and the amplitude increases considerably. In one case this has been shown to be due to one single day with strongly differing phase and amplitude. This day had the same phase and amplitude in Uppsala and Murchison Bay but affected the means for the two stations in different ways.

The amplitude of the second harmonic is very small. The phase of the second harmonic varies considerably from one year to another.

**Acknowledgements**

Funds for the erection of the cosmic ray station at Murchison Bay under the Swedish-Finnish-Swiss IGY-expedition were granted by the Swedish National Committee for Geodesy and Geophysics.

The work of the Cosmic Ray Group at Uppsala University has been sponsored by the Swedish National Science Research Council and the Swedish Committee for Atomic Research.

The research in this paper is supported in part by contract AF 61 (514)—1312 with the Air Research and Development Command, United States Air Force, through its European Office.

A grant from the foundation of Knut and Alice Wallenberg made it possible to carry on the work at Murchison Bay for another year after the end of the IGY-expedition.

We are especially indebted to Professor Gösta H. Liljequist, the leader of the Swedish-Finnish-Swiss IGY-expedition, for the excellent facilities at Murchison Bay and for his interest in the cosmic ray enterprise. We thank him also for putting the meteorological records of the expedition at our disposal.

We also wish to thank Mr Karl-Erik Heikkilä who during the first year assisted one of us (E. Dyring) in the work at Murchison Bay and Mr Lars O. Andersson, who during the second year had the responsibility for the cosmic ray equipment. We are also indebted to the technician of the IGY-expedition, Mr Hans Engström, for valuable services. We thank him as well as everyone else who helped in securing the cosmic ray records.

## REFERENCES

Alfvén, H., 1954: On the origin of cosmic radiation, *Tellus* **6**, p. 232.

Brunberg, E. Å., 1953: Experimental Determination of Electron Orbits in the Field of a Magnetic Dipole, Part I, *Tellus* **5**, p. 135.

— 1956: Cosmic Rays in the Terrestrial Magnetic Dipole Field, *Tellus* **8**, p. 215.

— 1958: The optics of cosmic ray telescopes, *Arkiv f. Fys.* **14**, p. 195.

Brunberg, E. Å., and Dattner, A., 1953: Experimental Determination of Electron Orbits in the Field of a Magnetic Dipole, Part II, *Tellus* **5**, p. 269.

— 1954: On the Interpretation of the Diurnal Variation of Cosmic Rays, *Tellus* **6**, p. 73.

DATTNER, A., and VENKATESAN, D., 1959: Anisotropies in Cosmic Radiation, *Tellus* **11**, p. 239.

DORMAN, L. I., 1957: *Cosmic Ray Variations* (Variatsii Kosmicheskikh Luchey) Translation prepared by Technical Documents Liaison Office, Wright-Patterson Air Force Base, Ohio.

DYRING, E., 1960: *Statistical Studies of the Performance of Cosmic Ray Recording Instruments.* In preparation.

DYRING, E., and ROSÉN, B., 1960: *The Standard Error in Harmonic Analysis of Cosmic Ray Time Series.* In preparation.

FIROR, J. W., FONGER, W. H., and SIMPSON, J. A.: Cosmic radiation intensity-time variations and their origin, V. The daily variation of intensity, *Phys. Rev.* **94**, p. 1031.

LILJEQUIST, G., 1959: Murchison Bay. Den svensk-finsk-schweiziska expeditionen till Nordostlandet 1957—58. *Ymer 1959*, p. 81.

MALMFORS, K. G., 1945: Determination of Orbits in the Field of a Magnetic Dipole with Applications to the Theory of the Diurnal Variation of Cosmic Rays, *Arkiv f. Matemat., Astron. och Fys.* **32 A**, Nr 8.

PARSONS, N. R., 1960: Phase Changes in the Daily Variation of the Cosmic Ray Nucleonic Component. *Tellus* (in manuscript).

POMERANTZ, M. A., SANDSTRÖM, A. E., POTNIS, V. R., and ROSE, D. C., 1960: Solar Disturbances and the Cosmic Ray Equator, *Tellus*, in manuscript.

ROTHWELL, P., 1958 a: Cosmic Rays in the Earth's Magnetic Field, *Phil. Mag.* **3**, p. 961.

SANDSTRÖM, A. E., 1955: On the correlation between Geomagnetic Activity and the Diurnal Variation of Cosmic Rays, *Tellus* **7**, p. 204.

— 1956: Experimental Evidence of the Directional Components of Cosmic Rays, *Tellus* **8**, p. 18.

— 1958 a: Cosmic Ray Diurnal Variation and Geomagnetic Activity, *Memoria del V Congreso Internacional de Radiación Cósmica*, Mexico, p. 340.

— 1958 b: The latitude effect of the cosmic ray nucleonic component in relation to the magnetic dip, *Ark. Fys.* **14**, p. 409.

SANDSTRÖM, A. E., and LINDGREN, S., 1959: First and second harmonics of the daily variation of the cosmic ray nucleonic component at Uppsala Aug. 31, 1956 to Aug. 31, 1957, *Ark. Fys.* **16**, p. 137.

SEKIDO, Y., and KODAMA, M., 1952: Diurnal variation of vertical cosmic rays, *Rep. of Ionosph. Research in Japan*, **6**, No. 2.

SIMPSON, J. A., FONGER, W., and TREIMAN, S. B., 1953: Cosmic Radiation Intensity-Time Variation Method and Meteorological Factors. *Phys. Rev.* **90**, p. 934.

ÅSTRÖM, E., 1956: Focusing of Paraxial Rays in a Magnetic Dipole Field, *Tellus* **8**, p. 254.

— 1958: Focusing of Paraxial Rays in a Magnetic Dipole Field, *Memoria del V Congreso Internacional de Radiación Cósmica*, Mexico, p. 332.

# Radiance Distribution in the Upper Layers of the Sea

By N. G. JERLOV, Oceanographic Institute, Göteborg,

and

M. FUKUDA, Faculty of Fishery, Hokkaido University, Hakodate

(Manuscript received March 2, 1960)

## *Abstract*

The angular distribution of underwater radiance for green light has been studied in the upper turbid layers of the Gullmar fjord by means of a radiance meter which is lowered in the sea along a guide wire with a fixed orientation. A theoretical discussion considers the different components entering into the light field, *viz.* direct sunlight, skylight, and scattered light. On the basis of available measurements of the volume scattering function the scattered light is evaluated by integrating light scattered from the predominant sun beam alone. The experimental angular distributions of radiance compare well with the theoretical distributions. In particular it is demonstrated that the radiance in the angle interval $\pm 45°$ from the sun attains a maximum below the surface.

Our present knowledge of the angular distribution of underwater radiant energy from sun and sky and its change with depth has been attained through a number of investigations employing specific instrumentation (JERLOV and LILJEQUIST, 1938; TAKENOUTI, 1940; WHITNEY, 1941; DUNTLEY *et al.*, 1955; SASAKI *et al.*, 1955; TYLER, 1958). It is manifest that in the upper layers the radiance distribution is much predominated by direct sunlight whereas with increasing depth the light takes a more diffuse character. At great depths an equilibrium state of distribution is approached which is symmetrical round a vertical axis. We do not know with certainty where this asymptotic radiance distribution is reached. Measurements in clear ocean water suggest a depth of about 400 m (JERLOV, 1951).

The theoretical conceptions of underwater radiance are to be based on some assumption about the volume scattering function (POOLE, 1945; LENOBLE, 1957; PREISENDORFER, 1959). Considering the great variety of particles suspended in the sea it is realized that this critical factor should preferably be determined by experiments. ATKINS and POOLE (1952) have initiated such experimental work through a laboratory study of the angular scattering of light by sea water. Recently TYLER and RICHARDSON (1958) and JERLOV (unpublished) have built and used *in situ* instruments to record the significant volume scattering function.

A great deal of interest is connected with the passage of radiant energy through the interface air-water. In his above-mentioned investigation TYLER has studied this problem in the near-surface layer of homogeneous lake water and with an overcast sky and has demonstrated some principal optical effects. The present work is also directed to the surface stratum of the sea and aims at computing for a clear sky the radiance as the resultant of different components by employing radiance quantities observed above the sea together with a simple model for integrating the scattered energy. The predicted distributions are compared to data collected by field work, especially in the near-surface layer.

**Apparatus**

The setting of the radiance meter at different angles requires in the first place a fixed reference direction. It is wellknown that the vertical position of a wire even if weighted is not easily established in the sea. For these experiments conducted in the Gullmar fjord at Bornö Station an accurate orientation of the radiance meter was obtained in the following way. A heavy weight was anchored at 50 m depth off the station. A wire was tightened between the weight and the station bridge in the direction west-east and with an angle of 60° from the vertical. At the observations the meter, which was provided with two wheels, was lowered along this guide wire (Fig. 1). The meter was stabilized with a weight so that its measuring head could be set at different vertical angles in a meridional plane. Land was far away from the observation point in this plane, and the disturbing effect of land contours was judged to be inconsiderable.

The meter was devised so as to present equally large surfaces above and below the guide wire so that the vertical angle would be little affected by the drag of prevailing currents. The depth change of the measuring head when rotating it was negligible.

Sufficient sensitivity was obtained by using a photovoltaic cell as detector in connexion with an Ising galvanometer (sensitivity $4 \cdot 10^{-10}$ ampères per scale-unit). By means of a lens-pinhole system the apex angle of the cone of acceptance was limited to 7.0° in water which is equivalent to 9.3° in air. A high resolving power is desirable but there is not much to gain by choosing a smaller angle because of the wave-induced fluctuations in radiance which especially tend to disturb observations close to the sun.

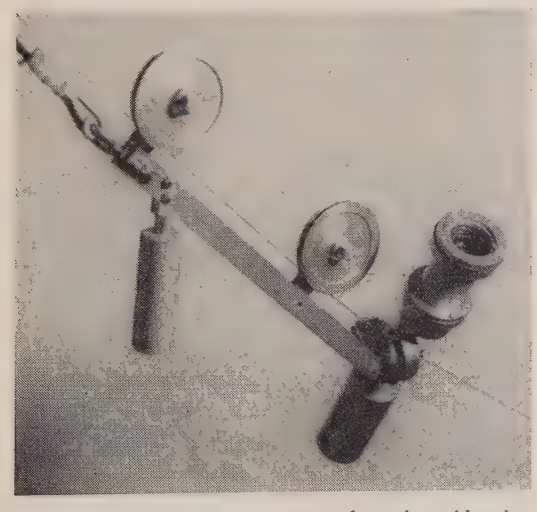

Fig. 1. The radiance meter mounted on the guide wire.

**Measurements**

The radiance was measured solely in a meridional plane. Usually the following settings of vertical angle at both sides of the vertical line were employed: 0°, 20°, 30°, 40°, 45°, 60°, 90°, 135° and 180°. Observations with settings close to the sun were obviously critical and must be made when the sun passed the meridian. The radiance at other angles being less dependent on the azimuth was recorded as near noon as possible. In the deep layers no attention was paid to radiance from below which is probably affected by the bottom.

Experiments were conducted in June 1958 and completed in June 1959. Weather conditions were clear sky and low wind. The sun's altitude was 48—50° which corresponds to a refraction angle in the water of about 30°.

As the chief object was to study the radiance distribution for wavelengths having maximum transmittance in the fjord water the meter was provided with a green Schott filter (4 mm VG 9, centre 535 mμ).

At the measurements the water of the Gullmar fjord showed a typical stratification with a top layer of less salinity and lower transparency than underlying layers. This water structure was studied by collecting water samples from different depths and determining their attenuation coefficient by means of an ELKO meter. The characteristic result was a homogeneous top layer with a thickness of 2 m having an attenuation coefficient of 0.5 $m^{-1}$. Towards greater depth the attenuation decreased rapidly. Through comparative tests on these water samples in a scattering meter (Jerlov, 1958) the total scattering coefficient in the top layer was estimated at 0.3 $m^{-1}$.

It would be too voluminous to present the whole supply of observations. The material lends itself to a combined representation as the data were obtained very much under the same conditions. Radiance in a logarithmic scale as a typical function of depth for different angles is given in Fig. 2. It is noted that the

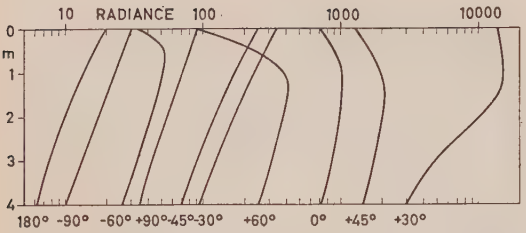


Fig. 2. Observed radiance for green light (535 mμ) as a function of depth for different vertical angles. The sun at +30°.

radiance for angles between 0° and + 60° attains a maximum below the surface. This maximum is most conspicuous for + 60°.

The representation of the angular distribution is restricted to 0 m and 1.86 m depth, *i.e.* to the homogeneous top layer (Fig. 3). These curves will later be compared to those theoretically derived.

An instance of radiance distribution followed to great depth is adduced in Fig. 4. It is evident that the approach to a pattern symmetrical round the vertical is for green light not fully accomplished at 30 m depth.

## Theory

The different components will be considered separately, *viz.* direct sunlight, skylight and scattered light, which enter into the total flux

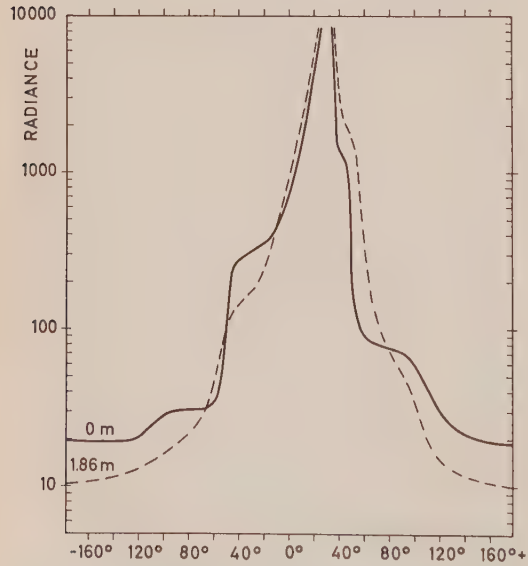


Fig. 3. Angular distribution of observed radiance (535 mμ) at surface and at 1.86 m depth.

available to the radiance meter. The discussion is confined to the vertical plane through the sun.

Most of the energy passing the surface layers

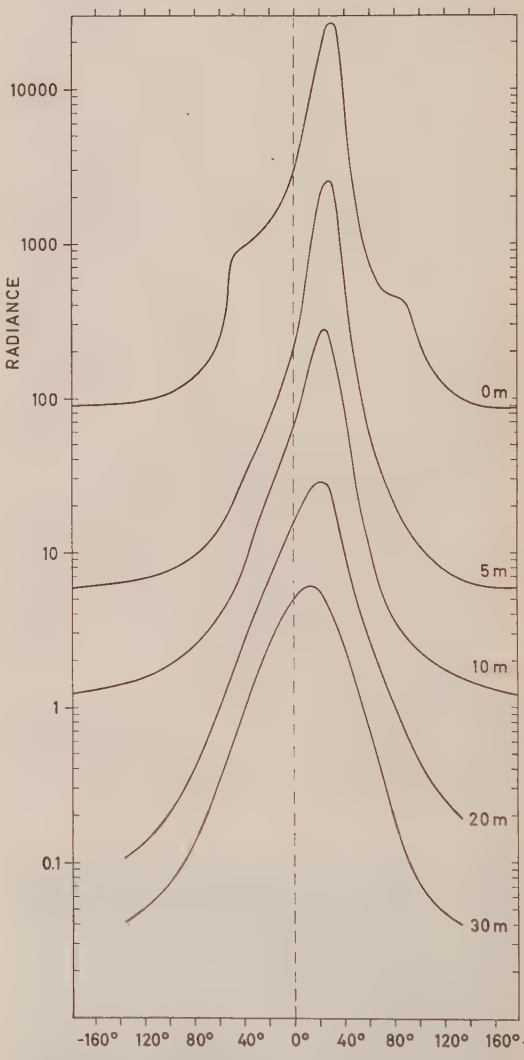


Fig. 4. Angular distribution of observed radiance (535 mμ) followed down to 30 m depth in order to illustrate the approach to a distribution symmetrical round the vertical.

is direct sunlight. Accordingly, the radiance distribution solid is in the surface layer much elongated in the sun's direction. This is fluctuating in a degree dependent on the formation of surface waves.

The penetration into the sea of the diffuse skylight exhibits some wellknown features.

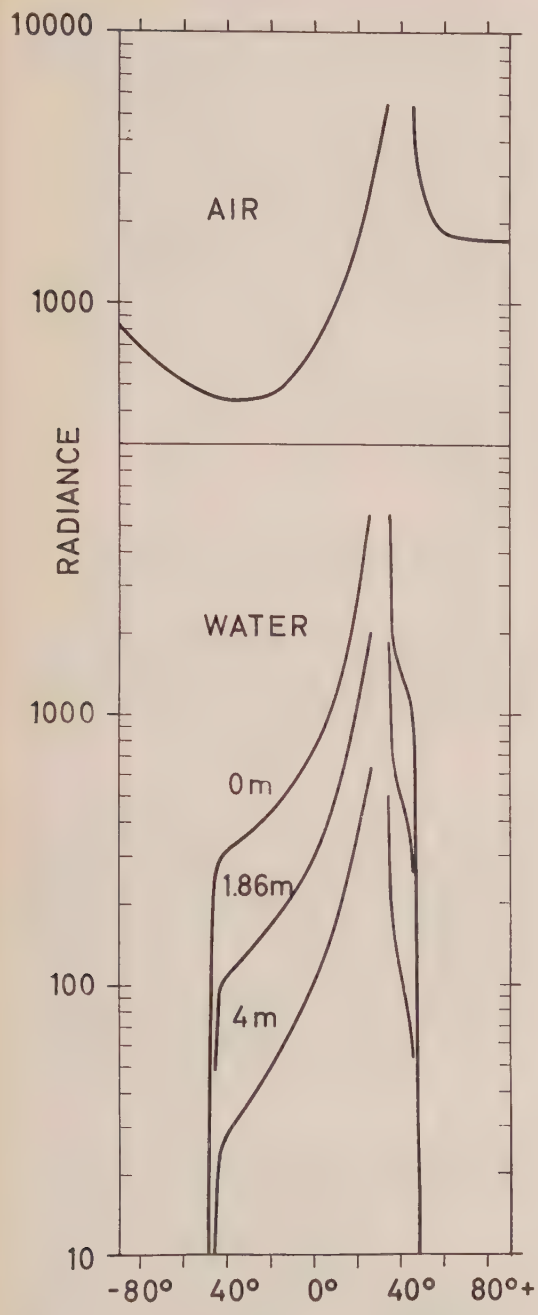


Fig. 5. Change and compression of skylight (535 mμ) from air to water (surface, 1.86 m and 4 m depth).

With a flat surface the light field is by refraction compressed within a cone of an apex angle $2 \times 48.6°$. It is evident from Snell's law that the edge of this cone corresponding to high angles of incidence is fairly stable and not much affected by waves.

Leaving, for the present, reflexion losses out of account a beam of radiant energy is considered which passes from air to water through a flat water surface, the angles of incidence and refraction being $i$ and $j$ respectively. The geometry of the light beam is characterized by the solid angle $\Delta\omega_a$ in air and $\Delta\omega_w$ in water. The relation between these solid angles is

$$\frac{\Delta\omega_a}{\Delta\omega_w} = \frac{2\pi \sin i \Delta i}{2\pi \sin j \Delta j}$$

With the aid of Snell's law, $\sin i / \sin j = n$, it follows

$$\frac{\Delta\omega_a}{\Delta\omega_w} = n^2 \frac{\cos j}{\cos i} \qquad (1)$$

As mentioned this type of radiance meter collects flux within a solid angle which in air is $n^2$ times as large as in water. Consequently, readings taken in air in the direction $i$ should be multiplied with $\cos i / \cos j$ in order to convert them to readings in water in the direction $j$. It remains to pay regard to reflexion losses at the water surface. The magnitude of this reflexion is evaluated according to Fresnel's formula for unpolarized light. Furthermore it is observed that the window of the measuring head in air reflects a percentage of 4 % which almost disappears in water.

The typical change and compression of the skylight field from air to water is illustrated in Fig. 5. These underwater values depicted for 0, 1.86 and 4 m have been computed on the basis of observed atmospheric values by applying the above conversion.

An interpretation of the scattered light must proceed from a determination of the volume scattering coefficient $\beta(\varphi)$. JERLOV has measured for green light the factor $\beta(\varphi)/b$, where $b$ is the total volume scattering coefficient. By definition

$$b = \int_{4\pi} \beta(\varphi)\, d\omega = 2\pi \int_0^{\pi} \beta(\varphi) \sin\varphi\, d\varphi \qquad (2)$$

These results shown in Fig. 6 are well representative for the Gullmar fjord in the

early summer. They give evidence of a pronounced forward scattering and of minimum scattering at about 120°.

It is reasonable to presume that in the near-surface layer the sun is the primary source of scattered light. The radiance from the upper hemisphere may accordingly be derived by a simple integration if multiple scattering is neglected.

Let $E_0$ be the irradiance at the surface. The small volume element, $dv$, at P is irradiated by (see Fig. 7)

$$E_0 e^{-cx \sec j}$$

The irradiance at Q will be

$$dE = E_0 e^{-cx \sec j}\, \beta(\theta - j)\, dv \frac{1}{r^2} e^{-cr}$$

where $dv = r^2\, d\omega\, dr$.
By integrating with respect to $r$ and introducing the radiance $L = dE/d\omega$ it is found

$$L(\pm) = E_0 \frac{\beta(\pm\theta \mp j)}{c} \frac{\sec\theta}{\sec j - \sec\theta} \cdot \cdot \left(e^{-cz \sec j} - e^{-cz \sec\theta}\right) \qquad (3)$$

$L(+)$ referring to positive and $L(-)$ to negative $\theta$.

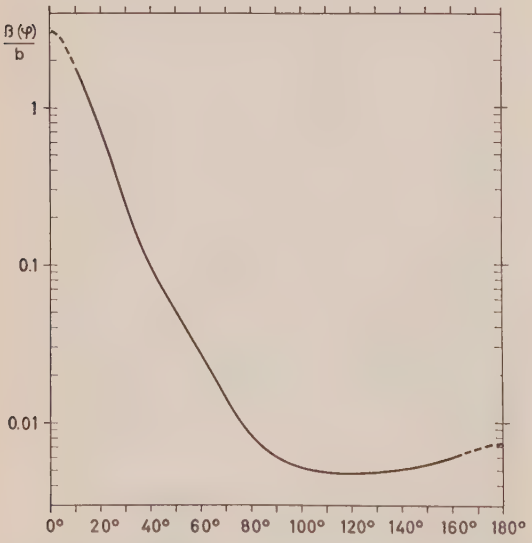


Fig. 6. The ratio between the volume scattering function $\beta(\varphi)$ and the total scattering coefficient $b$ for green light (JERLOV).

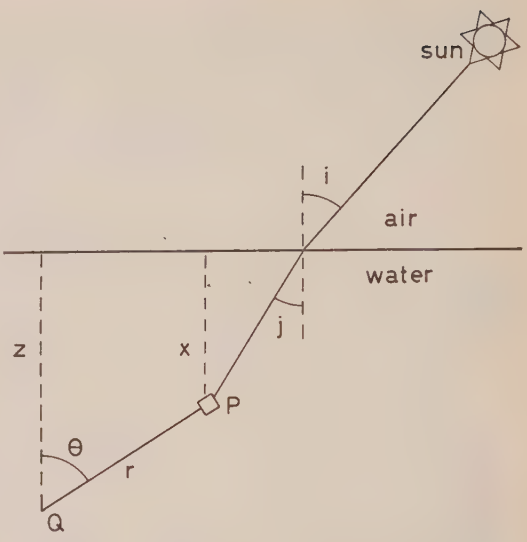


Fig. 7. Sketch of primary scattering of sunlight.

In the special case of $|\theta| = |j|$, which has a significance only for negative $\theta$-values, equation (3) reduces to the simple form

$$L(-) = E_0 z \frac{\beta(2j)}{\cos\theta} e^{-cz \sec j} \qquad (4)$$

Similar integrations have been performed by LE GRAND (1939) assuming isotropic scattering, by LAUSCHER (1947) and by TAKENOUTI (1949) both dealing with pure Raleigh scattering.

Equation (3) has some important applications. Maximum in radiance is attained at a depth $z_m$

$$z_m = \frac{1}{c} \frac{\ln\sec\theta - \ln\sec j}{\sec\theta - \sec j} \qquad (5)$$

This formula is identical with that found by LAUSCHER who also points out that for $\theta = j$

$$z_m = \frac{1}{c} \cos\theta \qquad (6)$$

In this case

$$L(-)_{\max} = E_0 \frac{\beta(2j)}{c} e^{-1} \qquad (7)$$

It is gathered that the field of scattered light is built up in magnitude unto a certain depth which is independent of the scattering function.

An application of equations (3)—(7) will give a concrete illustration of the radiance of scattered light as a function of depth. With reference to the measurements, the $j$-value is chosen at 30°, the $c$-value at 0.5 $m^{-1}$ and the $b$-value at 0.3 $m^{-1}$. The estimating of $E_0$ is beset with some difficulty. We have adopted the atmospheric value converted to underwater irradiance according to the same arguments as given for skylight. Thus we take it for granted that the glitter pattern of the sun has the same angular subtense as the radiance meter. Though

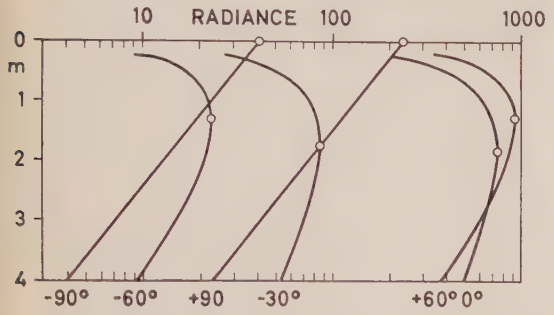


Fig. 8. Computed radiance of downward scattered light (535 m μ) as a function of depth for some vertical angles. Positions of radiance maximum are indicated by small circles.

this is supported by the observations it is notwithstanding subject to uncertainty.

The set of computed curves are shown in Fig. 8. They demonstrate that the radiance maximum is encountered at the greatest depth, 1.86 m, for $\theta = 0°$ and that it moves to the surface when $\theta$ grows to 90°.

The radiance of light scattered from the lower hemisphere is deduced in a similar way. It will come out by integrating from the depth $z$ to infinite depths as follows

$$L(\pm) = E_0 \frac{\beta(\pm\theta \mp j)}{c} \frac{\sec\theta}{\sec j + \sec\theta} e^{-cz\sec j} \quad (8)$$

In this case the light field continuously reduces in magnitude when the depth increases.

It must not be disregarded that upward scattered light is reflected against the water surface and enters into the light field of the upper hemisphere. Particularly in the angle interval 48.6°—90° (with a flat surface), where total reflection takes place, this light contribution is appreciable.

The light scattered upwards from an infinite

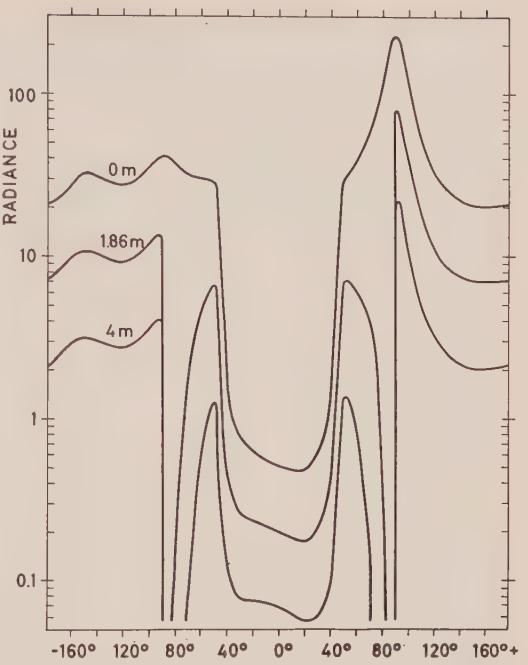


Fig. 9. Angular distribution of upward scattered light (535 mμ) at surface, 1.86 m and 4 m depth. Reflexion takes place at the sea surface in the interval +90° to −90°, and total reflexion between +48.6° and +90° as well as between −48.6° and −90°.

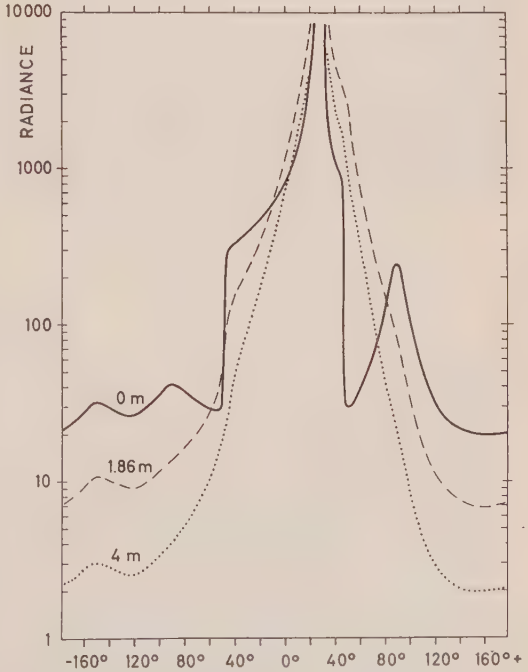


Fig. 10. Angular distribution of computed radiance (535 mμ) at surface, 1.86 m and 4 m depth.

path is thus distributed over all angles. The radiance is evaluated from equation (8) with the mentioned numerical values and with reflexion values obtained from Fresnel's formula. The resulting surface distribution (Fig. 9) exhibits a profound minimum between + 48.6° and − 48.6°, where reflexion is low, as well as two maxima at + 90° and − 90°. The former, being against the sun, is much more conspicuous than the latter. Another slight maximum at − 150° is attributed to pure backscattering (at 180° from the sun). The change of radiance with depth is very drastic for the totally reflected light close to 90° on account of the depth function $e^{-cz \sec \theta}$.

Finally the total light field is yielded by adding the different components examined under the assumption of clear sky and flat water surface. The three curves in Fig. 10 representing distributions at 0, 1.86 and 4 m give evidence of the strong predominance of radiance near the sun. The sudden fall of surface radiance at the critical angle of 48.6° becomes less conspicuous towards greater depth. The two outstanding peaks at 90° in the surface distribution are almost extinguished at depth.

## Discussion

The conclusions centre on a comparison between radiance distributions obtained experimentally (Fig. 3) and those obtained theoretically (Fig. 10). On the whole the characteristic features in the two sets of curves are consistent. The 1.86 m curve is in both pictures well above the surface curve between − 10° and + 80°, or about in the interval ± 45° from the sun, and also in a small angle interval at − 55°. Existing discrepancies may be explained as the effect of wave motion at the measurements which is apt to smooth out fine details in the theoretical pattern derived for at flat surface. Thus the minimum at + 50° combined with the maximum at + 90° in the theoretical surface distribution is almost completely levelled off in the experimental distribution, chiefly on account of fluctuations of the scattered light from below totally reflected at the surface. The computed slight maximum at − 150° does not show up in Fig. 3 because of lack of sufficiently dense observations in this region.

The radiance distribution in the sea has been sketched in its general outline twenty years ago. Improved technique has later made possible the finding of significant details. An investigation by SASAKI *et al.* has given clear evidence of the peak of radiance which occurs at 90° though they did not interpret this as a maximum. The mentioned distributions with an overcast sky obtained by TYLER are in comparable features consistent with the present results.

It may be inferred that the observed radiance in the upper layers of the sea conforms with a theoretical conception based on a simple integration of light scattered from the sun beam alone. This assumption does not hold true at greater depths where the direct sunlight has lost its predominating character.

## REFERENCES


ATKINS, W. R. G., and POOLE, H. H., 1952. An experimental study of the scattering of light by natural waters. *Proc. Roy. Soc. B*, **140**, p. 321.

DUNTLEY, S. Q., UHL, R. J., AUSTIN, R. W., BOILEAU, A. R., and TYLER, J. E. An underwater photometer. *Journ. Optical Soc. America*, **45**, p. 904 (A).

JERLOV, N. G., and LILJEQUIST, G., 1938. On the angular distribution of submarine daylight and on the total submarine illumination. *Svenska hydrogr.-biol. Komm. Skr., Hydrogr.*, **14**, p. 3.

JERLOV, N. G., 1951. Optical studies of ocean waters. *Rep. Swedish Deep-Sea Exp.*, 1947—48, **3**, No. 3.

JERLOV, N. G., 1958. Distribution of suspended material in the Adriatic Sea. *Estratto dall'Archivio di Oceanografia e Limnologia*, **11**, p. 227.

LAUSCHER, F., 1947. Zur Strahlungstheorie der Hydrosphäre. *Sitzungsberichte Akademie der Wissenschaften in Wien, Abt. II A*, **155**, p. 281.

LE GRAND, Y., 1939. La pénétration de la lumière dans la mer. *Ann. de l'Inst. Océanographique*, **19**, p. 393.

LENOBLE, JACQUELINE, 1957. Étude de la pénétration du rayonnement ultraviolet naturel dans la mer. *Bull. d'Information du Comité Central d'Océanographie et d'Étude des Côtes*, **9**, p. 8.

POOLE, H. H., 1945. The angular distribution of submarine daylight in deep water. *Scient. Proc. Roy. Dublin Soc.*, **24**, p. 29.

PREISENDORFER, R. W., 1959. *Journ. Marine Res.*, **18**, p. 1.

SASAKI, T., OKAMI, N., WATANABE, S., and OSHIBA, G., 1955. Measurements of the angular distribution of submarine daylight. *Journ. Scient. Res. Inst.*, **49**, p. 103.

— 1957. *Measurements of the angular distribution of daylight in the sea.* Records Oceanogr. Works Japan (spec. number), p. 42.

TAKENOUTI, Y., 1940. Angular distribution of submarine solar radiation and the effect of altitude of the sun upon the vertical extinctions coefficient. *Bull. Jap. Soc. Sci. Fish.*, **8**, p. 213.

TAKENOUTI, Y., 1949. On the diffusion-ratio of underwater illumination. *The Oceanogr. Mag.*, **1**, p. 43.

TYLER, J. E., 1958. Comparison of light distribution above and below water. *Journ. Marine Res.*, **16**, p. 96.

TYLER, J. E., and RICHARDSON, W. H., 1958. Nephelometer for the measurement of volume scattering coefficient *in situ*. *Journ. Opt. Soc. America*, **48**, p. 354.

WHITNEY, L. V., 1941. The angular distribution of characteristic diffuse light in natural waters. *Journ. Marine Res.*, **4**, p. 122.

# LETTERS TO THE EDITOR

## *Diurnal Wind Variation*

"*The diurnal variation of the wind*" by G. J. Haltiner, *Tellus*, **II**, pp. 452—458 (1959).

Dear Sir,

In this article, G. J. Haltiner obtained numerical solutions for the diurnal variation of wind in the friction layer, allowing the coefficient of eddy viscosity to vary with height and time. Concluding that the results of this study showed some agreement between the theoretical representation of the diurnal wind variation and observed data evaluated by BUAJITTI and BLACKADAR (1957), Dr. Haltiner attributed disagreement in significant features of the wind field to the functional forms used for the coefficient of eddy viscosity. I would like to suggest that there is another possible source of disagreement, namely, the diurnal variation of the geostrophic wind, a factor that apparently has not been considered in models of this type.

To illustrate the likelihood of such an effect, we may compare the magnitudes of the "local acceleration", $\partial u'/\partial t$, and the pressure gradient force in the first of the equations of motion, linearized to satisfy the diurnal variations only (HARRIS, 1959). For the data in Figure 4 of Dr. Haltiner's paper, a representative value of the amplitude of the wind component in the friction layer appears to be about 2.5 m sec$^{-1}$, so that the amplitude of $\partial u'/\partial t$ would be about $1.8 \times 10^{-2}$ cm sec$^{-2}$. I do not know what corresponding value for the variation of the geostrophic wind would be appropriate to these data, but at Washington, D.C., I found the diurnal variation of the component of the pressure gradient force per unit mass, $\partial p'/\bar{\varrho}\partial x$, to be

$$1.45 \times 10^{-2} \sin(\omega t + 123°) \text{ cm sec}^{-2},$$

the semidiurnal term being much smaller. This value, which applies to the surface and the month of June, was found by analyzing maps of the amplitude and phase of the diurnal pressure variation for stations in the eastern U.S., graphing the results along a section through Washington, and evaluating the spatial derivatives of the amplitude and the phase.

The value of $1.45 \times 10^{-2}$ cm sec$^{-2}$, incidentally, is very nearly an order of magnitude larger than one would infer from the passage of a simple progressive wave of the appropriate amplitude (0.9 mb). It must be somewhat greater than the average for the United States as a whole, for the pressure wave shows unusually marked changes along the Atlantic seaboard. Presumably the magnitude should decrease with elevation, like the pressure wave itself, but I believe it would still be appreciable throughout the friction layer. At Washington in June a representative amplitude for $\partial u'/\partial t$ is about $0.6 \times 10^{-2}$ cm sec$^{-2}$ for the first harmonic, so that the diurnal variation of the pressure gradient force in the lower layers of the atmosphere at Washington is probably even larger than the acceleration.

It may be that at other localities also the diurnal change of the geostrophic wind is appreciable in comparison with other terms in the equation of motion, and must therefore contribute to the observed wind variation. I feel that one should be aware of this possibility in comparing the results of theoretical models, based on the usual assumptions, with the results of observation.

Sincerely yours,

MILES F. HARRIS

U. S. Weather Bureau
Washington, D. C.

## REFERENCES

BUAJITTI, K., and BLACKADAR, A. J., 1957: Theoretical studies of diurnal wind variations in the planetary boundary layer. *Quarterly Journal of the Royal Meteorological Society*, **83**, pp. 486—500.

HARRIS, M. F., 1959: Diurnal and semidiurnal variations of wind, pressure, and temperature in the troposphere at Washington, D. C., *Journal of Geophysical Resarch*, **64**, pp. 983—995.

## *Reply*

Dear Sir,

Mr. Harris' suggestion that part of the diurnal variation of the wind is due to the diurnal pressure variation is certainly a valid one, and the information he has furnished regarding the pressure variation permits an evaluation of this influence. Some indication of the possible magnitude of this contribution may be obtained by integrating the horizontal equations of motion with the following simplifying conditions: constant density, no friction and zero horizontal variation of velocity. If we now express the pressure in terms of the mean pressure $\bar{p}$ plus the component which varies diurnally $p'$, namely, $p = \bar{p} + p'$; the equations of motion may be written

$$\frac{\partial u}{\partial t} = -\frac{1}{\varrho}\frac{\partial \bar{p}}{\partial x} - \frac{1}{\varrho}\frac{\partial p'}{\partial x} + fv$$
$$\frac{\partial v}{\partial t} = -\frac{1}{\varrho}\frac{\partial \bar{p}}{\partial y} - \frac{1}{\varrho}\frac{\partial p'}{\partial p} - fu \qquad (1)$$

where $f$ is the Coriolis parameter.

Next we may express the mean pressure force in terms of the equivalent geostrophic wind components,

$$f\bar{u}_g = -\frac{1}{\varrho}\frac{\partial p}{\partial y}, \quad f\bar{v}_g = \frac{1}{\varrho}\frac{\partial \bar{p}}{\partial x} \qquad (2)$$

Finally, utilizing Harris' expression for the periodic component of the pressure force

$$-\frac{1}{\varrho}\frac{\partial p'}{\partial x} = 1.45 \times 10^{-2} \sin(\omega t + 123^\circ); \frac{1}{\varrho}\frac{\partial p'}{\partial y} = 0 \qquad (3)$$

we obtain the following system of equations:

$$\frac{\partial u'}{\partial t} = 1.45 \times 10^{-2} \sin(\omega t + 123^\circ) + fv'; \frac{\partial v'}{\partial t} = -fu' \qquad (4)$$

$$\text{where } u' = u - \bar{u}_g, \quad v' = v - \bar{v}_g \qquad (5)$$

The expressions on the left in Eqs. (4) are permissible since $u_g$ and $v_g$ are invarient with time.

The solution of the system (4) is easily found to be

$$u' = k_1 \sin ft + k_2 \cos ft + \frac{1.45 \times 10^{-2}\omega}{f^2 - \omega^2} \cos(\omega t + 123^\circ)$$
$$v' = k_1 \cos ft - k_2 \sin ft - \frac{1.45 \times 10^{-2} f}{f^2 - \omega^2} \sin(\omega t + 123^\circ) \qquad (6)$$

where $k_1$ and $k_2$ are constants and $f \neq \omega$.

The first two terms on the left in the expression for $u'$ and $v'$ give the inertial oscillations, while the last term in each expression gives the contribution resulting from the diurnal pressure variation. At 45° latitude the latter terms give velocities of about three to four knots which represent deviations from the mean geostrophic wind.

If the friction force is added to Eqs. (4) the solution is not so simple; and the effect of the diurnal pressure variation is more difficult to assess. It may be noted however that the effects of the diurnal pressure variation and the inertial oscillations are similar in the solution given by (6). Hence they may act somewhat similarly when friction is included. In the solution for the diurnal wind variation which did not include the diurnal pressure variation (HALTINER 1959), inertial oscillations are damped where the friction force is large. However, aloft where the friction force is comparatively small, any unbalance between the pressure and Coriolis forces gives rise to a distinct inertial oscillation. A similar condition may occur when the diurnal pressure variation is taken into account. In order to determine these influences more completely some numerical solutions are being obtained through the use of a high-speed electronic computer. It would be desirable here to know the vertical variation of the component of the pressure gradient resulting from the diurnal pressure variation.

Yours very truly,

G. J. HALTINER
U. S. Naval Postgraduate School
Department of Meteorology
and Oceanography
Monterey, California

## REFERENCE

HALTINER, G. J., 1959: The diurnal variation of the wind *Tellus*, **11**, pp. 452—458.